Particulate Air Monitoring Mathematical Sourcebook Revision 2

William C. Evans
nikenuke@ieee.org

May 2020

Preface

Chapter 1 Mathematical Response Models

Chapter 2 Quantitative Methods

Chapter 3 Concentration Modeling and Response Prediction

Chapter 4 Fast-Filter-Speed Method

Chapter 5 Incorrect Interpretation of Moving-Filter Responses

Chapter 6 Geometric Efficiency Correction

Chapter 7 Selected Formulas

Chapter 8 Integrated-Count Processing

Chapter 9 Reactor Coolant Leakage Rate Estimation

Appendix A Nonconstant Flowrate Effects in Sampling

Appendix B Decay-Chain Concentration Estimation in Sampling

Appendix C Bias in MDC Estimates due to Autocorrelation

Appendix D Activity / Countrate Profile Plots

Preface

This sourcebook is primarily a collection of my published papers on particulate air monitoring. The papers have been re-formatted but have the same content as the published versions, although a few small corrections or clarifications have been made. There is some redundance in the material across the chapters. There is also a considerable amount of unpublished work here, notably the chapter on geometric efficiency correction and the chapter on reactor coolant leakage rate estimation. It is important to recognize that this book does not deal with topics such as pump specification, or line loss estimation, or how to adjust the detector high voltage, etc. Some of the material is still unpolished or incomplete; the document will be updated from time to time to clean up and complete the work.

Consider the processes in an air monitor. Air is pulled through a collection medium, which is viewed in real time by a radiation detector. The output of that detector is a random stream of pulses. Somehow that random sequence must be converted into an estimate of the countrate. With this in hand, the next process is to somehow convert that countrate estimate into an estimate of the *input* to the monitor, namely, the time-dependent air concentration of a nuclide. The latter step is impossible without some form of mathematical model that relates the input (air concentration) to the output (net countrate) of the monitor. Thus, the subject matter of this book is primarily the mathematical modeling of continuous particulate air monitor time-dependent responses. These models can, in some cases and under certain assumptions, be inverted to provide an estimate of the input concentration, or quantities related to it, such as its time integral.

This sourcebook also provides a collection of selected algebraic solutions for the monitor response models, as well as some *Mathematica* code that can provide purely numerical calculation of monitor responses, independent of the algebraic solutions. This is an important point, namely, that evaluating the math herein, e.g., triple integrals, by hand, is not necessary, nor are any sort of approximations to bypass those calculations needed. Just use *Mathematica*.

There is some limited material here on air *sampling*, which of course is related to, but quite different from, air *monitoring*. Expressions are provided for the analysis of decay-chain nuclides in air sampling.

An important point is that my original monitor-response models assumed a constant or “flat” detection efficiency across the deposition window. This is incorrect, since the geometric efficiency will vary with the position of a differential area in that window. This problem is addressed in Chapter 6, where a relatively simple solution is presented, along with *Mathematica* code for evaluating an effective "average" (flat) efficiency, for both RW and CW. If that average efficiency is used in my original models, the fractional difference in the predicted monitor response is within a few percent of the "exact" numerical solution (i.e., the solution that explicitly includes the geometric efficiency variations).

For reference, below are the citations for my published material in this book:

Some Analysis of Integrated-Count Processing for Fixed-Filter Continuous Particulate Air Monitors
Health Physics, Vol. 111,September 2016, pp. 290-299

Incorrect interpretation of Moving-Filter Continuous Particulate Air Monitor Responses
Health Physics, Vol. 104, April 2013, pp. 437-443

Estimation of High-Level, Rapidly-Changing Concentrations Using Moving-Filter Continuous Particulate Air Monitors
Health Physics, Vol. 102, April 2012, pp. 410-418; Erratum Vol. 102, June 2012, p.708

Concentration Dynamics Modeling for Continuous Particulate Air Monitor Response Prediction
IEEE Transactions on Nuclear Science, Vol. 49, No. 5, October 2002, pp. 2574-2598

Bias in Concentration Estimates Due to Nonconstant Flowrate During Particulate Air Sampling
Health Physics, Vol. 82, No. 1, January 2002, pp. 114-119

Quantitative Methods for Continuous Particulate Air Monitoring
IEEE Transactions on Nuclear Science, Vol. 48, No. 5, October 2001, pp.1639-1657

Mathematical Models for the Dynamic Response of Continuous Particulate Air Monitors
IEEE Transactions on Nuclear Science, Vol. 48, No. 2, April 2001, pp. 202-218

My hope is that the material in this book will provide a useful reference for the development of improved air monitoring systems, especially in nuclear power applications. I know from experience that such a sourcebook would have been invaluable in the mid-1970's when I was working on RMS design at Bechtel Power, and a few years later for my work on the Shoreham RMS, especially for the calibration of air monitors in that system. That calibration was a critical-path item for the plant, and affected the fuel-loading schedule. If I had this mathematical material in one place, in a consistent notation, at the time, it would have been extremely useful. I believe it will be just as helpful for a new generation of nuclear engineers.

A personal note: my first real experience with CPAMs was at the SM-1 Nuclear Power Plant, operated by the Army Corps of Engineers at Ft. Belvoir, VA. I was there from March 1968 - March 1971. In late May 1969 I was assigned Health Physics Supervisor at the plant. My predecessor was showing me various things around the plant that I had to do, one of which was to get some readings off the temporary stack monitor (a Tracerlab moving filter; that monitor was patched in, replacing the inoperative Eberline monitor discussed in Chapter 2). There was a graph taped to the filter box on top, and I was being shown how to take a reading of the ratemeter, enter the graph, put that number into a form, etc. How I knew this is a mystery, but I distinctly remember thinking at the time "There is *no possible way* this could be correct..."

And thus began the journey.

Chapter 1

Mathematical Response Models

IEEE Transactions on Nuclear Science, 48(2), April 2001; 202-218

Mathematical models are developed for the dynamic, time-dependent countrate response of fixed-filter (FF), rectangular-window moving filter (RW), and circular-window moving filter (CW) continuous particulate air monitors. These models relate the monitor input, a time-dependent concentration, to the monitor output, its dynamic countrate. The models take the form of a single integral for the FF case, the sum of two double integrals for the RW case, and the sum of three triple integrals for the CW case. The models apply for a single isotope of any half-life, and for sampled concentrations of any time-dependence, at any time during a concentration transient. The models are solved for selected concentration behaviors, providing analytical expressions for the prediction of monitor response, and plots comparing these responses of the three monitor types are presented. A numerical simulation of monitor response has also been developed, which starts from first principles and does not use the analytical solutions. It is shown that this simulation agrees with the analytical solution.

Introduction

Continuous particulate air monitors (CPAMs) are widely used in nuclear facilities. In order to obtain quantitative results, a mathematical relation between the input to the monitor and its output is required. The input is a time-dependent concentration of airborne particulate radioactivity, notated as $Q(t)$, of any half-life, while the output of the monitor is a time-dependent countrate. Monitor response models are used to understand and predict how a monitor will react to various input behaviors, and also to provide the explicit mathematical relationships needed to explore quantitative methods that might be used to solve the "inverse" problem, of relating the observed response of the monitor to its input.

The purpose of this paper, the first in a planned series of three, is to develop relations for the monitor's output, given its input, for the three most-commonly used monitor types: fixed-filter (FF); rectangular-window moving filter (RW); circular-window moving filter (CW). The second paper will present a review of some methods for estimating the input (concentration, or quantities derived from it), given an observed output (countrate, or quantities derived from it). The third paper will develop mathematical models, using linear-systems techniques, for calculating the concentration dynamics for systems commonly encountered in nuclear facility air monitoring, including the effects of HVAC. This mathematics is helpful in relating CPAM-estimated concentrations to source terms, such as reactor coolant leakage rates.

The mathematical models to be developed in this paper will permit the calculation of the monitor response for any concentration time dependence, for any nuclide. These response models, in the form of a set of integrals, will then be solved for several example concentration behaviors, and analytical expressions will be provided for these solutions. Plots of the monitor responses will permit comparison of the three monitor types. The starting point for the development is the fixed-filter monitor, which is relatively straightforward, and the FF model is the starting point for the RW model. In turn, the RW model acts as a template for the CW model.

The development below treats the activity on the filter one nuclide at a time. In some applications, however, there will be multiple nuclides in the sampled air, and thus on the filter. When the activity is measured with a "gross" counting device such as a GM tube, treating the mixture as if it came from a single nuclide is not a very good assumption. One could imagine an "effective" nuclide, using a concentration-weighted average half-life, efficiency, etc. But of course this assumes that one knows the concentrations, in which case there would be little need to use a monitor.

For applications with multiple nuclides it is best to use high-resolution spectroscopy if at all practical. This permits treating the nuclides independently, and we can then apply the monitoring analysis herein to each nuclide, one at a time. If gross (nonspecific) measurements are made, we must assume that the activity is from a single, predominant nuclide. This is not as preposterous as one might think, at least in some power reactor applications. It is certainly possible, by the linear nature of these instruments, to superpose the solutions for several nuclides. But the interpretation of the resulting responses is very difficult, and to use them quantitatively is impossible (ambiguity). Therefore we will consider only one nuclide at a time.

Monitor Response Model Development

Fixed Filter

Introduction

The fixed-filter (FF) monitor is of course the simplest case, and there have been models in the literature for its response since at least the 1960's. The FF model is just a straightforward differential equation, based on consideration of the source and loss of activity on the collection medium (filter). This is for a single nuclide, which is the usual application for nuclear-facility monitoring. However, another important application is the monitoring of natural airborne radioactivity, commonly referred to as "radon-thoron" (RnTn), which involves a decay series. That is, there are multiple nuclides on the filter, and some of these nuclides have two sources- the sampled air, and the decay of a precursor on the filter. There are many papers in the literature which present analyses of a fixed-filter monitor for radon progeny monitoring; one excellent early example is [1].

Development

The dynamic response of a fixed-filter monitor for a single nuclide is governed by the linear, first-order, ordinary differential equation (ODE)

$$\frac{d\dot{C}}{dt} = \varepsilon k F_m \phi Q(t) - \lambda \dot{C}, \tag{1-1}$$

where: $\dot{C}$ =monitor countrate, cpm; ε=detector efficiency (including a gamma abundance if spectroscopy is used); k=conversion constant (2.832×10^4 cm^3/ft^3 times 2.22×10^6 dpm/μCi); F_m=monitor sampling flowrate, ft^3/min; ϕ=filter collection efficiency (possibly also incorporating a line-loss and/or anisokinetics fraction); $Q(t)$=time-dependent concentration of the nuclide in the sampled air, μCi/cc; λ=decay constant of collected activity, min^{-1}.

There are several ways to solve this familiar kind of ODE, but it will prove to be helpful to make use of the scalar convolution integral [2] to provide the FF countrate response model:

$$\dot{C}_{FF}(t) = \varepsilon k F_m \phi \exp(-\lambda t) \int_0^t Q(\tau) \exp(\lambda \tau) d\tau + \dot{C}_0 \exp(-\lambda t) \tag{1-2}$$

The initial condition here, and in all subsequent development, is taken to be zero, that is, a clean filter at time zero, so the last term in (2) vanishes. Time zero is when the concentration $Q(t)$ begins its transient. In this form of solution we are convolving the driving function (the dynamically-varying concentration in the sampled air) with the impulse response of the filter/monitor. This solution format will prove to be very useful in the subsequent development, and it also has a straightforward extension to the case of multiple, decay-chain nuclides, via linear-systems modeling and a matrix convolution.

Note that the monitor flowrate is taken to be constant over the interval of interest, usually a few hours. If this is not a reasonable assumption, then a time-dependent flowrate can be placed inside the integral, assuming that the form of the time-dependence is known (e.g., a linear or exponential ramp-down due to dust loading, although this is usually insignificant on a time scale of a few hours).

The fixed-filter response model (2) is of fundamental importance to the subsequent development.

Rectangular-Window Moving Filter

Introduction

In some applications a fixed-filter monitor will suffer from the buildup of dust, reducing the air flow. This means that the filter must be changed frequently. To remedy this, moving-filter monitors were developed. Typically there is a roll of filter paper or "tape" which advances slowly across a deposition window, through which air is drawn. This window is usually either rectangular or circular in shape, and this deposition area is viewed by a detector. The paper supply is sufficient to last about a month at a nominal filter speed of one inch per hour. Other speeds are of course possible; some monitors also permit the filter to be left fixed, then "stepped" or advanced, periodically, such as hourly or daily. Moving-filter monitors have been widely

used in nuclear facilities, even in situations where dust loading is not an issue at all, such as a prefiltered stack.

There is surprisingly little mathematical information in the literature on these monitors. It isn't clear how one would hope to interpret the dynamic, time-dependent countrate responses of a moving-filter monitor without some explicit mathematical relation between the input and the output of the unit. Of course, in some applications, monitors are used in a "hypothesis-testing" mode (is there an alarm condition or is there not), as opposed to an "estimation" mode (what is the concentration). In the former case, we still need to understand the monitor input/output relation in order to calculate detection limits and setpoints, although sometimes the latter is done just by setting the alarm at a level slightly above the background response.

Some definitions are needed before presenting examples of what material has been available on moving-filter monitors. First, we note a distinction between long-lived (LL) and short-lived (SL) activity. LL activity does not decay significantly during the period of study of the response, which is typically no more than several hours (although effluent applications can extend for days or even weeks). SL activity may decay significantly during the period of study. Second, an important parameter in moving-filter analysis is the "transit time" T. This is the time required for a differential-area element to traverse the entire length of the RW deposition window. For CW monitors the transit time is defined to be along the diameter of the window. For many monitors T is about two hours.

Three examples of material on moving-filter monitors are as follows:

a) An early paper [3] presented an intuitive argument for the response of a RW monitor, for the commonly-assumed case of a constant concentration of LL and SL activity. The RW countrate expressions given in [3] are correct for LL activity, but incorrect for SL activity (this will be discussed in the RW countrate solutions section). Both expressions apply only after the transit time T.

b) Another paper [4], written by authors affiliated with a monitor vendor, shows the correct RW countrate result for a constant concentration of LL activity for times less than T. The result for times after T is also correct. However, no derivation is provided; the expression is referenced to a private communication. Also, the limitation of LL activity is not explicitly stated, and the requirement for a constant concentration is not as clear as it might be. The fact that their monitor is RW is not stated, although it appears to be so in a photo. Without this caveat, one might conclude that the given expression could be used for any moving-filter monitor, including a CW.

c) A second monitor vendor supplied a countrate expression in their catalog. The expression is correct for times after T for a constant concentration of LL activity, assuming that their monitor was RW. This was not stated, and no derivation or reference was provided. Further, the limitation of LL activity was not stated, which is a serious oversight. Information from this vendor at a later date implied that their monitor was CW, in which case the earlier expression was incorrect.

The point of these examples is that there has not only been little, if any, mathematical analysis available for moving-filter monitors (RW or CW), but what information there *has* been, even from monitor vendors, would require extraordinary care in its use, and has sometimes been misleading at best, and incorrect at worst. The moving-filter countrate models to be developed below provide the necessary foundation for analysis of the response of these CPAMs, without the restrictive assumption of a constant concentration of LL activity.

Development

For the rectangular-window (RW) monitor, consider the sketch in Fig. 1-1. We have the collection medium moving from left to right at speed v, with a deposition area of length L and width w. Assume that this entire deposition area is viewed by the detector, which could, for example, be cylindrical with a diameter equal to the diagonal length of the rectangle. Importantly, we also assume that the deposition is uniform across the window.

The approach is to break this rectangular region down into differential areas, of length dx. Each of these areas is a vertical strip, moving from left to right with the filter speed v. Clearly, each strip entirely leaves the window at position $x=L$ and so there is no y-axis (vertical) dependence.

We assume that the monitor is observing background (perhaps including RnTn, depending on the application), when at some time zero, a concentration transient begins. That is, at time zero, we initiate a nonzero $Q(t)$ behavior. For both types of moving-filter monitors, we must note that there will be two classes of differential areas: those that are in the deposition window at time

zero, and those that are not yet in the window. This is an essential fact, needed to model the dynamic behavior of these monitors.

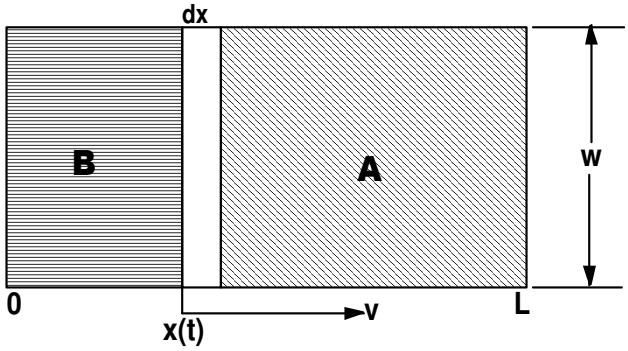

Figure 1. Rectangular window geometry sketch.

For the RW monitor we define the "key" strip to be that differential area at the leftmost position in the window at time zero. It will take this strip a time L/v to transit the window; hence this is T, the "transit time" for a RW monitor. Before this time T, the key element and all elements to its right were in the window at time zero (region A in Fig. 1-1), while those elements to its left were not (region B). The time-dependent countrate will be the sum of the contributions from these two regions, up to the transit time T. After this time the entire window is region B. Thus we will need separate solutions, for times before, and after, T. These solutions will be continuous across the time T.

The approach to modeling the dynamics of the RW monitor is to consider each differential strip to be a fixed filter, whose collection time depends on its initial position at time zero. That is, we apportion the source term (the incoming $Q(t)$ in the sampled air stream) equally across the strips, and integrate using the fixed-filter solution, (1-2). The key to this is that the strips have different integration limits. Next we consider these integrals for the two regions for times less than T, and then for times after T.

a) Region A, $t \le L/v$: A simple way to develop this part of the RW model is to consider the strips to the right of the key element to be a fixed-filter monitor of continuously-decreasing area. All these elements have the same limits of integration, since they have all been in the window, exposed to $Q(t)$, for the same length of time. Thus we can write

$$\dot{C}_{RW-A}(t) = \left(1-\frac{vt}{L}\right) \varepsilon k F_m \phi \exp(-\lambda t) \int_0^t Q(\tau)\exp(\lambda\tau)\, d\tau \tag{1-3}$$

which is the FF countrate solution (1-2) multiplied by a linearly-decreasing area-adjustment factor. At $t=L/v$, this factor is zero and the expression vanishes. Also note that if the filter speed v is zero, this reduces to the FF solution, as we would expect.

b) Region B, $t \le L/v$: Next we need to consider the elements to the left of the key strip. These have been in the deposition window varying lengths of time, depending on their current position, which can range from zero to some position x (not greater than L). In fact, an element at position x has been in the window for x/v units of time (minutes). Since t is the current time, we can write for this portion of the countrate

$$\dot{C}_{RW-B}(t) = \frac{\varepsilon k F_m \phi \exp(-\lambda t)}{L} \int_0^{vt} \int_{t-\frac{x}{v}}^{t} Q(\tau)\, \exp(\lambda\tau)\, d\tau\, dx \tag{1-4}$$

so that the inner (fixed-filter; convolution) integral is done over the time that the element has been in the window. The outer integral, over x, goes from the left side (0) to the current position of the key element, vt. Since this position must not be greater than L, this portion of the countrate model only applies for times less than T. Note that the inner integral will result in a function of x, which is then integrated across the x-limits of the outer integral. The division by L results from apportioning the source Q equally across all the strips (there is an implicit division, then a subsequent multiplication, by w).

The limit of this integral as the filter speed approaches zero is not as obvious as for the other region, but the lower limit of the inner integral will approach minus infinity. We define the response to be zero for negative times, since there is no source term then. So this integral would yield a nonzero result only for times greater than zero. The outer integral approaches zero to zero, which will yield zero. Hence the first portion, (1-3), will apply, and we have the FF result.

c) RW Countrate Model, $t \le L/v$: The result in (1-3), the decreasing-area fixed-filter countrate contribution, can also be obtained via a double integral similar to (1-4); adding this to (1-4) we can write the rectangular window countrate model for times before *T*:

$$\dot{C}_{RW}(t) = \frac{\varepsilon k F_m \phi \exp(-\lambda t)}{L} \left[\int_0^{vt} \int_{t-\frac{x}{v}}^{t} Q(\tau)\exp(\lambda\tau)\, d\tau\, dx + \int_{vt}^{L} \int_0^{t} Q(\tau)\exp(\lambda\tau)\, d\tau\, dx \right] \quad (1\text{-}5)$$

d) RW Countrate Model, $t \ge L/v$: Finally, we must consider what happens after the transit time *T*. Then, none of the elements in the window were there at time zero, and the entire window is region B. Hence we have another integral of the form of (1-4), with the upper limit of the outer integral now at *L,* that is, the full window length:

$$\dot{C}_{RW}(t) = \frac{\varepsilon k F_m \phi \exp(-\lambda t)}{L} \int_0^{L} \int_{t-\frac{x}{v}}^{t} Q(\tau)\exp(\lambda\tau)\, d\tau\, dx \quad (1\text{-}6)$$

Equations (1-5), (1-6) represent a completely general response model for the countrate of a rectangular-window moving filter monitor, for an input concentration of any time dependence and any half-life, at any time during the concentration transient. Once a form is specified for *Q(t)*, using, for example, one of the solutions developed via compartmental modeling, these integrations can be carried out and the monitor response predicted.

Circular-Window Moving Filter

Introduction

Most of the comments above, in the RW Introduction, also apply for the circular-window (CW) case. However, there was an interesting and detailed, if not so easy-to-find, paper published in 1967 which presented an analysis for CW monitors [5]. This paper, in French, was published in an IAEA book reporting the proceedings of an IAEA Symposium held in Vienna, Austria. The work is based primarily on an exponentially-decreasing concentration, and the mathematical treatment is comprehensive. However, while there are a number of specific solutions provided, there is not a general model for the countrate response for concentration dynamic variations of any arbitrary shape.

This is not as much of a limitation as it might appear. As will be discussed below, and in a later paper on concentration dynamics modeling, for a great many real-world nuclear facility monitoring applications the concentration time dependence can be expressed as linear combinations of exponentials. Since the monitors are linear instruments, we can superpose the solutions for the individual exponential terms to obtain the complete countrate response for a great many concentration behaviors. Baron [5] presents a set of solutions for the countrate, including the effects of an analog ratemeter time constant, for the exponentially-decreasing concentration.

In the same IAEA book there is another paper [6], also in French, which in passing presents expressions for the attained countrate at the transit time, for a constant, LL concentration, for both RW and CW moving filter monitors. There is no derivation nor reference for where these expressions came from, but they are correct. The CW result is the same as can be developed from the material in [5], and this same relation is also derived below. As mentioned in [6], for a given concentration, it is the case that, at time *t=T*, and with *L=2R* and the RW and CW filter speeds equal, the FF monitor will have twice the countrate of the RW, and $3\pi/4$ (2.36) times the CW countrate. This will be illustrated below, in plots comparing the responses of all three monitors to various concentration behaviors for LL and SL activities.

Another paper that presents a mathematical treatment of CW monitors is [7]. This paper is directed at constant concentrations of RnTn. The results are presented in an appendix containing a number of very complicated equations, involving integrals that cannot be evaluated in closed form. As a practical matter these results, while detailed and thorough, are not especially useful

for the typical nuclear facility monitoring application. There are no expressions given to relate the output of a CW monitor to its input, in a generalized and readily-usable way. This is what we will do, next.

Development

The geometry of the circular-window (CW) monitor is sketched in Fig 1-2. There are several ways to approach this analysis, and a typical way is to use circular arc segments [5]. The present setup is different, and is used so that the analytical mathematics will parallel a numerical simulation of monitor responses, to be discussed later.

The basic premise is to model the circular region with a series of horizontal strips, each of which represents a small rectangular-window moving filter. Each strip will contain differential "cells," or "elements," analogous to the vertical strips in the RW case. Since we already have the solution for the RW case, it should be relatively simple to extend this to the CW situation. A horizontal strip, with one cell highlighted, is illustrated in Fig. 1-2.

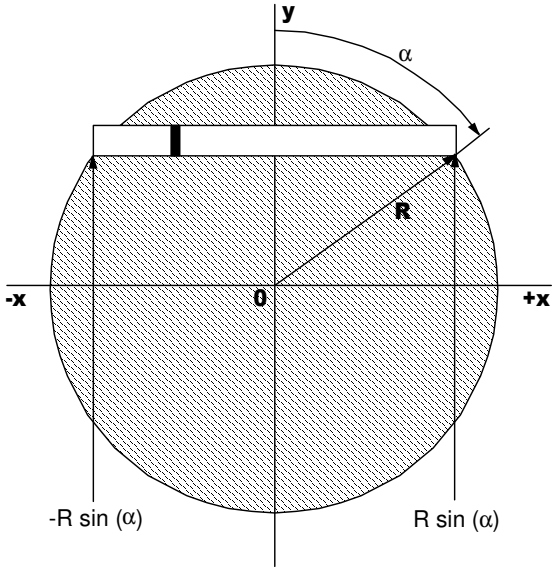

Figure 1-2. Circular window geometry sketch. A single rectangular strip, and one cell, is shown.

The coordinate system is Cartesian and is centered at the center of the circular deposition area, which is assumed to be viewed by a detector of the same diameter. Thus the *x*-coordinates range from *-R* to *R*, and the analysis takes the *y*-coordinate range to be *0* to *R*, or the top half of the deposition. The countrate result is of course doubled to get the final answer. The deposition is assumed to be constant across the window area.

The *y*-position of the bottom of each horizontal strip is defined using an angle α, measured clockwise from the positive *y*-axis. The *y*-coordinate of the strip bottom is $R\cos(\alpha)$ and the corresponding right-side *x*-coordinate is $R\sin(\alpha)$. Each strip will have a length of $2R\sin(\alpha)$, which is zero at the top of the circle and $2R$ at $\alpha=\pi/2$. An important variable is the *x*-coordinate of the left side of each strip, $-R\sin(\alpha)$, since this is the point at which new differential-area elements for that strip enter the window. Clearly the entry, and exit, times vary with the angle α.

With this geometry setup we have a small complication in that the cell sizes are not constant, if the angular steps are constant. The strips nearer the diameter will have larger cells than those near the top of the circle. Fig. 1-3 illustrates the cells in the window (this figure was generated by the numerical simulation). We need to allow for this size difference in allocating the input source term $Q(t)$ to the cells.

The differential area is $dA=dxdy$. Since $y(\alpha)=R\cos(\alpha)$ then $dy=-R\sin(\alpha)d\alpha$. We can drop the minus sign, since for the coordinate system in use, when α increases, *y* decreases. So the source allocation ratio becomes

$$\frac{dx\, R\sin(\alpha)\, d\alpha}{\pi R^2}, \tag{1-7}$$

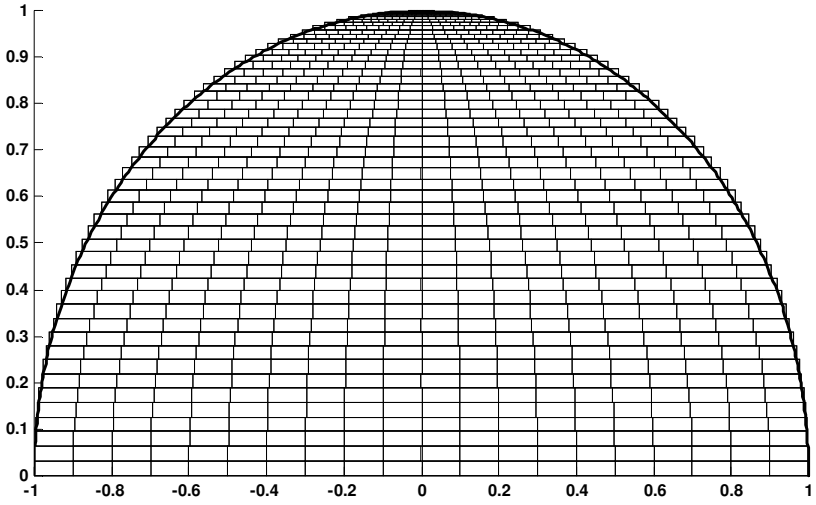

Figure 1-3. Circular window differential areas, showing their unequal size as a function of y-position.

and we will also need another factor of 2 in the numerator of the model to account for the fact that the region considered is only the top half of the window. Note that, in both Fig. 1-2 and Fig. 1-3, the rectangular strips "overhang" the end of the circle. In the mathematical limit, however, each cell has an infinitesimally small height and width and so this overhang vanishes. In the numerical simulation, this overhang cannot be ignored, since the number of strips and cells is finite, and so this small error is corrected in the calculations.

We can now proceed to develop the CW model; consider the diagram in Fig. 1-4. There are three regions in the deposition area at any time after time zero, and the relative proportion of the deposition area taken up by each region varies with time. At exactly time zero, the entire window is region A, which, as with the rectangular window, consists of the elements (cells in the horizontal strips) which were in the deposition window at time zero. At time $T=2R/v$, none of these elements is in the window, and there is no longer any region A.

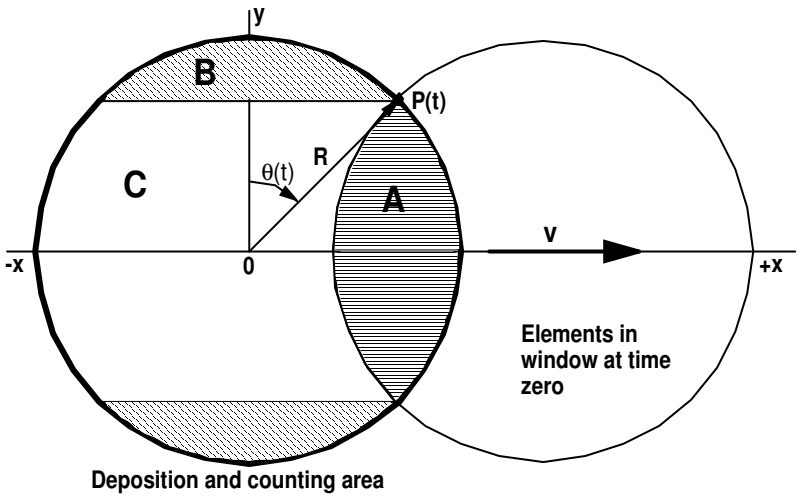

Figure 1-4. Illustration of regions of circular window.

Region B is comprised of horizontal strips whose elements have entered the deposition area after time zero and which have reached their individual transit times, given in (1-8) below. The lower boundary of region B is the horizontal strip whose rightmost cell is at position *P(t)*. The strips above this have already passed their transit time. At time *T* the entire window is region B.

There are horizontal strips with some elements that were not in the window at time zero, and some that were. These strips have not yet attained their respective transit times. This means that the key elements of these strips are still inside the deposition area. The elements to the right of these key elements comprise region A, while the elements to the left are region C. At time T, the key element of the longest horizontal strip (along the diameter) will have reached the right border of the deposition area, and so region C vanishes, as does A. All elements then are region B.

The point of intersection $P(t)$ of the moving and fixed circles starts at $x=0$, $y=R$ (the top) and moves down along the circle, to the right, until it reaches $x=R$, $y=0$ at time T. The angle, measured from the y-axis to the line connecting the point $P(t)$ to the center of the deposition area, is $\theta(t)$. This angle as a function of time, which is very important in defining the countrate model, is given in (1-9) below. (Note that the angle α used above is general, for any horizontal strip, while $\theta(t)$ is specifically for the point of intersection $P(t)$, which is at the end of one particular strip.)

The sketch in Fig. 1-5 may help clarify the geometry. The key element (the leftmost cell in each horizontal strip at time zero) for horizontal strips in region B (strips 1,2) is at or beyond the deposition area boundary, and thus no cells in these strips were in the window at time zero. The remaining horizontal strips (3,4) have not attained their respective transit times, and their key elements are still in the window. The portion of the strips to the left of the key element is included in region C, while the portion to the right is in region A.

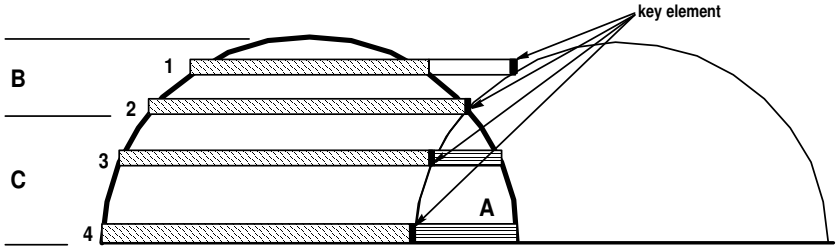

Figure 1-5. Sketch showing positions of key elements for circular window.

Region A of the filter will be, similarly to the RW case, effectively a fixed-filter of continuously-decreasing size. Thus we could look for a solution similar to that of a rectangular-window monitor for each horizontal strip common to regions A and C. But, since each strip has a different entry and exit point, unlike the RW case, we can expect to need another integral, to cover the angular variation. Thus the solutions will be triple, rather than double, integrals- one for time, one for the x-direction, and one for the angular direction (which is a surrogate for the y-direction). Since there are three regions for times less than $2R/v$, the countrate model will consist of the sum of three triple integrals (compared to the sum of two double integrals for the RW model).

Using the second term of (1-5) as a template, we recognize that the RW upper limit L will be replaced by $R\sin(\alpha)$ since this is the exit x-coordinate for each CW strip. Similarly, the RW lower limit vt is implicitly $0+vt$, since the RW strips all start at $x=0$. In the CW case the strips start at $x=-R\sin(\alpha)$, so that the lower limit of the second integral will be $-R\sin(\alpha)+vt$. This is the current x-position of the "key" cell, or element, in each horizontal strip. These key cells form the boundary between regions A and C.

Next we need to define the angular variation, for the limits of integration across angle. Clearly the upper limit is just $\pi/2$. The lower limit of the α integration is a bit more subtle. This is the value of α for the region defined by the fact that the per-strip transit time has been attained (region B). For any strip, we have the transit time

$$T_s = \frac{2R\sin(\alpha)}{v}. \tag{1-8}$$

As time progresses, the short strips at the top of the circle (α near 0) will reach T_s almost immediately, while at the diameter ($\alpha=\pi/2$) the transit time is the maximum, $2R/v$. The current value of the angle $\theta(t)$ where the transit time has just been attained, at point $P(t)$, the juncture of regions A, B, and C, is, solving (1-8) for α:

$$\theta(t) = \sin^{-1}\left(\frac{vt}{2R}\right). \tag{1-9}$$

To simplify the subsequent notation, define

$$\beta \equiv \frac{vt}{2R} = \frac{t}{T}.$$

Now we can develop the integrals for each of the regions.

a) Region A, $t \le 2R/v$: For this region we can write the first triple integral for the CW model, for the countrate due to the decreasing-fixed-filter portion:

$$\dot{C}_{CW-A}(t) = \frac{2\varepsilon k F_m \phi \exp(-\lambda t)}{\pi R^2} \int_{\theta(t)}^{\frac{\pi}{2}} \int_{-R\sin(\alpha)+vt}^{R\sin(\alpha)} \int_{0}^{t} Q(\tau)\exp(\lambda\tau)\, d\tau\, dx\, R\sin(\alpha)\, d\alpha \tag{1-10}$$

The innermost integral is as usual the FF convolution integral. Since all these elements were in the window at time zero, zero is the lower limit of this integration. This result is in turn integrated across x, the horizontal strips, from the left boundary of region A to the right side of the deposition area. The angle is then integrated from the current transit-time-attained angle, $\theta(t)$, corresponding to the current position of the intersection point $P(t)$, to $\pi/2$. These integral limits define the bounds of region A. The source term $Q(t)$ has been allocated using the differential area of (1-7). The factor of two, correcting for our use of only the top half of the window, has been applied.

b) Region B, $t \le 2R/v$: Next we consider the set of strips that have attained their transit times, in region B of the diagram above. The cells in these strips were not in the window at time zero, and so they each have had a different exposure to the source $Q(t)$. This is going to vary as a function of the angle, since the length of each strip depends on α. The distance moved by a cell will be its current x-position minus its starting coordinate (the left side of its strip), and the time required to move this far is of course just this distance divided by the filter speed. So the lower limit of the inner integral becomes

$$t - \frac{x + R\sin(\alpha)}{v} = \Phi.$$

The next integral, across x, will range across the full length of each of the horizontal strips in this region. The outer, angle, integral will range from the top of the circle ($\alpha=0$) down to the current angular position $\theta(t)$ where the transit time has been attained. With this we can write the second triple integral for the countrate, due to the elements in region B:

$$\dot{C}_{CW-B}(t) = \frac{2\varepsilon k F_m \phi \exp(-\lambda t)}{\pi R^2} \int_{0}^{\theta(t)} \int_{-R\sin(\alpha)}^{R\sin(\alpha)} \int_{\Phi}^{t} Q(\tau)\exp(\lambda\tau)\, d\tau\, dx\, R\sin(\alpha)\, d\alpha \tag{1-11}$$

c) Region C, $t \le 2R/v$: We now consider the cells that were not in the window at time zero, in the strips that have not yet attained their respective transit times. These are the cells to the left of the key cell in each strip, region C in the diagram. The inner-integral lower limit is again dependent on the current position (x and α) of the cell, since these cells all have different exposure times. The x-variation covers the range from the left side of the strip to the current position of the key strip (compare to the second integral for region A). The angular variation, the outer integral, covers the same range as the angle integral for region A (since this boundary serves both regions). Then we can write the third triple integral, for the countrate due to region C, as

$$\dot{C}_{CW-C}(t) = \frac{2\varepsilon k F_m \phi \exp(-\lambda t)}{\pi R^2} \int_{\theta(t)}^{\frac{\pi}{2}} \int_{-R\sin(\alpha)}^{-R\sin(\alpha)+vt} \int_{\Phi}^{t} Q(\tau)\exp(\lambda\tau)\, d\tau\, dx\, R\sin(\alpha)\, d\alpha \tag{1-12}$$

d) CW Countrate Model, $t \le 2R/v$: The final model consists of the sum of these three triple integrals, (1-10 to 1-12). This model is completely general, and applies for a single nuclide of any half-life or concentration time dependence. Consider the effect of taking the filter speed to zero in these equations. In (1-11) and (1-12) we again, as in the RW case, have the innermost integral ranging from minus infinity to t, while in (1-12) the second integral approaches zero to zero, and in (1-11) the outer integral approaches zero to zero. Thus these two components vanish, leaving (1-10), which will approach integration across the entire window, and we then will have the equivalent of (1-2), the FF response.

e) CW Countrate Model, $t \geq 2R/v$: We also need a model for $t>2R/v$. After this time, all the strips consist of cells that were not in the window at time zero. Thus we use (1-11), for region B, with a new upper limit on the angle integral, of $\pi/2$, covering the entire top half of the window. So the fourth triple integral, for the post-transit-time countrate response, is

$$\dot{C}_{CW}(t) = \frac{2\varepsilon k F_m \phi \exp(-\lambda t)}{\pi R^2} \int_0^{\frac{\pi}{2}} \int_{-R\sin(\alpha)}^{R\sin(\alpha)} \int_{\Phi}^{t} Q(\tau)\exp(\lambda\tau)\, d\tau\, dx\, R\sin(\alpha)\, d\alpha \tag{1-13}$$

Approximate Circular-Window Monitor Response

Observation of a large number of CW and RW response plots from the numerical simulation, for varied $Q(t)$ behaviors, led to speculation that the responses seemed to be keeping a more-or-less constant ratio to each other. Since the only difference between them is one of geometry, it seemed like there could be some way to obtain the more complex result (CW) from the simpler result (RW), by applying a correction factor.

The first naive approach to this was simply to equate the "equilibrium" responses to a constant concentration of long-lived activity. This leads to[1]

$$\varepsilon k F_m \phi Q_0 \frac{L}{2v} = \varepsilon k F_m \phi Q_0 \frac{8R}{3\pi v},$$

which we can solve for the RW window length

$$L = \frac{16R}{3\pi}. \tag{1-14}$$

The implication is that if we operate a RW monitor with this window length we will obtain (nearly) the same response as a CW monitor of radius R. Interestingly enough, this conjecture was supported by simulation runs. However, there is a more sophisticated way to derive this approximation.

Consider the fact that, for the CW monitor, there are as many transit times as there are horizontal strips in the window. The RW monitor of course has only one transit time, $T=L/v$. The length of each CW strip is $2R\sin(\alpha)$, and its y-position is $R\cos(\alpha)$, so that its differential height is $-R\sin(\alpha)$. Since the y-values decrease with increasing α, we can discard the minus sign to obtain the differential area of each horizontal strip

$$2R\sin(\alpha)\, R\sin(\alpha) = 2R^2 \sin^2(\alpha).$$

What we want is some effective or average transit time across the window. Since the areas of the strips vary with α, we should weight the individual strips by their contribution to the total countrate, which is proportional to their area. The transit time per strip is given by (8), and so we can write for the area-weighted transit time

$$T = \frac{\int_0^{\pi} \frac{2R\sin(\alpha)}{v}\left[2R^2\sin^2(\alpha)\right] d\alpha}{\int_0^{\pi} 2R^2 \sin^2(\alpha)\, d\alpha}, \tag{1-15}$$

which, when solved and equated to the RW $T=L/v$, will yield the same L as given in (1-14). This is an elegantly simple relation, which produces an excellent approximation to the CW response, especially when noise is added (as is usually the case). Using this approximation means that closed-form solutions (the RW solutions) can be obtained and used for CW analyses, with this adjustment to the RW window length. This can be very useful, and is in fact the default CW response generation method for the numerical simulation, since it saves a lot of execution time.

However, the geometry is, obviously, different between the monitors, so we would not expect the responses to be *exactly* the

[1] These response results will be developed below, (1-26) and (1-41).

same. Fig. 1-6 shows the fractional difference for the simple constant-concentration, long-lived activity case; the transit time is 120 min. The worst difference is less than 3% under most circumstances. The approximation fails, however, when we have a short burst of LL activity, as in Fig. 1-7 (although the approximation is reasonable for times less than about 75% of the transit time). Of course when it is important to have the best accuracy, or for the LL "puff" case, we would use the exact CW response calculations.

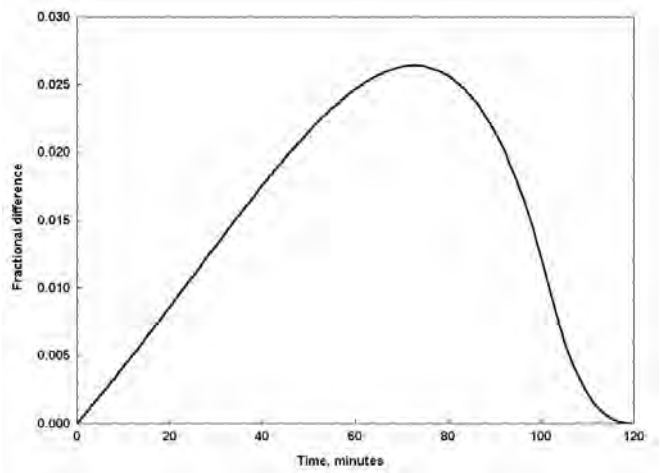

Figure 1-6. Fractional difference for CW approximation, constant-Q.

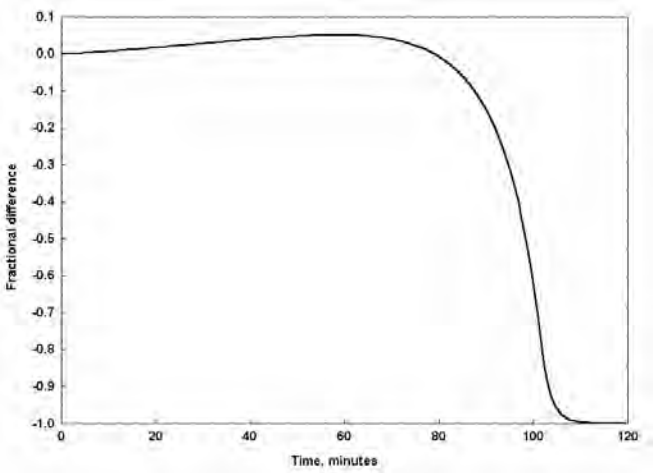

Figure 1-7. Fractional difference for CW approximation, short-burst Q(t), LL

Analytical and Numerical Monitor Response Solutions

Introduction

For any concentration time dependence $Q(t)$, we will need to develop five countrate solutions. There is one for the FF, and two each for the RW and CW (one before and one after the transit time). Since there are many possible $Q(t)$ behaviors, we require a way to condense this multitude of algebraically-messy solutions into a manageable number. Fortunately there is a way to do this, and the approach will have wide applicability.

As it happens, in the vast majority of monitoring applications, the $Q(t)$ behavior will result from the dynamics of a compartmental system. Such a system may be trivial, as in the commonly-assumed case of a well-mixed single compartment, or it may be very complex, with many mutually-exchanging compartments with multiple, time-varying sources, all under an HVAC flow, with filtration. The matrix-based formalism of compartmental modeling can readily handle all these situations.

It is the case that the $Q(t)$ behavior of a compartmental system can be expressed as a linear combination of exponentials [8]; in general, for p compartments:

$$Q(t) = \sum_{j=1}^{p} \Gamma_j \exp(\omega_j t) , \tag{1-16}$$

where the Γ represent coefficients derived from the eigenvectors of the compartmental matrix[2], and the ω represent the system eigenvalues [9]. Since for most problems of interest for monitoring applications the Γ are constants, we can find a solution for a single-exponential $Q(t)$ function, and then, making the appropriate substitutions, add together several of these solutions to get the overall monitor response, by the principle of superposition. This will save a great deal of tedious work.

We will consider two $Q(t)$ cases, for developing analytical solutions. One is the simple constant-Q case, which might occur

[2] The compartmental matrix contains the rate constants for the exchanges between the system compartments.

after a system has reached equilibrium. The other is a three-component exponential, with the sum of two exponentials defining a buildup to a *Q(t)* peak (which implies a decreasing source term); to this is added an initial concentration which simply decreases exponentially. This function provides great flexibility in modeling many practical *Q(t)* behaviors. For the constant-*Q* case we will have $p=1$; $\Gamma=Q_0$; $\omega=0$. For the three-component behavior, $p=3$, the Γ are nonzero constants, and the ω are negative constants.

Analytical solutions have been found for these *Q(t)* behaviors, for all five of the cases mentioned above. We will find the countrate solutions for the general "any-half-life" case, and then find a few selected LL solutions (of historical interest) by taking a limit as the decay constant approaches zero. The latter results have been compared to those derived directly, i.e., by using the LL case in the monitor response models (using zero for the decay constant), and they agree. The constant-*Q* case is covered by using a single exponential and taking its ω value to zero in the countrate expressions; these also can be shown to agree with the countrate solutions obtained using the respective models with a constant-*Q* directly.

Three-Component Exponential Q(t)

First we need to set up the appropriate factors for the three-component *Q(t)*. The form of this concentration behavior is

$$Q(t) = \frac{S}{r_2 - r_1}\left[\exp(-r_1 t) - \exp(-r_2 t)\right] + Q_0 \exp(-r_3 t) \tag{1-17}$$

where S is a source emission rate, including an implicit division by a free-air volume; r_1 is the source rate of decrease (which may be zero); r_2 is the loss rate from the system; Q_0 is the initial concentration, and r_3 is a separate loss rate, although usually in most physical systems r_2 and r_3 would be the same. These are kept separate here for more generality and ability to model various behaviors. This *Q(t)* expression results from the solution of a single compartment system driven by an exponentially-decreasing source, with a nonzero initial condition.

Clearly this *Q(t)* is the sum of three exponentials. For use in (1-16), these definitions are straightforward:

$$\Gamma_1 = \frac{S}{r_2 - r_1}; \quad \Gamma_2 = \frac{-S}{r_2 - r_1}; \quad \Gamma_3 = Q_0; \quad \omega_{1,2,3} = -r_{1,2,3}.$$

This is a useful, relatively general form for the concentration behavior. Given a countrate solution for this case, a number of other *Q(t)* cases follow easily, by appropriate substitutions. In the solutions below, if we have only the first subscript active, and all parameters with subscripts greater than one are defined to be zero, then we will obtain the single-exponential *Q(t)* countrate solution. Further, within the single-exponential case, if the rate constant ω_1 is zero then we have the constant-*Q* solution. So the three-component solution implicitly contains several others. Since the constant-*Q* solutions are of some historical interest, especially those for long-lived activity, we will write them out explicitly, for easy reference.

Analytical Fixed-Filter Countrate Response Solutions

Three-Component Exponential Q(t)

Using the FF model, (1-2), and substituting the *Q(t)* defined above, we find the FF countrate solution:

$$\dot{C}_{FF}(t) = \sum_{i=1}^{p} \varepsilon k F_m \phi \Gamma_i \frac{\exp(\omega_i t) - \exp(-\lambda t)}{\lambda + \omega_i}. \tag{1-18}$$

Constant-Q, General

In (1-18) if p is *1* and ω is zero, we have this familiar solution, using some $\Gamma = Q_0$, a constant:

$$\dot{C}_{FF}(t) = \varepsilon k F_m \phi Q_0 \frac{1 - \exp(-\lambda t)}{\lambda}. \tag{1-19}$$

Constant-Q, Long-Lived

If we take the limit of (1-19) as λ approaches zero (i.e., as the activity's half-life increases), we obtain the well-known LL, constant-Q solution

$$\dot{C}_{FF}(t) = \varepsilon k F_m \phi Q_0 t \,. \tag{1-20}$$

Note that we cannot just substitute zero for the decay constant, we must take a limit as it approaches zero. We can, however, return to the response model (1-2) and use zero for the decay constant there, and then carry out the integration. This is also the case for the RW and CW solutions.

Analytical Rectangular-Window Moving Filter Countrate Response Solutions

Three-Component Exponential Q(t), t ≤ L/v

Substituting the $Q(t)$ into the RW model, (1-5), and carrying out the integrations, we obtain the RW countrate for times less than the transit time L/v:

$$\dot{C}_{RW}(t) = \varepsilon k F_m \phi \sum_{i=1}^{p} \left\{ \frac{\Gamma_i}{(\lambda+\omega_i)^2} \frac{v}{L} \left[\begin{array}{c} \exp(\omega_i t)\cdot\{t(\lambda+\omega_i)-1\} \\ +\exp(-\lambda t) \end{array} \right] + \frac{\Gamma_i}{\lambda+\omega_i}\left(1-\frac{vt}{L}\right)\cdot\left[\exp(\omega_i t) - \exp(-\lambda t)\right] \right\} \tag{1-21}$$

Three-Component Exponential Q(t), t ≥ L/v

Using the RW model for times after the transit time, (1-6), we obtain the RW countrate

$$\dot{C}_{RW}(t) = \sum_{i=1}^{p} \frac{\varepsilon k F_m \phi \Gamma_i}{(\lambda+\omega_i)^2} \left\{ \exp(\omega_i t)\left(\lambda+\omega_i-\frac{v}{L}\right) + \frac{v}{L}\exp\left[\omega_i\left(t-\frac{L}{v}\right)-\frac{L}{v}\lambda\right] \right\} \tag{1-22}$$

Constant-Q, t ≤ L/v, General

Setting the parameters $p=1$ and $\omega=0$ in (1-21), we can obtain the constant-concentration (Q_0) countrate solution directly:

$$\dot{C}_{RW}(t) = \frac{\varepsilon k F_m \phi Q_0}{\lambda^2}\frac{v}{L}\left[\lambda t - 1 + \exp(-\lambda t)\right] + \frac{\varepsilon k F_m \phi Q_0}{\lambda}\left(1-\frac{vt}{L}\right)\left[1-\exp(-\lambda t)\right] \tag{1-23}$$

Constant-Q, t ≤ L/v, Long-Lived

If we take the limit of (1-23) as the half-life becomes long, we find

$$\dot{C}_{RW}(t) = \varepsilon k F_m \phi Q_0 \left(t - \frac{vt^2}{2L}\right). \tag{1-24}$$

This result has been seen in various places, e.g., [4], over the years, but, to my knowledge, without a published derivation.

Constant-Q, t ≥ L/v, General

For times after L/v, we again use $p=1$ and $\omega=0$, this time in (1-22), to obtain the constant countrate

$$\dot{C}_{RW}(t) = \varepsilon k F_m \phi Q_0 \left\{ \frac{1}{\lambda} - \frac{1}{\lambda^2 T}\left[1 - \exp(-\lambda T)\right] \right\} \tag{1-25}$$

As mentioned previously, an early paper [3] shows an expression for this case, namely[3]

$$\dot{C}_{RW}(t) = \varepsilon k F_m \phi Q_0 \left\{ \frac{1}{2\lambda}\left[1 - \exp(-\lambda T)\right] \right\},$$

[3] This is (15) from [3], recast using the notation of the present paper.

which is just one-half of the FF response for this case, (1-19). This is not appropriate for SL activity, since it does not properly account for the varying decay times of the differential elements in, and leaving, the window during the deposition period up to time *T*.

Constant-Q, t ≥ L/v, Long-Lived

Taking the limit of (1-25) as the decay constant approaches zero we obtain

$$\dot{C}_{RW}(t) = \varepsilon k F_m \phi Q_0 \frac{L}{2v}, \tag{1-26}$$

which is another result that has appeared in print over the years, without a mathematical derivation, e.g., [2], [6]. Also, the expression from [3], above, will, correctly, have this limit for LL activity.

Note that the RHS of (1-26) is a constant, and it is half of the FF response at the RW transit time *T*. Thus while the FF response continues to increase (LL activity), the RW response flattens out and becomes constant. This is a sort of "equilibrium" where the input to and loss from the window are in balance. The loss is of course due only to the filter movement, since by definition the LL activity, once deposited, remains on the filter for the duration of the analysis.

It is important to note that the RW solution is continuous at the transit time *T*. Substituting *L/v* for *t* in (1-23) will produce (1-25). Also, by inspection it can be seen that if the filter speed *v* is taken to zero in the $t < L/v$ solutions, we will obtain the corresponding FF solution. Thus, separate FF solutions are not even necessary for the various *Q(t)* behaviors since the RW (and CW) solutions contain them implicitly if we simply use a zero filter speed.

Analytical Circular-Window Moving Filter Countrate Response Solutions

It will be convenient to define a variable to stand for a nonelementary integral which arises in these solutions:

$$Z(a,b) = \int_0^a \exp\left[-\frac{b}{v} 2R \sin(\alpha)\right] R \sin(\alpha)\, d\alpha. \tag{1-27}$$

In the application of these response models this integral can of course be evaluated numerically; it occurs in the solution of the third and fourth triple integrals in the CW model, (1-12) and (1-13).

Three-Component Exponential Q(t), t ≤ 2R/v

Using the CW response model (1-10) to (1-12) we find the following solutions for the regions:

$$\Psi_1(t) = \sum_{i=1}^{p} \frac{\varepsilon k F_m \phi \Gamma_i}{\lambda + \omega_i} \left[\exp(\omega_i t) - \exp(-\lambda t)\right] \left\{1 - \frac{2}{\pi}\left[\beta\sqrt{1-\beta^2} + \sin^{-1}(\beta)\right]\right\} \tag{1-28}$$

Note that this is the continuously-decreasing 'fixed-filter' portion of the response (region A), with the trailing brackets a geometry factor which approaches zero as *t* approaches the transit time *T*. For region C we find

$$\Psi_2(t) = \sum_{i=1}^{p} \frac{2\varepsilon k F_m \phi \Gamma_i}{(\lambda+\omega_i)^2} \left\{\exp(-\lambda t) + \exp(\omega_i t)\left[(\lambda+\omega_i)t - 1\right]\right\} \frac{v}{\pi R}\sqrt{1-\beta^2} \tag{1-29}$$

For region B we have

$$\Psi_3(t) = \frac{2\varepsilon k F_m \phi \Gamma_i \exp(\omega_i t)}{\lambda+\omega_i} \frac{1}{\pi} \left\{ \begin{array}{l} \sin^{-1}(\beta) - \beta\sqrt{1-\beta^2} + \\ \frac{v}{R(\lambda+\omega_i)}\left[\frac{Z\left[\sin^{-1}(\beta),(\lambda+\omega_i)\right]}{R} + \sqrt{1-\beta^2} - 1\right] \end{array} \right\} \tag{1-30}$$

The monitor countrate is the sum of these three components,

$$\dot{C}_{CW}(t) = \sum_{j=1}^{3} \Psi_i(t) . \tag{1-31}$$

Note that if the filter speed v is taken to zero we obtain the FF response once again, as was the case with the RW countrate response.

Three-Component Exponential Q(t), t ≥ 2R/v

Using the CW response model (1-13) we find this countrate solution

$$\dot{C}_{CW}(t) = \varepsilon k F_m \phi \sum_{i=1}^{p} \frac{\Gamma_i \exp(\omega_i t)}{\lambda + \omega_i} \cdot \left\{ 1 - \frac{2v}{\pi R(\lambda + \omega_i)} + \frac{2v}{\pi R^2 (\lambda + \omega_i)} Z\left[\frac{\pi}{2}, (\lambda + \omega_i) \right] \right\} \tag{1-32}$$

Constant-Q, t ≤ 2R/v, General

With the usual substitutions into the three-component solution found above, we obtain for this case:

$$\Psi_1(t) = \frac{\varepsilon k F_m \phi Q_0}{\lambda} \left[1 - \exp(-\lambda t) \right] \left\{ 1 - \frac{2}{\pi} \left[\beta \sqrt{1-\beta^2} + \sin^{-1}(\beta) \right] \right\} \tag{1-33}$$

$$\Psi_2(t) = \frac{2\varepsilon k F_m \phi Q_0}{\lambda^2} \left[\lambda t - 1 + \exp(-\lambda t) \right] \frac{v}{\pi R} \sqrt{1-\beta^2} \tag{1-34}$$

$$\Psi_3(t) = \frac{2\varepsilon k F_m \phi Q_0}{\lambda} \frac{1}{\pi} \left\{ \sin^{-1}(\beta) - \beta \sqrt{1-\beta^2} + \frac{v}{\lambda R} \left[\frac{Z\left[\sin^{-1}(\beta), \lambda \right]}{R} + \sqrt{1-\beta^2} - 1 \right] \right\} \tag{1-35}$$

The CW countrate is the sum of these three contributions, i.e., (1-31).

Constant-Q, t ≥ 2R/v, General

The CW countrate response model for times after the transit time (1-13), gives

$$\dot{C}_{CW}(t) = \frac{\varepsilon k F_m \phi Q_0}{\lambda} \left[1 - \frac{2v}{\lambda \pi R} + \frac{2v}{\lambda \pi R^2} Z\left(\frac{\pi}{2}, \lambda \right) \right] \tag{1-36}$$

Baron [5] has, for this situation, the series approximation

$$\dot{C}_{CW}(t) \cong \varepsilon k F_m \phi Q_0 \frac{2R}{v} \frac{4}{3\pi} \left[1 - 0.2945 \lambda T + 0.0667 (\lambda T)^2 - 0.0123 (\lambda T)^3 \right] \tag{1-37}$$

if the product λT is less than 2, and

$$\dot{C}_{CW}(t) \cong \varepsilon k F_m \phi Q_0 \frac{2R}{v} \frac{0.4535}{\lambda T} \left\{ 1 + \left(1.205 - \frac{2}{\lambda T} \right) \left(1 - \frac{1}{\lambda T} \left[1 - \exp(-\lambda T) \right] \right) \right\} \tag{1-38}$$

otherwise. All three of these expressions agree very well for LL activity. The ratio of (1-38) to (1-36) as a function of half-life is shown in Fig. 1-8. The ratio happens to be worst near Rb-88 (18 min), which is a nuclide of considerable interest in CPAM applications. Nonetheless, the approximation is still acceptable, and (1-38) can be used as a convenient approximation for the attained countrate after the transit time for a constant concentration, for any half-life of practical interest in air monitoring. This avoids the need to evaluate the numerical integral Z in (1-36).

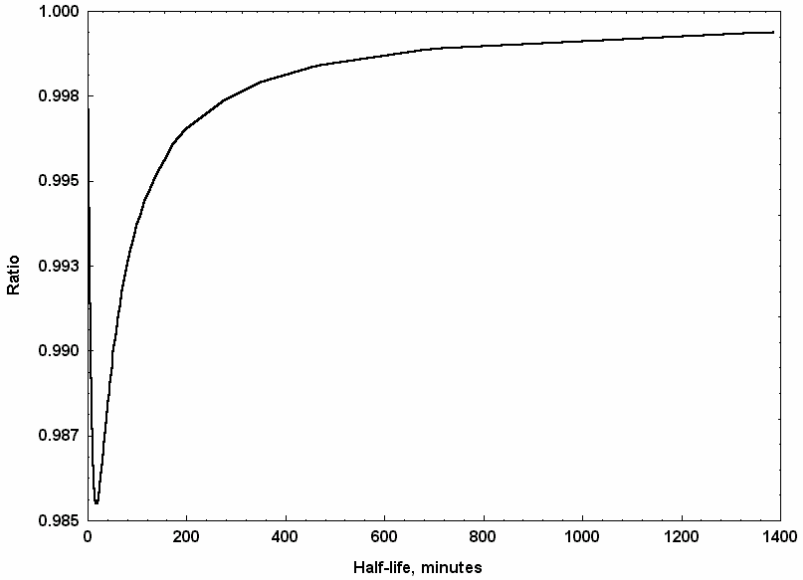

Figure 1-8. Ratio of Baron [5] approximation to (1-36) solution as a function of half-life.

Constant-Q, t ≤ 2R/v, Long-Lived

As usual, one way to find this solution is simply to take limits of the expressions above, as the decay constant λ approaches zero. Another method is to go back to the CW countrate response model (1-10) to (1-12) and substitute zero for λ, and carry out the integrations. As it happens this substitution greatly simplifies the work, since the exponential inside the triple integrals will vanish. And, very significantly, the nonelementary integral which arises from the third triple integral when λ is not near zero becomes tractable, and we can obtain a closed-form solution.

Carrying out these integrations, the result for this case for times less than *2R/v* is

$$\dot{C}_{CW}(t) = \varepsilon k F_m \phi Q_0 \left\{ t\left[1 - \frac{2}{\pi}\left(\beta\sqrt{1-\beta^2} + \sin^{-1}(\beta) \right) \right] + \frac{8R}{3\pi v}\left(1 - \sqrt{1-\beta^2} \right) + \frac{2vt^2}{3\pi R}\sqrt{1-\beta^2} \right\} \qquad (1\text{-}39)$$

This can also be written[4], a bit more simply, as [10]

$$\dot{C}_{CW}(t) = \frac{2\varepsilon k F_m \phi Q_0}{\pi}\left[\frac{4R}{3v}\left(1 - \sqrt{1-\beta^2} \right) - \frac{vt^2}{6R}\sqrt{1-\beta^2} + t \sin^{-1}\left(\sqrt{1-\beta^2} \right) \right] \qquad (1\text{-}40)$$

If we take the limit of (1-39) as the filter speed *v* approaches zero, we obtain the fixed-filter result for this case.

Constant-Q, t ≥ 2R/v, Long-Lived

The CW response model (1-13) produces a simple result for this particular situation:

$$\dot{C}_{CW}(t) = \varepsilon k F_m \phi Q_0 \frac{8R}{3\pi v}, \qquad (1\text{-}41)$$

which agrees with two references [5], [6]. Another way to obtain this result is to recognize that the countrate is continuous across the transit-time boundary, so that substituting *2R/v* for *t* (i.e., β=*1*) in (1-39) will yield this same result. This value is of course a constant, and the CW response flattens out and stays at this level as long as the constant concentration is active.

[4] This was developed independently, using a different approach for the CW geometry, similar to that used in [7].

Sample Analytical-Solution Plots

Figures 1-9 to 1-15 are some example plots of the analytical monitor countrates for a few typical *Q(t)* behaviors. These are, of course, deterministic responses, with no noise. The plots were generated using the expressions developed in the sections above. In fact they were produced by the most general form, the three-component exponential *Q(t)* solutions, since this case can handle the other cases by simple substitution of appropriate parameter values. The monitor setup for these runs was: flowrate, 5 ft^3/min; detection efficiency, 0.25; filter collection efficiency, 0.90.

Constant-Q, LL

This is the simplest case, shown in Fig. 1-9. Note that the countrate responses are nearly identical in the first 10-15 minutes or so, since in this time the moving filters have not moved very much (typical speed is 1 inch/hour, typical deposition window length is 2 inches). The moving filters flatten out and remain constant after the transit time- the RW at 0.5 times the FF countrate at $t=T$, while the CW is at 0.424 ($4/3\pi$) times the FF level. This moving-filter "equilibrium" is of course due only to the loss of activity due to the filter movement.

Constant-Q, SL

The isotope used in Fig. 1-10 is Rb-88, half-life 18 minutes. Here the countrates all reach an equilibrium, the FF due only to the decay, while the moving filters lose countrate due both to decay and the filter movement. Again note that the initial countrates are nearly identical, for the same reason as above (and as they are for any concentration behavior).

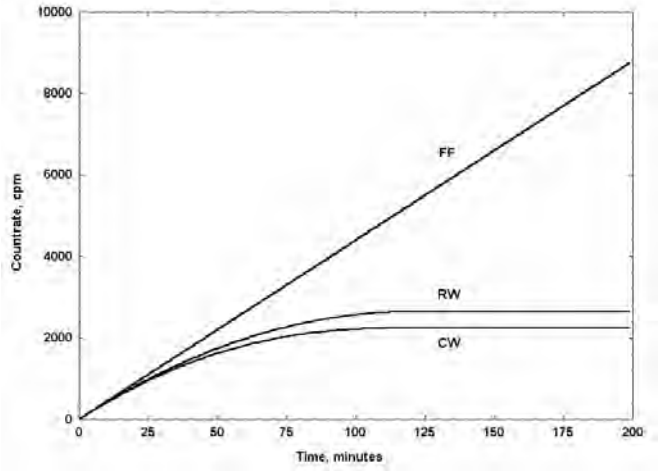

Figure 1-9. Countrate responses, constant-Q, LL activity. Detection efficiency, 0.2; flowrate, 5 cfm; collection efficiency, 0.7; concentration, 10^{-9} μCi/cc; L, 2 inches; R, 1 inch; v, 1 inch/hour; transit time, 120 minutes.

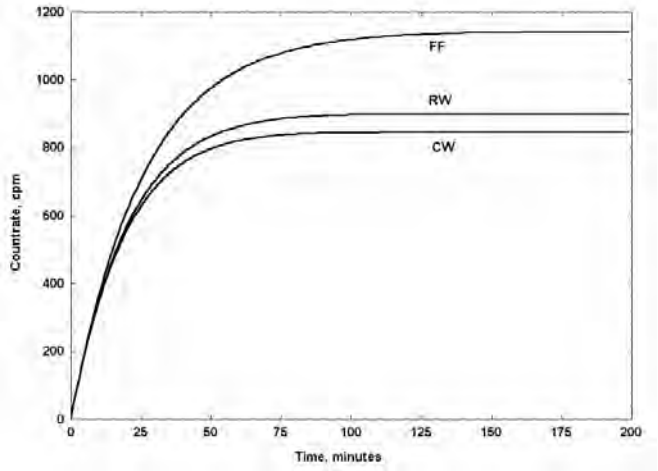

Figure 1-10. Countrate responses, constant-Q, SL activity (Rb-88). All parameters are the same as Fig. 1-9.

Single-Exponential Decrease, LL

Fig. 1-11 exhibits what appears to be an equilibrium for the FF countrate response. However, what has happened is that the source *Q(t)* has vanished and the countrate on the FF becomes constant, since the activity is long-lived. For a fixed-filter monitor viewing LL activity the countrate cannot decrease. It will either increase or stay (essentially) constant. Clearly, examining the FF response here and for the case above, one would be hard-pressed to tell which was happening- a short burst of LL activity or a continuing source of SL activity. Here is where the moving filters have an advantage. If one can wait long enough, (i.e., about two hours) they will clear the LL activity and return to background, if the source has vanished. In the case above, the source is constant, so the moving-filter responses stay up. In Fig. 1-11 the FF will in effect have a background of some 9000 cpm, rendering it useless for detection of subsequent, especially lower-level, activity transients. The only solution is to change the filter.

Single-Exponential Decrease, SL

In Fig. 1-12 the FF response does drop back down, indicating that the activity must be short-lived, and that the concentration transient is finished. Again the isotope is Rb-88. In this situation there is not much to choose between the three monitors- their responses are very similar.

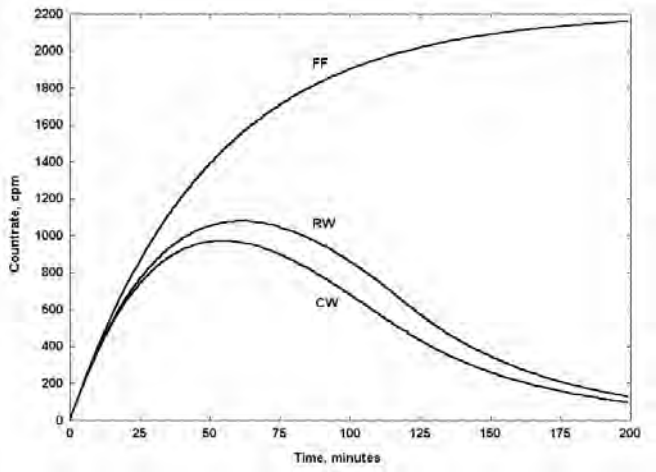

Figure 1-11. Countrate responses, exponential-decrease Q(t), LL activity. Same parameters as Fig. 1-9 except for exponential-decrease rate constant of 0.02 min^{-1}.

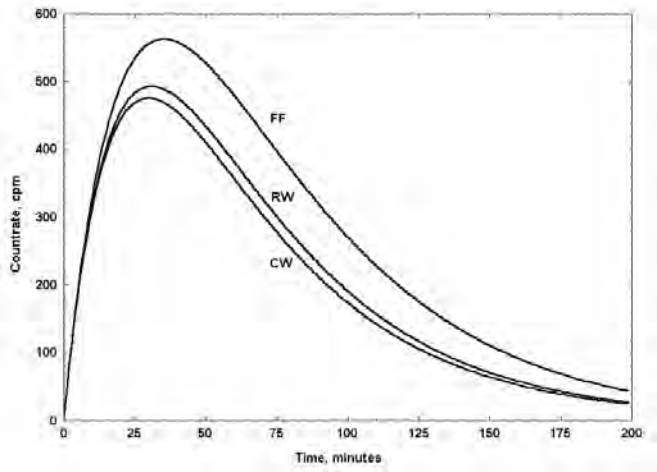

Figure 1-12. Countrate responses, exponential-decrease Q(t), SL activity (Rb-88). Same parameters as Fig.1-11.

Three-Component Exponential, LL

Fig. 1-13 shows an example of a three-component *Q(t)* behavior. This is a situation where the initial concentration is small (but not zero) and the concentration increases for some time, then begins to decrease. This is not an uncommon *Q(t)* behavior in the real world. In Fig. 14 we have the countrate responses to this *Q(t)*. Note the initial slope for all three monitors is near zero. This S-shape response is diagnostic of a peaked-shape *Q(t)*, although with noise it can be difficult to see.

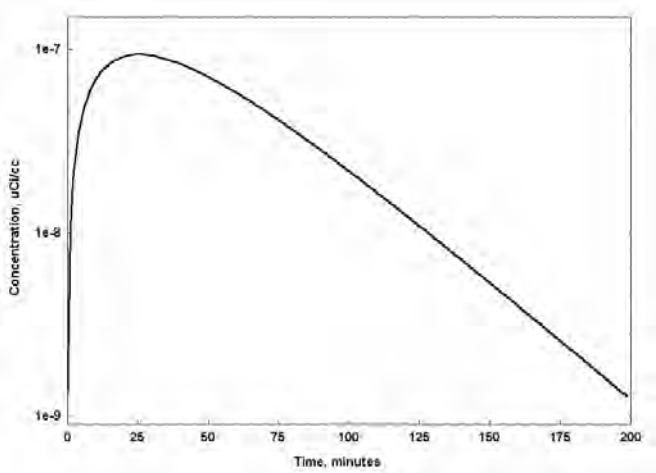

Figure 1-13. Three-component exponential Q(t) vs. time; S, 10^{-8} μCi/cc-min; r_1, 0.03 min^{-1}; r_2, 0.05 min^{-1} ; r_3, 0.02 min^{-1} ; initial concentration, 10^{-9} μCi/cc.

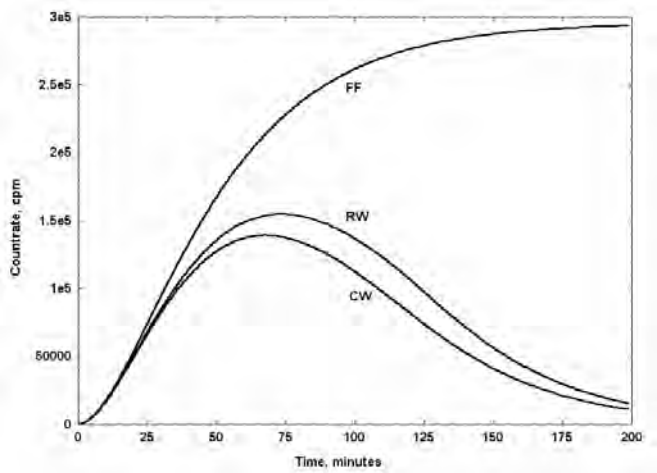

Figure 1-14. Countrate responses, three-component exponential Q(t), LL activity; Q(t) parameters as in Fig. 1-13, monitor parameters as in Fig. 1-9.

Three-Component Exponential, SL

For the same *Q(t)* behavior, for SL (Rb-88) activity we have the countrates shown in Fig. 1-15. Note the difference in vertical scale from Fig. 1-14.

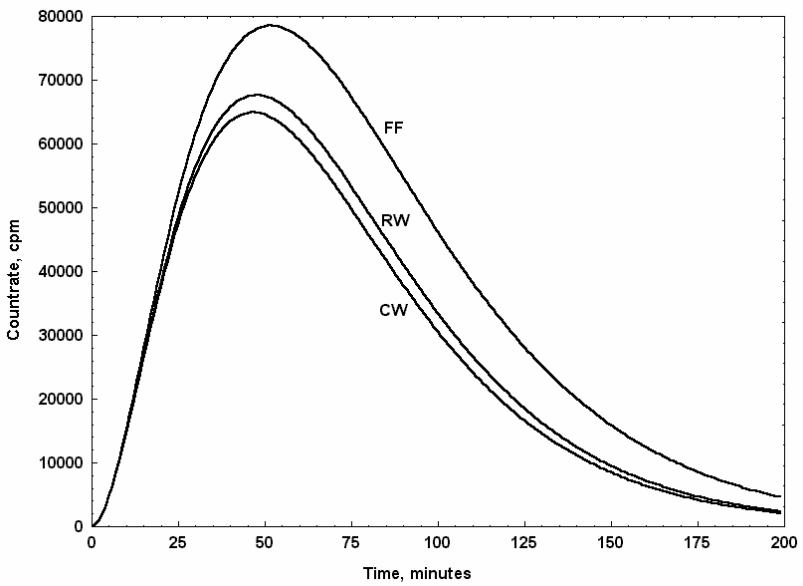

Figure 1-15. Countrate responses, three-component exponential Q(t), SL activity (Rb-88); parameters as in Fig. 1-13 and Fig.1- 9.

Countrate Components

Finally, we will plot the contributions from the regions of the moving-filter monitors. The moving-filter responses above are of course the sums of these "regional" contributions. Fig. 1-16 shows the rectangular-window response for the three-component exponential *Q(t)* for SL activity (Rb-88). The curve RW-A is the countrate due to the portion of the filter to the right of the key element, i.e., the decreasing-FF region. The curve RW-B is the countrate due to the region to the left of the key element. After time *T* (120 min), all of the response is due to elements that were not in the window at time zero.

In Fig. 1-17 we have the response of the circular-window monitor to the same *Q(t)*. Curve CW-A is the countrate from the decreasing-FF region, to the right of the key cells in the strips, which becomes zero at the transit time *T*. Curve CW-C is the countrate from the cells to the left of the key cells in the strips, which also will have all left the window by time *T*. Curve CW-B is the countrate from the strips at the top of the window, all of whose cells were not in the window at time zero. This region becomes the entire response after the transit time *T* (*2R/v*), again 120 min. Recall that, at the start of the transient, region A is the entire window, so the contributions from B and C are small at the start.

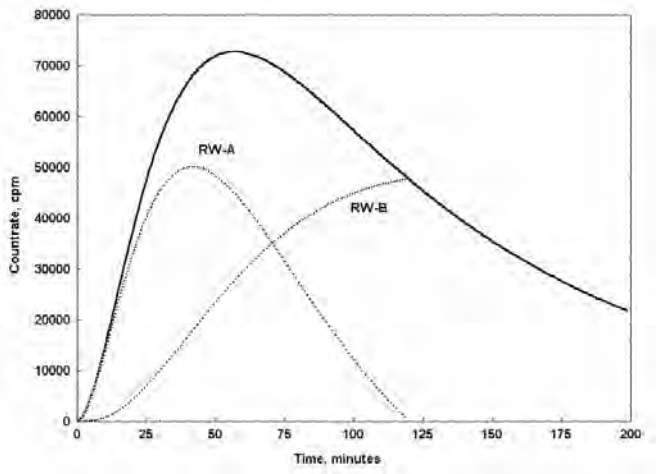

Figure 1-16. Countrate components, RW, three-component exponential Q(t), SL activity (Rb-88). S, 10^{-8} μCi/cc-min; r_1, 0.01 min^{-1}; r_2, 0.08 min^{-1} ; r_3, 0.01 min^{-1} ; initial concentration, 10^{-9} μCi/cc. Monitor parameters as in Fig. 1-9.

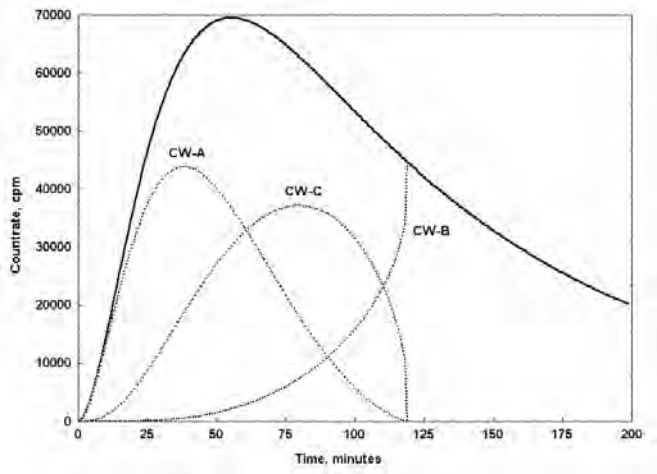

Figure 1-17. Countrate components, CW, three-component exponential Q(t), SL activity (Rb-88). Same parameters as in Fig. 1-16.

Numerical Response Solutions

Introduction

An interactive, GUI-driven program has been developed to allow the exploration of CPAM responses to various concentration time-dependencies. The solutions for the monitor responses are generated numerically, rather than via the use of deterministic solutions. This permits the exploration of more general *Q(t)* behaviors without the need to solve the monitor response models for each *Q(t)* and then code the resulting analytical solution. The numerical solutions also act as a check of the analytical monitor response solutions for a few selected *Q(t)* cases, whose solutions have been derived. The numerical solutions start from "first principles" and do not explicitly use any monitor response model. All three monitor types discussed in this paper are implemented: fixed-filter (FF); rectangular-window moving filter (RW); circular-window moving filter (CW).

The numerical solutions for the monitor countrates can have Poisson-distributed noise added to them, for additional realism. Background is added, and there is an option to have RnTn on the filter also. RnTn is modeled using linear-systems matrix methods, and has three-component decay chains for both Rn and Tn. The RnTn can be in equilibrium on the filter or not; the air concentrations of all components are assumed constant over the analysis interval.

Many parameters are interactively adjustable, using sliders on the GUI. A set of *Q(t)* behaviors is available, selected by GUI radio buttons. The *Q(t)* data for the run is generated numerically, including a complicated numerical solution using linear-systems matrix methods for a containment monitoring application, with HVAC. The monitor countrate responses are found by solving a large set of differential equations, numerically, where the ODE source term is provided at each time step by the *Q(t)* generator.

The solutions are generated for a long-lived, or short-lived (Rb-88), isotope. There is an option to combine these, that is, to have both present at the same time. The monitor countrate can be processed using an adaptive exponentially-weighted moving average (EWMA) [11], or a fixed-gain EWMA (simulating an analog ratemeter), or this processing can be bypassed, yielding the raw countrate data. A number of plots are generated by the simulation, including the countrates for all monitors (on the same plot), concentration estimates, and release estimates. These are all dynamic, that is, they are generated for each time step as they would be in a real monitoring application.

The RW module begins by breaking up the window into a set of elements, i.e., vertical strips, typically 100. The initial position of each strip is found, across the window length *L*.

The source term is allocated equally across the strips via a simple ratio, which is just the reciprocal of the number of strips. Recall that the approach is to model the RW as a set of small fixed-filter monitors. Thus each vertical strip is a FF monitor, which is exposed to the source term (the sampled air) for a different length of time.

The key to the moving-filter numerical models is in keeping track of which strips (or "cells" for the CW) are in the window at any time. Those elements in the window at any time step have their *Q(t)* and RnTn activities integrated as if they were small fixed-filter monitors. Next, all the elements are advanced one step to the right, by the distance $v\Delta t$, where Δt is the digital time-step[5] size (e.g., 5 seconds) and v is the filter speed. If an element has left the window at the right ($x \geq L$), it is "moved back" to the left boundary ($x=0$) and all of its integrations are reset to zero. The RW countrate at any time is just the sum of the per-strip countrates.

The CW module also begins by breaking down the window into a set of elements, or "cells." As was discussed in the analytical response models section, the cells are created within horizontal strips which are defined by an angle. Typically 200 angle steps are used to define 200 horizontal strips, and 20 cells are defined in each strip. The initial positions in x and y of all cells are defined, as is the left boundary as a function of y (since this is not constant, unlike the RW case). The RnTn is set up for each cell in the window, as for the other monitors. This time, however, we have many more "little fixed-filter monitors" to keep track of. Nonetheless the principles are the same.

The source term is allocated to the cells; this is a bit more complicated than the RW case since the CW cell sizes are not constant. As was shown in Fig. 1-3, the horizontal strips nearer the x-axis are taller than the ones nearer the top of the circle ($y=R$). Also, since there is a finite number of cells, a small correction is made to account for the "overhang" of the cells at the

[5] This is the time during which a digital monitor accumulates count data from the detector (sampling interval). This raw data is processed into a countrate estimate, using, for example, the algorithm in [11].

left and right end of each horizontal strip.

The cell activities are integrated at each time step, both the activity from *Q(t)* and RnTn, if enabled. Again the idea is to keep track of which cells are still in the window, contributing counts and being exposed to the source term. The cells are advanced to the right, just as was done for the RW, at each time step. The way the bookkeeping is implemented is to find the norm, or Euclidean distance, from the center of the window, of all cells. Those cells whose norm exceeds *R*, the window radius, at any time step have exited the window (at the right). They are moved back to the appropriate starting point at the left side of the window (which differs for each horizontal strip), and their integrations are reset. The total CW countrate at any time is the sum of all the per-cell countrates. The rest of the processing is the same as for the RW.

This program has been used to generate countrate responses for comparison to the analytical solutions developed above, for a variety of *Q(t)* behaviors, for LL and SL activity. In all cases the agreement is excellent. One example will be presented below.

Filter Isoactivity Contour Plots

Since the numerical simulation keeps track of the activities in the differential elements ("strips" for RW, "cells" for CW), it is possible to analyze these to find contours of constant activity. This can lead to some insight into how the activity builds up on the filter as it moves. Recall that we assume a uniform deposition of particulates across the window area, at all times. The activity will build up in proportion to the length of time each differential area is in the window, so that we end up with variations in activity across the window. Since the detector response is not position-dependent, a given amount of deposited activity could be in one small portion of the deposition window, or it could be evenly spread out, and the countrate would be the same in either case.

Fig. 1-18 is a graphic showing contours of constant activity for both RW and CW. Note how the activity levels are similar across both deposition areas. The CW contours look like a "bent" version of the RW contours. This is because the horizontal strips near the top of the CW deposition area reach their transit times faster than the strips nearer the main diameter.

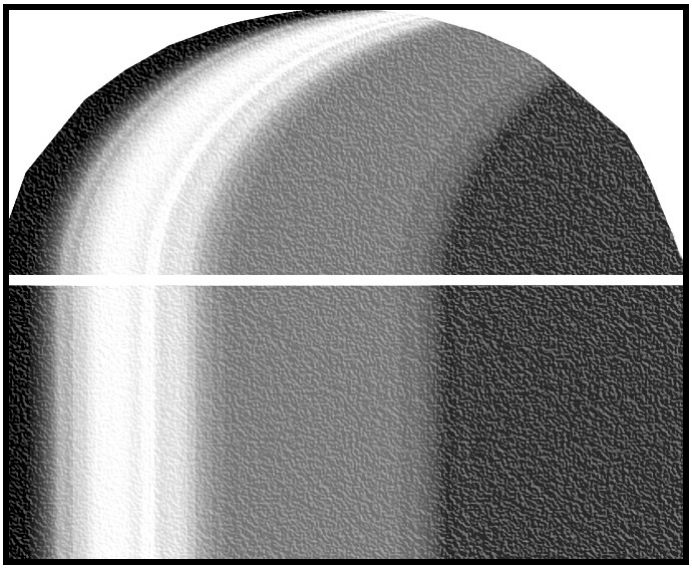

Figure 1-18. Isoactivity contours, RW (bottom), CW (top).

Numerical/Analytical Response Comparisons

Fig. 1-19 shows the numerical and analytical responses for a constant concentration of Rb-88, with no noise added. The dotted lines are the components of the analytical response, from the two regions of the filter. The transit time is 120 minutes. The numerical and analytical results are so close at this resolution that they appear to be identical. Fig. 1-20 is an expanded view. Now we can see the variations in the numerical response as the individual filter strips leave the window. This variation ranges over about 20 cpm out of 2200, or about one percent (there are 100 strips). When Poisson noise is added, this variation is not noticeable at all.

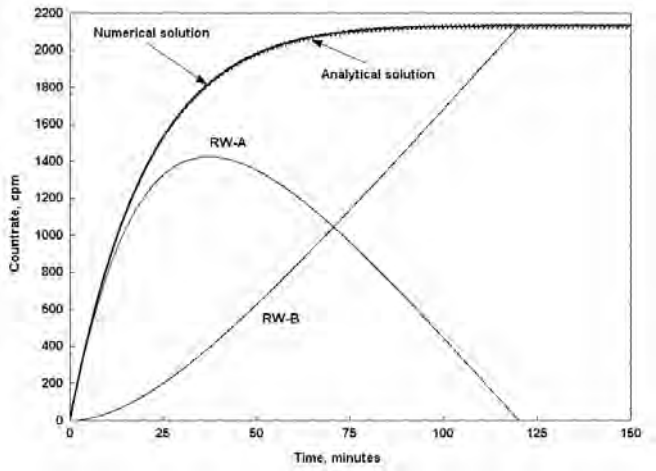

Figure 1-19. Analytical and numerical countrates, RW, constant-Q, SL activity (Rb-88), with components. Detection efficiency, 0.15; flowrate, 5 cfm; collection efficiency, 0.7; concentration, $3.2x10^{-9}$ μCi/cc; L, 2 inches; v, 1 inch/hour.

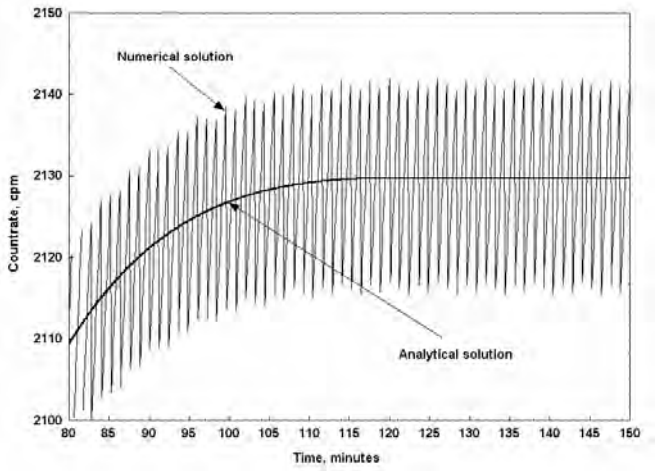

Figure 1-20. Analytical and numerical countrates, RW, constant-Q, SL activity (Rb-88), expanded view.

Fig. 1-21 shows the "exact" (as opposed to approximate) numerical CW response, and the analytical response, with no noise added. This is, again, a constant concentration of Rb-88. The dotted lines are the contributions from the three regions of the filter. The transit time is 120 minutes. As with the RW, the responses appear to be identical at this resolution In Fig. 1-22 we have an expanded view, which now shows the variations in the numerical response as the cells exit the window. Again this variation is about one percent, and is of no concern by the time Poisson noise is added.

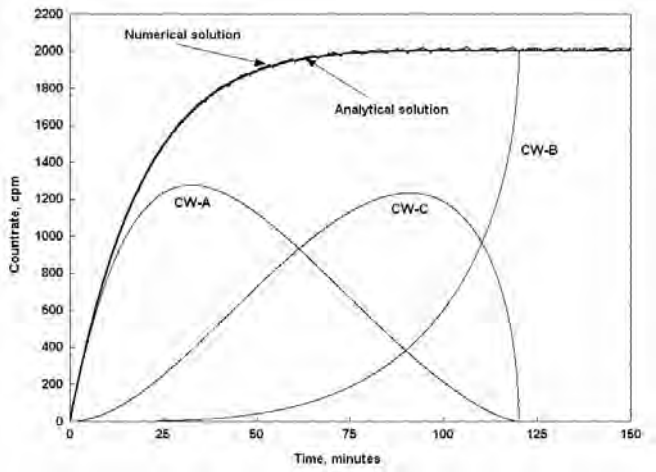

Figure 1-21. Analytical and numerical countrates, CW, constant-Q, SL activity (Rb-88), with components. Same parameters as Fig. 1-19; R, 1 inch.

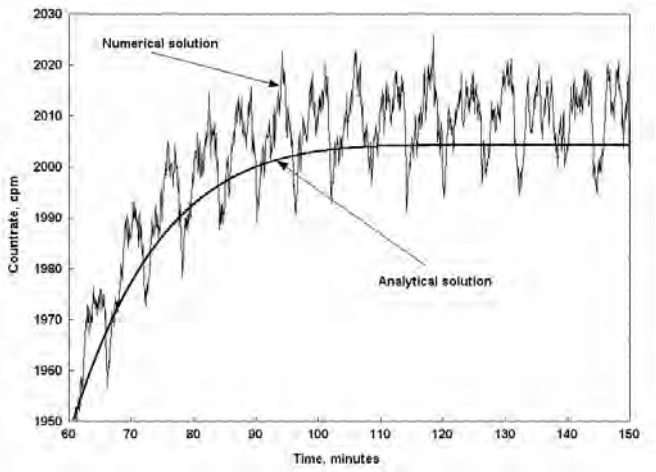

Figure 1-22. Analytical and numerical countrates, CW, constant-Q, SL activity (Rb-88), expanded view.

Analytical Moving-Filter Response Time

A major standard that relates to CPAM quantitative methods is ANSI N42.18-1980 [12], reaffirmed in March 1991. This standard has been around since the mid-1970s (under the designation ANSI N13.10-1974). It is cited in several regulatory documents, for example Regulatory Guide 8.37 [13], which states in section 3.1 that "Effluent monitoring systems should be designed in accordance with" this standard.

An interesting requirement in this standard is in paragraph 5.3.1.7, which says: "For moving filter particulate monitors, a curve of activity buildup versus time should be stated. The buildup coordinate should be expressed in percentages from 0 to 100 percent for the system response to nuclides in equilibrium deposited on the filter." Apparently the intent of this is to show how the monitor responds, as a function of time. We have the mathematical tools to do this, via the countrate response models developed above, although all the standard requires is for a "curve" to be "stated."

Presumably the concentration is to be held constant, and the time period is measured from a clean initial condition, up to the transit time of the moving-filter monitor, although this is not specified. It is not clear what "nuclides in equilibrium" means in this context, since we usually deal with the response to one nuclide at a time. We also usually do not work with the activity on the filter, but rather with the observable quantity, the monitor's countrate, although these are of course proportional. The response curve is to be normalized to the limiting value attained by these monitors when the concentration is constant, namely, (1-25) for RW and (1-36) for CW.

We can provide a completely general response-time function to satisfy this requirement, for both RW and CW monitors. For RW we have the response ratio consisting of (1-23) divided by (1-25). For CW we have a similar, but considerably more complicated, expression, consisting of the sum of (1-33), (1-34), and (1-35), divided by (1-36). If we plot these fractional responses as a function of a normalized time, namely the fraction of the transit time t/T, we find the curves shown in Fig. 1-23. In the figure, the lower two curves are for long-lived activity (the half-life was not specified in the standard), and the upper two curves are for a short-lived nuclide, Rb-88. The solid lines are for the RW monitor and the dotted lines are the CW monitor.

These equations and the resulting curves will be applicable to any RW or CW monitor; simply multiply the time axis by the appropriate transit time, and we will have satisfied this requirement from this standard, for any long-lived nuclide or for Rb-88. If other nuclides are of interest, return to the equations cited, and re-evaluate them using the appropriate decay constants.

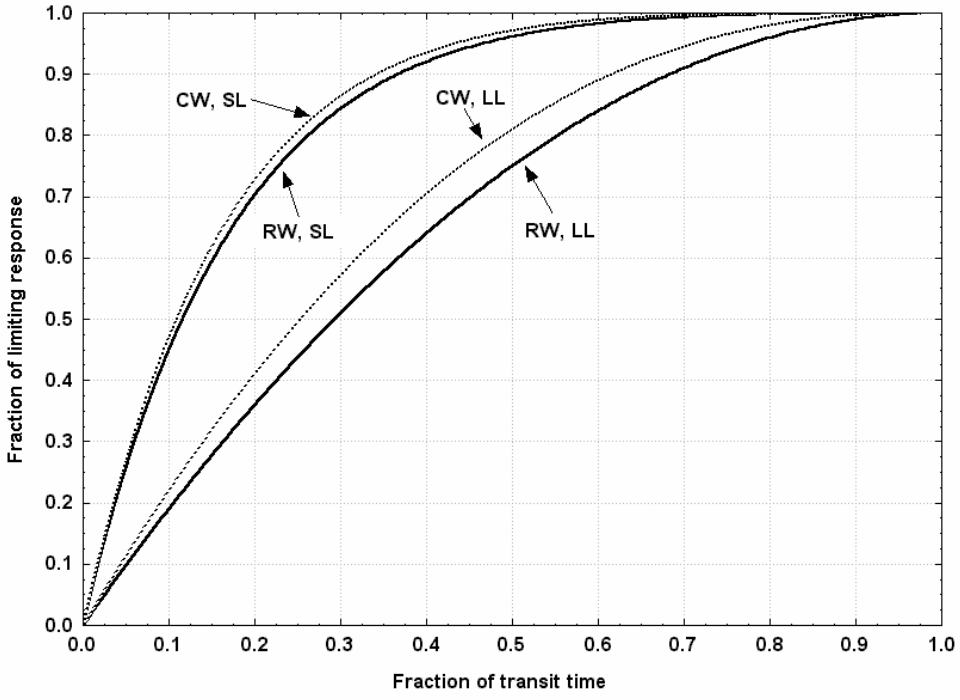

Figure 1-23. Normalized response time for moving-filter monitors.

Conclusions

In this paper we have developed mathematical models for the dynamic responses of FF, RW, and CW monitors. These models provide a way to predict the output of a monitor (countrate), given a mathematical description of its input (concentration time-dependence). No restrictions are applied to the concentration behavior, nor to the half-life of the monitored nuclide. We found that the FF response model is a single integral, in fact it is the well-known scalar convolution integral. The RW response model is the sum of two double integrals for times less than the transit time *T*, and a single double integral for times after *T*.

The CW response model is the sum of three triple integrals for times less than *T*, and a single triple integral for times after *T*. In the general case (no restriction on half-life), one of the CW triples leads to an integral which cannot be evaluated in closed form, and so countrate predictions must be found numerically. As a practical matter, however, this is not much of a limitation, since most implementations of these models would be done numerically. The RW model is considerably simpler to use than is the CW response model. We found an approximation which allows the use of the RW model to predict CW responses, for many practical applications (it does, of course, have some limitations).

We also found analytical solutions for the countrate responses for a few selected concentration behaviors. These solutions are quite general, and can readily be extended to apply to a variety of other concentration behaviors, by appropriate parameter substitution, and by superposition of solutions, as needed, for more complicated concentration behaviors. We also compared the responses of the three monitor types to several concentration behaviors, using plots.

A numerical simulation has been developed, starting from first principles. That is, it starts at the individual differential areas on the moving filters, and solves the resulting ODE sets, numerically. This simulation does not use the analytical solutions in any way. We have shown via plots that the numerical simulation agrees with the analytical solution for a selected case (constant concentration of Rb-88), for both RW and CW monitors.

The work reported here provides a solid foundation for the analysis of CPAM applications in nuclear facilities, showing how the output of a CPAM can be predicted from its input. A planned future paper will address the "inverse" problem, that of estimating the concentration (input) given the observed countrate (output). Another future paper will develop mathematical models, using linear-systems techniques, for calculating the concentration dynamics for systems commonly encountered in nuclear facility air monitoring, including the effects of HVAC. This mathematics is helpful in relating CPAM-estimated concentrations to source terms, such as reactor coolant leakage rates.

References

[1] R. D. Evans, "Engineer's Guide to the Elementary Behavior of Radon Daughters," *Health Physics,* vol. 17, pp. 229-252, 1969.

[2] W. J. Palm III, *Modeling, Analysis, and Control of Dynamic Systems.* New York:Wiley, 1983, p. 178.

[3] G. L. Helgeson, "Determination of Concentrations of Airborne Radioactivity," *Health Physics,* vol. 9, pp. 931-942, 1963.

[4] G. L. Bleher and D. J. Holloway, "Selection of Monitors for Airborne Particulate Radioactivity," presented at 19th Annual Meeting, American Nuclear Society, 1973.

[5] H. Baron, "Response Dynamique D'Un Appariel De Detection Des Aerosols Radioactifs," *Assessment of Airborne Radioactivity*, STI/Pub/159, International Atomic Energy Agency, Vienna, 1967.

[6] M. Lafont-Rapnouil, "Choix Du Mode De Collection Et De Mesure Pour Un Moniteur D'Aerosols A Filtre," *Assessment of Airborne Radioactivity*, STI/Pub/159, International Atomic Energy Agency, Vienna, 1967.

[7] T. H. Ping and A. Piatkowski, "The Method of Alpha-Beta Activity Multiple Correlation For Assessment of Airborne Radioactivity," *Health Physics* vol. 28, pp. 127-138, 1975.

[8] K. Godfrey, *Compartmental Models and Their Application*. New York:Academic, 1983, pp. 27-28.

[9] D. H. Anderson, *Compartmental Modeling and Tracer Kinetics*. New York:Springer-Verlag, 1983, p. 46.

[10] W. C. Evans, "Dynamic Response of Continuous Particulate Air Monitors," School of Nuclear Engineering, Georgia Institute of Technology, 1975.

[11] W. C. Evans, "Digital Countrate Estimation Using Adaptive Exponentially-Weighted Moving Averages," *Trans. Am. Nucl. Soc.*, vol. 32, p. 134, 1979.

[12] American National Standards Institute, "Specification and Performance of On-Site Instrumentation for Continuously Monitoring Radioactivity in Effluents," ANSI N42.18-1980.

[13] U. S. Nuclear Regulatory Commission, Regulatory Guide 8.37, "ALARA Levels for Effluents from Materials Facilities" July 1993.

Updates

Errata

In the published paper the region labels for (1-29) and (1-30) were reversed. The equation numbers were not changed here, so as to remain consistent with the published version. Thus, (1-29) is for region C and (1-30) is for region B. This error is not of much consequence since the three regions are added to get the overall CW response.

Decay-Chain Extension

The mathematical models in this chapter have been extended to accommodate decay chains, e.g., Radon-Thoron (RnTn). The principal concept is to use *matrix* exponentials in the integrals defining the RW and CW responses. The relevant equations are presented in Chapter 7. In that chapter are many specific solutions for the time-dependent responses for decay chains. Length three is used, since that is the case for the Rn or Tn chain; this could be modeled as a 6-chain system but the results would be very cumbersome and since the responses combine linearly it is better to use two chains of length three for modeling RnTn. For fission product air monitoring, a two-chain is sufficient. The solutions for the top-of-chain nuclide are the same as those shown in the present chapter, since the progeny do not affect the parent nuclides.

Example plots of the decay-chain responses for FF, RW, and CW (using the RW approximation (1-14)) are shown in Fig. 1-24, for a constant concentration of the top-of-chain nuclide, and zero air concentration for the progeny. Thus all progeny response is from ingrowth. Figure 1-25 is similar, for an exponentially-decreasing concentration. Figure 1-26 shows how well the RW approximation (1-14) works, even for the decay-chain application.

Geometric Efficiency / Shelf Effect

In the models reported in this paper/chapter, it was assumed that the detection efficiency was constant ("flat") across the deposition area. This is not the case, since the geometric efficiency will vary with the position of an emitting differential area. This problem is addressed in Chapter 6. The essential result is that reasonable (i.e., within a few percent, well within statistical variability) countrate predictions can be obtained by using the models developed in this paper/chapter, but with an *effective* detection efficiency, found by averaging a specific function across the deposition area geometry. See Chapter 6.

It was also assumed that the detector's field of view was restricted to the deposition area, perhaps by collimation. If this is not the case then material that has left the deposition area can still be "seen" by the detector, inflating the countrate response above that predicted by these models. This issue has been analyzed and modeled, but it is felt that this is not a major problem in the practical application of CPAMs, and in any case would be so specific to the particular geometric arrangement of a CPAM that there is no point in attempting some generalized-correction analysis.

CW Solution

An analytical solution has been obtained for the single-nuclide CW $t \geq T$ case, (1-36) in this chapter; that equation involves the nonelementary integral Z and thus must be evaluated numerically. Here is the new result, for a sum-of exponentials $Q(t)$:

$$\frac{F\,k\,\phi\,\Gamma_i\,e^{-t\,\omega_i}\left(\pi\,R\,(\lambda_1-\omega_i)+\pi\,v\,\mathbf{L}_{-1}\left(\frac{2\,R\,(\lambda_1-\omega_i)}{v}\right)-v\left(\pi\,I_1\left(\frac{2\,R\,(\lambda_1-\omega_i)}{v}\right)+2\right)\right)}{\pi\,R\,(\lambda_1-\omega_i)^2}$$

where $L_{-1}(\ )$ is the "StruveL" function and $I_1(\ )$ is the Bessel I function. Since these are tabulated functions, this can be evaluated readily, but its real usefulness is in the "fast-v" Taylor series process (Chapter 4). It can be shown that this series results in the same $Q(t)$ in the first-order term behavior as happens in the RW case. Remarkably, the result is the same as simply using (1-14) in the RW equations for the fast-v process.

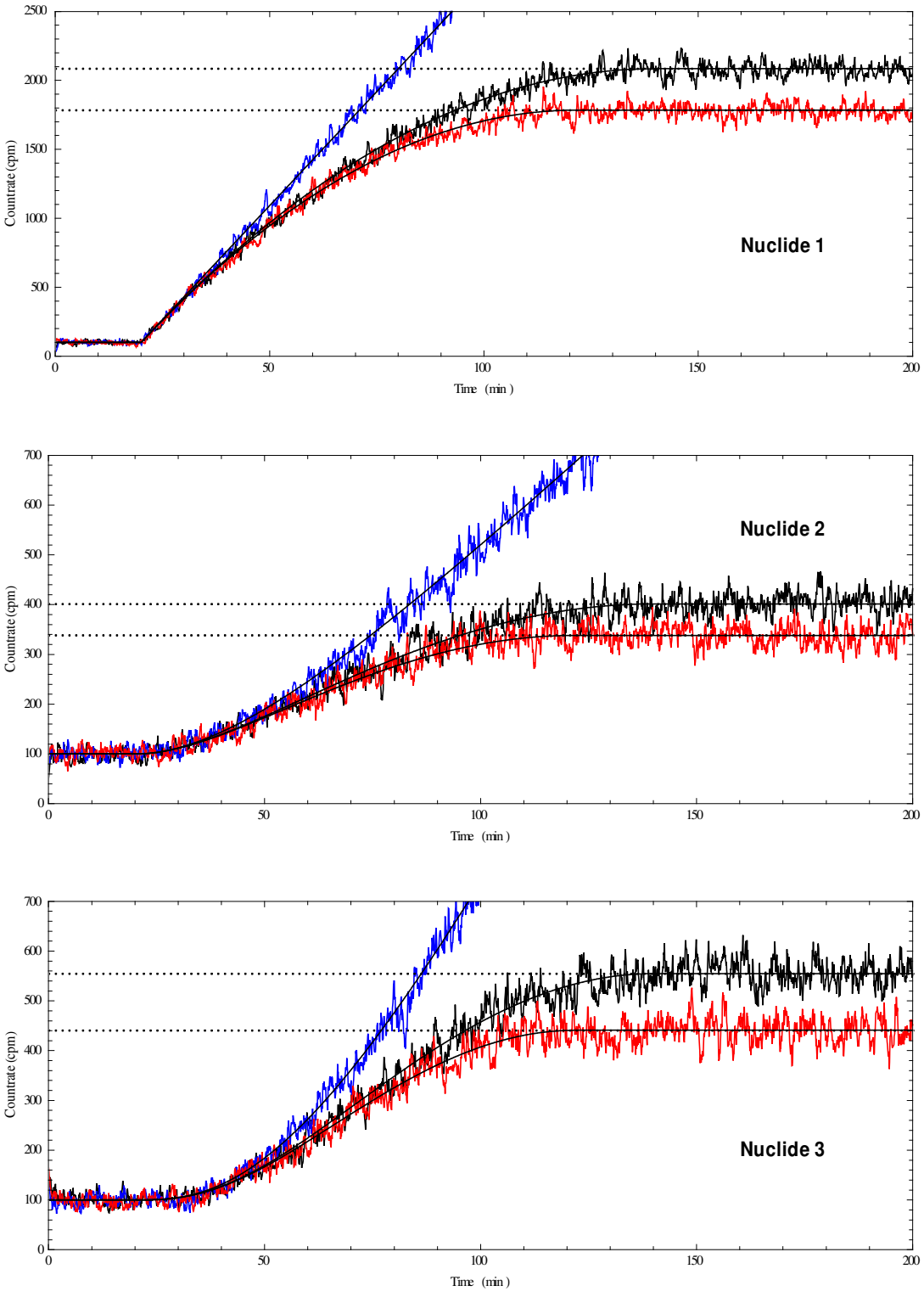

Figure 1-24. Decay-chain FF (blue), RW (black), CW (red) countrate responses for a constant concentration of nuclide 1 (top-of-chain) only. Horizontal lines from equations 4.1.2, 4.2.2, 4.3.2 in Chapter 7. Note the zero initial slope for the progeny curves. The half-lives were: nuclide (1) long, (2) 20 min, (3) 10 min.

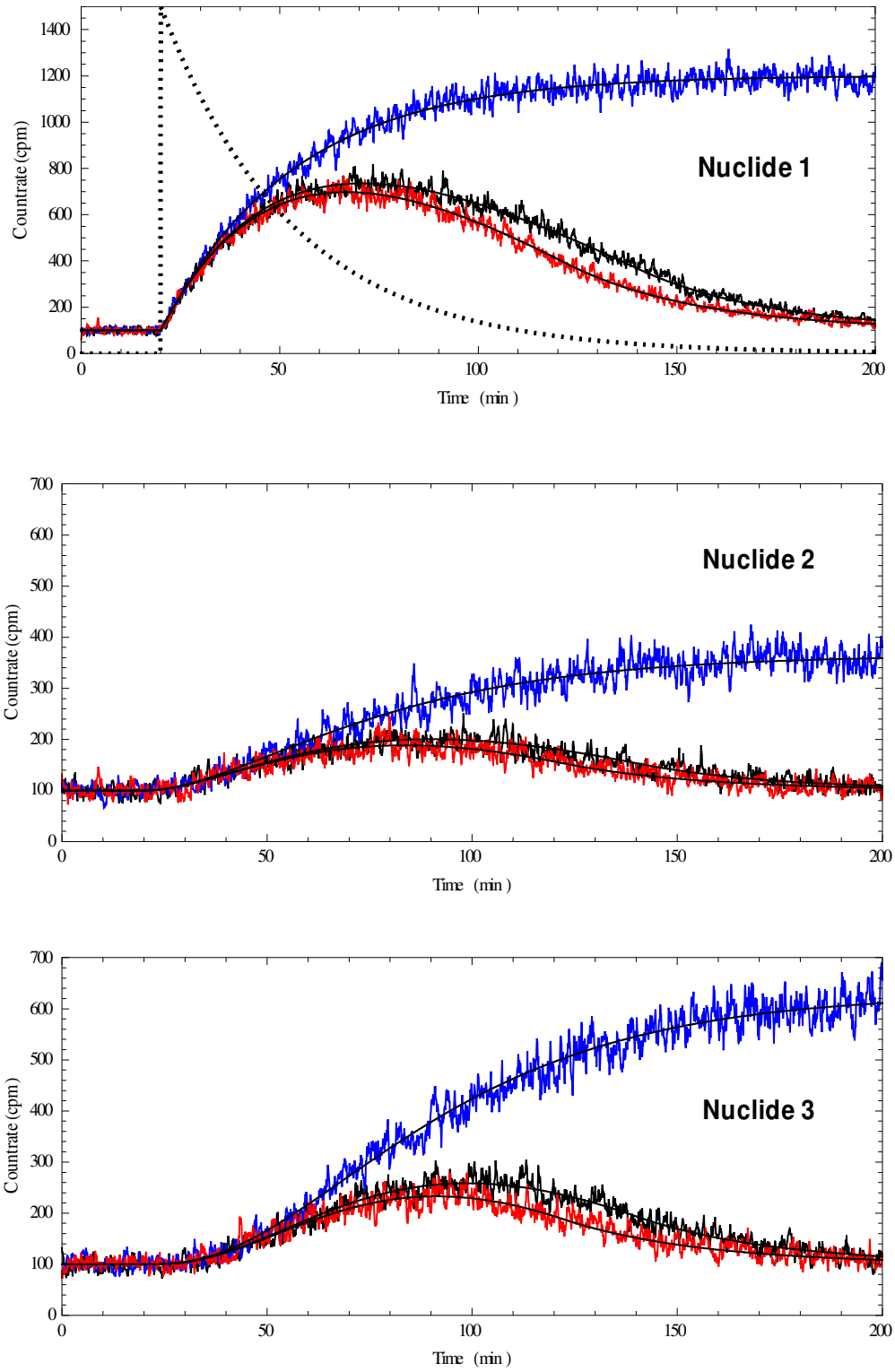

Figure 1-25. Same setup as Figure 1-24, with an exponentially-decreasing concentration (shown in first pane).

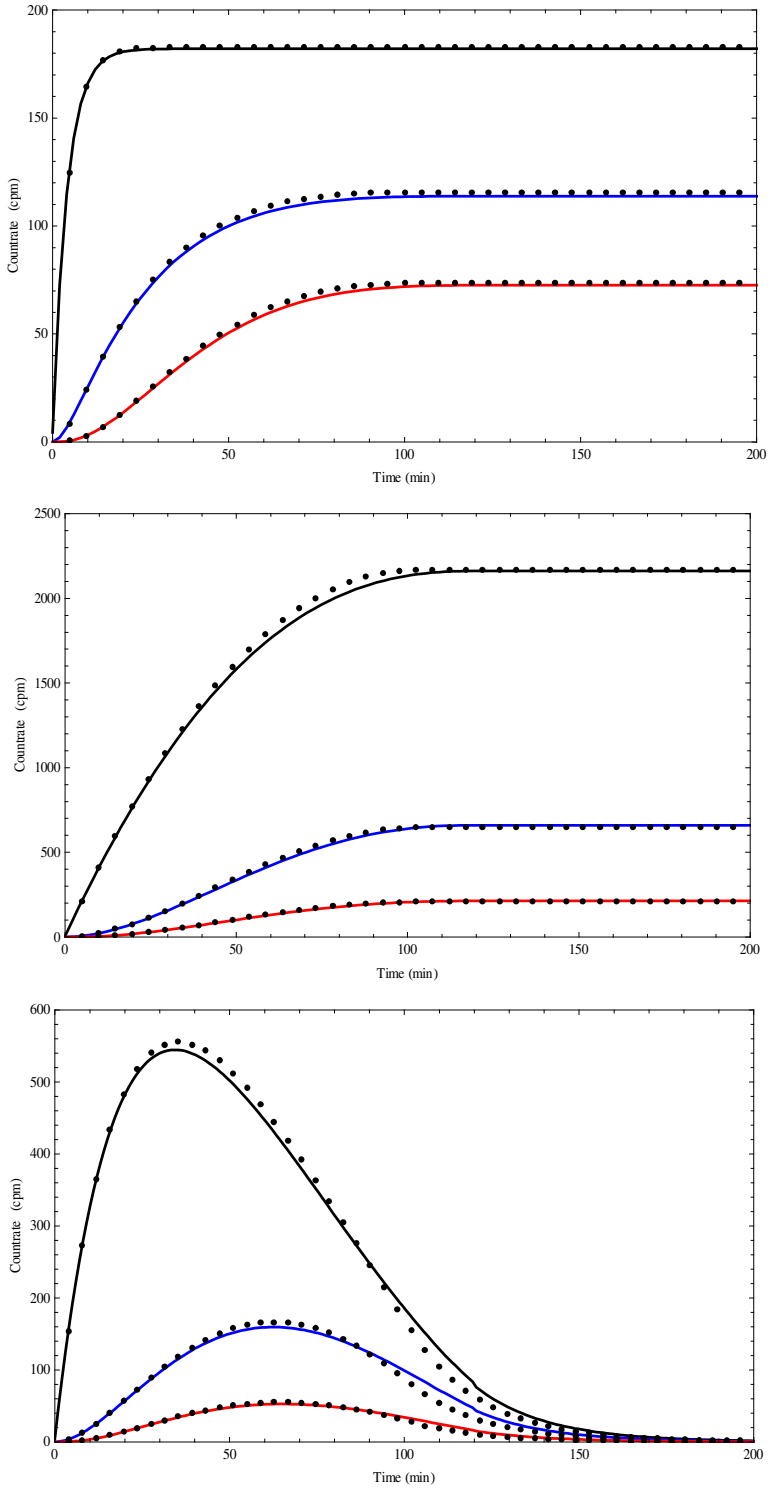

Figure 1-26. CW responses; direct numerical integration of full CW model (Chapter 7, Section 2.2) vs. the RW approximation (dots). Top pane, Rn chain; note that the 3-minute top-of-chain nuclide comes to equilibrium very quickly. (Its detection efficiency is artificial, for illustration; as an alpha emitter, in many systems it would not be observed.) Middle and bottom pane, Tn. The "exact" solution is still numerical, due to a nonelementary integral in the full CW model.

Chapter 2

Quantitative Methods

IEEE Transactions on Nuclear Science, 48(5), Oct 2001; 1639-1657

Quantitative methods for the estimation of concentrations and time-integrals of concentrations of airborne radioactivity using continuous particulate air monitors are discussed. For fixed-filter and moving-filter monitors, methods based on countrate derivatives and integrals are summarized, with plots of simulation results. An approach for estimating a total-episode activity release, using moving-filter monitors, is described. Also presented is an unusual concentration measurement technique, that of an integrated-count step-advance filter (ICSAF) monitor. The instrument uses an integrated count for the concentration estimate, and it also advances the collection medium ("filter"), held fixed during the measurement interval, after each measurement is made. The measurement interval can be determined by either a preset count or a countrate-controlled integration time. This instrument's performance is mathematically analyzed in some detail, with graphical simulation results. The ICSAF monitor has excellent transient-following abilities, and good sensitivity. Its quantitative approach does not depend on assumptions of constant concentrations of long-lived activity, nor is there a need to wait for the monitor to attain some "equilibrium" countrate, as with moving-filter monitors. This instrument would be an excellent choice for many monitoring applications.

Introduction

Continuous particulate air monitors (CPAMs) are used in many nuclear facilities, usually in one of two modes. In a qualitative role, these monitors perform a continuous hypothesis test, that is, deciding whether or not an alarm condition exists. In a quantitative mode, the monitor is used to estimate some quantity, usually the concentration of a nuclide in the sampled air. It is possible for a given monitor to fulfill both purposes at the same time, but generally they focus on one or the other.

Hypothesis testing requires a setpoint or threshold to be defined, and this can be done using the mathematical monitor response models developed in [1], for fixed- or moving-filter monitors, which apply for arbitrary concentration behaviors, for nuclides of any half-life. Setpoint calculations are usually done via a relation that can predict the monitor's output (countrate) for some specified input condition, which is usually based on a limiting concentration of a particular nuclide.

This paper seeks to address the quantitative mode of application for CPAMs, which might be viewed as the "inverse" of the qualitative problem: given an observed monitor output, what can be inferred about the input? An early paper [2] addressed this problem for fixed-filter (FF) and rectangular-window (RW) moving-filter (MF) monitors. These and other methods for FF and MF monitors will be briefly reviewed, including methods based on derivatives, and integrals, of the monitor's net countrate.

In the first section below, we present an overview of methods for obtaining quantitative results from fixed-filter and moving-filter CPAMs. This will include: (a) direct use of the countrate; (b) countrate derivatives; (c) initial countrate derivative; (d) attained countrate after delay; (e) countrate integrals. The second section presents the re-introduction of a monitoring approach first implemented in the early 1960's, a stepped-advance filter monitor. This instrument's performance, enhanced with modifications to its original calculations, will be analyzed in some detail.

Overview of CPAM Quantitative Methods

Introduction

For the quantitative application of CPAMs, what we seek to do is to estimate some quantity, which is not necessarily constant, by analyzing the time-dependent response of the instrument. For CPAMs the input is the dynamically-varying concentration, denoted by $Q(t)$, of a nuclide in the sampled air, and the output is the net countrate above background.

This background is the sum of the countrates due to: (a) the external radiation field in the vicinity of the detector; (b) natural airborne radioactivity (usually referred to as radon-thoron, or RnTn) on the filter; (c) contamination of the monitor;

(d) electronic interference or noise; (e) a checksource, if installed. The external component is nearly always present, and is usually nearly constant, while RnTn may or may not be in the sampled air, depending on the application, and if present can in some cases vary significantly, over periods of several hours. This variation can cause problems for some quantitative methods, notably, those based on countrate derivatives.

Monitor contamination is generally correctable, although some material may have become attached in difficult-to-clean areas. This contribution to background should be essentially constant. Electronic noise tends to be sporadic, and is a difficult problem to overcome, no matter what quantitative methods are used. Finally, some checksources can cause a countrate response in the detector even in the retracted position. This component of background can be considered constant.

Next we will examine the quantitative relations that monitor vendors have often provided with CPAMs, and then move on to review and develop several quantitative approaches for these monitors.

Monitor-Vendor Calibrations

Monitor vendors, in their sales literature and operation manuals, usually provide some "calibration" expressions or curves which are to be used to establish the quantitative relation between the monitor's net countrate and a concentration in the sampled air. For fixed-filter monitors this often takes the form of a log-log plot of the countrate's rate of increase, e.g., in counts per minute (cpm) per minute, vs. the concentration. The curves are implicitly parameterized on detector efficiency, and are often plotted for a few selected nuclides. While the nuclide names are given, what it is about them that leads to the respective curves is often not stated.

We will see below that the FF derivative can be directly used, at any time, if, and only if, the nuclide is long-lived (LL)[1]. That is, if we can somehow obtain a reliable countrate derivative estimate, and the activity is LL, then the vendor curve can be used. If the nuclide of interest is not LL, such as Rb-88, then an additional correction is required.

The primary issues with these FF vendor "calibrations" are: (a) when only curves are provided, there is no explicit statement of how to generalize the quantitative relation to, e.g., various flow rates or detection efficiencies; (b) the countrate-derivative relation will only work properly for long-lived nuclides, unless a correction is applied; (c) this limitation is usually not stated.

For moving-filter monitors, what monitor vendors have often done is to provide equations or graphs, as with the FF monitors; these graphs indicate countrate vs. concentration. However, it is essential to be aware that these relations correspond to a very specific and limited special case. The restrictions are: constant concentration; long-lived activity; the time of concentration estimation must be at least the transit time[2], or greater. Frequently at least one of these conditions is not explicitly stated, and, often, none of them are. Sometimes it is not even stated whether the monitor is RW or circular-window (CW).

Using (1-26) for RW monitors, for this special situation we have the constant countrate, for the constant concentration Q_0, in μCi/cc,

$$\dot{C}_{RW}(Q_0) = \varepsilon k F_m \phi Q_0 \frac{L}{2v}$$

while for CW we have, using (1-41),

$$\dot{C}_{CW}(Q_0) = \varepsilon k F_m \phi Q_0 \frac{8R}{3\pi v}$$

In these expressions, ε is the detection efficiency (including a gamma abundance if spectroscopy is used); k is a conversion constant (2.832×10^4 cm^3/ft^3 times 2.22×10^6 dpm/μCi); F_m is the monitor flowrate, ft^3/min (cfm); ϕ is a collection efficiency, including line loss and/or anisokinetic corrections as needed; L is the length of the rectangular window; R is the radius of the circular window; v is the filter speed.

[1] Long-lived activity does not decay appreciably during the analysis period. Short-lived (SL) activity may decay significantly.

[2] The transit time is the time required for a differential-area element of the collection medium to completely traverse the deposition window. See [1]. Note that this "transit" time should not be confused with the "transport" time for material to reach the monitor from the sampling point.

For the simulations reported here, and for the figures, the default values for ε, F_m, and ϕ were 0.2, 5 cfm, and 0.7, respectively, while L, R, and v were 2 inches, 1 inch, and 1 inch/hour, respectively. The transit time for RW is L/v, while for CW it is $2R/v$.

The expressions above are the limiting or "equilibrium" countrates attained at and after the transit time, for constant-Q, LL activity. The transit time is typically about two hours. Some vendors provide plots of the above linear function of countrate vs. concentration, parameterized on ε as a function of energy, for a given flow rate F. Given just this curve, it would not be apparent to most users how they would generalize even this restricted quantitative relation for the other flowrates, efficiencies, window sizes, filter speeds, etc. which might occur in their application.

The major issue is that these curves, or equations, are very misleading, implying that the countrate at any time, and for any isotope, regardless of half-life, can be directly interpreted in terms of a concentration. This is not the case at all, and these curves have led to some misunderstanding about the application of moving-filter monitors. With only these curves provided, there is no hope of interpreting what is really going on, dynamically, with the instrument as it responds to various plant conditions. For that, we need the response models developed in [1]. These curves, or, as some vendors have provided, equations similar to those above, should have explicit labeling, making their limitations clear.

Next we consider several approaches, which either use the countrate, or quantities derived from it, to estimate the concentration, or quantities derived from it. For each we will look at fixed-filter and moving-filter monitors.

Countrate to Concentration (Instantaneous)

Fixed Filter

The starting point for the input/output analysis of this monitor type is the FF ordinary differential equation (ODE):

$$\frac{d\dot{C}}{dt} = \varepsilon k \phi \, Q(t) \, F_m(t) - \lambda \dot{C} \tag{2-1}$$

and its solution, via the scalar convolution integral,

$$\dot{C}_{FF}(t) = \varepsilon k \phi \exp(-\lambda t) \int_0^t Q(\tau) F_m(\tau) \exp(\lambda \tau) d\tau \tag{2-2}$$

where $\dot{C}(t)$ is the monitor net countrate, cpm; $Q(t)$ is the time-dependent concentration of the nuclide in the sampled air, μCi/cc; λ is the decay constant for the nuclide of interest. We consider a single nuclide at a time; if multiple nuclides are present in the sampled air, then high-resolution spectroscopy is indicated. The flow rate is assumed constant over the analysis interval. If this is not the case, then the flow rate as a function of time must be defined and used inside the integral in (2-2), as indicated in (2-2). For example, the flow rate might be an exponential, or perhaps linear, decrease with time.

Clearly we do not have an explicit relation between the FF output countrate and its input concentration. The relation is via the integral of the concentration. We can get the countrate from the integral of the concentration, or we can get to the concentration through the derivative of the countrate. Both of these approaches will be discussed below. However, we cannot directly relate an instantaneous countrate to an instantaneous concentration for a fixed-filter monitor. Intuitively this makes sense, because particulate monitors are integrating instruments- they must accumulate some material on the collection medium before a countrate can be developed.

Moving Filter

For these monitors there is one very limited case where we can directly relate the monitor countrate and a concentration. Since this involves a time delay, it will be discussed in a later section, on that topic. However, aside from this special case, as with the FF monitor, it is not possible to directly relate the instantaneous countrate and instantaneous concentration for moving-filter monitors. This can be seen from the moving-filter monitor response models in [1].

Some preliminary simulation results indicate that using a variable filter speed might lead to a direct proportionality between a moving-filter countrate and its input concentration. This needs further research, but even a simple linear scaling of the filter speed with countrate produces countrate traces that appear to follow the concentration profile reasonably well.

Countrate processing

An important consideration in using monitor countrates, for any mode of concentration estimation, is that of providing variance reduction. Even though, as discussed above, we rarely use the countrates directly, it is still important as a component of some estimation methods to have a variance-reduced countrate available.

One way of developing a variance-reduced or "smoothed" countrate is to use a digital filter, such as the exponentially-weighted moving average (EWMA), which can be considered a fixed-gain Kalman filter:

$$z_i = z_{i-1} + \alpha\left(x_i - z_{i-1}\right) \tag{2-3}$$

Here z is the processed output and x is the raw input, at each time step. This is also known as an "alpha" filter, with gain α. The EWMA will suffer from lag problems when the countrate is changing [3], especially when small gains are used to obtain a larger amount of variance reduction. It is possible to use various rules to adjust the EWMA gain, e.g., based on the countrate decade, similar to analog ratemeters.

A better approach is to use an adaptive exponentially-weighted moving average (AEWMA) [4]. This filter has effective variance reduction, while also providing rapid response to transients. The algorithm for this processing is

$$\begin{aligned}
\psi_i &= C_i - \Lambda_{i-1} \\
q_i &= q_{i-1} + \gamma\left(\psi_i - q_{i-1}\right) \\
\delta_i &= \delta_{i-1} + \gamma\left(\left|\psi_i\right| - \delta_{i-1}\right) \\
\alpha_i &= \left|\frac{q_i}{\delta_i}\right| \\
\Lambda_i &= \Lambda_{i-1} + \alpha_i\,\psi_i \\
\dot{C}_i &= \frac{\Lambda_i}{\Delta t}
\end{aligned} \tag{2-4}$$

where ψ is the prediction error; C is the count accumulated each time step; Λ is the smoothed count; q and δ are the smoothed error and smoothed absolute error, respectively; γ is a gain, typically 0.1; α is now an adaptive gain used for the count smoothing. The variance-reduced countrate is just the smoothed count divided by the time step size Δt. Larger prediction errors will occur when the count data is changing rapidly, and so the filter gain will "speed up" to track the input more closely. As the data settles back into a constant level, the AEWMA gain will decrease, producing more variance reduction.

The digital step size Δt is an important consideration. If it is too short, e.g., one second, then at low concentrations there will be few counts accumulated per time step, making the AEWMA's variance-reduction job that much more difficult. If it is too long the monitor will not be of much use for applications requiring rapid response. Thus this parameter should be optimized for each application. For the simulations presented herein, the step was set at five seconds.

Countrate Derivative

Fixed filter

It has long been recognized that the ODE for the FF monitor, (2-1), says that the time derivative of its countrate is proportional to the instantaneous concentration, for long-lived activity only. In (1) the loss term will vanish as λ approaches zero, and we have a simple linear proportionality relating the countrate derivative to $Q(t)$. This is a straightforward theoretical result, but in practice it is not especially useful. One reason for this is that the derivative estimation must be done numerically, using noisy data, and simple countrate-derivative estimates are very erratic unless the countrate (and thus the concentration) level is high.

For a nuclide of any half-life we can rearrange (2-1) and solve for the concentration:

$$Q(t) = \frac{1}{\varepsilon\, k\, F_m\, \phi}\left(\frac{d\dot{C}}{dt} + \lambda\dot{C}\right) \tag{2-5}$$

if we have a time-dependent derivative estimate and of course the countrate itself. Both of these are net, background-corrected

values. The monitor flow rate can be nonconstant as long as we have a dynamic estimate of it, as we might in a digital system. In applications where RnTn is an issue, the effects of this interference must be removed prior to taking the derivative. This is not simple. Note that, for short-lived activity, we must know which nuclide is being monitored so that we have its decay constant. For gross monitors this means that we need a single, or at least strongly predominant, nuclide in the sampled air.

Concentration estimates using (2-5) will be very noisy, due to the derivative. Nonetheless, there could be some restricted applications where this approach might work reasonably well. The problem of "clearing" any long-lived activity from the filter remains an issue, since this will make it nearly impossible to see lower concentrations once a high concentration transient has been experienced.

An improved approach for derivative estimation from noisy data is a radar tracking filter [5], which can be expressed as

$$\begin{aligned} \varphi_i &= \frac{C_i}{\Delta t} - \hat{z}_{i-1} \\ z_i &= \hat{z}_{i-1} + \alpha \varphi_i \\ r_i &= r_{i-1} + \frac{\beta}{\Delta t} \varphi_i \\ \hat{z}_i &= z_i + r_i \Delta t \end{aligned} \tag{2-6}$$

where α and β are fixed gains, C is the count accumulated during a time step Δt, and r is the derivative output. This is often referred to as an "alpha-beta" filter, for obvious reasons. The performance of this filter, with regard to variance reduction vs. lag, is very much dependent on the settings of these gains, which are usually adjusted empirically. For the work reported here, α was 0.1 and β was 0.005. The input to this filter can be either the raw countrates, as indicated in (2-6), or the output of the AEWMA, (2-4). Generally, the latter will perform better under most circumstances, as we would expect, although the difference is not large.

Fig. 2-1 shows concentration estimates for a simple first backward difference numerical derivative, for an exponential *Q(t)* of Rb-88, using raw countrate data (accumulated counts divided by the digital time step size, five seconds). Clearly, these concentration estimates are all but useless. Fig. 2-2 shows the same situation, but using the AEWMA countrates in the derivative. These estimates are much less scattered, but still not of much value. Interestingly, however, as we will see below in the section on concentration integrals, the numerical integral of these noisy estimates can in fact produce a usable result.

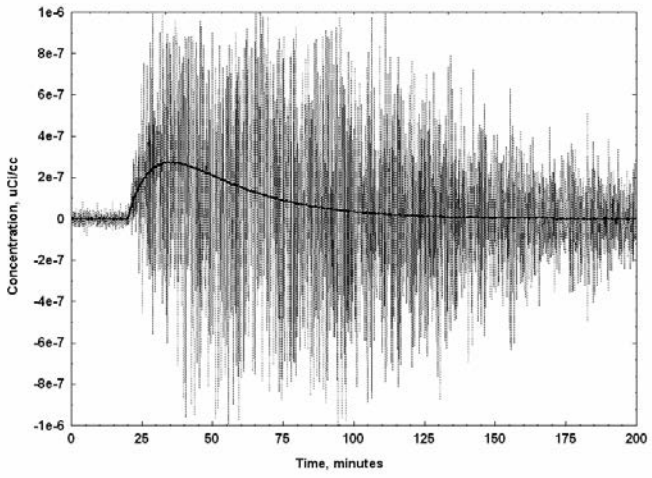

Figure 2-1. First-difference numerical derivative concentration estimates, using raw countrate data. Solid line is known concentration.

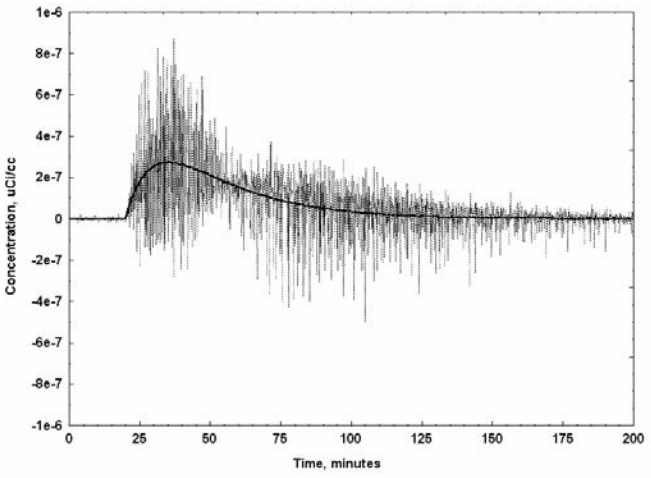

Figure 2-2. First-difference numerical derivative concentration estimates, using AEWMA countrate data. Solid line is known concentration.

Fig. 2-3 shows the concentration estimates for the radar filter (2-6), using as input both the raw and AEWMA countrates. At the plot resolution we cannot separate these estimates. Note the lag at the start of the *Q(t)* transient. This is the price we pay for the superior variance reduction of the digital filter derivative estimator.

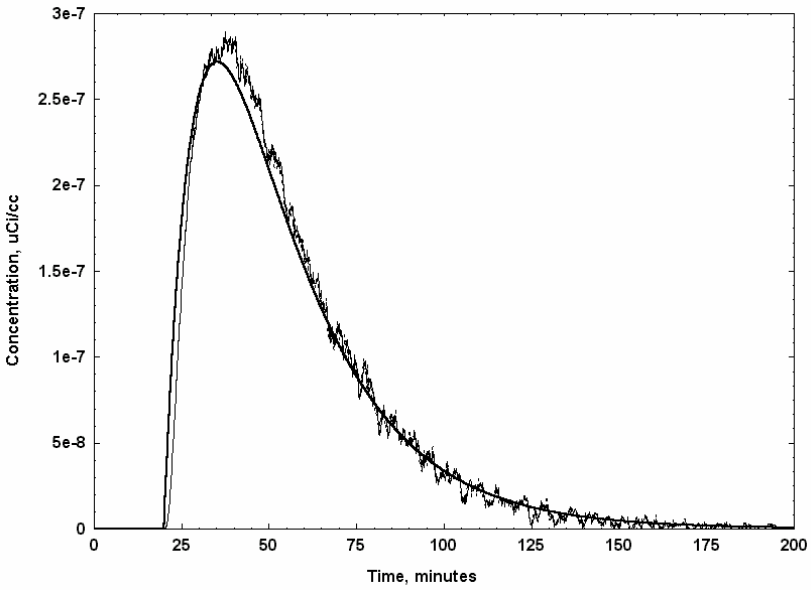

Figure 2-3. Radar-filter derivative concentration estimates, using both raw and AEWMA countrates as input. Same Q(t) as in Fig. 2-1 and Fig. 2-2.

Moving filter

Examination of the moving-filter response models in [1] will show that there is no straightforward relationship between derivatives of those countrates and the concentration; this has been verified with numerical studies, using the detailed monitor-response simulation also described in [1]. Intuitively, this happens because the filter movement acts as a loss term, in a differential-equation sense, and the amount of this loss per unit time is not simply-related to the instantaneous concentration, since the filter elements leaving the window have integrated the *Q(t)* behavior for various lengths of time.

Initial-Slope Approach

Fixed filter

Consider again the FF ODE, (2-1). At time zero, when the *Q(t)* transient begins, we have a zero net countrate, due to the assumed zero initial condition (clean filter at time zero). Thus the loss term is negligible, and the slope (derivative) of the countrate will be directly proportional to the concentration *at time zero*, for a nuclide of any half-life.

$$Q(0) \approx \frac{1}{\varepsilon k F_m \phi} \left. \frac{d\dot{C}}{dt} \right|_{t \approx 0} \tag{2-7}$$

In this case, the monitor flow rate can be taken as constant since we are only examining a short time span.

Moving filter

Moving-filter countrate response models reduce to the FF case when the filter speed approaches zero [1]. For the first few minutes of a transient, the filter does not move much, and we can consider the moving-filter monitors to be fixed-filter, briefly. In Fig. 2-4 note that in the first 15 minutes or so after the start of the *Q(t)* transient at 50 minutes, the moving-filter countrates are indistinguishable from the fixed-filter countrate. Thus the moving-filter initial slopes are also proportional to the initial concentration. This is the case no matter what the *Q(t)* behavior may be, or what the nuclide half-life is.

In fact, it can be shown analytically that, for all three monitor types (FF, RW, CW), the initial slope is proportional to the initial concentration. One way to show this is to use a constant concentration, with a general half-life, find the countrate solutions, take their time derivatives, and evaluate them at time zero. This was done, using a symbolic-mathematics program, and the result, after a lot of algebra, is as stated.

If the concentration is constant, then we could use the initial slope to quickly obtain an estimate of it, rather than waiting for the moving-filter monitors to attain their steady-state values. This time delay can be significant, on the order of two hours.

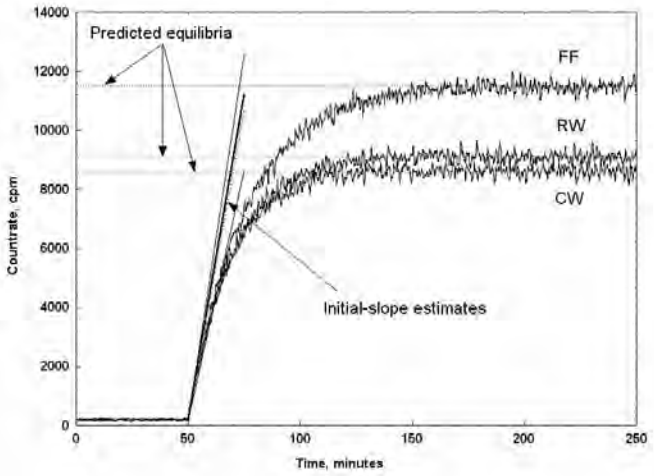

Figure 2-4. Countrate responses, FF, RW, CW monitors, constant-Q, 10^{-8} μCi/cc, Rb-88. Equilibria predicted using (2-8) for FF; (2-9) for RW; (2-11) for CW. Countrates are AEWMA-processed.

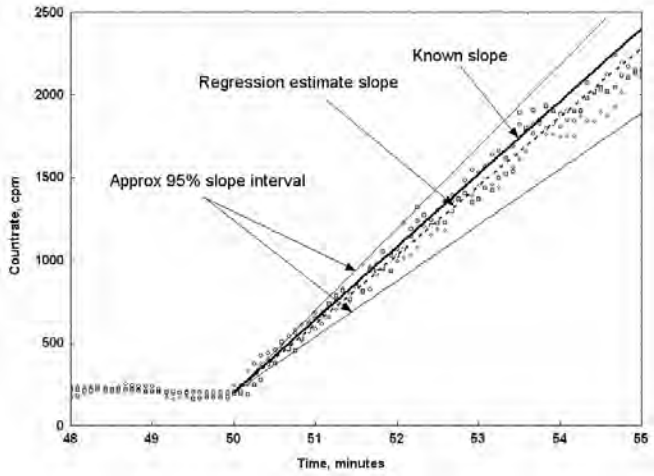

Figure 2-5. Expanded view of initial slope estimates, same data as Fig. 2-4.

Example

To illustrate the initial-slope concept, again consider Fig. 2-4. Here we see the buildup of the countrates of FF, RW, and CW monitors for a step change in the concentration. The initial slope was estimated using the first minute's worth of FF countrate data, which for the digital step used, 5 seconds, means the first 12 samples. This data was processed using linear regression [6], and the initial-slope lines drawn in the figure include the point estimate and approximate 95% confidence bounds on either side. The known concentration was 10^{-8} μCi/cc; the slope point estimate was 0.948×10^{-8} μCi/cc, with a 95% confidence interval of $[0.769 \times 10^{-8} \;\; 1.13 \times 10^{-8}]$, which covers the known value. In Fig. 2-5 we have an expanded view of Fig. 2-4, at the start of the transient, so that the slope lines and data can be seen more clearly.

Thus, a regression approach can provide very good estimates of the initial concentration. This assumes, however, that we have a way of estimating when the transient has started. In this example this time was of course known without error. To automate the detection of the transient's start time, we might consider the methodology in, e.g., [7]. In principle, the detection of the transient and the estimation of the initial slope can be mechanized.

Note that in this context we extend the meaning of "net countrate" to be that due to activity, not only above the ambient background and RnTn, if present, but above any pre-existing, constant countrate. The latter may result from, e.g., a FF monitor sampling a constant-*Q*, SL activity for a time sufficient to attain equilibrium, or a MF monitor sampling SL or LL activity for at least its transit time. The *Q(0)* that we estimate using (7) is in addition to any constant level of activity that may already be in place.

The initial-slope approach differs from the countrate derivative method (2-5) in that it does not require a half-life correction, and it can be used for MF monitors. However, it only estimates the initial concentration *Q(0)*; how useful this will be of course depends on the application.

Attained Countrate After Delay

Fixed filter

In some contexts it is acceptable to define a time delay after which a FF monitor will produce some net countrate, for a given concentration input. A typical value for the delay is one hour. The concentration is of some specified isotope and is assumed

constant over this time delay. The countrate attained will be, using (2-2) with a constant flow rate, and constant concentration Q_0,

$$\dot{C}_{FF}(t) = \frac{\varepsilon k F_m \phi Q_0}{\lambda}\left[1 - \exp(-\lambda t)\right] \tag{2-8}$$

This sort of specification is often used in defining detection sensitivities, so that the concentration used in the countrate solution would be some lower-limit value. The issue then is, will the monitor produce a reliably-detectable countrate increase above its background when it responds to this low-level concentration over a period of one hour.

For dynamic concentration-quantification purposes the idea of waiting one hour and then seeing what net countrate is attained has little practical value. In principle one could use the monitor-response solutions in [1], substitute one hour (or any other fixed value) for the time t, and then solve for the constant concentration, using the observed net countrate at the delay time, for a given nuclide. For the FF monitor this is trivial, especially for long-lived activity, as is often assumed in these performance specifications. The countrate simply increases linearly with time, and the question reduces to finding whether the countrate increases sufficiently above the monitor background to be "reliably detectable."

A variation on the time-delay approach, if we can assume a constant concentration, is to observe the time required for a FF monitor to, e.g., double its countrate. Once the monitor has reached an alarm setpoint, not far above its background, we can record the time required for the countrate to reach some multiple of the alarm level. Using (2-8) for a given nuclide, we can calculate how long it would take to increase the countrate to the multiple, for some particular concentration. If it takes this amount of time or less, then that concentration limit has been exceeded.

Moving filter

Recalling that this time-delay approach requires a constant concentration, we have the necessary expressions for the countrate of moving-filter monitors at any time, for any half-life, from [1], namely (1-23) and (1-25) for rectangular-window, and (1-33) to (1-36) for circular window monitors. Since the usual delay-time specification is one hour, and the typical moving-filter transit time T is two hours, we will need to use the $t \le T$ expressions. This is algebraically messy, but manageable. The CW case will require a numerical approach, due to the nonelementary integral in this solution, if the nuclide of interest is not long-lived. If it is LL, the expressions have closed forms. All else being equal, after one hour, the moving-filter monitors will have a substantially lower countrate than will the FF monitor, thus reducing their sensitivity (i.e., their ability to rise above their background countrates to a reliably-detectable level). This can be seen in Fig. 2-4, which used a short-lived nuclide (Rb-88); the difference is more pronounced for a long-lived nuclide.

If we wait until at least the transit time, typically two hours[3], things become considerably simpler. Taking the RW monitor first, we have, assuming a constant monitor flow rate and using (1-25), the constant countrate

$$\dot{C}_{RW}(t) = \varepsilon k F_m \phi Q_0 \left\{ \frac{1}{\lambda} - \frac{1}{\lambda^2 T}\left[1 - \exp(-\lambda T)\right] \right\} \tag{2-9}$$

from which we can define a proportionality constant

$$\xi_{RW} = \frac{\dot{C}_{RW}}{Q_0}\frac{1}{\varepsilon k F_m \phi T} = \frac{1}{T}\left\{ \frac{1}{\lambda} - \frac{1}{\lambda^2 T}\left[1 - \exp(-\lambda T)\right] \right\} \tag{2-10}$$

This idea is based on [8], and the constant will prove to be useful below. The division by the transit time T makes the constant dimensionless. Note that if the activity is long-lived, the limit of (2-10) as λ approaches zero is ½.

For the CW monitor we have the constant countrate after the transit time, using (1-36):

$$\dot{C}_{CW}(t) = \frac{\varepsilon k F_m \phi Q_0}{\lambda}\left[1 - \frac{2v}{\lambda \pi R} + \frac{2v}{\lambda \pi R^2} Z\left(\frac{\pi}{2}, \lambda\right) \right] \tag{2-11}$$

where Z is the nonelementary integral

[3] Or increase the filter speed to make the transit time one hour.

$$Z(a,b) = R \int_0^a \exp\left[-bT\sin(\alpha)\right] \sin(\alpha)\, d\alpha \tag{2-12}$$

which arises in the CW model; this is (1-27). The proportionality constant can now be defined for CW monitors:

$$\xi_{CW} = \frac{\dot{C}_{CW}}{Q_0} \frac{1}{\varepsilon k F_m \phi T} = \frac{1}{\lambda T}\left\{1 - \frac{4}{\lambda \pi T}\left[1 - \frac{1}{R} Z\left(\frac{\pi}{2}, \lambda\right)\right]\right\} \tag{2-13}$$

For LL activity the limit of this expression is 4/3π. For the common case of a transit time of 120 minutes, the value of (2-13) for Rb-88 is 0.1588, with Z evaluated numerically. Note that the window radius R will cancel, in this expression. As noted in [1], there are approximations given in [8] which can avoid the integral Z, but evaluating Z numerically is to be preferred, and this is straightforward with modern computing capabilities. With these expressions for the attained countrates of the RW and CW monitors, we can easily solve for the constant-concentration estimate, given an observed net countrate after the delay time T.

Returning to Fig. 2-4, we have a plot of the FF, RW, and CW responses to a step change in the concentration, and the respective equilibrium countrates are indicated by horizontal dotted lines. These lines were calculated using (2-8), (2-9), and (2-11), for FF, RW, and CW, respectively. The agreement is good. Note that the noisy countrates (AEWMA-processed) were generated by the numerical simulation discussed in [1], and this simulation is independent of any analytical models.

Concentration Time-Integrals

Fixed filter

If we revisit the FF ODE solution, when it is written in the form of the convolution integral, (2-2), it is clear that we could make some progress by thinking in terms of the integral of the concentration, rather than its instantaneous value. The integral will be time-dependent, and it includes the effect of the dynamic variations in the concentration. The question is, of what use is the integral of the concentration?

This integral turns out to be very useful, arguably more so than the "instantaneous" concentration. Consider the following expressions:

$$R(\eta) = \int_0^\eta Q(\tau) F_s(\tau)\, d\tau \tag{2-14}$$

$$U(\eta) = \int_0^\eta Q(\tau) F_b(\tau)\, d\tau \tag{2-15}$$

$$\bar{Q}(\eta) = \frac{1}{\eta}\int_0^\eta Q(\tau)\, d\tau \tag{2-16}$$

Equation (2-14) is for the release of activity from the facility in an effluent stream, where F_s is the "stack" flowrate. The release integrand product $Q(t)F_s(t)$ is often referred to as a "release rate." Equation (2-15) is for the human uptake (or "intake") of activity via the respiration pathway, with F_b an inhalation ("breathing") rate. Equation (2-16) is the definition for the average of a varying concentration over some time η. If we assume the stack flowrate and breathing rate are constant then they come outside the release and uptake integrals respectively, leaving just the concentration time integral. If they are not exactly constant, we can usually break down the interval $[0\ \eta]$ into subintervals where these flows can be considered reasonably constant, and then sum the resulting integrals.

Looking at the FF solution (2-2), we see that we have an exponential inside the integral, so that we cannot write the three integrals above directly in terms of the observed countrate, unless we assume long-lived activity. (We do not want to impose this restriction.) However, we can re-write the original ODE (2-1) as we did in (2-5), and if we integrate both sides of this with respect to t, we obtain, for a zero initial condition (clean filter) and a constant monitor flow rate:

$$\dot{C}(t) + \lambda \int_0^t \dot{C}(\tau)\, d\tau = \varepsilon k F_m \phi \int_0^t Q(\tau)\, d\tau \tag{2-17}$$

This says that the sum of the countrate and a multiple of the integral of the countrate is proportional to the integral of the concentration. Now we can do the algebra to solve for the release, uptake, or average concentration using the countrate and its integral (the countrate integral can be evaluated using an analog scaler or digital numerical integration). The results are

$$R(\eta) = \frac{F_s \left[\dot{C}(\eta) + \lambda \int_0^\eta \dot{C}(\tau)\, d\tau \right]}{\varepsilon k F_m \phi} \tag{2-18}$$

$$U(\eta) = \frac{F_b \left[\dot{C}(\eta) + \lambda \int_0^\eta \dot{C}(\tau)\, d\tau \right]}{\varepsilon k F_m \phi} \tag{2-19}$$

$$\bar{Q}(\eta) = \frac{\dot{C}(\eta) + \lambda \int_0^\eta \dot{C}(\tau)\, d\tau}{\varepsilon k F_m \phi\, \eta} \tag{2-20}$$

Note that in order to apply these expressions, we must choose an isotope so that we have its decay constant λ. This approach will not work for gross (nonspecific) monitors that are observing isotopic mixtures. High-resolution gamma spectroscopy is indicated for such situations, and then these relations can be applied to one isotope at a time. Note also that if the isotope of interest is long-lived, then the decay constant is small, and the contribution from the count integral vanishes. This says that for a fixed-filter monitor and LL activity, the release, or uptake, is directly proportional to the attained countrate, no matter what the concentration dynamics were.

A complication in applying these expressions is that the countrate used must be a *net* countrate, above background. This is of course for both the countrate itself and its integral. In many applications the background is reasonably constant and can be estimated by the monitor, periodically, and then subtracted. In other cases the plant environment may cause a fluctuating background. RnTn might be a significant concern, for some applications.

However, (2-18) and a stack monitoring system based on it were developed by the author at a PWR in the late 1960's [9], and neither the ambient background nor RnTn was a problem. The approach worked very well for the effluent monitoring situation at that plant. The particulate releases consisted almost exclusively of episodic purges of Rb-88 from the containment, prior to entry. This means a rapidly-changing concentration of a short-lived, single isotope. Because of this history, (2-18) is termed the "Rb-88 Method."

In Fig. 2-6 we have an example run, showing the Rb-88 Method release estimate, compared to the known release. The agreement is excellent; the estimate cannot be distinguished from the known values. The relative error is also shown, and it is less than 0.1 percent. Note that the estimate is dynamic, that is, it follows the release value as it changes during the concentration transient.

DAC-hour estimation

An important CPAM application for occupational exposure assessment is that of estimating the "DAC-hour" exposure of workers. The DAC, or derived air concentration, is based on an ALI, or annual limit on intake, for a given nuclide. The "exposure" is the time integral of the concentration. If we divide (2-19) by the breathing rate, and then divide again by the DAC for a given nuclide, we will have

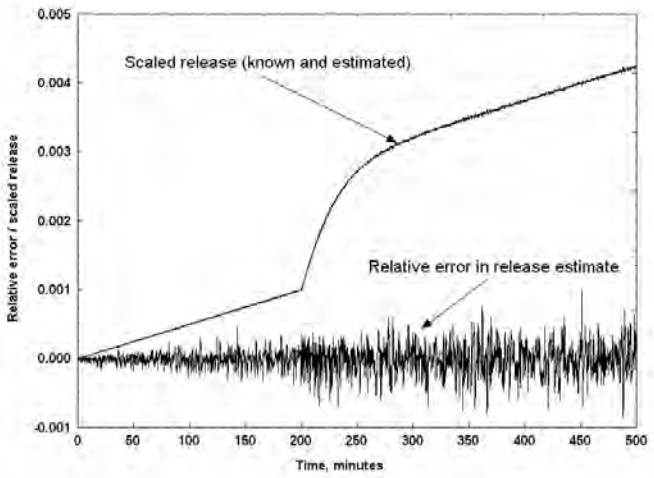

Figure 2-6. Release (concentration integral) estimate using (2-18), and relative error, compared to known value. Release is scaled arbitrarily to fit on relative error vertical scale.

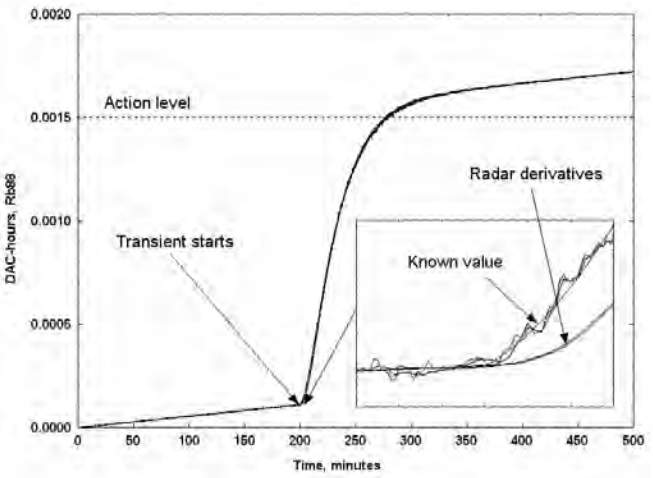

Figure 2-7. DAC-hour estimates for all FF methods, including first-difference derivatives. Inset shows data at start of transient. Lag of radar derivatives at start of transient is evident. First-difference and Rb-88 Method (2-22) track closely together (remaining curves in inset).

$$DAChr(\eta) \;=\; \frac{\dot{C}(\eta) \;+\; \lambda \int_0^{\eta} \dot{C}(\tau)\, d\tau}{\varepsilon\, k\, F_m\, \phi\; DAC} \tag{2-21}$$

so that a FF monitor can estimate the exposure continuously. This is a dynamic estimate, which evolves during the work period [*0* η], so that alarms can be set on the basis of DAC-hour exposure, rather than (or in addition to) concentration. In addition, any method that periodically estimates a concentration can of course be numerically integrated to produce a DAC-hour estimate, but (2-21) will be continuous.

In Fig. 2-7 we have DAC-hour estimates from (2-21) for Rb-88, as well as those from the numerical integration of all four derivative concentration estimates (first difference using raw and AEWMA data; radar filter using raw and AEWMA data). The agreement of all five of these estimates with the known values (solid line) is excellent, although in the inset, an expanded view near the start of the transient, we can see that the radar-filter-based estimates are lagging. This is the same behavior we saw in Fig. 2-3.

The *Q(t)* behavior for this example is a constant-*Q* at a low level, and then at 200 minutes a rapid increase occurs, followed by a rapid exponential decrease (the same shape as in Fig. 2-3). This simulates a work situation with a nominal *Q(t)* level, during which some event causes a higher concentration to occur very quickly. The "action level" shown in the figure is just for illustration, since the DAC-hour levels in this example are very small. The point is to show that an alarm, or evacuation order, can be generated dynamically by the monitor, in real time.

Note that in the inset in Fig. 2-7 we can see that the first-difference derivative DAC-hour estimates (thin solid lines) and those from (2-21) (dashed line) are following each other closely. This is because a numerical integration of the derivative concentration estimates from (2-5) will amount to the same thing as the numerator of (2-21). So, even though the derivative-based concentration estimates may be very erratic (if we did not use the radar filter, or some equivalent), their integral is still a usable estimate for a concentration integral, such as a DAC-hour estimate.

Rb-88 Method concentration estimates

Equation (2-18) is intended to be used for effluent applications, over relatively long time intervals of many days or even weeks. However, there is nothing preventing us from using the closely-related expression (2-20) over short time steps, such as five minutes. This will produce a series of average concentration estimates over those time steps, assuming that we clear the scaler (integral) at each start, and use the *change* in countrate, over the time interval. This can be written as

$$\bar{Q}(\eta) = \frac{1}{\varepsilon k F_m \phi \eta}\left\{\left[\dot{C}(\eta) - \dot{C}(0)\right] + \lambda \int_0^{\eta} \dot{C}(\tau)\, d\tau\right\} \tag{2-22}$$

where η is the averaging interval and the time variable is zero at the start of each interval. The countrates are as usual net, although the countrate difference can be gross, since the background will cancel.

One might expect that this estimate would not be correct for cases where there was a release episode and the fixed filter was not replaced prior to the next episode. However, it can be shown that the "residual" countrate due to the previous episode, whether LL or SL, will not affect the concentration estimate (2-22). What that elevated countrate will do is raise the effective background countrate of the instrument, so that its detection capability will be reduced, particularly for a LL nuclide. This could "mask" a smaller release after a larger one. Hence it would be best, where practical and where releases tend to be episodic (e.g., containment purges), to replace the filter after each release episode. This would not be much of a burden since in most instances we would want to take the filter to the laboratory for detailed spectral analysis after each release episode.

In Fig. 2-8 we have the concentration estimates produced by this approach, for an exponential *Q(t)*. The squares show the estimate, at the time it is evaluated, and the line to the left shows the five-minute time interval covered by that estimate. The dotted line to the right indicates that this will be the concentration estimate we have, until the next estimate becomes available.

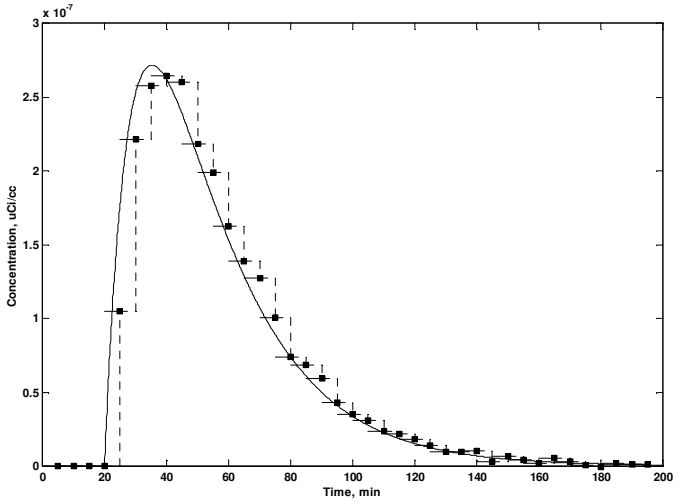

Figure 2-8. Concentration estimates for five-minute Rb-88 Method averages, based on (2-22). Exponential pulse of Rb-88.

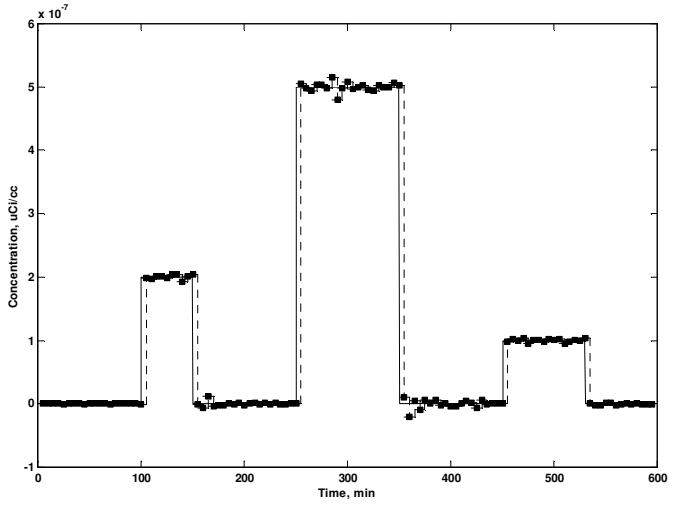

Figure 2-9. Concentration estimates for five-minute Rb-88 Method averages, based on (2-22). Pulses of Rb-88 activity.

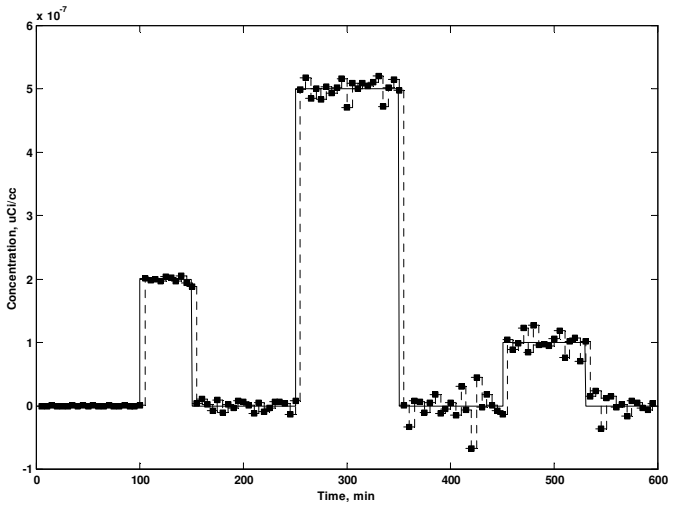

Figure 2-10. Concentration estimates for five-minute Rb-88 Method averages, based on (2-22). Pulses of long-lived activity.

The concentration estimates follow the *Q(t)* behavior well, as long as we recognize that the indicated concentration is the average over the previous five minutes. In Fig. 2-9 we have three pulses of Rb-88, while in Fig. 2-10 we have the same *Q(t)* for a long-lived nuclide. Note the additional scatter in the estimates in the latter case, due to the residual LL activity after a pulse.

Moving filter

Consider the RW and CW response to an exponential buildup/decay *Q(t)* transient, in Fig. 2-11. This is for a long-lived nuclide; the response is very similar for SL. We observe that the countrate response has the same general shape as that of the concentration. This would not be the case for a FF monitor, which would stay at an elevated countrate after the *Q(t)* had become small. We might speculate that there could be some proportionality between the integral of the moving-filter countrate and the integral of the concentration. This was proposed in [8], for CW monitors, expressed as

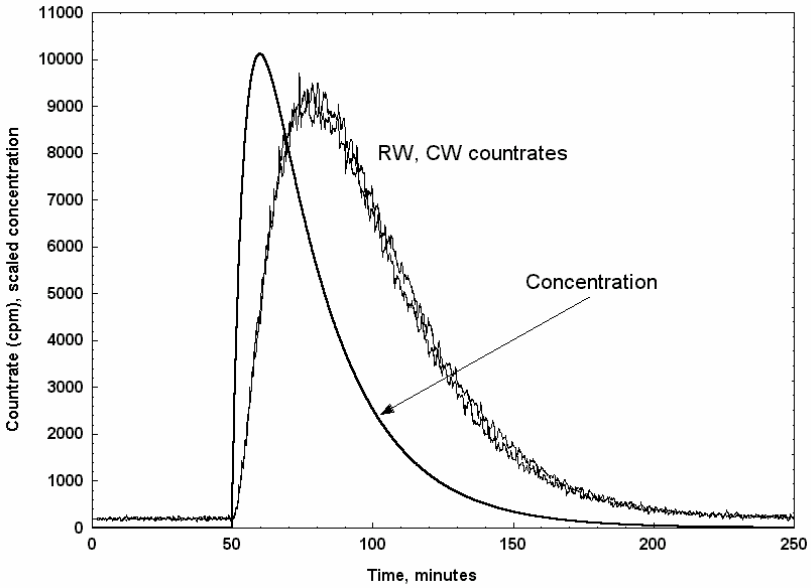

Figure 2-11. Countrates for RW and CW monitors for exponential Q(t). Concentration arbitrarily scaled to fit on countrate axis.

$$\xi = \frac{\int_0^\infty \dot{C}(t)\,dt}{\varepsilon k F_m \phi T \int_0^\infty Q(t)\,dt} \tag{2-23}$$

where ξ is a constant of proportionality, and T is the transit time. As usual the countrate is net, background-corrected, and the monitor flowrate is constant.

The constant ξ is independent of the shape of *Q(t)*, as long as *Q(t)* tends to zero as time increases. This will not apply for the constant-*Q* case. Since the integrals are taken to infinity, any quantitative method based on (2-23) only applies after the concentration transient is completed, and after the monitor response has returned to zero (i.e., background). As a practical matter this would mean a delay of at least two hours, and possibly much more, depending on the shape of *Q(t)*. In some applications this delay would be unacceptable, in others it would not be an issue.

This constant of proportionality ξ is the same as was discussed above, in the section on attained-countrate. There, we found an expression for this constant, for RW monitors, (2-10), using a constant concentration. We can use the RW response model for an exponential-decrease *Q(t)* to derive ξ again, this time using (2-23), to show that they are equivalent. From (1-21) we have the RW response to a single-exponential decrease *Q(t)* for time less than *T*:

$$\dot{C}_{RW-1}(t) = \frac{\varepsilon k F_m \phi Q_0}{(\lambda - r)^2} \frac{v}{L}\left[\exp(-rt)\left\{t(\lambda - r) - 1\right\} + \exp(-\lambda t)\right] + \frac{\varepsilon k F_m \phi Q_0}{\lambda - r}\left(1 - \frac{vt}{L}\right)\left[\exp(-rt) - \exp(-\lambda t)\right] \quad (2\text{-}24)$$

where r is the parameter controlling the $Q(t)$ decrease. For time after T we have from (1-22):

$$\dot{C}_{RW-2}(t) = \frac{\varepsilon k F_m \phi Q_0}{(\lambda - r)^2}\left\{\exp(-rt)\left(\lambda - r - \frac{v}{L}\right) + \frac{v}{L}\exp\left[-r\left(t - \frac{L}{v}\right) - \frac{L}{v}\lambda\right]\right\} \quad (2\text{-}25)$$

Then we can write

$$\xi = \frac{\int_0^T \dot{C}_{RW-1}(t)\,dt + \int_T^\infty \dot{C}_{RW-2}(t)\,dt}{\varepsilon k F_m \phi T \dfrac{Q_0}{r}} \quad (2\text{-}26)$$

which when evaluated is the same as (2-10). Thus we have found the same ξ for a constant and an exponential $Q(t)$; the relation is via a countrate for a constant Q, and via the integrated counts for a time-dependent Q.

The expression for the concentration integral for the RW monitor, using its constant (10), is

$$\int_0^\infty Q(t)\,dt = \frac{1}{\varepsilon k F_m \phi T \xi_{RW}} \int_0^\infty \dot{C}_{RW}(t)\,dt \quad (2\text{-}27)$$

while for the CW monitor we have, using its proportionality constant (2-13),

$$\int_0^\infty Q(t)\,dt = \frac{1}{\varepsilon k F_m \phi T \xi_{CW}} \int_0^\infty \dot{C}_{CW}(t)\,dt \quad (2\text{-}28)$$

Recall that in both cases the proportionality constants become very simple for LL activity. As a practical matter, the upper limit of the integrals can be replaced with the time at which the monitor net countrate returns to "zero" counts per minute. Using this finite time means that we can estimate an average concentration over the episode, by dividing the concentration integral by the total time, i.e., (2-16).

In Fig. 2-12 we have an example run for an exponentially-decreasing $Q(t)$. We see that at the time corresponding to the sum of the transit time (120 minutes) and the time needed for the $Q(t)$ to become small, when the LL activity has been cleared (i.e., the net countrates are small), the integral estimates (2-27) and (2-28) agree with the true value, but not before. A similar plot can be made for SL activity.

A number of simulation runs of cases of $Q(t)$, including non-exponential behaviors, have verified (2-27) and (2-28). That is, no matter what the $Q(t)$ behavior is, as long as it, and the monitor net countrate, approach zero within the analysis period, we can obtain a *single* estimate of the integral of the concentration over the *entire* episode (not dynamically during it), by using the integrated countrate in (2-27) or (2-28). On the other hand the FF expressions above (2-18) to (2-20) are dynamic, and evolve during the course of the transient. Thus we can keep track of the current level of release (or uptake) as the situation develops. We note that both attempts at a quantitative use of moving-filter monitors (attained countrate or integrated counts) require a delay of some two hours before a result is possible. The only exception to this is the initial-slope method (2-7).

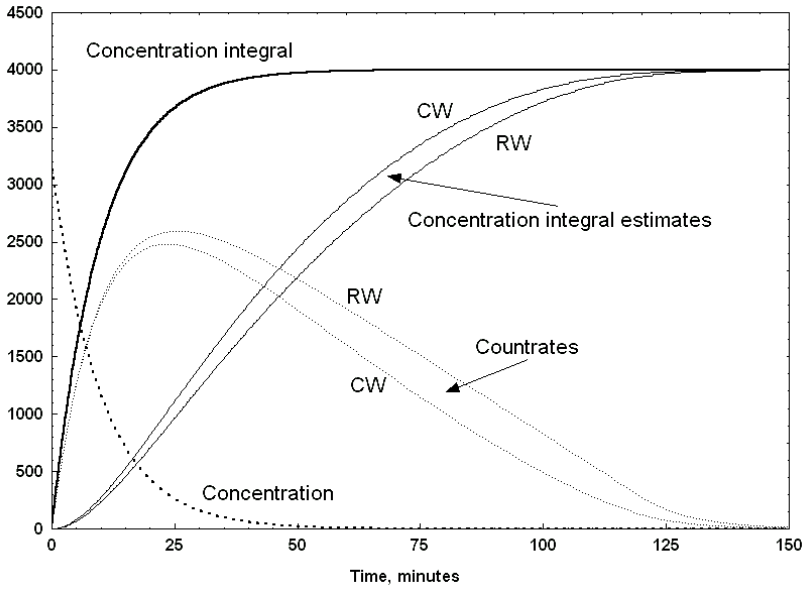

Figure 2-12. Moving-filter monitor estimation of concentration integral. Concentration and integral arbitrarily scaled to fit on countrate axis.

Integrated-Count Step-Advance Filter (ICSAF) Monitor

Introduction

In the early 1960's a new air effluent monitoring system was installed at the SM-1 Nuclear Power Plant, a small PWR operated by the U.S. Army Corps of Engineers Reactors Group, at Ft. Belvoir, VA. This system, built by Eberline Instrument Corp., had a number of novel features. Notable among these was the use of a stepped-advance particulate filter, operated as a fixed-filter until such time as a preset count was attained. That is, the net countrate from the particulate monitor's detector (a large plastic scintillator) was integrated by a scaler, and when the preset count was reached, a concentration estimate was output. At the same time, the filter paper, on a large roll, was advanced, clearing any accumulated activity, and the process was started anew.

In addition to this unusual quantification scheme, the system also had two parallel detection paths, one from the plant stack, and the other from the ambient air outside the plant. The idea was to subtract the countrate contribution from RnTn so that the monitor signal would represent only activity from the plant.

This system did not operate properly, mainly in the sense that it usually generated negative concentrations. Considerable time and money was spent attempting to get it to work correctly. The author, assigned to this plant from 1969-71, determined that the RnTn subtraction was the problem. The stack air was HEPA-filtered, and thus contained little or no RnTn, while the outside air of course did. This would lead to negative net counts, upon subtraction. Upon reporting this to those in command, who for their own reasons wanted it removed, the system was in fact removed from the plant.[4]

However, the Eberline system was well ahead of its time, and a question has remained as to whether it could have been made to work properly. In implementing the CPAM mathematical models in [1], this system was also coded. This was done strictly from memory, since no documentation of the system operating methodology was available. In running the numerical simulations, it became apparent that, with some adjustments to the basic principles of operation, this system could perform very well indeed, usually outperforming the more traditional monitors using the quantification methods discussed above.

The purpose of this section is to re-introduce this monitoring approach, and extend it with some mathematical analysis. It will be seen that this quantification scheme does perform very well, and monitors designed on these principles could be useful in a number of nuclear facility monitoring applications.

[4] Since the SM-1 still needed a stack effluent monitor, a replacement system, based on the Rb-88 Method (18) mentioned above, was developed and installed.

Principle of Operation

A continuous filter tape, similar to that used in an ordinary moving-filter monitor, is held fixed. Activity from the sampled air accumulates on the tape, just as for a fixed-filter monitor. The net countrate (background is subtracted) from the detector is accumulated in a scaler[5]. For reasons to be discussed below, the gross counts and background counts are also accumulated. When either a preset net count, or optionally, a countrate-dependent integration time, is reached, the filter is advanced quickly, clearing the deposited material, and the scalers are also reset to zero.

Thus this system might be called a "step-advance filter" (SAF). Although some monitors can be operated with a timed step-advance, with a constant preset time between filter advances, here we have the step advance occurring based on a control law, which responds to the activity seen by the monitor. Since the quantification method uses an integrated count, we can call this system an "integrated-count step-advance filter" (ICSAF) monitor.

Fig. 2-13, generated by the numerical simulation reported in [1], shows the ICSAF countrate response and scaler integrated counts for an exponential pulse of SL activity (Rb-88). The resets can clearly be seen. The count attained in the integration time period is used to calculate a concentration estimate, which is then output, and the process starts again. Thus, no countrate is output, only a concentration estimate. In Fig. 2-13 the curvature in the countrate due to the SL decay can just be seen, especially at the longer integration times (lower concentrations). The curvature of the integrated counts can also be seen.

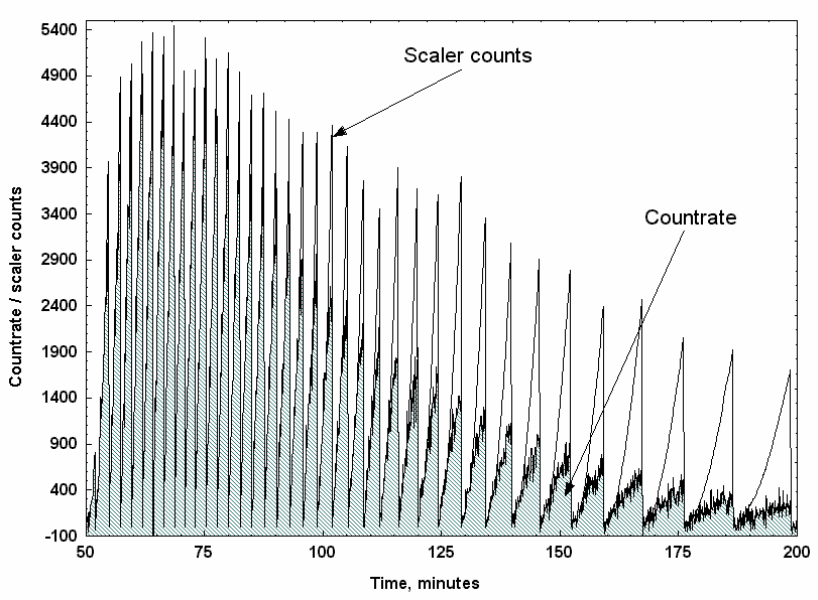

Figure 2-13. ICSAF scaler counts and countrate, exponential Q(t), SL activity.

For the mathematical basis of this quantitative approach, consider a fixed-filter monitor, with zero initial condition. The net counts integrated during an interval $0 \le t \le \eta$ will be, integrating (2),

$$C(\eta) = \varepsilon k \phi \int_0^{\eta} \exp(-\lambda t) \int_0^{t} Q(\tau) F(\tau) \exp(\lambda \tau) \, d\tau \, dt \tag{2-29}$$

In order to use this we need some form for both *F(t)* and *Q(t)*; let us begin by assuming both to be constant. Note that this means constant only over the interval [0 η], which is on the order of at most tens of minutes. Carrying out the integrations and solving for this constant concentration, we have

$$\hat{Q}_0 = \frac{C(\eta)}{\varepsilon k F_m \phi \frac{1}{\lambda^2} \{ \lambda\eta - [1 - \exp(-\lambda\eta)] \}} \tag{2-30}$$

[5] The familiar term "scaler" is used, for convenience, but in modern implementations this accumulation would be done in software.

For long-lived activity, the limit of (2-30) as the decay constant approaches zero is

$$\hat{Q}_0 = \frac{2\,C(\eta)}{\varepsilon\, k\, F_m\, \phi\, \eta^2} \tag{2-31}$$

which was the calculation done by the original system. However, since the primary particulate effluent from the SM-1 was Rb-88, the estimated concentrations, based on (2-31), would have been incorrect even if the system had functioned properly.

The fundamental idea of this monitor is that, every so often, we estimate a concentration, advance the filter, reset the scalers, and start the whole process all over again as if it had never been done before. There is no memory effect from one time period to the next. Thus we obtain a series of stepwise, independent estimates of the concentration, during its dynamic variation, whatever it may be.

A way of visualizing this is as a bank of FF monitors, each of which is used for some finite time, at the end of which a concentration estimate is generated, and we switch the air sampling to the next monitor, which is of course starting from a clean (zero) initial condition. In fact, the measurement defined by (2-30) could be viewed as a separate quantitative method for FF monitors, for a constant-Q.

Timeout Control

A "timeout" is a convenient term for the event when the instrument advances the filter and outputs a concentration estimate. A strategy for controlling these timeouts is an essential part of the instrument design. Since the monitor uses integrated counts for quantification, the behavior of the "scaler" (a count integrator, whether digital or analog) is of considerable interest. We are concerned with the time-dependent behavior of the scaler, unlike in most counting situations, where we just use the reading at the end of the counting time, since, as we will see, the dynamic behavior has an effect on our choice of a control strategy for the timeouts.

Scaler dynamics

Consider the accumulation of counts in a scaler, driven by a net countrate. We have, at the i-th step in a digital, discrete-time system with stepsize Δt,

$$C_i = C_{i-1} + \dot{C}_n\, \Delta t \tag{2-32}$$

The net countrate $\dot{C}_n$ is of course the gross countrate from the detector minus the background countrate. The background estimate we subtract may be either a fixed value, or random values that we observe at each time step, in a separate background detector.

What we have in (2-32) is a difference-equation form of a stochastic differential equation. It is "stochastic" because the quantity being integrated, the net countrate, is random. If no activity is present we will be subtracting our *estimate* of the background from an observed *sample* of the background and so the net counts per time step will be a zero-mean, constant-variance random process. This form of differential equation leads to a process called a "random walk" [10] for the counts in the scaler as a function of time.

When activity is present, the scaler-count process is a random walk with "drift" [11]. The drift represents a forcing function, which may be time-dependent, for the differential equation for the scaler counts. Once again, this forcing function will be stochastic. The general analytical solution for the scaler-count differential equation, with no random behavior, is just (2-29), and for the specific case of an assumed constant concentration (over relatively short time intervals), the solution is contained in (2-30).

As the activity increases, the drift dominates in (2-32) and the scaler counts increase in a manner that appears to be deterministic as the noise is dominated by the signal. In practice what happens is that, even at quite low concentration levels, the count integration results in the accumulation of many hundreds or even thousands of counts over modest time spans, on the order of tens of minutes.

We will illustrate the behavior of the scaler counts, for both zero- and nonzero-signal cases, but first we need to consider the time-dependent variance of the counts. This is more subtle than one might expect, given that the accumulation of counts is a simple process. The key issue is that the scaler-count random walks are realizations of a nonstationary random process. This

implies that any given realization of the process has no mean, or rather, mean values calculated over various subspans of the total time will not be equal.

However, an ensemble of realizations of the process will have a mean, and a variance which is *N* times the variance of the net countrate; *N* is the number of steps in the walk. For the zero-signal case this is exact, since that random walk will consist of the sum of *N* independent samples from a zero-mean, constant-variance random process. When there is activity present, the variance is approximate, since the net countrate is increasing, and so does the variance at each step (Poisson counts).

As will be developed below, we can write the standard deviation of the stochastic forcing function (i.e., the net countrate) in (2-32) as

$$\sigma_n = \sqrt{\sigma_s^2 + f\sigma_b^2}$$

where σ_s is the component due to the signal, that is, the activity, and σ_b is the component due to the background. For a fixed background, *f* is unity, while for a live-detector background, *f* is two.

The standard deviation of the random walks as a function of time will be

$$\sigma(t) = \sqrt{N}\,\sigma_n = \sqrt{\frac{t}{\Delta t}}\,\sigma_n$$

since we have taken *N* steps in time *t*, each of size Δt. We know that the mean and variance of Poisson counts are equal,

$$\sigma_{s,b}^2 = \dot{C}_{s,b}\,\Delta t$$

so that

$$\sigma_n = \sqrt{\dot{C}_s\,\Delta t + f\,\dot{C}_b\,\Delta t}$$

from which

$$\sigma(t) = \sqrt{\frac{t}{\Delta t}\left[\dot{C}_s + f\,\dot{C}_b\right]\Delta t}$$

$$\dot{C}_s = \frac{\varepsilon k F_m \phi Q_0}{\lambda}\left[1 - \exp(-\lambda t)\right]$$

and finally we have

$$\sigma(t) = \sqrt{t\left\{\frac{\varepsilon k F_m \phi Q_0}{\lambda}\left[1 - \exp(-\lambda t)\right] + f\,\dot{C}_b\right\}} \qquad (2\text{-}33)$$

Now we can illustrate the behavior of the counts. Consider Fig. 2-14. Here we have a set of 20 realizations of a zero-signal random walk, with one walk highlighted as a darker solid line. The background is 200 cpm, fixed estimate, and the isotope is Rb-88. The upper and lower bounds of an approximate 95% confidence interval, based on (2-33), on the walks are represented by the thinner solid lines. We see that this small ensemble does appear to stay within these bounds, across the 120-minute integration interval. Longer-time runs, with many more realizations, confirm this.

Next we have Fig. 2-15, which is the same as Fig. 2-14 except it has a nonzero Q_0 at 10^{-11} μCi/cc, a low level for a CPAM. Now we see the upward trend of the counts across the interval; the solid line at the center is the analytical solution, from (2-29). The "error bounds" again are describing the ensemble behavior nicely.

Timeout on preset count

The original system used a preset count; as far as is known today, this preset was fixed. A fixed preset count has problems at both high and low concentrations. At high concentrations, the system will timeout too often, since the preset count can be attained very quickly. This would lead to excessive filter movement. On the other hand, low concentrations may lead to very long timeout intervals.

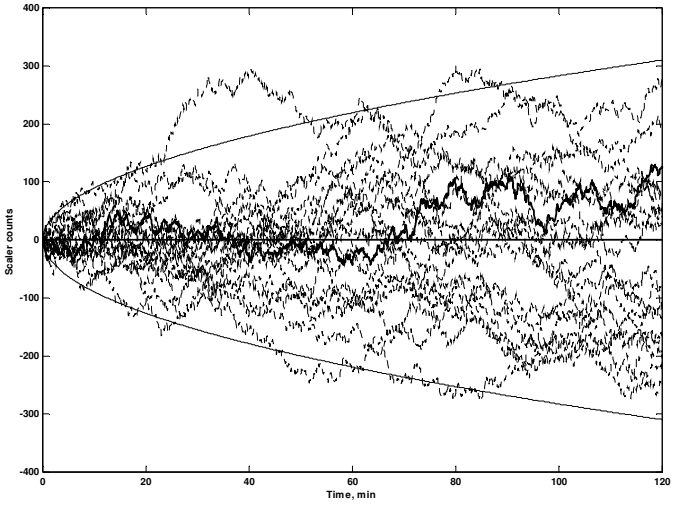

Figure 2-14. ICSAF scaler random walk, 20 realizations, zero signal, background 200 cpm. Bounds drawn using (2-33). One realization highlighted in bold line.

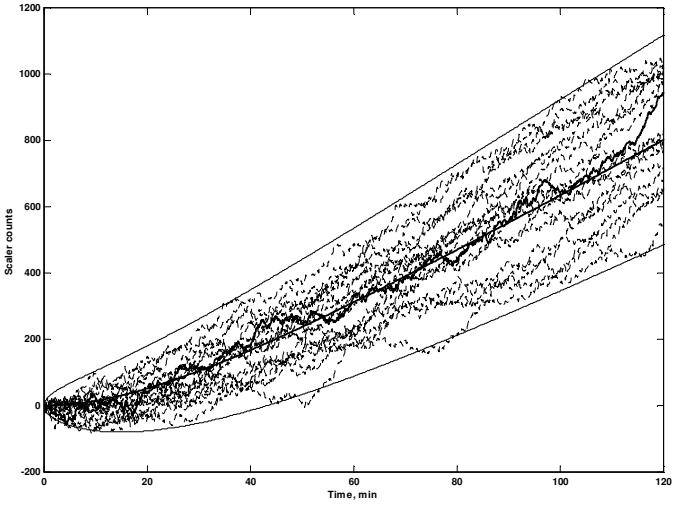

Figure 2-15. ICSAF scaler random walks, Rb-88 constant concentration 10^{-11} μCi/cc, 20 realizations. Bounds drawn using (2-33), central line using solution from (2-29).

To correct this, in the numerical simulation adjustments were made to the preset count, based on the time intervals between resets. If these were too short, the preset count was scaled up by a factor of ten. If they became too long, the preset was scaled back down. A minimum preset of 100 counts was enforced. This worked reasonably well, but the scaling rules were entirely ad hoc, and the system could sometimes run for extended times without a measurement output.

Consider Fig. 2-16, a zero-signal random walk, where we have one timeout, based on attaining 100 counts, early in the run, and then none at all for several hours. When, eventually, the scaler random walk finally reaches the preset count, the concentration calculation will use the elapsed time since the last timeout. This timeout is not caused by the buildup of activity on the filter, which is assumed by the quantification expression, (2-30), so that the indicated concentration will be incorrect. We will discuss this further, below.

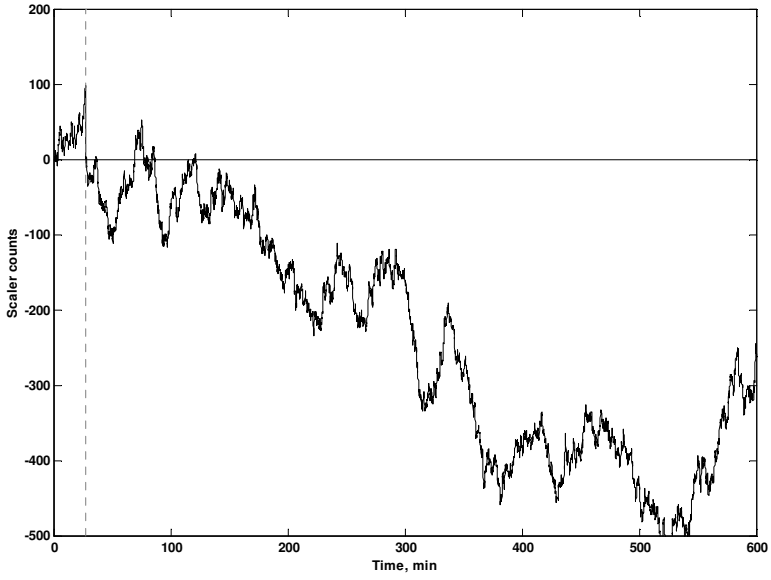

Figure 2-16. Zero-signal ICSAF scaler counts vs. time, background 200 cpm, using preset count (100 counts) control, illustrating a long random walk, of several hours, with no timeout.

These long random walks provide an alternate explanation for the negative concentrations seen in the original system at the SM-1. Even without the RnTn subtraction, the scaler, if read periodically before the preset count was reached, would show negative counts during some portions of these random walks. Since the system would not have produced an output for, perhaps, several hours, it may have been designed to output a concentration estimate every so often, say, every hour. If the scaler was negative at this time, then of course the concentration estimate would also be negative.

Timeout on countrate-controlled time

Another approach for controlling the instrument is to vary the time periods between timeouts, using shorter periods at higher concentrations, but with a minimum, and longer periods at lower concentrations, but with a maximum. We would like to have concentration estimates more frequently when the concentration is at higher levels, and we can wait longer at lower concentration levels. However, there should be some upper limit on this integration time, so that we can get a reading reasonably often. We can use the countrate as an indicator of current concentration level.

One simple control law, tested empirically, is to define the integration time η by

$$\eta = 1 + \frac{100\,\Delta t}{C_g} \tag{2-34}$$

where C_g is the gross count observed in one digital time step, of size Δt seconds, and η is restricted to some maximum, e.g., 20 minutes. The shortest allowable time is one minute. The factor of 100 is arbitrary, and scales the time values η, in minutes, into a convenient range. This is the relation used in the ICSAF simulation.

Analytically, we would like to relate these integration times to concentrations, via the countrate. To do this, we can write for the gross countrate, for a constant concentration over the time η,

$$\dot{C}_g(\eta) = \frac{\varepsilon k F_m \phi Q_0}{\lambda}\left[1 - \exp(-\lambda\eta)\right] + \dot{C}_b$$

and we can then multiply by the time step Δt to obtain counts, and use the result in (2-34). If we then try to solve for the time η, we will have a transcendental equation, which can only be solved numerically (or perhaps via a series expansion). We can make progress more readily by considering a long-lived nuclide, for which we can write

$$\eta = 1 + \frac{100\,\Delta t}{\left(\varepsilon k F_m \phi Q \eta + \dot{C}_b\right)\frac{\Delta t}{60}}$$

where the denominator is the LL gross countrate, cpm, times the digital step size, in minutes, to obtain gross counts. We can then solve this for η, which gives

$$\eta(Q) = 0.5\left[1 - \frac{\dot{C}_b}{a} + \sqrt{\left(1 + \frac{\dot{C}_b}{a}\right)^2 + \frac{24000}{a}}\right] \tag{2-35}$$

$$a = \varepsilon k F_m \phi Q$$

To illustrate, (2-35) leads to integration times as follows, for a background of 200 cpm and LL activity: 10^{-5} μCi/cc or greater, 1 minute; 10^{-6}, 1.1 minutes; 10^{-7}, 1.8 minutes; 10^{-8}, 4.0 minutes; 10^{-9}, 10.2 minutes; 10^{-10} or less, 20 minutes. For SL activity, solutions found numerically indicate, for the same concentrations and background, values which are only slightly larger than these, with about a ten percent increase for concentrations below about 10^{-9} μCi/cc.

Note that the control law is evaluated at each time step, i.e., on a scale of a few seconds. Thus η can quickly be brought to a short value when there is a concentration transient. Other control laws are of course possible, and the maximum and minimum periods can also be adjusted. A minimum of less than 1 minute is not recommended, since the filter would be advancing too frequently. In some applications, a maximum of greater than 20 minutes might be acceptable.

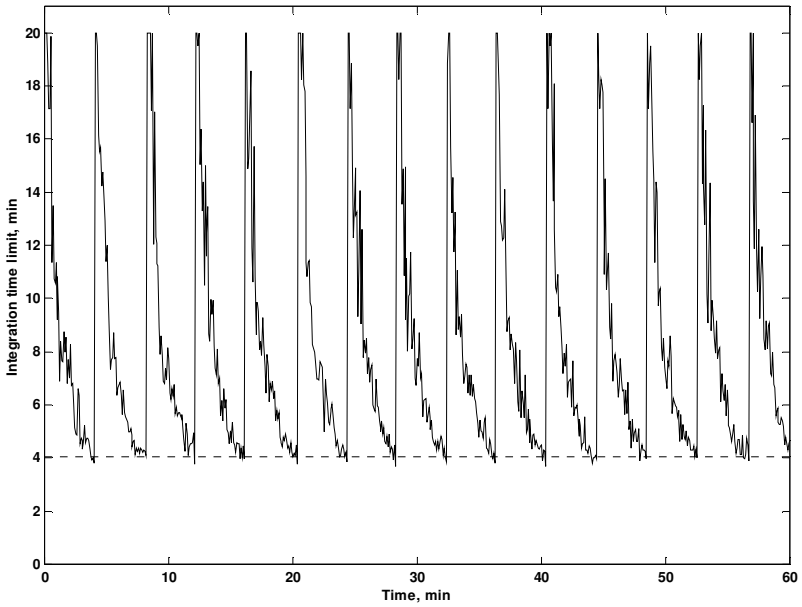

Figure 2-17. ICSAF timeout limit as dynamically calculated per time step, with a constant concentration of 10^{-8} μCi/cc. Dotted line is integration time from (2-35).

Fig. 2-17 illustrates how the integration times vary during an episode of a constant concentration at 10^{-8} μCi/cc. Here, the timeouts are occurring about every four minutes. The integration time starts out at 20 minutes (the maximum η) at the start of each interval, because, then, the countrate is low. As activity builds up on the filter, the countrate increases, so the calculated integration time decreases, as shown. Eventually the integration time and the elapsed time intersect, and a timeout is declared. In the figure, the value from (2-35) is indicated with a horizontal dotted line. Clearly the actual timeout periods are matching this value.

As we saw in Fig. 2-16, if we operate on preset count, we can have long random walks for low concentrations. With the countrate-dependent integration time mode of operation, we force timeouts, and reset the scalers periodically, resulting in a process where the zero-signal random walk is constrained to 20 minutes, and long negative walks are no longer possible. The random process stays closer to the zero level.

However, at a forced timeout, the net scaler can of course still have a negative reading. We could output some flag value for the concentration, or not output anything at all, and just carry on to the next interval. The instrument should have some visible output, however, at all times, such as the current scaler reading, or the current net countrate, so that we know it is operating correctly. It may also be possible to detect that no activity is present, and to reset the scalers without advancing the filter, thus saving a considerable amount of filter paper. At a minimum this can be done when the net scaler is negative at the 20-minute forced timeout.

Example concentration-estimate plots

In Fig. 2-18 we have the same *Q(t)* as in Fig. 2-8. The concentration estimates (circles) are plotted at the time of evaluation. As with the five-minute Rb-88 Method (2-22), the ICSAF follows the concentration dynamics well. Fig. 2-19 is an expanded view of the same data as Fig. 2-18, and here we can see the estimates following the concentration during each integration interval (the solid lines to the left of each circle). Note that these intervals become longer as the concentration decreases.

Fig. 2-20 shows the ICSAF concentration estimates for a complex, wide dynamic-range *Q(t)* behavior, for Rb-88. The estimates are clustered so close to the true values (solid line) near the peak that they cannot be separated. A series of pulses of Rb-88 activity will produce concentration estimates very similar to those shown in Fig. 2-9; the ICSAF will track these pulses closely.

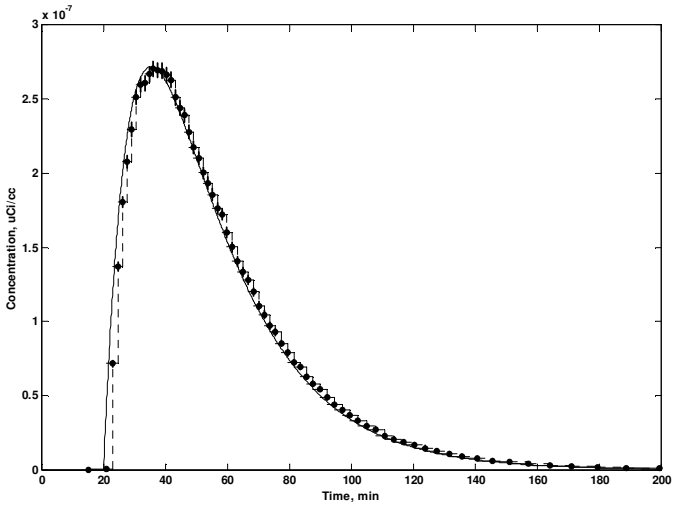

Figure 2-18. ICSAF concentration estimates, exponential Q(t), Rb-88.

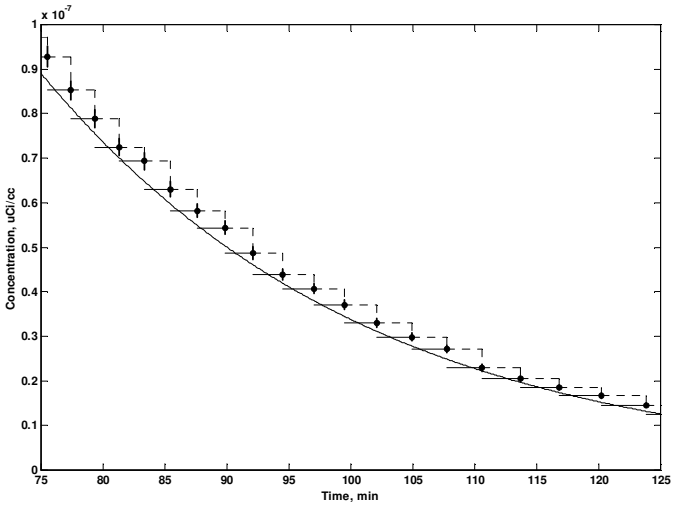

Figure 2-19. Expanded view from Fig. 2-18.

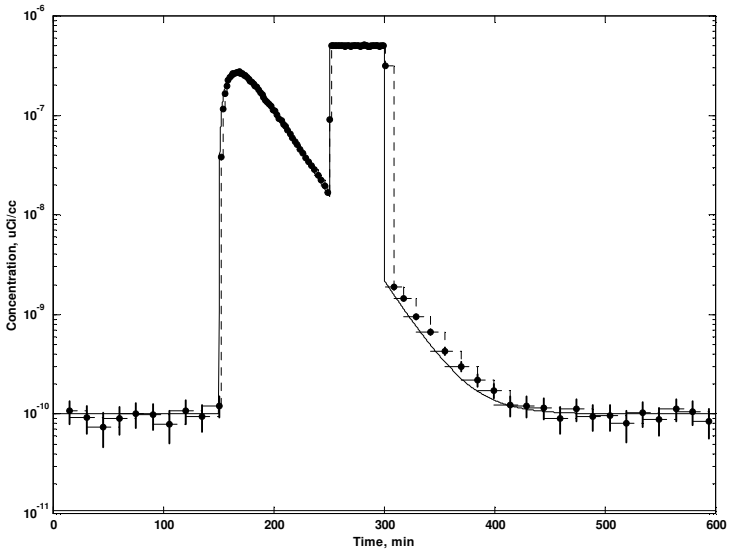

Figure 2-20. ICSAF concentration estimates, exponential plus pulse, Rb-88 activity.

Uncertainty Analysis

As with any measurement system, we would like to have some idea of the uncertainty (loosely, "error") in the instrument's output. For the ICSAF, this will be the concentration estimates.

Concentration error

To simplify the notation, first define a factor which is a function of the integration time η; this is the denominator of (30):

$$v(\eta) = \frac{\varepsilon k F_m \phi}{\lambda^2} \left\{ \lambda\eta - \left[1 - \exp(-\lambda\eta) \right] \right\} \tag{2-36}$$

which for LL activity is

$$v(\eta) = \varepsilon k F_m \phi \frac{\eta^2}{2}$$

From (2-30), the error in the concentration estimate is controlled by the error in the integrated net counts, if we ignore the errors in the flow rate, efficiency, etc.[6] and also consider the integration time to be nonrandom, so that

$$\mathrm{var}\left[\hat{Q}\right] = \frac{\mathrm{var}\left[C_n(\eta)\right]}{\upsilon(\eta)^2} . \tag{2-37}$$

where C_n is the net count attained in the integration time η. The gross count C_g, which we observe, is of course the sum of the signal count C_s and background count C_b, so that

$$\begin{aligned} \mathrm{var}\left[C_n(\eta)\right] &= \mathrm{var}\left[C_g(\eta)\right] + \mathrm{var}\left[C_b(\eta)\right] \\ &= \mathrm{var}\left[C_s(\eta)\right] + \mathrm{var}\left[C_b(\eta)\right] + \mathrm{var}\left[C_b(\eta)\right] \end{aligned} .$$

When we use a well-estimated, stable, fixed background, we could find a variance estimate for it, but more likely we would just assume the uncertainty in this estimate is negligibly small, and we can then drop the last term in the variance expression above. For a live background we do need to include the uncertainty in that estimate.

We will have, using the fact that counts are Poisson distributed, making the mean and variance equal,

$$\sigma\left[C_n(\eta)\right] = \sqrt{C_s(\eta) + f\, C_b(\eta)} \tag{2-38}$$

where f is unity for fixed background, and two for a live background. This is similar to the development in, e.g., [13]. Note that what is termed a "fixed" background here corresponds to "well-known blank" in [13], and "live" here is "paired" there. The factor f in (2-38) relates these two cases.

Combining (2-37) and (2-38) we obtain the concentration error estimate, based on the observable quantities C_g and C_b:

$$\sigma\left[\hat{Q}\right] = \frac{\sqrt{C_g(\eta) + (f-1)C_b(\eta)}}{\upsilon(\eta)} \tag{2-39}$$

The relative error in the concentration estimate is

$$\frac{\sigma\left[\hat{Q}\right]}{\hat{Q}} = \frac{\sqrt{C_g(\eta) + (f-1)C_b(\eta)}}{\upsilon(\eta)\,\hat{Q}} \tag{2-40}$$

We can also write, replacing C_s in (2-38) with its analytical counterpart, from (2-30),

$$\frac{\sigma\left[\hat{Q}\right]}{\hat{Q}} = \frac{\sqrt{\upsilon(\eta)\,Q + f\,\dot{C}_b\,\eta}}{\upsilon(\eta)\,Q} \tag{2-41}$$

for use in parametric studies of the relative error, where we can assume values for the concentration and background countrate.

In Fig. 2-21 we have a plot of (2-41) as a function of the concentration, for both fixed and live background, at 200 cpm. The integration time η was obtained using (2-35), so we must use LL activity. The simulation was run for 1000 minutes at several settings of a constant concentration, and the mean, median, and standard deviation of the estimated concentrations were found. The mean of the calculated errors, using (2-39) for each estimated concentration, was also found.

The solid line is the function (2-41), while the symbols represent the relative errors corresponding to the observed standard deviations of the many estimated concentrations at each setting. That is, at each concentration setting, many ICSAF concentration estimates were generated (at least 40, at the low concentrations, and many hundreds at the higher concentrations). We find the scatter of these concentrations, and compare that to the predicted relative error, (2-41). This was done for a fixed (lower curve, squares) and live (upper curve, asterisks) background.

[6] However, see [12] for some background on this aspect of the error analysis. These errors are often significant and should be considered.

Fig. 2-21 has a horizontal line drawn at the 10% level. This leads to a concentration on the *x*-axis which represents that concentration which can be estimated to 10% relative error at "one sigma." This could be a performance specification for the measurement capability (not detection limit) of the instrument. The bend upward at the low-concentration end of Fig. 2-21 is due to the 20 minute limit on the integration time. At the high-concentration end the curve turns downward due to the one-minute limit; this is more count time than is needed at high concentrations, thus improving the relative error, but we don't want the filter to advance more rapidly than this.

We see in Fig. 2-21 that the agreement between (2-41) and the observed relative errors is reasonably good. There is, however, a subtle issue that arises for concentrations in the area of 10^{-9} or 10^{-10} μCi/cc. Close inspection of the clusters of error estimates, especially those from (2-39), which have small dispersion, show that the curve of (2-41) slightly underestimates the uncertainty in the concentration estimates. Investigation reveals that the reason for this is that the integration time from (2-35) tends to slightly overestimate the attained integration time, particularly for low concentrations and high backgrounds. This is because the integration time η, from (2-34), is in fact a random variable, due to the gross counts, and it has substantial scatter under these conditions. What happens is that the dynamically-calculated integration time from (2-34) can, randomly, be several minutes less than the deterministic value from (2-35). This, randomly, leads to a shorter integration interval in the simulation data than (2-35) and (2-41) expect, and so the observed relative errors are slightly above the curve. At lower concentrations we have a fixed η, at 20 minutes, so that this problem vanishes. At higher concentrations the gross count per time step is large enough that the behavior of (2-34) looks very much like that predicted by (2-35).

In Fig. 2-22 we have a plot of the relative error vs. concentration as the background varies, using (2-41) with integration times from (2-35). This is similar to Fig. 2-21, but for several values of the background. The fixed background ranges from 50 cpm to 500 cpm in steps of 50 cpm. The lower backgrounds produce smaller relative errors, seen in the curves toward the bottom of the plot. A plot for live background is very similar, just shifted slightly (somewhat larger relative error for a given concentration and background level, due to the live estimation of the background).

In Fig. 2-22 the maximum integration time is 60 minutes, which leads to smooth curves. If the maximum integration time was artificially forced to be, e.g., 10 minutes, we would see an upward "bending" of the curves, resulting from too short an integration time being used at the lower concentrations. That is, the relative errors would be larger than they would be if we had used a longer integration time. This is of course well understood in concept, but with (2-41) and (2-35) we can explore these effects quantitatively.

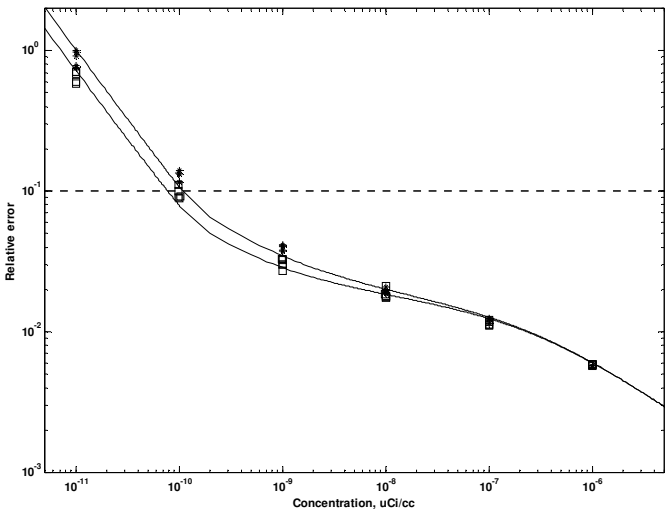

Figure 2-21. ICSAF concentration relative error vs. concentration. Symbols are for data generated by simulations. Lower curve is from (2-41) for fixed background of 200 cpm, upper curve for live background. Integration times vs. concentration from (2-35), with maximum of 20 minutes. Squares, fixed background; asterisks, live background.

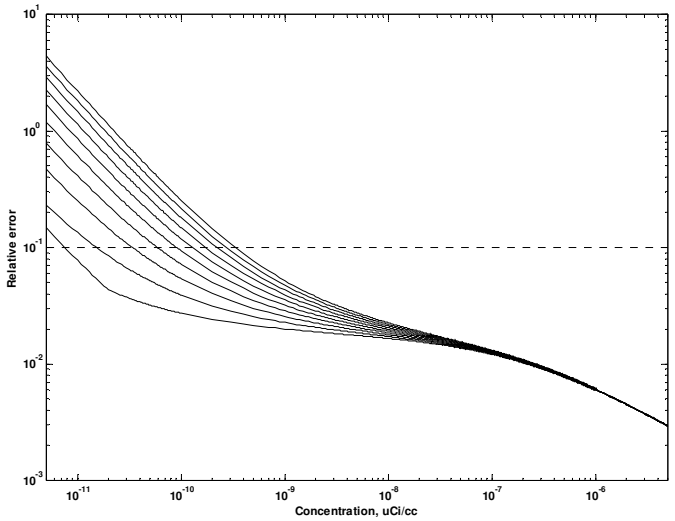

Figure 2-22. ICSAF concentration relative error from (2-41), vs. concentration, with 60 minute limit on maximum integration time. Parameter is (fixed) background, from 50 to 500 cpm in steps of 50, with 50 cpm at bottom of set. Integration time vs. concentration from (2-35).

Zero-Signal Indicated Concentration

The ICSAF will generate a concentration estimate whenever the scaler counts are positive at a timeout. When the concentration is low, timeouts are forced, e.g., every 20 minutes. If the scaler count is positive, a "zero-signal indicated concentration" will be produced. It would be useful to have some idea as to the level of these outputs, since this acts as a sort of "floor" below which we cannot obtain a meaningful reading. Note that these outputs treat the attained scaler count as if it had come from activity, when in fact this is not the case.

From (2-33) the standard deviation of the random walks during the integration time will be, when the concentration is zero,

$$\sigma(\eta) = \sqrt{f \dot{C}_b \eta} \tag{2-42}$$

This describes the scatter in the scaler counts at time η. Note that this is just the usual Poisson relation, the square root of the counts attained at the end of the counting time. This variation is about a mean of zero, but we are only interested in the positive half of the data, since negative scaler counts are meaningless. The upper bound of the positive scaler counts would be some multiplier, based on a percentage point of a probability distribution function (PDF), times (2-42). We often would use the Normal PDF for this. If so, then we might consider the average, or mean, level of positive scaler counts we would expect to observe for a given value for (2-42).

This mean value is given by

$$\mu = \frac{\frac{1}{\sqrt{2\pi}\,\sigma}\int_0^\infty x \exp\left(\frac{-x^2}{2\sigma^2}\right) dx}{\frac{1}{\sqrt{2\pi}\,\sigma}\int_0^\infty \exp\left(\frac{-x^2}{2\sigma^2}\right) dx} = \sqrt{\frac{2}{\pi}}\,\sigma$$

so that the mean zero-signal indicated concentration is

$$Q_{mean}(\dot{C}_b, \eta) = \frac{\mu}{\upsilon(\eta)} \approx \frac{0.8\sqrt{f \dot{C}_b \eta}}{\upsilon(\eta)} \tag{2-43}$$

We can also write for the minimum detectable concentration (MDC), using one of the standard formulations [13]:

$$MDC(\dot{C}_b, \eta) = \frac{2.71 + 3.29\sqrt{f \dot{C}_b \eta}}{\upsilon(\eta)} \tag{2-44}$$

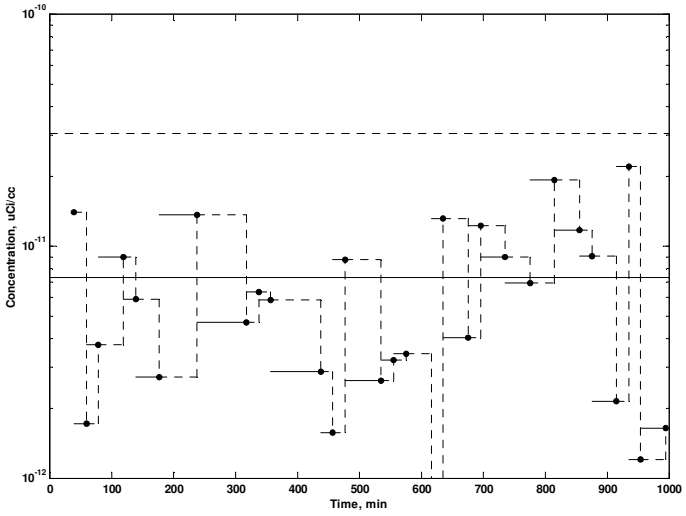

Figure 2-23. ICSAF zero-signal indicated concentrations. Fixed background, 200 cpm, Rb-88 estimation. Solid horizontal line is mean value expected, from (2-43), dotted horizontal line is MDC, from (2-44).

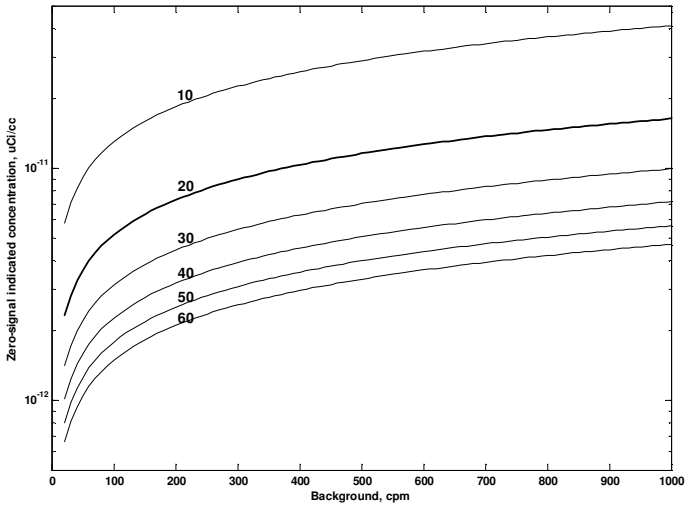

Figure 2-24. ICSAF zero-signal indicated concentration mean values vs. background and maximum integration time, from (2-43). Fixed background, Rb-88 estimation.

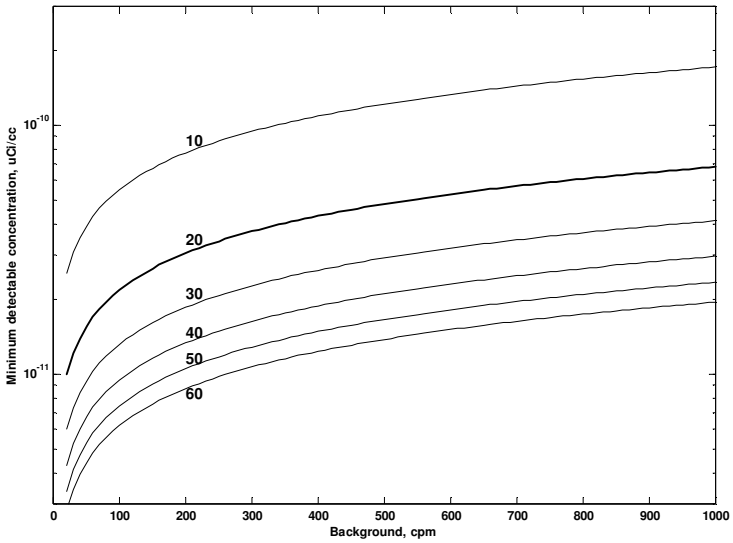

Figure 2-25. ICSAF MDC vs. background countrate and maximum integration time, from (2-44). Background fixed, Rb-88 estimation.

In Fig. 2-23 we have a long zero-signal run, with a fixed background at 200 cpm, estimating Rb-88 concentrations, with the maximum integration time at 20 minutes. The solid line is (2-43), while the dotted line is (2-44). There is a lot of scatter in the concentration estimates, but simulation runs have shown good agreement between (2-43) and the observed mean of the zero-signal indicated concentrations, for both fixed and live backgrounds.

In Fig. 2-24 are curves of (2-43) evaluated as a function of the (fixed) background level, for several settings of the maximum integration time, for Rb-88. Fig. 2-25 has curves of the MDC (2-44) for the same variations.

Conclusion

Methods and applications

We have discussed a number of methods for using CPAMs for quantitative assessments of airborne radioactivity. The measurements can be of concentrations or the time integral of concentration. We have the following candidate measurement methods, for a given application (equation numbers indicated in parentheses):

(a) FF derivative (2-5)
(b) FF initial slope (2-7)
(c) MF initial slope (2-7)
(d) FF attained countrate after delay (2-8)
(e) MF attained countrate after delay (2-9), (2-11)
(f) FF continuous concentration integration (2-18), (2-19), (2-21)
(g) FF short-cycle concentration integration (2-22)
(h) MF continuous concentration integration (2-27), (2-28)
(i) ICSAF (2-30)
(j) Numerical integral of FF derivative $Q(t)$ estimates
(k) Numerical integral of ICSAF $Q(t)$ estimates

We might break down CPAM applications into four main groups: effluent monitoring; occupational exposure assessment and monitoring; process monitoring and control; containment leak detection. Each application will have its requirements, for such considerations as response time, detection sensitivity, estimation of concentration vs. integrated concentration, and so on. Similarly, each measurement approach will have its strengths and weaknesses as a candidate for a given application.

There are far too many combinations of measurement methods and application requirements for a thorough analysis here. However, we can try to suggest, based on the material presented above, a few methods that might have a good chance of success in some applications.

For effluent monitoring of concentrations, methods (a), (g), (i) can all work well. For releases, methods (f), (j), (k), and in some cases, (h) are good possibilities. The same candidates will serve for occupational exposure assessment, with the concentration time-integral estimation for effluent releases being analogous to those for DAC-hour exposures. In process control we have a need for rapid response, and are usually only concerned with concentrations, so that (a), (b), (c), (i) are worthy of consideration, although the one-minute minimum response time of (i) might be too slow for some applications. Containment leak detection[7] is also a concentration-based measurement for which we might use methods (a), (d), (e), (g), and (i).

General comments on methods

The countrate derivatives are excessively noisy as concentration estimates for FF monitors, unless some variance reduction is applied, such as the radar filter (6). The latter can provide reasonably good, real-time tracking of concentration behaviors. It will, however, exhibit lag for rapidly-changing concentrations. The filter gains should be optimized for the specific application.

The initial-slope approach can provide a rapid estimate of the initial level of a concentration, for FF and MF monitors. However, some $Q(t)$ behaviors have a zero initial level, and in those cases the initial slope method will not be of any use. Thus it is important to have models for the dynamics of the $Q(t)$ behavior, so that the applicability of the various measurement methods can be assessed.

Moving-filter monitors cannot provide real-time concentration estimates, and we must wait some two hours in order to use them for estimation of a constant concentration (which in practice is not likely to be constant for two hours), or for use as a total-episode concentration integral, such as a DAC-hour estimate. In both cases the output is a single number and is not dynamic. These monitors will clear LL activity and/or attain an "equilibrium" countrate for LL activity, so that in some applications where LL activity was present, MF monitors would be useful. Of course, another consideration is dust loading, in situations where that is a problem; MF monitors were developed primarily to alleviate this concern.

The FF Rb-88 Method is an excellent choice for episodic effluent releases, and for DAC-hour estimation. Its short-cycle cousin, the five-minute average concentration estimate, can follow concentration transients well, if we can accept the five-minute lag. In some cases this would not be acceptable, and in others a measurement every five minutes would represent great progress and would be very useful.

The ICSAF monitor also provides good tracking of dynamic concentration behaviors. Its output of periodic concentration estimates can readily be integrated, to provide release or DAC-hour estimates. It has a lag also, but it is shorter at higher concentrations, as we would require. This is a more complex instrument, but it has the best performance in terms of, simultaneously, detection sensitivity in a given length of time, ability to track changes in the concentration, and precision of estimation, as we will see next.

Concentration-estimate relative errors

Finally, we can consider the quality of the concentration measurements made by several of the methods, and compare them via the relative error of the estimates.

For the FF derivative method (2-5), in addition to the uncertainty in the countrate estimate, there is of course also uncertainty in the rate (derivative) estimate. The magnitude of this error depends on the technique used to estimate the derivative. Using the radar-filter derivative, the square symbols in Fig. 2-26 show the results of a simulation study for the relative error in these concentration estimate vs. the concentration. The best this approach can do, at the higher concentrations, is only about ten percent (these are "one-sigma" relative errors). Below a concentration of about 10^{-9} μCi/cc the relative error is nearly 100 percent, making the estimate useless as a measurement.

The short-cycle Rb-88 Method (22) uses both a countrate and the integral of the countrate. Note that, used as a concentration estimator, it runs only over short times, e.g., five minutes. Thus it will not accumulate many counts at lower concentrations. Its relative error performance is also shown in Fig. 2-26 (circles), and it is essentially the same as that of the derivative method.

These two sets of simulation runs consisted of sets of five 200-minute runs at a constant concentration, from which the

[7] This application will be discussed in detail in a future paper, using matrix-based linear systems compartmental modeling.

observed scatter was estimated. Some simulation results for initial-slope relative errors are also shown (asterisks) in Fig. 2-26. These are quite good at the higher concentrations, since they are based on a regression. However, this approach fails for lower concentrations, below about 10^{-9} μCi/cc, where the signal-to-noise ratio becomes poor.

The FF attained-countrate-after-delay approach is shown as the dotted curve in Fig. 2-26. This uses the same delay time as the ICSAF η in a relation similar to (41), namely

$$\frac{\sigma\left[\hat{Q}\right]}{\hat{Q}} = \frac{\sqrt{v_{FF}(\eta)Q + f\,\dot{C}_b\,\kappa^2}}{v_{FF}(\eta)Q}$$

$$v_{FF}(\eta) = \frac{\varepsilon\, k\, F_m\, \phi}{\lambda}\left[1 - \exp(-\lambda\eta)\right] \qquad (2\text{-}45)$$

where κ is a constant, 1.6, estimated from Monte Carlo experiments that relate the AEWMA countrate variance to the countrate level. This is necessary since the gain of the AEWMA adaptive linear filter is a random variable, so no closed-form relation is available.

The solid curve in Fig. 2-26 is the ICSAF relative error, using (2-41) with integration times η from (2-35). We see that the ICSAF relative error is at least as good as the FF methods, and is superior at the lower-concentration end of the range.

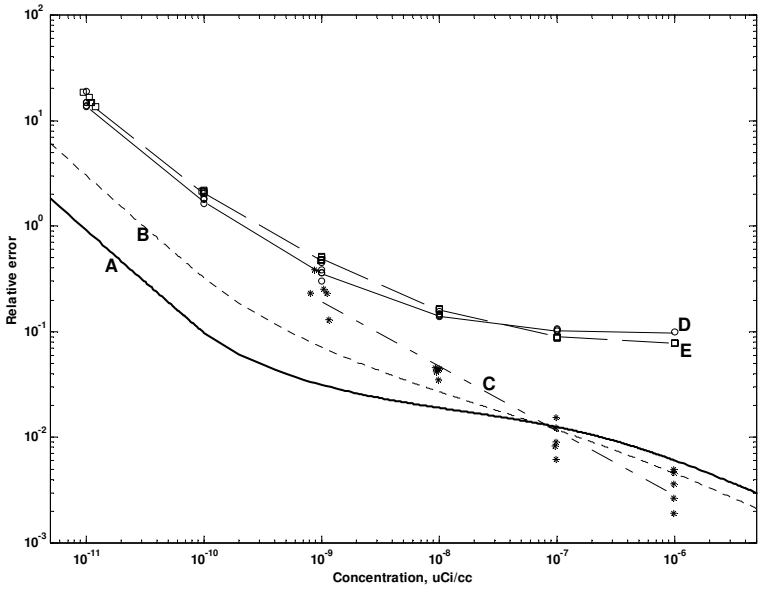

Figure 2-26. Concentration-estimate relative errors. Curve A is ICSAF; B is FF attained countrate at same delay times as ICSAF integration times; maximum integration time 20 minutes. Data symbols: C, initial slope; D, Rb-88 Method five-minute averages, using (2-22); E, FF derivatives, radar filter. Rb-88 estimation, fixed background 200 cpm.

Minimum detectable concentrations

A closely related issue is the MDC performance of the methods. For concentration estimation, the FF derivative is not going to provide much competition to the ICSAF, since the former is based on counts accumulated over only a few seconds. The initial-slope method fails at low concentrations. The only other candidates would be the FF and MF attained-countrate approaches. Of these, the FF is the best, since its countrate is always larger than that of the MF monitors, all else being equal.

The MDC for the FF attained countrate is, using the same formulation as for the ICSAF,

$$MDC_{FF}(\dot{C}_b, \eta) = \frac{2.71 + 3.29\kappa\sqrt{f\,\dot{C}_b}}{\upsilon_{FF}(\eta)} \tag{2-46}$$

Here we use the countrate-variance factor κ since, unlike the ICSAF, the FF utilizes a countrate rather than an accumulated count. Also note that the time η is not multiplied under the radical, unlike (2-44).

For the RW monitor we would usually have an integration time η which is less than the monitor transit time T, so that we can re-use (2-46) with

$$\upsilon_{RW}(\eta) = \varepsilon k F_m \phi \left\{ \begin{array}{l} \frac{1}{\lambda^2 T}\left[\lambda\eta - 1 + \exp(-\lambda\eta)\right] \\ + \frac{1}{\lambda}\left(1 - \frac{\eta}{T}\right)\left[1 - \exp(-\lambda\eta)\right] \end{array} \right\}$$

in the denominator to obtain the RW MDC. This denominator is based on (1-23). If the time η should be greater than or equal to T, then we use, from (1-25),

$$\upsilon_{RW} = \varepsilon k F_m \phi \left\{ \frac{1}{\lambda} - \frac{1}{\lambda^2 T}\left[1 - \exp(-\lambda T)\right] \right\}$$

in (2-46). Note that this denominator is not a function of η, since the monitor attains a constant countrate after the transit time T. The RW of course also uses a countrate, like the FF, so that the variance factor κ in (2-46) still applies. The MDC for a CW monitor can be approximated using the RW expressions, and substituting for the window length a value

$$L = \frac{16\,R}{3\pi}$$

where R is the CW window radius. This is (1-14).

Using these expressions it can be shown that the ratios of the ICSAF MDC to that of the FF and RW, using for the latter the same delay time as the maximum integration time of the ICSAF, are

LL, 20 min integration..... 0.273, 0.250
SL, 20 min integration..... 0.242, 0.225
LL, 60 min integration..... 0.157, 0.118
SL, 60 min integration..... 0.116, 0.097

where the first result in each row is FF and the second is RW, and the latter is smaller (worse) than the FF in each case. These ratios are for a fixed background of 200 cpm, and the values are nearly constant with increasing background above this level. At lower backgrounds the ratios are even more strongly in the ICSAF's favor. The SL nuclide is Rb-88.

In conclusion, from the above analyses we see that the ICSAF performance, both in terms of qualitative detection and quantitative measurement, is very good, and thus this monitoring approach should be considered for nuclear facility particulate air monitoring.

References

[1] W. C. Evans, "Mathematical Models for the Dynamic Response of Continuous Particulate Air Monitors," *IEEE Trans. Nucl. Sci.* vol. 48, no. 2, pp. 202-218, April 2001. Chapter 1 here.

[2] G. L. Helgeson, "Determination of Concentrations of Airborne Radioactivity," *Health Physics* vol. 9, pp. 931-942, Sept. 1963.

[3] D. C. Montgomery, L. A. Johnson, *Forecasting and Time Series Analysis*, New York: McGraw-Hill, 1976, p. 57.

[4] W. C. Evans, "Digital Countrate Estimation Using Adaptive Exponentially-Weighted Moving Averages," *Trans. Am. Nucl. Soc*., vol. 32, p.134, June 1979.

[5] D. R. Frieden, *Principles of Naval Weapons Systems*, Annapolis, MD: Naval Institute Press, 1985, p. 164.

[6] N. R. Draper, H. Smith, *Applied Regression Analysis*, 2nd Ed., New York: Wiley, 1981, Chapter 2.

[7] M. Basseville, I. V. Nikiforov, *Detection of Abrupt Changes*, Englewood Cliffs, New Jersey: Prentice-Hall, 1993.

[8] H. Baron, "Response Dynamique D'Un Appariel De Detection Des Aerosols Radioactifs", in *Assessment of Airborne Radioactivity.* Vienna, Austria: International Atomic Energy Agency, 1967.

[9] W. C. Evans, "Quantitative Assessment of Time-Varying Rb-88 Using Continuous Air Monitors," *Trans. Am. Nucl. Soc*. vol. 24, p. 129, 1976.

[10] G. E. P. Box, G. M. Jenkins, G. C. Reinsel, *Time Series Analysis: Forecasting and Control*, 3rd Ed., Englewood Cliffs, New Jersey: Prentice-Hall, 1994, p. 129.

[11] J. D. Hamilton, *Time Series Analysis,* Princeton, NJ: Princeton University Press, 1994, p. 495.

[12] U. S. Nuclear Regulatory Commission, NUREG-1507, "Minimum Detectable Concentrations with Typical Radiation Survey Instruments for Various Contaminants and Field Conditions", Section 3, Statistical Interpretations of Minimum Detectable Concentrations.

[13] L. A. Currie, "Limits for Qualitative Detection and Quantitative Determination: Application to Radiochemistry", *Analytical Chemistry*, vol. 40, no. 3, pp. 586-593, March 1968.

Updates

A new quantitative method for moving-filter monitors which uses a fast filter speed is discussed in Chapter 4. The geometric efficiency adjustment (i.e., using an appropriate average across the deposition window) should be applied, in order for the methods in this chapter to produce correct estimates; see Chapter 6. The "shelf effect" could inflate the countrates observed, such that quantitative estimates would be somewhat larger than expected for given concentration behavior; this effect is not believed to be of any real consequence for most applications.

Chapter 3

Concentration Modeling and Response Prediction

IEEE Transactions on Nuclear Science, 49(5), Oct 2002; 2574-2598

A linear-systems, matrix-based mathematical formulation for predicting continuous particulate air monitor (CPAM) responses when monitoring a system of compartments served by an HVAC system is developed. The CPAM responses, for both fixed- and moving-filter monitors, are found using a "quasi-numerical" approach, combining numerical eigenvector/eigenvalues with closed-form analytical solutions, for sources with exponential time-dependence. This formulation is general and can handle complex or simple systems with no changes to the mathematics. Parent-progeny (decay chain) nuclides, with branching, are handled directly. The monitor responses are found via several alternative methods. The computations are readily mechanized, providing a valuable analytical tool for the efficient analysis of many CPAM applications. Two example cases are presented: (1) a multi-compartment, multi-source system, for a single nuclide; (2) a two-compartment, ^{88}Kr-^{88}Rb decay chain system, as found in an actual PWR containment building.

Introduction

Background

This paper is the third in a series that has provided some mathematical analysis for continuous particulate air monitors (CPAMs). The first paper [1] developed mathematical models for finding the countrate responses for fixed-filter (FF), rectangular-window moving filter (RW), and circular-window moving filter (CW) monitors, given a mathematical expression for the time-dependent concentration $Q(t)$ that is the input to the monitor. The second paper [2] developed a number of approaches for the "inverse" of the input-output problem addressed in the first paper, namely, estimating the $Q(t)$ or quantities related to it, from the observed CPAM response.

In this paper we seek to predict the CPAM response given only a description of a physical monitoring situation, rather than the $Q(t)$ behavior that would exist in that system. To do this we will implicitly find the $Q(t)$, but that is incidental to our main purpose. We seek a mathematical formulation that can *directly* relate the system and source parameters to the expected CPAM response, without an explicit solution for $Q(t)$.

The theme is that of a design-stage analysis of how a monitor will be expected to respond in a given nuclear facility monitoring application. While the methodology is in principle applicable to any nuclear facility, the main emphasis is on power reactor radiation monitoring system (RMS) design. Note that we seek only to predict the monitor response; the assessment of whether or not that response is in some sense acceptable or adequate is beyond the scope of this paper.

Monitor Response Prediction

We will begin with the system definition, e. g., the number and configuration of physical compartments, the HVAC service to those compartments, the use of filtration and/or ventilation. Then, given a mathematical description of the expected sources that provide airborne radioactivity to the compartments, including into which compartments each source provides activity, we will be able to find the CPAM responses, for both fixed- and moving-filter monitors.

Three methods for finding the monitor response will be discussed. One approach (“Method A”) predicts the dynamic response of the fixed- or moving-filter monitors by using a particular form of solution for the time-dependent concentration in the monitor response models reported in [1]. The model handles parent-progeny[1] (PP; decay chain) nuclides, for both fixed- and moving-filter monitors, but it does not account for PP "ingrowth" of a progeny nuclide from the decay of its parent on the filter medium (since this was not part of the models in [1]), so that for some analyses one of the other methods should be used.

[1] Also known as "parent-daughter."

For the same monitoring setup as Method A, the second method (B) predicts FF monitor dynamic responses by integrating a linear-systems model for the FF response into the physical-compartment/HVAC/source linear system. The FF response is found directly, without using the models from [1]. PP cases are handled correctly, since the FF linear system includes PP activity transfers on the filter medium. Method B does not apply to moving-filter monitors.

The third method (C) comprises a series of recursive convolution integrals that find the correct FF response for PP systems, when the concentrations of the PP nuclides have been found "externally." This approach permits the use of more sophisticated concentration dynamics models. It is intended to be implemented numerically, given a vector of concentration values, per nuclide in the PP chain. The shape of the concentration profile is arbitrary (it need not be exponential). Method C does not provide a response solution for moving-filter monitors. However, for RW monitors, for some applications we can use a response model in [1] via a numerical multiple integration of the concentration vector.

Modeling Context

The overall modeling approach, for methods A and B, can be considered a "middle ground" between two extremes. On the one hand, we could assume that the HVAC monitoring application comprises, effectively, a single compartment system (SCS), due to the mixing effect of the HVAC. The SCS approach is often unrealistic, in that the HVAC flow rate required to attain this "convergence" is very high. On the other hand, we could invoke a sophisticated computation of the concentration behavior in the multicompartment system (MCS) that actually exists, using a code such as the CONTAM series.[2] The complex MCS calculations require a great deal of information, which may or may not be available, about the system being modeled.

In both cases, we would attempt to calculate the concentration dynamics, and then use a numerical implementation of the analytical monitor response models in [1] to obtain the predicted responses. Our objective here is to get directly, in a single analysis, to the monitor responses, using a level of modeling detail that "splits the difference" between these alternative approaches.

One application for which the modeling described below will not be especially useful is the case where we have a single compartment, with workers more-or-less continuously present. The CPAM is to be placed inside this compartment, rather than at an HVAC exhaust point or elsewhere in the HVAC system; the monitor is present for the purpose of alerting the workers that a release has occurred, so that their exposures can be minimized. In some such cases, where there is a low rate of HVAC air exchange, and/or poor mixing, we can have a persistent spatial dependence of the concentration, that is, $Q(t,x,y,z)$. The placement of the monitor sample point in the compartment then becomes an issue, since the concentration is not uniform. If concentration profiles have been computed for such a situation, so that we have $Q(t,x,y,z)$, then for a selected monitor location (x,y,z), we could use an appropriate model from [1] to predict the CPAM response.

The modeling in this paper, on the other hand, assumes instantaneous mixing of the input activity from a source, uniformly throughout the compartment(s) driven by that source. That is, we use the familiar "lumped-parameter" approach to system modeling; spatial dependencies are ignored, so that we consider only $Q(t)$. This is entirely appropriate for larger-scale systems such as a power reactor RMS, where we use monitors to observe several compartments simultaneously. Many of these compartments will be equipment "cubicles" which do not have human occupants during normal operations. Indeed, CPAMs are installed in power reactors for worker-protection purposes, as in the single-compartment case, but also for, e.g., leak detection, process monitoring and control, and effluent monitoring purposes.

The concentration dynamics modeling in this paper is neither unique nor especially sophisticated; it is intended to provide a modest capability to represent the contaminant movement in a MCS, with emphasis on the effects of HVAC, since this is the monitoring configuration found in power reactor applications. The value of the methodology described here is that it provides an integrated model for readily generating CPAM dynamic responses, for a variety of system conditions (number of compartments, source dynamics, HVAC flow rates, filtration/ventilation fractions, etc.), so that these responses can be evaluated. This might be done during the design of a new plant, or for design reviews of an existing plant. Issues such as how many monitors are required, where their sample points should be placed, their response times for source transients, and so forth, can be addressed by analyzing data generated by the models presented below.

[2] Currently CONTAMW, available from the National Institute of Standards and Technology (NIST), free of charge; visit the NIST web site at *www.bfrl.nist.gov/IAQanalysis*. See the "Publications" section there for a bibliography relating to the modeling of contaminant transport.

Paper Overview

The development begins with a brief review of the matrix-based linear systems formalism used in the modeling. This is then specialized to "compartmental" modeling, because linear systems analysis is more general than we need for this problem. The compartmental model is then extended to include the effects of HVAC, including filtration and ventilation. The approach is further generalized so that we can handle parent-progeny decay chain situations.

Each of the sources that drive the linear system is modeled as a sum of two exponentials, one of which may be switched off. By adjusting the parameters in each source's model, we can cover many time-dependencies of interest in air monitoring. We may have any number of sources, driving any number of compartments, in any linear combination. Each source has its own set of parameters, including a delay time. In PP systems we may have sources of any of the nuclides in the chain, in any combination.

The compartmental system with its sources results in a vector-matrix differential equation for the activities in the compartments. This differential equation can of course be solved by a variety of methods, including numerical, or analytical, via Laplace transforms. The solution approach for the compartmental activities is a "quasi-numerical" combination of an analytical solution, for the exponential-shaped sources, and the numerical eigenvectors and eigenvalues needed by these solutions. This approach was taken because modern scientific/engineering software will readily provide numerical eigenvalues and eigenvectors. The several monitor response methods are then developed.

Finally, we consider two example analyses; in each case we will find the concentrations and CPAM responses, and check them against purely numerical solutions. The first example is meant to represent the monitoring of a typical power reactor building, such as an LWR auxiliary building, with multiple compartments, served by an HVAC, with filtration and ventilation, and multiple sources. The second example is of a two-compartment system, with the decay chain ^{88}Kr-^{88}Rb, as found in an operating PWR containment. In this case there was an unusual pathway for exchange of the airborne radioactivity between a small, high-concentration compartment and the rest of the containment building. A recirculating HVAC with filtration was also present. This situation is modeled and solutions are found for both a pre-entry recirculation and a subsequent purge of the containment.

System Modeling

Linear Systems Review

The state-variable, or linear-systems, formulation provides a convenient, powerful, and compact way to represent the sets of ordinary differential equations that describe the time-dependent behavior of many dynamic systems. We will focus on the dynamics of the activity due to one or more airborne radionuclides in a multicompartment system. The vector-matrix differential equations are written as

$$\dot{\mathbf{x}} = \mathbf{A}\mathbf{x} + \mathbf{B}\mathbf{u} \tag{3-1}$$

where the column vector **x** contains the state variables, and the matrix **A** contains the system rate parameters, which are assumed to be constants, so that this is a time-invariant system. If the rate parameters depend on the state variables, then the system is nonlinear. We will have *p* variables, so the matrix **A** is *(p,p)*.

The product **Bu** allocates the forcing functions into the system; we can have any number of functions *m* in the *(m,1)* column vector **u** forcing the response of the *p* state variables, in combinations defined by the *(p,m)* matrix **B**. The product **Bu** reduces to a (*p,1*) column vector of forcing function combinations, which may be functions of time.

The linear-systems formalism also includes the algebraic "observation" equation

$$\mathbf{y} = \mathbf{C}\mathbf{x} \tag{3-2}$$

where the *(p,p)* matrix **C** maps the state variables **x** into a vector of observed quantities **y**. Finally, we will also need a vector of initial conditions $\mathbf{x}_0$ for the state variables.

A very useful property of the linear-systems formulation is that we can find the equilibrium values for the state variables, regardless of the initial states, for constant forcing functions, via [3]

$$\mathbf{x}_{\infty} = -\mathbf{A}^{-1}\,\mathbf{B}\mathbf{u} \tag{3-3}$$

for nonsingular **A,** without solving the ODE system. We will have occasion to use this, below. The inverse of **A** can of course be found numerically, and indeed the calculation of the equilibrium values can be executed in a single statement in many scientific/engineering programming languages.

Compartmental Systems

We now make the general linear-systems analysis more specific to the concentration-modeling problem. The state variables **x***(t)* will be the time-dependent activities in a set of "compartments." For the present purpose, a compartment is a well-mixed region within which we consider the concentration of a nuclide to be uniform. A physical compartment like a room may be subdivided into more than one mathematical compartment, if we are not willing to assume a homogeneous mixture in the room. Also, it will be convenient to consider the nuclides in a parent-progeny chain to each be a compartment, mathematically, even though they all may exist in one physical compartment.

The forcing functions **u***(t)* will now be the time-dependent emission rates of sources of airborne radioactivity in the compartments, in units of activity per unit time. For air monitoring applications the matrix **C** is usually just a diagonal matrix containing the reciprocals of the compartmental volumes, so that the observations **y***(t)* are of concentrations rather than activities.

Physical compartments exchange activity amongst themselves via thermal air currents or other unforced air movements. This is as opposed to the action of an "HVAC" or air-handling system that forces the movement of air at much higher rates than the unforced exchanges. Often in industrial facilities, compartments do not directly exchange air with each other, but may do so through a common area such as a corridor. The primary mechanism for the movement of activity is via the HVAC, which may include filtration and ventilation. Our main concern is with the activity in the HVAC return air, which is where monitor sample points are often placed. We do not usually monitor static air volumes, although there are exceptions.

A key aspect of compartmental analysis is the use of the eigenvalues of **A** in the study of system dynamics. These eigenvalues, which can readily be found numerically by most scientific/engineering software, appear in the arguments of the exponentials that comprise the time-dependent solution for the state variables **x**. That is, the solution is nearly always of the general form

$$\mathbf{x}(t) = \sum \mathbf{\Gamma}\,\exp(\omega t)$$

where the ω are the eigenvalues of **A**, and the factors $\mathbf{\Gamma}$ are found using the eigenvectors of **A** (more on this below). This "sums-of-exponentials" solution applies when the eigenvalues are real and distinct [4], as they usually are for the systems found in monitoring applications.

The activity-transfer-rate parameters in the **A**-matrix are defined as $k_{i,j}$, where i is the receiving compartment, and j is the emitting compartment. These k-factors are

$$k_{i,j} = \frac{f_{i,j}}{v_j} \tag{3-4}$$

where $f_{i,j}$ is the volumetric flow rate from compartment j to compartment i, v_j is the volume of compartment j, and the $k_{i,j}$ have units of reciprocal time. Note that $k_{i,i}$ is defined to be zero. A subscript (index) of zero represents the environment (i.e., the "world" outside any compartment in the system). In most nuclear applications the loss directly to the environment from a compartment can be assumed to be negligible.

The elements of the **A**-matrix can be expressed as [5]

$$A_{i,i} = -k_{0,i} - \lambda - \rho_i - \sum_{j=1}^{p} k_{j,i}$$
$$A_{i,j} = k_{i,j} \tag{3-5}$$

There are two other first-order losses on the main diagonal of **A**; the loss due to decay (λ), and to other mechanisms, such as plateout (ρ). The latter may vary by compartment although we will usually take it to be the same across compartments. Thus, the main-diagonal elements of **A** contain the losses from the respective compartments, while the off-diagonal elements represent the gain of material to the row compartment, from each of the respective column compartments.

For a compartmental system, as opposed to a general linear system, the **A** matrix has the following properties [4, p. 37]

- All elements are constants.
- The main diagonal elements are nonpositive.
- The off-diagonal elements are nonnegative.
- The column sums are nonpositive and are the negative of the sum of the first-order loss rates for the compartment corresponding to each column. These loss rates include decay, exfiltration, plateout.

If **A** meets these conditions, then it is the case that [4, pp. 46-48]

- The solution for the activities is nonnegative.
- If the eigenvalues of **A** are real and distinct, the solution consists of sums of exponentials.
- If the eigenvalues are real and repeated, the solution consists of sums of exponentials and time-exponential products.
- If the eigenvalues are complex, the solution consists of sums of exponentially-damped sinusoids.
- There are at least as many exponentials in the solution for each compartmental activity as there are compartments.
- The arguments of these exponentials are the product of time and the eigenvalues of **A**; these eigenvalues are nonpositive.

A compartmental system that has no first-order losses is termed "closed" otherwise it is "open." A compartment with no first-order losses is a "trap." This would correspond to a long-lived isotope (small decay constant), no plateout, no exfiltration, and neither ventilation nor filtration (i.e., a pure recirculating HVAC). Traps induce zeroes as eigenvalues of **A**, and then **A** is singular; thus, **A** will be invertible (a condition we need) only if there are no traps [4, p. 71].

HVAC Model

Development

A typical layout for a simple HVAC system is sketched in Fig. 3-1; this system will be used below for an example analysis. We will consider a constant HVAC flow, although this is not always the case. If it is not the case then the entries in the **A** matrix, as we will see shortly, will be time-dependent rather than constants, and a different solution approach will be required. We also will not consider the case of activity being present in the ventilation intake air of the HVAC, because this is rarely an issue for nuclear facilities, where the monitored nuclide is not present in the outside air.

Consider again the system matrix **A** defined in (5). When we include the effects of HVAC on this system, it is reasonable to postulate an additional loss from each compartment, which we will take to be a simple first-order loss, i.e., the loss rate is proportional to the concentration in the compartment. Thus we need to augment the main diagonal of the **A**-matrix with a new loss rate

$$k_{H,i} = \frac{f_{H,i}}{v_i}$$

where $f_{H,i}$ is the volumetric flow rate to the HVAC (i.e., the return) from compartment i. Next we assume that the HVAC creates on its supply side a flow-weighted average of the returning concentrations, so that

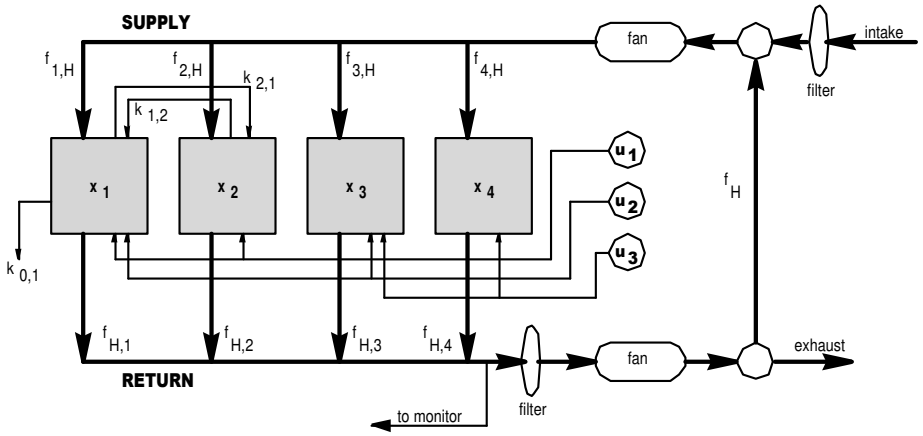

Fig. 3-1. System sketch for example 1. Only one set of unforced flows is shown.

$$\bar{Q}_S(t) = \frac{\sum_{i=1}^{p} \frac{x_i(t)}{v_i} f_{H,i}}{\sum_{i=1}^{p} f_{H,i}} \tag{3-6}$$

Because the source of material into a compartment due to the HVAC is a function of the state variables **x** (compartmental activities), through the flow-weighted average , we must include this source in the **A**-matrix, rather than including it in the **Bu** product, which we reserve for sources that do not depend on a state variable.

Next we need to extend the model to account for filtration and ventilation. The loss from each compartment to the HVAC return does not change, but the concentration in the supply from the HVAC will of course be affected by filtration and ventilation. Thus we modify (6) to account for the fractional loss due to filtration, Θ, and the fraction of the HVAC flow rate that is allocated to ventilation (fresh air intake), υ:

$$\bar{Q}_S(t) = \frac{\sum_{i=1}^{p} \frac{x_i(t)}{v_i} f_{H,i} (1-\Theta)(1-\upsilon)}{\sum_{i=1}^{p} f_{H,i}} \tag{3-7}$$

Here we can see that if the filtration efficiency Θ is unity, there will be no activity in the HVAC supply air, or if the HVAC is operating in a "purge" or once-through ventilation mode, where υ is unity, there will again be zero activity in the supply air.

Next, if we expand the flow-weighted average (3-7) and assign its individual terms to the appropriate columns of the **A**-matrix, we can collect the HVAC sources and losses into the augmented elements

$$A_{i,i} = -k_{0,i} - \lambda - \rho_i - \sum_{j=1}^{p} k_{j,i} + \left[\frac{f_{i,H}}{f_H} (1-\Theta)(1-\upsilon) - 1 \right] \frac{f_{H,i}}{v_i}$$

$$A_{i,j} = k_{i,j} + \frac{f_{i,H}}{f_H} (1-\Theta)(1-\upsilon) \frac{f_{H,j}}{v_j} \tag{3-8}$$

with f_H the total HVAC flow. The column sums of this **A** matrix can be shown to be the negative of the sum of the first-order loss terms, or

$$-\left\{ \lambda + \rho_i + k_{0,i} + \frac{f_{H,i}}{v_i} \left[1 - (1-\Theta)(1-\upsilon) \right] \right\}$$

so that **A** is a compartmental matrix. The last term is the net loss, per compartment, due to the HVAC; when there is no filtration or ventilation, there is no loss, and conversely if there is once-through ventilation (υ=1) or perfect filtration (Θ=1), then the loss rate is based on the full return flowrate.

Flow Allocation

A significant aspect of the analysis of HVAC systems is the manner in which the flow f_H is allocated to the compartments served by the system. Often this is done on the basis of heat loads, for temperature or humidity control. In this instance, the flow allocation could be considered random for modeling purposes, because we cannot predict the flow fraction for a given compartment, in general. Another strategy is to have a volume-proportional flow allocation, which will lead to an equal number of air changes per hour (ACH) in all compartments. This is written

$$f_{H,i} = f_H \frac{v_i}{\sum_{j=1}^{p} v_j}$$

Thus a larger compartment will receive more flow than a smaller one. We will denote this condition as E-ACH. A third approach would simply allocate the flow equally to all compartments, regardless of volume or heat load.

Since all compartments are served by the HVAC, when υ is less than unity the system is "strongly connected" [4, p.54] [3, p. 384]. This means that activity originating in any compartment can reach any other compartment.

Monitored Concentration

In many CPAM applications, notably in power reactors, the monitor will be sampling the air in an HVAC return duct, upstream of any filtration. This concentration tells us what is happening in the monitored compartment(s). We can write the average concentration in the HVAC return using the scalar product

$$\bar{Q}_R(t) = \mathbf{x}(t)' \mathbf{z} \tag{3-9}$$

where **z** is a $(p,1)$ vector with constant elements

$$z_i = \frac{f_{H,i}}{f_H v_i} \tag{3-10}$$

This concentration is just a flow-weighted average of the concentrations returning to the HVAC from the compartments, and is the same as (3-7) with Θ and υ zero. It will prove to be useful to combine (3-3) and (3-9) to find the HVAC-return equilibrium concentration when we have constant sources. This can be written

$$Q^{HVAC}(\infty) = \left(-\mathbf{A}^{-1} \mathbf{B} \mathbf{u}^* \right)^T \mathbf{z} \tag{3-11}$$

where the superscript T is transpose, and

$$u_i^* = \begin{cases} 0 & \text{if } u_i \text{ is not constant} \\ u_i & \text{if } u_i \text{ is constant} \end{cases}$$

Finally, to simplify the notation in the monitor response expressions, we define a variation of the **z** vector that will return the concentration for a single compartment, per nuclide, as follows:

$$z_k^S = 0 \;\; ; \;\; k = 1, p \;\; ; \;\; z_{mon}^S = v_{mon}^{-1}$$

where *mon* represents the monitored-compartment number. The superscript *s* indicates that this is the **z** vector for the single-compartment case. If we are monitoring the HVAC return, $\mathbf{z}^H$ will represent the **z** vector as originally defined, in (3-10).

Practical Considerations

In many applications we would not have good data on the unforced air flowrates that are used to define the *k* parameters. It is tempting to speculate that the HVAC flows dominate the unforced flows in the **A** matrix in such a manner that we could ignore the *k* values, i.e., set them to zero.

The first question that comes to mind is, how can we assess the effect of changes in the *k* values, for a given system and source configuration? Because our focus is on CPAM responses, and since the monitoring point is very often in the HVAC return, we could use the monitored concentration (Q_m), i.e., (3-9), in a response variable. Further, we can use constant sources, so that we will have a single equilibrium concentration value, given by (3-11), as the response.

To explore this, a number of numerical experiments were run, and it is was found that:

- if the HVAC allocation is E-ACH, the monitored concentration does not change as we increase or decrease or even completely remove the unforced intercompartmental flows;[3]
- if the flow allocation is random, there is a change in the equilibrium concentration of a few percent, as the unforced flowrates are varied across a wide range.

From these tests we can conclude that, if necessary, the *k* values can be set to zero without significantly changing conclusions about a CPAM's predicted response.

Decay Chains

The HVAC model can be extended to include PP problems. In general there are *N* nuclides in a decay chain, and *p* physical compartments. Taking each nuclide in each physical compartment to be a separate mathematical compartment, the state variables will be the activities of these *N* nuclides in the *p* compartments, so that the length of **x** is now *Np*. We can handle single-nuclide cases by setting *N*=1 in the expressions to follow.

We can organize the state vector in two ways; the elements can be grouped either by nuclide or by compartment. For example we might have, for *N*=2 and *p*=2,

$$\mathbf{x} = \begin{pmatrix} n=1;\, k=1 \\ n=2;\, k=1 \\ n=1;\, k=2 \\ n=2;\, k=2 \end{pmatrix} \quad or \quad \begin{pmatrix} n=1;\, k=1 \\ n=1;\, k=2 \\ n=2;\, k=1 \\ n=2;\, k=2 \end{pmatrix}$$

where *n* is the nuclide and *k* is the physical compartment. The issue is that the **A** matrix will be affected by our choice of organization for **x**. It turns out that the second choice, above, of arranging the nuclides and compartments leads to a simple way of generalizing the **A** matrix for PP systems.

This new **A** matrix will have *(N,N)* submatrices, each of which is *(p,p),* so that A is now *(Np,Np)*. On the main diagonal of **A** are *(p,p)* submatrices $\boldsymbol{\alpha}$, all with elements like the usual **A** matrix, i.e., (8), with parameters as appropriate for each nuclide.

[3] This can be shown analytically.

Each of these submatrices reflects the physical-compartment transfers of activity, for a given nuclide. Usually what would vary in the $\boldsymbol{\alpha}$ submatrix elements are the first-order losses, with of course the decay constant, and possibly the plateout or HVAC filtration efficiency, needing to be nuclide-specific. On the other hand, the physical properties of the system, such as volumes and HVAC flow rates, are re-used in the $\boldsymbol{\alpha}$ elements, because these properties do not change with the nuclide.

Below the main diagonal in **A** are submatrices $\boldsymbol{\mu}_n$ which are *(p,p)* diagonal with all elements equal to the decay constant λ_n multiplied by the branching ratio χ_n, for the transition to nuclide *n*. These submatrices provide for the inter-nuclide transfers of activity.

In (3-12) we have an illustration of these matrices, for *N=4* and *p=3*. The upper triangular region of **A** is zero-filled, because the progeny do not contribute to the parent activity. In the lower triangular region we have a band structure, since only the immediate parent contributes to the progeny activity.

$$\mathbf{A} = \left(\begin{array}{c|c|c|c} \boldsymbol{\alpha}_1 & \mathbf{0} & \mathbf{0} & \mathbf{0} \\ \hline \boldsymbol{\mu}_2 & \boldsymbol{\alpha}_2 & \mathbf{0} & \mathbf{0} \\ \hline \mathbf{0} & \boldsymbol{\mu}_3 & \boldsymbol{\alpha}_3 & \mathbf{0} \\ \hline \mathbf{0} & \mathbf{0} & \boldsymbol{\mu}_4 & \boldsymbol{\alpha}_4 \end{array}\right) \tag{3-12}$$

$$\boldsymbol{\mu}_n = diag\left(\chi_n \lambda_n\right)$$

Consider a ^{88}Kr-^{88}Rb 2-chain, three-compartment system, to illustrate this modeling. The **A** matrix is

$$\mathbf{A} = \left(\begin{array}{ccc|ccc} \alpha_{11}^{Kr} & \alpha_{12}^{Kr} & \alpha_{13}^{Kr} & 0 & 0 & 0 \\ \alpha_{21}^{Kr} & \alpha_{22}^{Kr} & \alpha_{23}^{Kr} & 0 & 0 & 0 \\ \alpha_{31}^{Kr} & \alpha_{32}^{Kr} & \alpha_{33}^{Kr} & 0 & 0 & 0 \\ \hline \lambda_{Rb} & 0 & 0 & \alpha_{11}^{Rb} & \alpha_{12}^{Rb} & \alpha_{13}^{Rb} \\ 0 & \lambda_{Rb} & 0 & \alpha_{21}^{Rb} & \alpha_{22}^{Rb} & \alpha_{23}^{Rb} \\ 0 & 0 & \lambda_{Rb} & \alpha_{31}^{Rb} & \alpha_{32}^{Rb} & \alpha_{33}^{Rb} \end{array}\right)$$

To construct the **A** matrix for this 2-chain we use (3-8) for the $\boldsymbol{\alpha}$-elements of (3-12). For the ^{88}Kr elements we use its decay constant, a zero plateout rate, and a zero HVAC filtration efficiency Θ. For ^{88}Rb's $\boldsymbol{\alpha}$-elements we have its decay constant and, presumably, a nonzero plateout rate and filtration efficiency. The compartmental volumes, unforced exchange rates, and HVAC flowrates are of course the same for both nuclides.

Once the **A** matrix is defined, we need to define the sources of all nuclides in the chain, and their allocation to the compartments. Hence the sources are defined as usual by the **Bu** product, which will be a *(Np,*1*)* column vector (more on this in the next section). The (*Np*,1) state vector, which will be a vector of activities, for a PP system is organized with all *p* physical compartments represented, in order, *N* times, with the parent nuclide(s) appearing above the progeny nuclide(s), in decay-chain order. For the Kr-Rb chain with three compartments we would have the activities

$$\mathbf{x} = \left(\begin{array}{ccc|ccc} x_1^{Kr} & x_2^{Kr} & x_3^{Kr} & x_1^{Rb} & x_2^{Rb} & x_3^{Rb} \end{array}\right)^T$$

This means that we can find the (scalar) activity for nuclide *n* in compartment *k* by using **x**-element

$$x_{(n-1)\ p\ +\ k}$$

Similarly, the compartmental-volume vector **v** consists of *N* replications of the physical compartment volumes, in numerical order, for a total length of *Np*. Using the same example, **v** will be a (6,1) column vector

$$\left(\begin{array}{ccc|ccc} v_1 & v_2 & v_3 & v_1 & v_2 & v_3 \end{array}\right)^T \tag{3-13}$$

Vector-valued concentrations can be found using the (*Np,Np*) observation matrix **C**, which is

$$\mathbf{C} = \left[diag(\mathbf{v}) \right]^{-1} \tag{3-14}$$

Finally, we also need to replicate the **z** vector used in (3-9), because it represents physical (not nuclide-specific) parameters. This is done exactly as for the volumes, above, so that we have the vector **z** constructed like (3-13), with z_k in place of the v_k..

Source Modeling

Source Allocation

To introduce this aspect of the analysis, consider first a single-nuclide problem. In the linear-systems format we can have any number of sources of that nuclide providing activity to any number of compartments. The allocation of the *m* sources to the *p* compartments is done via the *(p,m)* **B** matrix. To illustrate, suppose we have three sources and five compartments. Then we can write, for example,

$$\mathbf{B}\mathbf{u}(t) = \begin{pmatrix} 0 & 1 & 0 \\ 0 & 0 & 0.6 \\ 1 & 0 & 0 \\ 0 & 0 & 0 \\ 0.2 & 0.7 & 1 \end{pmatrix} \begin{pmatrix} u_1(t) \\ u_2(t) \\ u_3(t) \end{pmatrix}$$

for the source product **Bu**. The first source $u_1(t)$ drives compartment three at 100 percent strength, and it also drives compartment five at 20 percent strength. In some modeling situations we would expect that the column sums of **B** would be unity, but this is not a general requirement. Also, it is not required in general that there be one source per compartment; in the example, compartment five is driven by all three sources, while compartment four is not driven by a source at all. However, in many nuclear-facility applications, it would be unusual for a source to provide activity directly into a compartment other than the one containing it.

For PP systems, we need to partition **B** as was done for **x** and **A**; then **B** will be *(Np,m)*. For these systems we must define each of the *m* sources **u** as a source of a specific nuclide. Each nuclide has a set of *p* rows in **B**, and we assign the source to the row(s) in the source's nuclide's partition of **B** that correspond to the physical compartments driven by the source. For example, returning to the three-compartment Kr-Rb system, we might have

$$\mathbf{B}\mathbf{u}(t) = \left(\begin{array}{cc} 0 & 0 \\ 1 & 0 \\ 0 & 0 \\ \hline 0 & 1 \\ 0 & 0 \\ 0 & 1 \end{array}\right) \begin{pmatrix} u_1(t) \\ u_2(t) \end{pmatrix}$$

The top three rows of **B** are for the three physical compartments with the "parent" ^{88}Kr, and the bottom three rows are for the "progeny" ^{88}Rb. Here the first source is releasing ^{88}Kr into the second compartment only, while the second source is emitting ^{88}Rb into the first and third compartments.

We can consider the initial condition (activity) to be a special case of a source, i.e., a Dirac delta function at time zero. This means that the initial activity could be included in the source vector **u**. For clarity, however, we will keep the initial activities separate. We will define a *(Np,1)* vector of the initial activities of the *N* nuclides in the *p* compartments. For example,

$$\mathbf{x}_0 = \left(x_1^{Kr}(0) \quad x_2^{Kr}(0) \quad x_3^{Kr}(0) \mid x_1^{Rb}(0) \quad x_2^{Rb}(0) \quad x_3^{Rb}(0) \right)^T$$

Source Time-Dependence

Next, we need to define the time-dependence of the sources that drive the compartmental system. We can cover many cases by using an exponential shape for the source terms, and substantial flexibility in modeling source behaviors is available with a "double-exponential" (DE) function

$$u(t) = S\left[\exp(r_1 t) - f\exp(r_2 t)\right] \tag{3-15}$$

where S is a source emission rate (activity/time), f is a zero-or-one switch controlling the presence of the second exponential, and r_1 and r_2 are exponential-rate parameters, which are negative, with units of reciprocal time. The DE behavior can build up to a peak and then decrease, and the rise and fall times can be adjusted. If f is zero we have the single-exponential (SE) case,[4] with some initial emission rate S that decays toward zero, and if f and the parameter r_1 are both zero then we have a constant source.

Experimenting numerically with (3-15) for various parameter values will show that, as we adjust the time to attain the peak emission rate, given by

$$T_{\max} = \frac{\ln\left[\frac{r_2}{r_1}\right]}{r_1 - r_2},$$

the achieved emission rate will no longer be the desired value, S. To maintain this value for any settings of the parameters we need to normalize (divide) the emission rate by the factor

$$\Lambda = \begin{cases} 1 & f = 0 \\ \left(\frac{r_2}{r_1}\right)^{\frac{r_1}{r_1 - r_2}} - \left(\frac{r_2}{r_1}\right)^{\frac{r_2}{r_1 - r_2}} & f = 1 \end{cases} \tag{3-16}$$

Note that if f is unity (DE source), r_1 cannot be zero, and r_1 and r_2 must be different.

To apply this source behavior it would be useful to have an idea of how to set the exponential parameter values in order to attain some specified time-to-maximum. That is, we may have a source that reaches some maximum emission rate at, say, one hour after its initiation. However, the time-to-maximum expression cannot be solved in closed form for the time, even if we specify one of the parameters. Using a series expansion, it can be shown that if we have values for r_2 and T_{max}, then the parameter r_1 is given, approximately, by

$$r_1(r_2, T_{\max}) \approx \frac{1}{2T_{\max}\exp(-r_2 T_{\max})}\left\{-\exp(-r_2 T_{\max}) + \sqrt{\exp(-r_2 T_{\max})^2 + 4T r_2 \exp(-r_2 T_{\max})}\right\} \tag{3-17}$$

With some numerical experimentation, we find the parameter results shown in Table I, which can be used to guide the selection of the DE parameters for a time-to-maximum range from five minutes to ten hours. For example, to achieve a time-to-maximum of two hours, we would use r_2 at -0.05 min^{-1} and T_{max} at 120 min in (3-17), to obtain a value for r_1 of -1.26E-4 min^{-1}. We can add further flexibility in source modeling by using a delay time for the exponential sources. This is implemented using the Heaviside operator Φ, and with a delay time Ω included in the exponential argument. The operator $\Phi(\Omega)$ is zero for times less than Ω and is unity thereafter. Each source can have its own delay time. Then the DE function (15) now becomes, adding subscripts to indicate the source-dependent parameters,

$$u_j(t) = \frac{S_j}{\Lambda_j}\Phi(\Omega_j)\left\{\exp\left[r_{1,j}\left(t - \Omega_j\right)\right] - f_j\exp\left[r_{2,j}\left(t - \Omega_j\right)\right]\right\} \tag{3-18}$$

[4] SE sources can also be modeled using a "source compartment" rather than in the vector **u**. See [5, p. 48].

TABLE I

PARAMETER RANGES FOR DE SOURCE TIMING; TIME IN MINUTES

r_2	T_{max}	r_1	T_{max}	r_1
-0.5	5	-5.80E-2	20	-2.27E-5
-0.15	20	-9.14E-3	60	-1.85E-5
-0.05	60	-3.05E-3	150	-2.80E-5
-0.02	150	-1.22E-3	350	-1.84E-5
-0.01	350	-3.43E-4	600	-2.52E-5

Any compartment may be driven by any combination of these sources, and it may also have a nonzero initial condition. As a rule, in most practical situations we would have essentially constant, low-level (or zero) sources in most compartments, and then after some delay, a larger source would become active in one compartment. We would be interested in the monitor response to the new source.

Fig. 3-2 illustrates several source behaviors, with delays. The dotted line indicates the desired peak emission rate, and the plot shows a consistent emission rate being attained by several sources with various peak times, demonstrating that the normalization operates correctly.

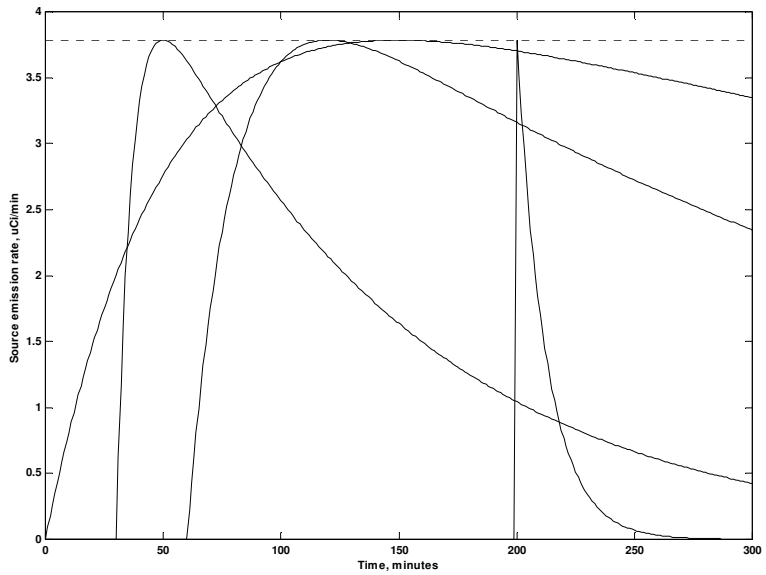

Fig. 3-2. Source emission rate examples, showing normalization.

Solution Methods

Introduction

Our objective is to find mathematical expressions for predicting monitor responses, given a description of the system and the sources. We can find the concentrations in the system, but this is not required. We will use the response models in [1], for the exponential concentration shape. We are using an exponential *source* shape also, but the concentration (system response) will

be exponential as well. Other concentration profiles are of course possible, and we would just use them in the models in [1] to find the corresponding monitor responses. In this section we will briefly review the analytical and numerical solution methods, and then develop the method of choice, which is a "quasi-numerical" approach, using eigenanalysis of the **A** matrix.

Analytical

Let us first consider a SCS; this system is defined by one ODE, the solution for which can be found in a number of ways. One such solution is given by the scalar convolution integral [6]

$$x(t) = \int_0^t u(\tau)\exp\left[\omega(t-\tau)\right] d\tau + x_0 \exp(\omega t) \tag{3-19}$$

where ω is the single, nonpositive, eigenvalue of this system, and x_0 is the initial activity in the compartment. The eigenvalue will just be the sum of the first-order loss rates for the system. The solution (3-19) is the sum of the response due to the forcing function *u(t)*, and that due to the initial condition x_0.

In the MCS case, there is a vector-matrix analog to the scalar convolution integral, and the vector-valued solution is given by the matrix convolution integral [7]

$$\mathbf{x}(t) = \int_0^t \mathbf{B}\mathbf{u}(\tau)\exp\left[\mathbf{A}\left(t-\tau\right)\right]d\tau + \mathbf{x}_0 \exp\left(\mathbf{A}t\right) \tag{3-20}$$

The quantity *exp(**A** t)* is called the "matrix exponential" or "transition matrix." A powerful technique for finding analytical solutions for the state variables **x** is the use of Laplace transforms. It can be shown that the solution to (3-20) can be written [5, p. 26]

$$\mathbf{x}(t) = \Im^{-1}\left[\left(s\mathbf{I}-\mathbf{A}\right)^{-1}\mathbf{B}\mathbf{U}(s)\right] + \Im^{-1}\left[\left(s\mathbf{I}-\mathbf{A}\right)^{-1}\mathbf{x}_0\right] \tag{3-21}$$

where $\Im^{-1}$ is the inverse Laplace transform, **I** is the *(p,p)* identity matrix, **U***(s)* is a vector of Laplace transforms of the sources, and *s* is the Laplace variable. The Laplace approach is useful for systems of dimension three or less, in general, because the algebra quickly becomes unwieldy for larger systems.

Using (3-21) will generate closed-form, algebraic expressions for the compartmental activities. An advantage of the Laplace transform solution is that many oddly-shaped source behaviors, such as square wave or sawtooth, have Laplace transforms [8]. Discontinuous or delayed sources can also readily be handled, using the Heaviside operator, which also has a Laplace transform [9].

Numerical

Of course, ODE systems can be solved by using any of a number of numerical solution methods. One advantage of the linear-systems approach is that the ODE system can be defined in a matrix format, which makes for a clean implementation of the solution.

We must, however, be careful in selecting an ODE-solver from the variety available. This is due to the presence of so-called "stiff" ODE systems, especially for HVAC applications. A stiff system has widely-spread eigenvalues, which means exponentials that decay on very different time scales. We must pay attention to stability, step size, and accuracy, as with any numerical solution, but especially so for stiff ODE systems. Most scientific/engineering software has one or more ODE solvers available that are appropriate for stiff systems.

We should use a numerical solution for problems with unusually-shaped and/or discontinuous sources, or problems where parameters in the **A** matrix are not constants. A numerical solution also provides a good check on an analytical solution, when we have developed the latter.

It is also possible, given a list of (scalar) concentration values, to use numerical integration to solve the integral forms of the countrate response models in [1]. For the FF monitor this is straightforward, while for the RW and CW monitors we need to use numerical multiple integration.

Quasi-Numerical: Eigenvector-Eigenvalue

This method of solution begins with the factorization or diagonalization of the system matrix **A**, sometimes referred to as a "spectral decomposition" [3, p. 377]. The factorization is

$$\mathbf{A} = \mathbf{V}\mathbf{D}\mathbf{V}^{-1}$$

where **V** consists of columns that are the eigenvectors of **A**. The matrix **D** is diagonal, with the eigenvalues along the main diagonal. For p=2 we will have

$$\mathbf{A} = \mathbf{V}\mathbf{D}\mathbf{V}^{-1} = \left[\begin{pmatrix} v_{11} \\ v_{12} \end{pmatrix}\begin{pmatrix} v_{21} \\ v_{22} \end{pmatrix}\right]\begin{pmatrix} \omega_1 & 0 \\ 0 & \omega_2 \end{pmatrix}\left[\begin{pmatrix} v_{11} \\ v_{12} \end{pmatrix}\begin{pmatrix} v_{21} \\ v_{22} \end{pmatrix}\right]^{-1}$$

where the columns in **V** are the eigenvectors of **A**, in the same order as the corresponding eigenvalues in **D**. What makes this approach attractive is that most scientific/engineering software will have commands for finding the eigenvalues and eigenvectors of a matrix.

This solution method is termed "quasi-numerical" because we will depend on numerical results for the eigenvectors and eigenvalues, but we will use these in analytical (closed-form) expressions. Another significant advantage is the fact that we can find solutions in a form that can be directly used in the monitor response models from [1], thus providing a complete analysis (concentration dynamics and monitor responses) for a specified system.

Activity Solution

For use in the monitor response models we would like to find concentration solutions in the form of linear combinations of exponentials, which, for the systems encountered in monitoring applications, is the form expected.

We begin by denoting the k-th eigenvector (column of **V**) as $\mathbf{W}_k$ and the k-th row of $\mathbf{V}^{-1}$ as $\boldsymbol{\beta}_k$. Each eigenvector is (Np,1), and each row vector $\boldsymbol{\beta}$ is (1,Np). It can be shown [10][3, p. 381] that the (Np,1) solution vector $\mathbf{x}(t)$ for the compartmental activities is

$$\mathbf{x}(t) = \sum_{k=1}^{Np} \mathbf{W}_k \int_0^t \boldsymbol{\beta}_k \mathbf{B}\, \mathbf{u}(\tau) \exp\left[\omega_k (t-\tau)\right] d\tau + \sum_{k=1}^{Np} \boldsymbol{\beta}_k \mathbf{x}_0 \mathbf{W}_k \exp(\omega_k t) \qquad (3\text{-}22)$$

The source emission-rate model is a linear combination of exponentials, so we begin the solution with a single generic exponential source function in (22). Writing out the matrix products as sums, this can then be written

$$\mathbf{x}(t) = \sum_{k=1}^{Np}\sum_{q=1}^{Np}\sum_{j=1}^{m}\left[\mathbf{W}_k \beta_{k,q} B_{q,j} \Phi(\Omega_j) \int_0^{t-\Omega_j} \left\{\exp\left[\omega_k \left(\{t-\Omega_j\}-\tau\right)\right] a_j \exp\left[b_j \tau\right]\right\} d\tau\right] + \sum_{k=1}^{Np} \boldsymbol{\beta}_k \mathbf{x}_0 \mathbf{W}_k \exp\left[\omega_k t\right] \qquad (3\text{-}23)$$

where a_j is a generalized emission rate and b_j represents either r_1 or r_2. Note that the convolution integral is now evaluated over a range from zero to the elapsed time since the j-th source initiated; this occurred at time Ω_j. The Heaviside operator Φ "zeroes-out" the contribution from the j-th source for times prior to Ω_j. Evaluating the integral in (3-23) and substituting the source parameters and normalization yields the activity vector

$$\mathbf{x}(t) = \sum_{k=1}^{Np}\sum_{q=1}^{Np}\sum_{j=1}^{m}\left\{\mathbf{W}_k\,\beta_{k,q}\,B_{q,j}\,\Phi\left(\Omega_j\right)\frac{S_j}{\Lambda_j}\left[\begin{array}{l}\dfrac{1}{r_{1,j}-\omega_k}\exp\left[r_{1,j}\left(t-\Omega_j\right)\right] - \\ \dfrac{f_j}{r_{2,j}-\omega_k}\exp\left[r_{2,j}\left(t-\Omega_j\right)\right] - \\ \left(\dfrac{1}{r_{1,j}-\omega_k}-\dfrac{f_j}{r_{2,j}-\omega_k}\right)\exp\left[\omega_k\left(t-\Omega_j\right)\right]\end{array}\right]\right\} + \sum_{k=1}^{Np}\boldsymbol{\beta}_k\,\mathbf{x}_0\,\boldsymbol{\alpha}_k\exp\left[\omega_k\,t\right] \tag{3-24}$$

This relation applies when the rate constants r are distinct from the eigenvalues ω, which will usually be the situation. If it is not so, then we must return to (3-23) and re-evaluate it using the equality of the rate constant(s) and eigenvalue(s), explicitly. In either case we will have an expression that can be "decomposed" into a sum of exponentials, each multiplied by a constant (or rather, a vector of constants). This is the format required for use in the monitor response models.[5]

The activity-vector solution (3-24) can be written in a more compact general form as

$$\mathbf{x}(t) = \sum_{j=1}^{m}\sum_{h=1}^{4}\sum_{k=1}^{Np}\left\{\mathbf{W}_k\,\Phi\left(\Psi_{h,j}\right)\;\Gamma_{h,j,k}\;\exp\left[\xi_{h,j,k}\left(t-\Psi_{h,j}\right)\right]\right\} \tag{3-25}$$

and we define the various factors in (3-25) using the components from (3-24), as follows:

$$\begin{array}{llll}\Psi_{1,j}=\Omega_j & \Psi_{2,j}=\Omega_j & \Psi_{3,j}=\Omega_j & \Psi_{4,j}=0 \\ \xi_{1,j,k}=r_{1,j} & \xi_{2,j,k}=r_{2,j} & \xi_{3,j,k}=\omega_k & \xi_{4,j,k}=\omega_k\end{array}$$

$$\Gamma_{1,j,k} = \frac{\dfrac{S_j}{\Lambda_j}}{r_{1,j}-\omega_k}\sum_{q=1}^{Np}\beta_{k,q}\,B_{q,j}$$

$$\Gamma_{2,j,k} = \frac{-f_j\dfrac{S_j}{\Lambda_j}}{r_{2,j}-\omega_k}\sum_{q=1}^{Np}\beta_{k,q}\,B_{q,j} \tag{3-26}$$

$$\Gamma_{3,j,k} = \frac{-S_j}{\Lambda_j}\left\{\frac{1}{r_{1,j}-\omega_k} - \frac{f_j}{r_{2,j}-\omega_k}\right\}\sum_{q=1}^{Np}\beta_{k,q}\,B_{q,j}$$

$$\Gamma_{4,j,k} = \frac{\boldsymbol{\beta}_k\,\mathbf{x}_0}{m}$$

The division by m in the last factor above corrects for the summation of the initial-condition portion of the solution over the sources. If there are no sources, we can find the activity vector by using only the last term in (3-24), which is the contribution to the solution due to the initial activities in the compartments.

We can add some additional flexibility for analysis purposes by generalizing the sum over the sources to have variable lower and upper limits. With this we have the activity vector

[5] This assumes that the shape of the concentration is that of a sum of exponentials. Other shapes are possible, and can be handled by the models in [1]. Exponential shapes are used because of their wide applicability and ability to model various time-dependencies.

$$\mathbf{x}(t, j_1, j_2) = \sum_{j=j_1}^{j_2} \sum_{h=1}^{4} \sum_{k=1}^{Np} \left\{ \mathbf{W}_k \, \Phi\left(\Psi_{h,j}\right) \, \Gamma_{h,j,k} \, \exp\left[\xi_{h,j,k} \left(t - \Psi_{h,j} \right) \right] \right\} \tag{3-27}$$

Note that the correction (denominator) for the IC gamma factor, *h=4* in (3-26), now needs to be generalized to $(j_2 - j_1 + 1)$. In practice, it is most useful to examine one source at a time, so that j_1 and j_2 will be equal. With (3-27) we can see the activity contributions by compartment, and by source, as well as the total response for all sources.

Concentration Solution

Once we have the eigenanalysis of the **A** matrix, we can proceed directly to the monitor response solutions, because the activity and concentration profiles in the system will have exponential shapes, and analytical solutions for the monitor responses are available for this form of dynamic behavior. However, it may be useful in some analyses to have explicit expressions for the concentrations. There are both vector and scalar concentrations that are of interest; the scalar concentrations will be used, implicitly, in the monitor response solutions.

The concentration vector is found from the activity vector (3-27) via

$$\mathbf{Q}(t, j_1, j_2) = \mathbf{C}\mathbf{x}(t, j_1, j_2) \tag{3-28}$$

by analogy to (3-2). This will be an (*Np*,1) column vector, arranged like the activity vector **x**. The equilibrium concentration vector is, using (3-3),

$$\mathbf{Q}(\infty) = \mathbf{C}\left[-\mathbf{A}^{-1}\mathbf{B}\mathbf{u}^{*} \right] \tag{3-29}$$

We can find the (scalar) concentration for nuclide *n* in compartment *k* by using **Q**-element

$$Q_{(n-1)\,p\,+\,k}$$

in (3-28) or (3-29).

The other scalar concentration of interest is that in the HVAC return. With **z** defined similarly to (3-13), we can use (3-9) with (3-27) to find the monitored concentration in the HVAC return; this will of course be separate for each nuclide. We can apply (3-9) by using only the subset of *p* elements in **x** that correspond to the respective nuclides, so that this flow-weighted average concentration can be written

$$\bar{Q}_n^{HVAC}(t, j_1, j_2) = \sum_{k=1}^{p} x_{(n-1)p+k}(t, j_1, j_2) \, z_k \tag{3-30}$$

The equilibrium HVAC concentration for nuclide *n* is

$$Q_n^{HVAC}(\infty) = \sum_{k=1}^{p} \left[-\mathbf{A}^{-1}\,\mathbf{B}\,\mathbf{u}^{*} \right]_{(n-1)p+k} \, z_k \tag{3-31}$$

which is based on (3-11).

Monitor Response Solutions

Introduction

We have several options for finding the monitor responses for a given system. The main purpose of the concentration modeling described above is to provide an integrated solution for the monitor responses, and this will of course lead to one countrate

solution option (Method A). With an extension of that modeling to include a FF monitor explicitly in the system definition, another solution is obtained (Method B). Finally, if we have some independent calculation of the concentration dynamics, resulting in a vector of concentrations per nuclide as a function of time, then numerical integration provides another solution approach (Method C). For FF monitors, methods A, B, and C are applicable. For RW monitors, method A and the equivalent of C, which we will call Method D, are available.

As with the concentration modeling, the formulation will assume a general PP system, of length N nuclides. All expressions developed below will provide correct results for a single-nuclide application by using N=1. The PP aspect is important, because one of the solutions (Method A) will not provide correct countrate predictions when precursors are collected on the monitor filter. This is due to the fact that the ingrowth of progeny activity from the decay of the parent is not accounted for in that model. The other two prediction methods properly account for this ingrowth.

Note that monitors respond to scalar concentrations, per nuclide. Thus we need to use (implicitly or explicitly, according to the method) scalar, time-dependent concentrations in the prediction calculations.

Fixed-Filter

Method A (FF)

This approach uses the activity vector solution developed above. We first define a factor similar to (3-27), for any nuclide, with decay constant λ:

$$\boldsymbol{\eta}^{FF}(t, j_1, j_2, \lambda) = \kappa F \sum_{j=j_1}^{j_2} \sum_{h=1}^{4} \sum_{k=1}^{Np} \left\{ \mathbf{W}_k \, \Phi\left(\Psi_{h,j}\right) \, \Gamma_{h,j,k} \;\; \varphi_{FF}(t, \lambda, j, h, k) \right\} \tag{3-32}$$

where F is the monitor flowrate, ft^3/min (cfm), κ is a conversion constant (2.22x10^6 dpm/μCi times 2.832x10^4 cm^3/ft^3), and

$$\varphi_{FF}(t, \lambda, j, h, k) = \frac{\exp\left[\xi_{h,j,k}\left(t - \Psi_{h,j}\right)\right] - \exp\left[-\lambda\left(t - \Psi_{h,j}\right)\right]}{\lambda + \xi_{h,j,k}} \tag{3-33}$$

This factor is developed using (1-18). It is important to recognize that the eigenvalues and exponential factors ξ must not be equal to the negative of the decay constant λ in these and subsequent expressions. This would seem unlikely to occur, but in some PP systems we can in fact have eigenvalues that are the negative of λ. When this is the case we use

$$\varphi_{FF}(t, \lambda, j, h, k) = \left(t - \Psi_{h,j}\right) \exp\left[-\lambda\left(t - \Psi_{h,j}\right)\right] \tag{3-34}$$

which follows from the countrate convolution integral (1-2) and the fact that the concentration is assumed to be a linear combination of exponentials. When the argument of any of the exponentials is equal to the negative of the decay constant, then the integration yields (3-34) for that term. This solution has been tested against an independent numerical countrate solution (the simulation described in [1]), and they agree.

The FF (or RW) countrate due to nuclide n will be

$$\dot{C}_n^{FF}(t) = \sum_{j=1}^{M_n} \varepsilon_{n,j} \, \gamma_{n,j} \, \zeta_n(t) = \varepsilon_n^{eff} \, \zeta_n(t) \tag{3-35}$$

where $\varepsilon_{n,j}$ is the detection efficiency and $\gamma_{n,j}$ is the abundance for emission j of M total emissions for nuclide n, whose activity is ζ. Here, "emission" may include alpha, beta, and gamma decays, in various combinations. To simplify subsequent expressions, we will use the "effective" efficiency ε^{eff} for a given nuclide, without the superscript.

The total FF monitor countrate response to all nuclides is obtained from (3-32) using

$$\dot{C}^{FF}(t, j_1, j_2) = \sum_{n=1}^{N} \varepsilon_n \, \phi_n \sum_{k=1}^{p} \left\{ \eta^{FF}_{(n-1)p+k}(t, j_1, j_2, \lambda_n) \; z_k^H \right\} \tag{3-36}$$

where ϕ_n is the collection efficiency for nuclide n on the monitor's sampling medium.[6] This expression is for the HVAC-return case; substitute z^S for the single-compartment case. For the response due to any specific nuclide in a PP system, restrict the outer sum in (3-36) to just that nuclide's index number.

For PP systems this solution will provide correct results when precursor nuclides are not collected on the monitor's filter. However, the ingrowth of the progeny from the decay of its parent, if the latter is collected (note that it need not be detected), is not accounted for in this formulation, and the solution will underestimate the monitor response in that case.

This FF monitor response solution is presented here because it works properly for single-nuclide (non-decay-chain) cases, and for the ^{88}Kr-^{88}Rb chain, which is frequently encountered in power reactor CPAM applications. For other FF situations the next two solution methods are recommended.

Method B

This approach is an extension of the basic formulation of the linear system itself. The idea is that, because the FF is also a linear system, we can combine it with the source/compartment/HVAC linear system into a single rate matrix **A**.

To see this, consider the ODE for the FF activity of nuclide n

$$\frac{d\zeta_n}{dt} = \kappa F \phi_n Q_n(t) - \lambda_n \zeta_n + \chi_n \lambda_n \zeta_{n-\Delta_n}$$

where the first term is the source from the sampled air, and the last term is the source from the decay of a precursor on the monitor filter. In the ODE Δ_n is the "distance" to the parent of nuclide n in the numbering scheme of the chain; it is either one or two (more on this below).

In the linear systems format we can consider the FF to be a single compartment, with a rate matrix

$$\mathbf{A}_{FF} = \begin{pmatrix} -\lambda_1 & 0 & 0 \\ \chi_2 \lambda_2 & -\lambda_2 & 0 \\ 0 & \chi_3 \lambda_3 & -\lambda_3 \end{pmatrix}$$

expressing the transfer of activity among the nuclides on the filter (here, e.g., three nuclides). The source of activity from the air is represented by the product

$$\mathbf{B}_{FF}\mathbf{u}_{FF}(t) = \mathbf{I} \begin{pmatrix} \phi_1 Q_1(t) \\ \phi_2 Q_2(t) \\ \phi_3 Q_3(t) \end{pmatrix} \kappa F \qquad (3\text{-}37)$$

where **I** is an (*N,N*) identity matrix, because each of the $m=N$ air concentrations only supplies activity to one nuclide.

The key to this extended-system formulation is to recognize that the source term (3-37) for activity from the air is just a transfer of activity from the compartments to the monitor filter, and so can be expressed as elements in a new **A** matrix, which we will denote as ***A***. The FF "compartment" does not have a source in the *system* **u** vector, because those sources supply activity only to the physical compartments.

We extend the system matrices by one "compartment," namely the FF collection medium. Thus the system dimension is now *P*, or the number of physical compartments *p* plus one. The total system dimension will now be *NP* rather than *Np*.

Consider again the **A** matrix definition in (3-12). Each of the compartmental-transfer submatrices $\boldsymbol{\alpha}$ is now to be extended to permit activity to be transferred from some combination of compartments to the FF monitor compartment, which is in row and column *P*. To illustrate, we use a three-physical-compartment system (p=3), and add the FF "compartment" as follows, for a given nuclide n in the PP system:

[6] This parameter could also include a correction for line losses and/or anisokinetic sampling.

$$\boldsymbol{\alpha}_n = \left(\begin{array}{ccc|c} \alpha_{11} & \alpha_{12} & \alpha_{13} & 0 \\ \alpha_{21} & \alpha_{22} & \alpha_{23} & 0 \\ \alpha_{31} & \alpha_{32} & \alpha_{33} & 0 \\ \hline \alpha_{n,P1} & \alpha_{n,P2} & \alpha_{n,P3} & -\lambda_n \end{array}\right) \tag{3-38}$$

where the elements in row P are the negative of the nuclide's decay constant λ, at element (P,P), and

$$\alpha_{n,P,k} = \kappa\, \phi_n\, F\, z_k^H \;\; ; \;\; k = 1, p$$

if we are monitoring the HVAC return, or

$$\alpha_{n,P1} = \frac{\kappa \phi_n F}{v_1} \qquad \alpha_{P2} = 0 \qquad \alpha_{P3} = 0$$

if we are monitoring, e.g., compartment one. The factors z^H are as defined in (3-10); these create the flow-weighted averaging of the compartmental concentrations as seen in the HVAC return. The appropriate collection efficiency and decay constant, per nuclide, must be used in each nuclide's $\boldsymbol{\alpha}$ submatrix.

Also, the $\boldsymbol{\mu}$ submatrices in (3-12) must be extended by one row and column. This extension accounts for the transitions in the decay chain on the FF collection medium, just as the other elements on the diagonal account for the transitions in the physical compartments. Thus these submatrices are now (P,P).

The source-allocation matrix **B** is also extended, to maintain the conformability of the matrices, but the monitor compartment does not receive any activity directly from a system source. Thus $\boldsymbol{B}$ is now (NP,m), where m is, again, the number of sources driving the physical system, and rows $(P, 2P, \ldots, NP)$ of $\boldsymbol{B}$ are zero-filled. These rows correspond to the FF compartments for each nuclide.

The volume vector $\boldsymbol{v}$ will now be defined as

$$v_{nP} = 1 \;\; ; \;\; v_{(n-1)P+k} = v_k \quad \left(k = 1, p \;\; ; \;\; n = 1, N\right)$$

with the FF elements having a value of unity. This is because the volume has already been accounted for in the FF elements in the submatrices $\boldsymbol{\alpha}$. This extended volume vector can be used in (14) to define a new (NP,NP) $\boldsymbol{C}$ matrix, which will permit finding both the concentrations (across nuclides and compartments) and the FF activities (across nuclides) in one step. Multiplying the FF activities by the respective efficiencies, per nuclide, will give the corresponding FF countrates. The initial-activity vector $\mathbf{x}_0$ is also extended, with the new entries, at elements nP, representing the activities on the monitor filter at time zero.

The state vector for this extended system will have the activities of the nuclides in the compartments in N sets of P elements, with the last in each set being the FF activity. Thus, the FF countrate is, using (3-27)[7] for the activity solution vector $\boldsymbol{x}$ (length NP),

$$\dot{C}^{FF}(t, j_1, j_2) = \sum_{n=1}^{N} \varepsilon_n\, x_{nP}(t, j_1, j_2) \tag{3-39}$$

while the concentration of nuclide n in compartment k is

$$Q_{n,k}(t, j_1, j_2) = \frac{x_{(n-1)P+k}(t, j_1, j_2)}{v_k} \tag{3-40}$$

This can also be written in vector form as

$$\boldsymbol{Q}(t, j_1, j_2) = \boldsymbol{C}\, \boldsymbol{x}(t, j_1, j_2)$$

and we find the concentrations at $\boldsymbol{Q}$-elements $(n-1)P+k$. The equilibrium concentration vector is

[7] Note that all sums in (3-27) are now taken over NP rather than Np.

$$\boldsymbol{Q}(\infty) \;=\; \boldsymbol{C}\left(-\boldsymbol{A}^{-1}\,\boldsymbol{B}\,\boldsymbol{u}^{*}\;\right) \tag{3-41}$$

If selected as the monitoring point, the HVAC return concentrations are used implicitly in finding the FF response, via the last row of the $\boldsymbol{\alpha}$ submatrices. To find the HVAC concentration for nuclide n from the solution vector $\boldsymbol{x}$, we can write

$$Q_n^{HVAC}(t, j_1, j_2) \;=\; \sum_{k=1}^{p} x_{(n-1)P+k}(t, j_1, j_2)\; z_k^H \tag{3-42}$$

The equilibrium HVAC concentration for nuclide n is

$$Q_n^{HVAC}(\infty) \;=\; \sum_{k=1}^{p}\left[-\boldsymbol{A}^{-1}\,\boldsymbol{B}\,\boldsymbol{u}^{*}\right]_{(n-1)P+k}\; z_k^H \tag{3-43}$$

With this approach we have a complete solution, for both the compartmental concentrations and the FF response, in a single formulation. This solution applies for single-nuclide or PP cases, and for the latter the ingrowth on the collection medium is included, if the collection efficiencies ϕ for precursors are nonzero.

Method C

This approach is best applied for more complex systems, with many compartments, or when the need for higher fidelity to actual contaminant transport/dispersal leads to the use of more detailed and sophisticated codes, such as CONTAM. The output from such codes, in the form of time-dependent concentrations of the nuclide(s), at the monitoring point, can then be used in a numerical integration to find the FF response. Of course, we could also use the concentrations generated by the solution (3-28).

Consideration of the ODE system for a decay chain on the FF collection medium will show that a straightforward extension of the convolution integral FF solution [1, (2)] for the activity ζ of the n-th nuclide is given by the recursive convolution integrals

$$\zeta_n(t) \;=\; \exp\left(-\lambda_n t\right) \int_0^t \left[\kappa F \phi_n Q_n(\tau) \;+\; \chi_n \lambda_n \zeta_{n-\Delta_n}(\tau)\right] \exp\left(\lambda_n \tau\right) d\tau \;+\; \zeta_n(0)\exp\left(-\lambda_n t\right) \tag{3-44}$$

where χ_n is, again, the branching ratio for the transition to nuclide n. Note that (3-44) includes an initial activity on the filter, although we usually take this to be zero (clean filter at start of analysis). If the forms of the $Q(t)$ are known analytically, then (3-44) can provide a closed-form solution for the FF activities. The concentration $Q(t)$ can have any shape; for the previous solution options we required it to be a linear combination of exponentials. If we define χ_1 to be zero, then (3-44) applies for a single nuclide as well.

To illustrate the parameter Δ, consider a decay chain with a branch at, e.g., nuclide three in the series. It decays to nuclides four and five, with branching ratios χ_4 and χ_5. In (44) when we find the activity of nuclide five due to the decay of its precursor (the second term in brackets inside the integral), that precursor will not be nuclide four (n-1) but rather nuclide three (n-2), so Δ_4=1 and Δ_5=2. If there is no branching in the chain, then Δ is unity for all nuclides in the chain.[8]

The countrate response solution per nuclide is obtained by using the output of (3-44) in (3-35). This approach explicitly accounts for the ingrowth of a nuclide on the filter due to the decay of its precursor on the filter. Using this with the concentration output (3-28) can thus provide a complete, correct solution for any PP system, for FF monitors (as can method B).

In some cases, notably including the ^{88}Kr-^{88}Rb chain that is of particular interest in power reactors, the precursor ^{88}Kr has a collection efficiency ϕ_1 of zero. This means that there is no ingrowth of ^{88}Rb because the second term in the integral in (3-44) for ^{88}Rb (n=2) will be zero. Thus, all three methods will produce the same countrate prediction.

[8] This "distance" also applies to (3-12); there, this principle is implemented by placing the $\boldsymbol{\mu}_n$ submatrix in column n-Δ_n.

Rectangular-Window Moving Filter

Method D

As with the FF monitor, if we have concentration values as a function of time, it is possible to use the RW countrate response model (1-5, 1-6) if numerical multiple integration is available.[9] The concentration time-dependence need not be exponential. However, this solution only applies for a single nuclide, or a PP system of length two if the precursor is not collected by the monitor (e.g., ^{88}Kr).

Method A (RW)

The RW countrate response for the exponential *Q(t)* formulated in Section IV is found using (1-21, 1-22). For moving-filter monitors we have the complication of a different response function for before and after the transit time. We will refer to the physical transit time T as the transit *interval*, to distinguish it from the "clock time" at which the transit interval elapses. Further, by definition, the transit-interval time is measured from the start of the respective concentration transient. Thus we will have different transit-interval-elapse clock times for the several sources. For a RW monitor the transit time T is the window length divided by the filter speed.

The countrate for time prior to the transit interval is found using the factor

$$\eta^{RW-1}(t, j_1, j_2, \lambda) = \kappa F \sum_{j=j1}^{j2} \sum_{h=1}^{4} \sum_{k=1}^{Np} \left[\mathbf{W}_k \, \Phi\left(\Psi_{h,j}\right) \, \Gamma_{h,j,k} \;\; \varphi_{RW-1}(t, \lambda, j, h, k) \left\{ 1 - \Phi\left(T + \Psi_{h,j} \right) \right\} \right] \tag{3-45}$$

with

$$\varphi_{RW-1}(t, \lambda, j, h, k) = \left\{ \begin{array}{l} \dfrac{1}{\left(\lambda + \xi_{h,j,k}\right)^2 T} \left[\begin{array}{l} \exp\left[\xi_{h,j,k} (t - \Psi_{h,j}) \right] \left(\left[t - \Psi_{h,j} \right] \left[\lambda + \xi_{h,j,k} \right] - 1 \right) + \\ \exp\left[-\lambda (t - \Psi_{h,j}) \right] \end{array} \right] \\ + \;\; \dfrac{1 - \dfrac{t - \Psi_{h,j}}{T}}{\lambda + \xi_{h,j,k}} \left\{ \exp\left[\xi_{h,j,k} (t - \Psi_{h,j}) \right] - \exp\left[-\lambda (t - \Psi_{h,j}) \right] \right\} \end{array} \right\} \tag{3-46}$$

when the arguments ξ are not equal to the negative of the decay constant λ. If they are equal, we use

$$\varphi_{RW-1}\left(t, \lambda, j, h, k\right) = \exp\left[-\lambda \left(t - \Psi_{h,j} \right) \right] \left\{ \left(t - \Psi_{h,j} \right) - \frac{\left(t - \Psi_{h,j} \right)^2}{2T} \right\} \tag{3-47}$$

The countrate for time after the transit interval is found using the factor

$$\eta^{RW-2}(t, j_1, j_2, \lambda) = \kappa F \sum_{j=j1}^{j2} \sum_{h=1}^{4} \sum_{k=1}^{Np} \left[\mathbf{W}_k \, \Phi\left(\Psi_{h,j}\right) \;\; \Gamma_{h,j,k} \;\; \varphi_{RW-2}(t, \lambda, j, h, k) \; \Phi\left(T + \Psi_{h,j} \right) \right] \tag{3-48}$$

with

$$\varphi_{RW-2}(t, \lambda, j, h, k) = \frac{1}{\left(\lambda + \xi_{h,j,k}\right)^2} \left[\exp\left[\xi_{h,j,k} (t - \Psi_{h,j}) \right] \left(\lambda + \xi_{h,j,k} - \frac{1}{T} \right) + \frac{1}{T} \exp\left[\xi_{h,j,k} (t - \Psi_{h,j} - T) \; - \; \lambda T \right] \right] \tag{3-49}$$

or, again, the special solution

$$\varphi_{RW-2}(t, \lambda, j, h, k) = \frac{T}{2} \exp\left[-\lambda \left(t - \Psi_{h,j} \right) \right] \tag{3-50}$$

[9] This has been exercised and does in fact produce the same responses as the solution developed here.

if needed. Note in (3-45) and (3-48) that we have a second Heaviside operator; this switches the solutions on or off as time passes through the transit times.

The complete RW countrate solution is obtained using

$$\dot{C}^{RW}(t, j_1, j_2) = \sum_{n-1}^{N} \varepsilon_n \phi_n \sum_{k=1}^{p} \left[\eta^{RW-1}_{(n-1)p+k}(t, j_1, j_2, \lambda_n) + \eta^{RW-2}_{(n-1)p+k}(t, j_1, j_2, \lambda_n) \right] z_k^H \tag{3-51}$$

where the same considerations apply as for (3-36). Note that, like this form of solution for the FF monitor, in a PP system where the precursor is collected by the monitor, the predicted RW response will be underestimated. This is because the ingrowth of the progeny due to the decay of the parent on the filter is not accounted for in the modeling. At this time there is no equivalent to either method B or C for RW monitors.

Circular-Window Moving Filter

We can proceed with the same analysis as for the RW, but now using the circular-window (CW) models (1-28) to (1-32). These expressions will be quite cumbersome, and for design purposes it will be sufficient to use the RW approximation for the CW response. This is done by using the adjusted RW window length

$$L_{CW} = \frac{16\,R}{3\pi}$$

where R is the CW window radius. This is (1-14), and the RW response will be close enough to the CW response for design purposes. See [1] for a comparison of the "exact" and approximate responses; they usually are within a few percent of each other.

Equilibrium Countrates

It will be useful to collect the expressions for the countrates attained by these monitors when the system is driven by one or more constant sources. These countrates can be found by using the expressions developed above, for a constant source, and taking limits as time becomes large. However, it will be simpler to note that the equilibrium of the concentration can be found using (3-3) or (3-11), and then use the response models from [1] for this constant concentration to find the monitor responses.

For method A, the limiting countrate for FF or RW is given by

$$\dot{C}(\infty) = \kappa F \sum_{n=1}^{N} \sum_{k=1}^{p} \varepsilon_n \phi_n \sigma_n \left[-\mathbf{A}^{-1} \mathbf{B} \mathbf{u}^* \right]_{(n-1)p+k} z_k^H \tag{3-52}$$

where σ_n is

$$\frac{1}{\lambda_n}$$

for FF, and

$$\frac{1}{\lambda_n} - \frac{1}{\lambda_n^2 T}\left[1 - \exp(-\lambda_n T)\right]$$

for RW. As usual, use z^S if monitoring a single compartment. (The subscripted-bracket notation means to use the indicated element of the vector that results from the matrix products in the brackets.)

For FF (3-52) is developed from (1-19), and it only applies when the product of the smallest decay constant and time is large, and if the nuclides are short-lived (SL).[10] For long-lived activity (LL), we see from (1-20) that the FF countrate will linearly increase without limit. The *slope* of the FF response would then be constant, but the countrate will not attain an equilibrium. For RW (3-52) is developed using (1-25), and it applies for either LL or SL activity. Recall that T is the RW transit interval. For LL activity the RW σ_n simplifies to $0.5T$, as seen in (1-26).

For CW we could use the models in [1] along with (11), but it will be much simpler to use the RW approximation, and then use (3-52) for RW with an adjusted transit interval,

$$T_{CW} = \frac{16\,R}{3\pi\theta}$$

where θ is the filter speed.

For method B, the equilibrium FF countrate is found directly, when no LL nuclides are present, using

$$\dot{C}^{FF}(\infty) = \sum_{n=1}^{N} \varepsilon_n \left[\boldsymbol{C} \left(-\boldsymbol{A}^{-1} \boldsymbol{B}\, \boldsymbol{u}^{*} \right) \right]_{nP} \tag{3-53}$$

where the italicized vectors/matrices are the extended versions. Note that the monitoring point (single compartment or HVAC) has already been accounted for in setting up the **A** matrix for this method.

There are no equivalent expressions for the equilibrium countrates for methods C or D, since these rely on external calculations of the concentrations.

Time to Equilibrium

It would be of interest to have some idea of the length of time needed for the concentrations and countrates to attain some fraction of their equilibrium values. In linear-systems analysis, the time-dependent behavior of the solution over long times is controlled by the "dominant root" [6, p. 304]. This is the eigenvalue with the smallest magnitude (minimum-magnitude eigenvalue, MME). With the MME found numerically from **A**, we can define a "time-to-equilibrium" (TTE) for the monitored concentration, with

$$TTE_Q = \frac{6\,\ln(2)}{MME}$$

by analogy to radioactive decay (six "half-lives"). This will be about 0.984 of the final equilibrium value, and will give an approximate idea of how long it will take the system to approach a constant monitored-concentration value. The clock time at which this occurs will be the sum of the TTE and the source's delay time Ω. The TTE is intended as a design guide, and not as a decision point in actual application of these calculations. It provides a rough indication, for a given system, of how long we will need to wait to be reasonably close to equilibrium.

A TTE for the countrates can be defined, for SL activity, as

$$TTE_C = \frac{6\ln(2)}{\lambda} + \frac{\ln\left(\dfrac{\lambda}{MME}\right)}{\lambda - MME}$$

where the second term is the inflection point of the countrate. For a RW monitor the TTE will be the smaller of this or the transit time, for any activity. The countrate TTE is somewhat longer than the concentration TTE, because the concentration must become more or less constant before the countrates can do the same.

To illustrate these calculations, consider the concentration behaviors in Fig. 3-3. This single-nuclide, four-compartment, three-source system will be discussed below, but for the present we use it with constant sources. The concentrations are found using

[10] Short-lived activity can decay significantly during the analysis period, while long-lived activity does not.

(3-28), and the horizontal dotted lines are the equilibria for the compartment concentrations from (3-29) and the monitored concentration from (3-31). The vertical dotted line is the TTE_Q, and it provides a good estimate for this E-ACH system.

In Fig. 3-4 we have the FF responses, using (3-36); the overall (sum) response has Poisson noise added.[11] The RW response for this example is very similar. The responses to the individual sources are indicated with dotted lines. Note the nonzero initial slope, due to the nonzero initial concentration in the system. The solid horizontal line is the predicted equilibrium, from (3-52); the countrate does attain this level and it stays there, because the nuclide is SL (^{88}Rb). The solid vertical line is the TTE_C, and this provides a reasonable indication of when the equilibrium countrate was attained.

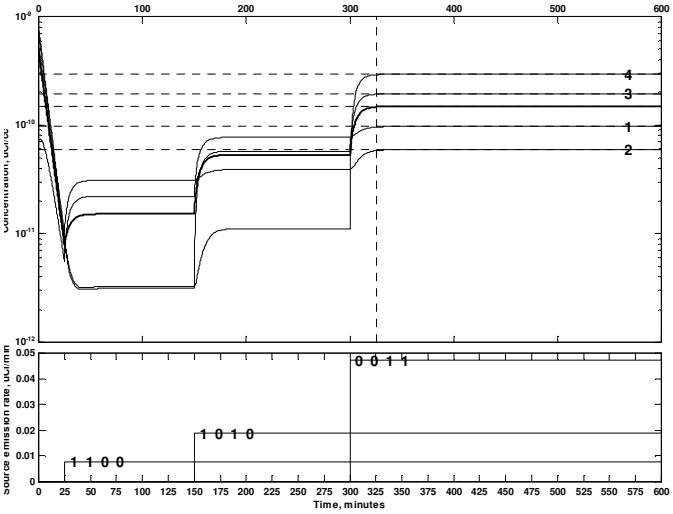

*Fig. 3-3. Constant-source concentrations and sources. Numbers on source lines indicate compartments driven by the source (i.e., transposed columns of **B**).*

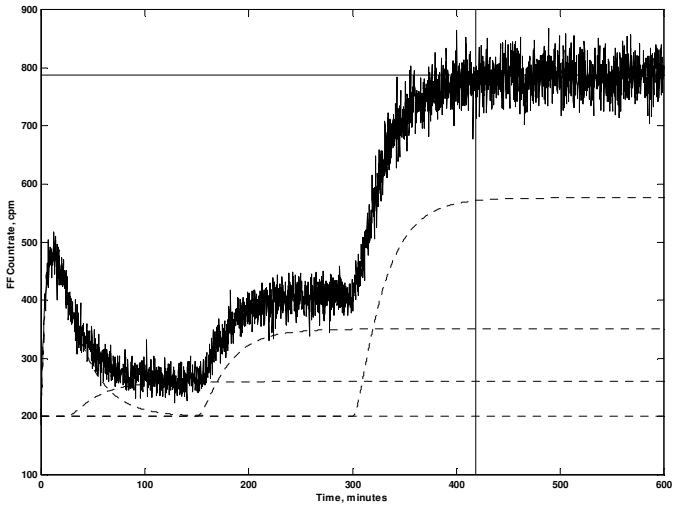

Fig. 3-4. Fixed-filter countrate response for constant sources of Fig. 3-3.

Example Analyses

Single Nuclide, Four-Compartment

Introduction

This example, one of many numerical experiments that have been run using the methodology developed above, is meant to illustrate the concentration dynamics and monitor responses for a multicompartment facility, with a single nuclide monitored via the HVAC return duct.

System

We have four compartments, interconnected as shown in Fig. 3-1. The compartments have no exfiltration to the environment, as is usually the case for a nuclear facility. One set of unforced flows is shown in the figure, but these are all set to zero. The HVAC service is balanced and is E-ACH. The HVAC has a ventilation fraction of 0.5, and a filtration efficiency of 0.5 as well. The nuclide being monitored is LL, so that we can see the difference in the FF and RW responses. (As shown in [1], for SL the responses are very similar.) Plateout is not used.

Sources

There are three sources, whose behavior is illustrated in the lower pane of Fig. 3-5. The first is a DE source, with a delay of 25 minutes, and a relatively low amplitude. Its peak is attained at about 60 minutes, after which it decays slowly. This source

[11] This data is processed with a variance-reducing countrate algorithm, described in [2, (4)].

drives compartments three and four. Next we have a constant source, with a delay of 200 minutes, and a somewhat larger magnitude. This source drives compartments one and two. Finally we have a "puff" source, a rapidly-decaying SE, at 400 minutes. This source drives compartments one and three. We also have nonzero initial conditions, with (randomly-selected) activity in all four compartments at time zero.

Concentration Dynamics

In the top pane of Fig. 3-5 we have the concentration behaviors for this system. The thinner lines are the four compartmental concentrations, via (3-28), while the thicker line is the HVAC-return, monitored concentration, from (3-30). The dotted horizontal lines are the equilibrium concentrations, due to the constant source, from (3-29), and (3-31) for the HVAC. The circles and squares on these lines are the results from an independent numerical ODE-solver solution for the concentrations; clearly the agreement is excellent.

Monitor Responses

The FF response is shown in Fig. 3-6. The thicker solid line is the overall response, i.e., the sum of the responses due to the individual sources, which are shown as dotted lines. The responses are found using (3-36), one source (and the initial condition) at a time. The circles are the results from the FF numerical model discussed in [1]; they agree well.

In Fig. 3-7 we have the RW responses for this run, using (3-51). Here we can see the clearing of the LL activity by this monitor, especially in the initial-condition and SE responses. In this case we have a countrate equilibrium, because there is a constant source; the equilibrium is found using (3-52), and it is indicated by the thin solid line. Note that the constant-source portion of the response does attain this equilibrium level, at a time equal to the transit interval of the monitor (120 minutes) plus the delay time of the constant source (200 minutes). The overall response will also attain this level, when the DE source has decayed away. Again the circles represent the output from the numerical model for RW, from [1], and the agreement is good.

Parent-Progeny, Two-Compartment

Introduction

In this example we will consider a case study of a monitoring application that arose at an operating nuclear power plant, the SM-1.[12] At issue was the interpretation of a CPAM (FF) response during preparations for entry into the reactor containment building. The main interest was in recognizing when the containment air concentration was at a level acceptable for the initiation of purging, and also to estimate the concentration for determination of respiratory protection needed for personnel entry.

During normal operations, primary coolant leakage into the control-rod-drive sump, directly below the pressure vessel, released significant quantities of ^{88}Kr into the sump air. The decay of ^{88}Kr of course produced ^{88}Rb. There was no air movement into or out of the sump (excepting perhaps some slight unforced flow due to temperature differentials), so this activity remained in the sump, and attained equilibrium, assuming that the ^{88}Kr emission rate was nearly constant.

When the need arose to enter containment, the reactor was shut down and the primary pressure reduced. This would greatly reduce the coolant leakage, and the source term for the Kr would essentially vanish. The sump activities would then decrease, with the ^{88}Kr half-life (2.8 h). The concentrations of Kr-Rb in the bulk of containment were very small, because there was no mechanism to move the highly contaminated air out of the sump, and there were no other comparable primary coolant leakages.

The SM-1 containment had a "decontamination-ventilation fan" (DVF) air handling system. In its decontamination mode the containment air was recirculated through HEPA filters; in the ventilation mode the air flow was directed to the plant stack, after opening the personnel hatch. During normal operations the DVF was secured. When the primary system pressure was reduced to atmospheric, the DVF was started, and, after some recirculation time, the personnel hatch was opened and the DVF was "valved to stack."

[12] The SM-1 was a small PWR operated by the U. S. Army Corps of Engineers Reactors Group at Ft. Belvoir, VA, ca. 1954-74.

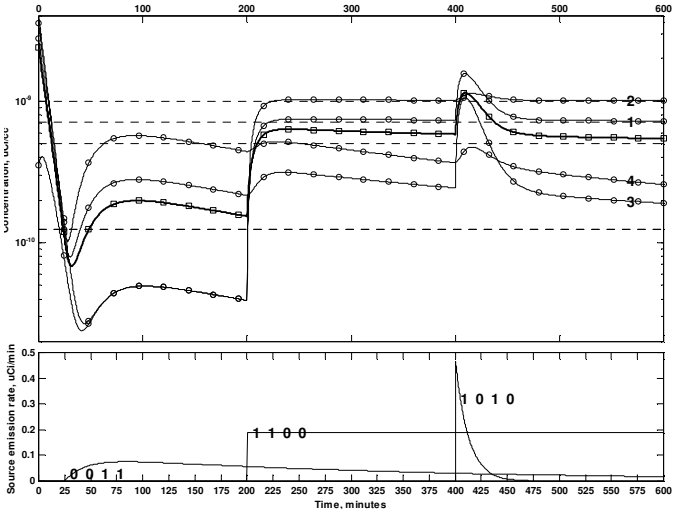

Fig. 3-5. Concentrations and sources for four-compartment system. Symbols represent independent numerical solutions. In upper pane, thicker line is HVAC-return concentration.

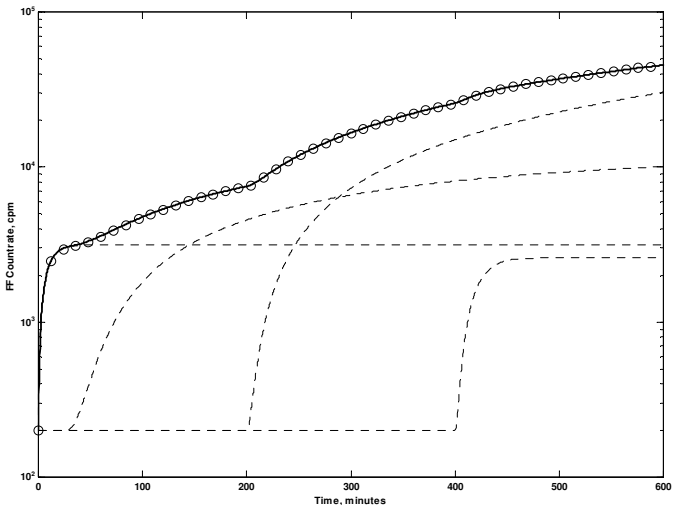

Fig. 3-6. Fixed-filter response for four-compartment system of Fig. 3-5. Circles represent independent numerical solution. Dotted lines are responses to individual sources.

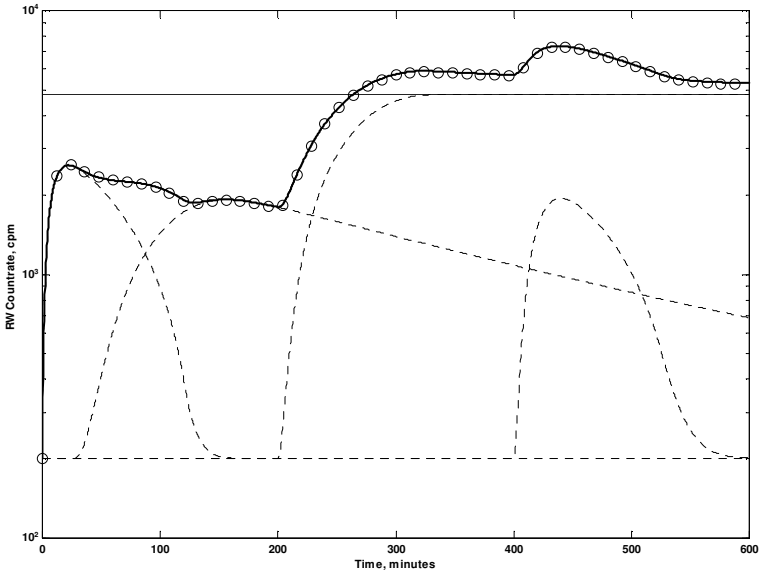

Fig. 3-7. RW response for four-compartment system of Fig. 3-5. Same notation as Fig. 3-6.

Recirculation was done while the containment was otherwise sealed (the DVF filters and some ductwork were outside containment). The idea, of course, was to use the DVF to reduce the levels of particulate nuclides in the containment air prior to personnel entry and prior to purge (ventilation). A FF monitor sampled the air in the DVF return, upstream of the filters.

During containment entries the FF monitor responses were used to estimate the concentration in containment, but when personnel entry was made, localized high-volume air sampling showed concentration estimates that were much lower than those indicated by the FF monitor. At the time, the methodology for interpreting the monitor response in terms of the concentration dynamics was not well-developed, so that some difference would be expected; however, the difference was large enough to indicate that there was some other inconsistency.

In studying and modeling this system, to understand the observed monitor responses so that improved procedures for containment entry could be developed, investigation of the "as-built" drawings for the plant showed that a condensate drain line

for the DVF led to the containment sump. The containment air was humid, so that during recirculation significant condensation would occur in the DVF return ducts. This moisture was to drain to the sump via a small pipe (about one inch diameter), that entered the sump about one foot above the floor. This entry point was not covered by water.

The DVF drain line was a "sneak circuit" that provided a direct path for highly contaminated air from the sump to enter the DVF return. The DVF's function was compromised by this unintended path, and it also had significant effects on the indicated (monitored) concentrations. Next we will model this system using the mathematics developed above, and investigate the monitor responses with regard to the actual concentration behaviors during recirculation and purge.

System

This system can be modeled as parent-progeny (^{88}Kr-^{88}Rb), two-compartment (sump and rest-of-containment), with HVAC (DVF), used in both pure recirculation/filtration (υ=0, Θ>0) and pure ventilation (υ=1) modes. In Fig. 3-8 we have a schematic of the system. The following points are important in defining the **A** matrix for this system; this assumes the DVF is on, in either recirculation or purge mode:

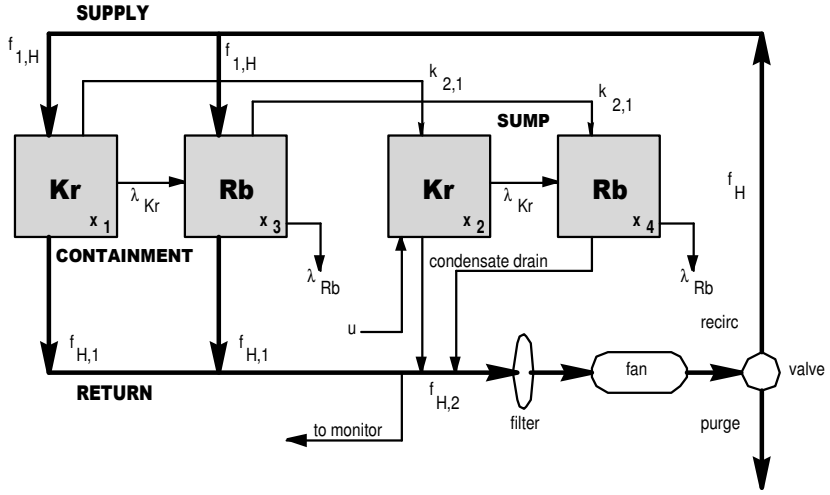

Fig. 3-8. System sketch for SM-1 containment example.

- There is no DVF flow directly to the sump volume (f_{2H}=0).
- The air flow from the sump to the DVF, via the drain line, (f_{H2}) is very small.
- The makeup air supply to the sump is from the containment air volume (k_{21}).
- The flow from containment to the sump equals the flow from the sump to the DVF (k_{21}=f_{H2}).
- There is no direct air flow from the sump to the containment (k_{12}=0).
- All the exchange rates are the same for Kr and Rb.
- The DVF filter efficiency for ^{88}Kr is zero.
- The DVF filter efficiency for ^{88}Rb is taken to be 0.5.
- The plateout, if any, of ^{88}Rb is ignored.
- As usual for containment buildings, the exfiltration rates are zero.

Adapting the general parent-progeny model (12) to this situation, we have a 2-chain and two compartments, so that the system matrix becomes:

$$\mathbf{A} = \left(\begin{array}{cc|cc} \alpha_{11}^{Kr} & \alpha_{12}^{Kr} & 0 & 0 \\ \alpha_{21}^{Kr} & \alpha_{22}^{Kr} & 0 & 0 \\ \hline \lambda_{Rb} & 0 & \alpha_{11}^{Rb} & \alpha_{12}^{Rb} \\ 0 & \lambda_{Rb} & \alpha_{21}^{Rb} & \alpha_{22}^{Rb} \end{array} \right)$$

The state variables are: x_1, ^{88}Kr in containment; x_2, ^{88}Kr in sump; x_3, ^{88}Rb in containment; x_4, ^{88}Rb in sump. Using (8) with substitutions as needed for this problem, we will have the **A**-elements

$$\begin{aligned} \alpha_{11}^{Kr} &= -k_{21} - \lambda_{Kr} + \left[(1-\upsilon)\frac{f_{1H}}{f_H} - 1 \right] \frac{f_{H1}}{v_1} \\ \alpha_{12}^{Kr} &= (1-\upsilon)\frac{f_{1H}}{f_H}\frac{f_{H2}}{v_2} \\ \alpha_{21}^{Kr} &= k_{21} \\ \alpha_{22}^{Kr} &= -\lambda_{Kr} - \frac{f_{H2}}{v_2} \\ \alpha_{11}^{Rb} &= -k_{21} - \lambda_{Rb} + \left[(1-\Theta)(1-\upsilon)\frac{f_{1H}}{f_H} - 1 \right] \frac{f_{H1}}{v_1} \\ \alpha_{12}^{Rb} &= (1-\Theta)(1-\upsilon)\frac{f_{1H}}{f_H}\frac{f_{H2}}{v_2} \\ \alpha_{21}^{Rb} &= k_{21} \\ \alpha_{22}^{Rb} &= -\lambda_{Rb} - \frac{f_{H2}}{v_2} \end{aligned}$$

The ventilation fraction υ is zero during recirculation, and is unity for purge. The HVAC flow to containment f_{1H} is the entire flow f_H, because no air flows directly from the HVAC to the sump. Thus these elements could be simplified further. The sump-to-DVF flow is one percent of the total flow, and the sump volume is five percent of the containment volume. The DVF flowrate is 4000 cfm and the containment total volume is 34000 ft^3.

Sources

The only source of activity in this system is of ^{88}Kr, and it is in the sump. However, this source is only active during normal operations, because it depends on the pressure in the primary system. We are analyzing the behavior during the operation of the DVF, which only occurs during shutdown, so that the coolant-leakage source of ^{88}Kr is no longer significant. Thus the only "source" for the system is the initial condition in the sump, which is nonzero; in the rest of containment we will assume a zero initial condition for both nuclides.

During operation we can assume an essentially constant emission rate of ^{88}Kr, so that (3-29) will give the equilibrium concentrations; with no plateout and no DVF flow the equilibrium activities, and concentrations, are equal. We will treat the ^{88}Kr source as remaining constant at its operational level, and then turning off instantaneously at the start of DVF recirculation.

The ^{88}Kr source term during operation is given by the product of the leakage rate, the coolant concentration, and the partition factor. For the example runs these parameters were 0.003 gpm, 0.01 μCi/cc, and unity, respectively. These values were selected arbitrarily; the concentration and countrate results will scale linearly with this product. The monitor parameters were: detection efficiency 0.2; flowrate, 5 cfm; collection and line-loss efficiency, 0.7. There is no **Bu** product for this problem, because there are no active sources.

Concentration Dynamics, Recirculation

In Fig. 3-9 we have a plot of the sump and containment concentrations for ^{88}Kr (squares) and ^{88}Rb (circles), for the recirculation mode. The sump concentrations have filled (solid) symbols. The lines are calculated from (3-27). The symbols are found using a numerical ODE solver, and the agreement is good. The thicker solid line is the DVF return concentration, from (3-30), which is what the monitor samples.

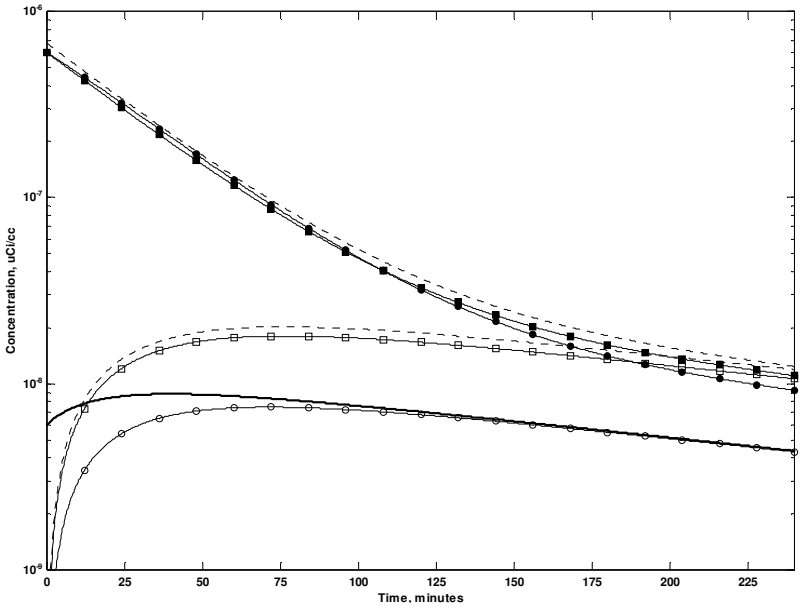

Fig. 3-9. SM-1 (2-compartment Kr-Rb) concentrations, for recirculation. Symbols represent independent numerical solutions: ■= ^{88}Kr, sump; ●=^{88}Rb, sump; = ^{88}Kr, containment; ○=^{88}Rb, containment. Thicker line is DVF (HVAC) return concentration, ^{88}Rb. Dotted lines indicate transient-equilibrium concentrations.

At the start of recirculation, the sump concentrations are relatively high, while the containment concentrations are very small. As the DVF operates, the sump concentrations decrease while the containment concentrations increase. This is contrary to the purpose of the DVF; if it was not used, the concentrations in containment areas other than the sump would remain low. On the other hand, if work needed to be done in the sump area, this unintended flow would help to reduce the high concentrations there, and this reduction would not likely happen otherwise, because there was no ductwork connecting the DVF to the sump area.

The monitored concentration starts at a level much higher than that in containment, increases for about an hour, and then decreases and tracks the containment ^{88}Rb concentration after about two hours. Thus the monitored concentration does not represent the concentration in containment for the first two hours of recirculation, although the difference is not large after about 30 minutes. The monitored concentration is higher than that in containment because the DVF return is receiving contaminated air from the sump, albeit at a low flow rate, via the condensate drain line.

The dotted lines in Fig. 3-9 indicate the ^{88}Rb levels that would occur during transient equilibrium with its parent. Note that, for the sump, the concentrations start out equal, and then the ^{88}Rb increases toward the equilibrium level, which is

$$\frac{\lambda_{Rb}}{\lambda_{Rb} - \lambda_{Kr}} = 1.12$$

That is, in the absence of filtration and any source term, the sump ^{88}Rb concentration would be 1.12 times the ^{88}Kr concentration as they both decay off with the ^{88}Kr half-life. With filtration, we see that the sump ^{88}Rb concentration crosses over and falls below the sump ^{88}Kr concentration, in about two hours. The containment Rb concentration stays below the containment Kr at all times. The difference between the containment dotted line and the actual containment ^{88}Rb concentration represents the effect of the DVF filtration.

As time proceeds past about four hours of recirculation the sump and containment ^{88}Kr concentrations become essentially equal, and then both decay at the ^{88}Kr half-life, as do both ^{88}Rb concentrations. The DVF filtration is not having a significant effect on the rate of removal of the ^{88}Rb; it produces an *offset* from the level that would obtain with no filtration (the dotted line), but the *rate* of the ^{88}Rb concentration's decrease is the same as that of the ^{88}Kr. This happens because ^{88}Rb is produced by the decay of ^{88}Kr, and the DVF does not remove the Kr.

Concentration Dynamics, Purge

In Fig. 3-10 we have the concentration behaviors for a containment purge, starting from about the concentration values at the end of the run in Fig. 3-9. The notation is the same, with the addition of the plus signs, which represent the rate of decrease due to pure dilution. The containment concentrations decrease rapidly, at the dilution rate, while the sump concentrations maintain a rate of decrease that is now larger than that due only to the ^{88}Kr decay. The (unintended) removal of air via the condensate drain line is hastening the reduction of the sump concentrations.

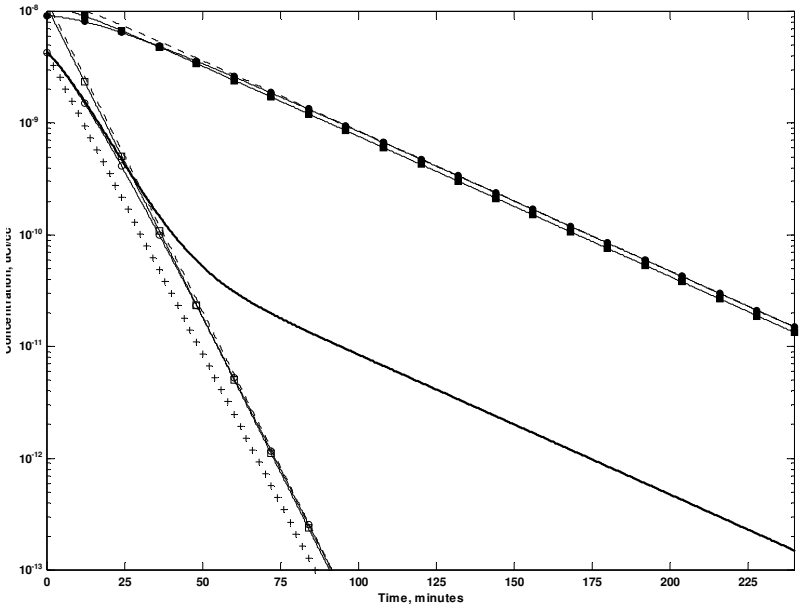

Fig. 3-10. SM-1 concentrations, for purge. Same notation as Fig. 3-9, with + representing pure dilution of ^{88}Rb from initial concentration.

In this mode, the monitored (DVF return) concentration follows the containment ^{88}Rb behavior, as it was doing at the end of the recirculation mode, for roughly the first half-hour. After this time, it decreases more slowly, now following the rate of decrease of the sump concentrations. This is due to the fact that as the containment concentration becomes smaller it reveals the contribution from the low-flowrate, but relatively high-concentration, sump activity. Thus the monitored concentration would indicate higher levels in containment than actually exist, although by the time this effect becomes significant the levels are low.

Note that the containment purge leads to a particulate effluent release of a rapidly-changing concentration of a short-lived nuclide, ^{88}Rb. Estimating the activity released due to this containment purge is of interest; see (2-18) for a FF measurement technique that was developed at the SM-1 specifically for this purpose.

Fig. 3-11 shows the concentrations for a continuous recirculation-to-purge run, with four hours of recirculation and four hours of purge. Note that the slope of the sump concentrations decreases as the recirculation period proceeds, and then regains the same level once the purge begins. The decrease in slope is due to the ^{88}Kr activity in containment re-entering the sump, until the two concentrations become equal, and then both decrease with the ^{88}Kr half-life until the purge begins.

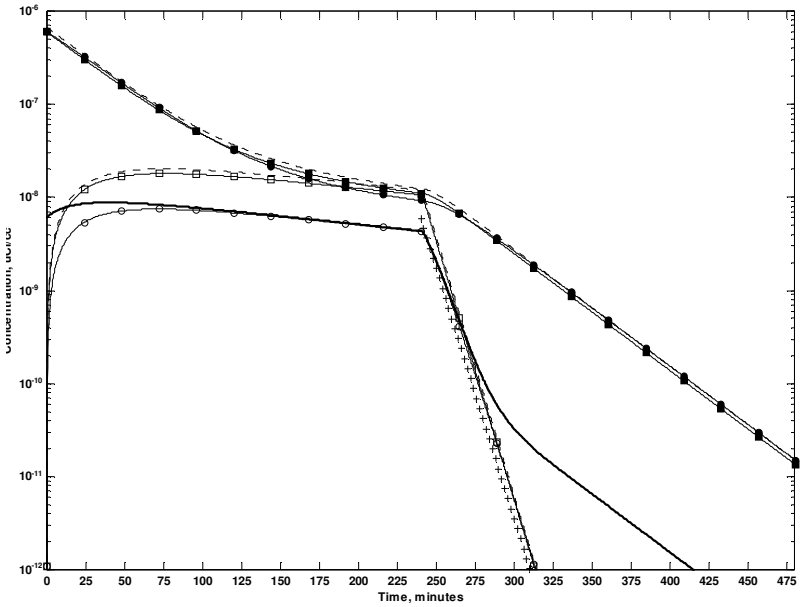

Fig. 3-11. SM-1 concentrations, continuous recirculation-to-purge. Same notation as Fig. 10.

Monitor Response, Recirculation and Purge

In Fig. 3-12 we have the FF response, generated by numerical integration of the monitored concentration in Fig. 3-11, and with Poisson noise added.[13] That is, the monitor response was found using method C rather than A. The squares in Fig. 3-12 show the output from the numerical model discussed in [1]; we see that the results agree well. If only FF responses are needed, and if the concentration behavior is available, then the direct integration of method C is a straightforward way of obtaining the FF response.

We see that the monitor, starting with a clean filter at the start of recirculation, exhibits a nonzero initial slope. This is due to the fact that there is a nonzero initial monitored concentration, as we can see in Fig. 3-11. Using (2-7) we could estimate this initial concentration. The containment ^{88}Rb concentration does not change very much once it has increased at the start of recirculation, so that we could use this initial estimate as an approximate measurement, for procedural purposes.

As recirculation continues, the monitor response reaches a broad peak and then decreases, following the slow decrease of the monitored ^{88}Rb concentration. When the purge begins, if we do not change the monitor collection medium the FF response will then decrease rapidly towards background.

If, as is more likely, we change the filter at the start of the purge, then the FF response is as shown in Fig. 3-13. This has the countrate obtained using (3-36), with noise added, and also the countrate from method C, as the thicker solid line. Here we also have a nonzero initial slope, which can be used to estimate the initial concentration at the start of the purge. We could use this along with the dilution rate of the DVF (f_H / v) to provide a procedural guideline as to the ^{88}Rb concentration in containment. This is the "plus sign" line in Figs. 3-10 and 3-11; note that it tracks the actual concentration much better than the concentration that would be indicated by a monitor observing the DVF return concentration, if we had a quantitative method for converting that monitor's dynamic response to a concentration estimate.[14]

[13] This data is also processed with the variance-reducing countrate algorithm of (2-4).
[14] See [2] for several approaches to this problem.

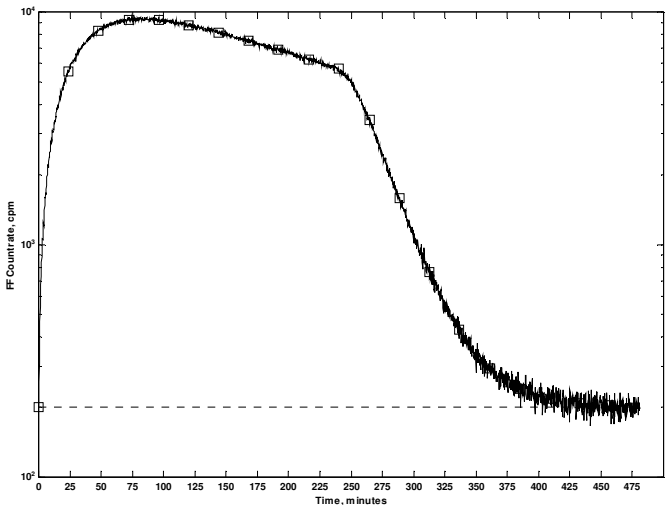

Fig. 3-12. SM-1 continuous recirculation-to-purge, fixed-filter response with Poisson noise, no filter change. Symbols represent independent numerical solution. Dotted line is background countrate.

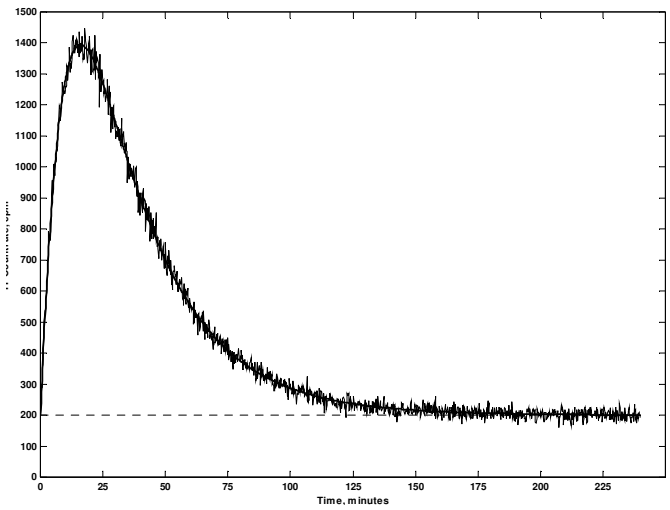

Fig. 3-13. SM-1 purge fixed-filter response with Poisson noise; filter change at start of purge. Thicker solid line is response from method C.

Conclusion

We have developed expressions that can be used to predict CPAM responses, for multicompartment systems with HVAC. Several options for these calculations are available, with three choices for FF monitors, and two choices for RW monitors. There are, however, some limitations on these prediction models; consider the nuclide behaviors in Table II.

TABLE II

NUCLIDE CASES, FOR MONITOR RESPONSE PREDICTION

Case	Chain Length	Collection Efficiency	Example
1	$N = 1$	$\phi_1 > 0$	^{137}Cs
2	$N = 2$	$\phi_1 = 0$	^{88}Kr – ^{88}Rb
3	$N \geq 2$	$\phi_n > 0$	Rn progeny

These cases arise because some of the calculations do not account for the ingrowth of a progeny nuclide due to the decay of its parent on the monitor filter. In Table II, the first and second cases do not have this problem, in the first instance because it is not a PP situation, and in the second because the parent nuclide is not collected on the filter. The third case applies when any precursor in a chain is collected, if its progeny is also collected. Methods that do not account for ingrowth when it is present will underestimate the monitor response.

The monitor response prediction methods are summarized in Table III, with regard to these nuclide cases. In this table the *u(t)* column indicates the assumed shape of the source behavior; the double-exponential form (18) was used in developing the solutions for methods A and B. Methods C and D are purely numerical and will apply for any (integrable) concentration behavior, which in turn could be generated by any source behavior.

TABLE III

SUMMARY OF MONITOR RESPONSE PREDICTION METHODS

Method	Equation	Monitor	Case	*u(t)*
A	(36)	FF	1,2	(18)
A	(51)	RW	1,2	(18)
B	(39)	FF	1,2,3	(18)
C	(35),(44)	FF	1,2,3	any
D	[1, (5-6)]	RW	1,2	any

Which of the methods we would select depends of course on the problem definition. If we have used "external" concentration calculations, e.g., from a code such as CONTAM, then methods C and D become useful, while if we are using the integrated approach developed in this paper, methods A and B are appropriate. For many power reactor RMS analyses, the straightforward modeling implemented in methods A and B will be a reasonable approach. The computations are readily mechanized, and they will provide a valuable analytical tool for the efficient analysis of many CPAM applications.

References

[1] W. C. Evans, "Mathematical models for the dynamic response of continuous particulate air monitors," *IEEE Trans. Nucl. Sci.*, vol. 48, pp. 202-218, Apr. 2001. Chapter 1 here.

[2] W. C. Evans, "Quantitative methods for continuous particulate air monitoring," *IEEE Trans. Nucl. Sci.*, vol. 48, pp. 1639-1657, Oct. 2001. Chapter 2.

[3] G. A. F. Seber and C. J. Wild, *Nonlinear Regression.* New York, NY: Wiley, 1989, p. 386.

[4] D. H. Anderson, *Compartmental Modeling and Tracer Kinetics.* New York, NY: Springer-Verlag, 1983, p. 63.

[5] K. Godfrey, *Compartmental Models and Their Application.* New York, NY: Academic, 1983, p. 29.

[6] W. J. Palm III, *Modeling, Analysis, and Control of Dynamic Systems.* New York, NY: Wiley, 1983, p. 178.

[7] R. A. DeCarlo, *Linear Systems: A State-Variable Approach with Numerical Implementation.* Englewood Cliffs, NJ: Prentice-Hall, 1989, p. 201.

[8] J. J. Tuma, *Engineering Mathematics Handbook*, 3rd ed. New York, NY: McGraw-Hill, 1987, pp. 242-247.

[9] P. V. O'Neil, *Advanced Engineering Mathematics*, 3rd ed. Belmont, CA: Wadsworth, 1991, pp. 236-245.

[10] F. L. Lewis, *Applied Optimal Control and Estimation*. Englewood Cliffs, NJ: Prentice-Hall, 1992, p. 81.

Updates

Need geometric correction; relation of this to full decay-chain RW/CW models??; redo 2compartment2nuclides incl SM1 with matrix expo not eigens

Chapter 4

Fast-Filter-Speed Method

Health Physics, 102(4) April 2012; 410-418. Erratum 102(6) June 2012; 708

A previously-published mathematical model for the dynamic response of moving-filter continuous particulate air monitors has been enhanced, to extend that model to include decay chains. During this work it was observed that a quantitative relation appeared to exist between the monitor count rate and the time-dependent particulate airborne radioactive material concentration if, and only if, the filter (tape) speed was much faster than the nominal 2.54 cm h^{-1} (one inch h^{-1}). The extended model demonstrated that operating moving-filter monitors at this nominal filter speed does not provide a quantitative measurement of a changing airborne particulate concentration of a fission product or other contaminant. By contrast, at faster filter speeds, e.g., 76.2 or 152.4 cm h^{-1} (30 or 60 inches h^{-1}), numerical experimentation with this model showed that the count rate trace has essentially the same shape as the concentration profile. It was then found that a quantitative relation applies, but only when the filter speed is sufficiently fast so that a Taylor series expansion of the monitor count rate can be reasonably well truncated at the first-order term. This mode of operation, which does not require any new monitor hardware, is capable of tracking rapidly-changing concentrations. Since the fast filter speed also reduces the monitor's count rate, all else being equal, the approach will best be used for relatively high-level concentrations, such as may occur in abnormal or "accident" conditions. The count rate suppression may also be useful for reducing the detector saturation that can occur with higher levels of airborne particulate radioactivity, in post-accident situations.

Introduction

Moving-filter continuous particulate air monitors have been used in nuclear facilities for decades. Usually they are deployed in situations where dust loading on the collection medium is a problem, such that a fixed-filter monitor would have its flow rate diminished too quickly, requiring frequent filter changes. Previous work [1,2] has shown, however, that only under the most restrictive assumptions is there any quantitative relation between an observed (net) count rate and the particulate air concentration, for a moving-filter monitor.

For applied radiological protection purposes in nuclear facilities it would be very useful to find a technique for using these monitors in a manner that would do more than just generate an alarm; the question is whether they can be used to actually measure a rapidly-changing air concentration, as it is happening. It seems that some users of these devices interpret the manufacturer's "calibration curves" to mean that, at any time, one can take the monitor's net count rate, multiply by a conversion constant read from those curves, and obtain an estimate of the air concentration at that time. It is the case, as shown in [2], that this simple conversion only applies if the radioactivity has a concentration which remains constant for a time on the order of several hours. If these conditions are not met, then there is no quantitative relation between a moving filter monitor's net count rate and the changing air concentration that drives that count rate.

In extending the moving-filter model reported in [1] to include decay chains, so that natural airborne radioactivity (radon-thoron) can be accounted for, the lack of a quantitative relationship was clear, in numerical experimentation with this extended model. However, it had previously been speculated in that earlier work that a variable-speed filter motion might show promise as a quantitative method. In exploring this idea, it was seen that using a constant but much faster filter speed than normal, e.g., perhaps 76.2 or 152.4 cm h^{-1} (30 or 60 inches h^{-1}) instead of the usual 2.54 cm h^{-1} (one inch h^{-1}), provided an apparent proportionality between the count rate and a changing concentration. This proportionality was numerically verified, and then a solid mathematical foundation was found for it. The purpose of this paper is to report on these developments, and to show that a moving-filter monitor can, for the first time, be used to quantitatively assess a changing air concentration.

Monitor Response Mathematical Model

Consider the sequential, "chain" decay of a series of nuclides, e.g., of length three, deposited from time-dependent concentrations in sampled air onto a collection medium simultaneously viewed by a detector. In order to calculate the count rate response of a particulate monitor, the starting point is a set of ordinary differential equations (ODE) for the time-dependent

activity on the collection medium, or "filter." For either a fixed filter, or a differential area of a moving filter, these equations are (the symbols are defined below):

$$\begin{aligned}
\frac{d\alpha_1}{dt} &= -\lambda_1 \alpha_1 && + k F \varphi Q_1(t) \\
\frac{d\alpha_2}{dt} &= \lambda_2 \eta_2 \alpha_1 - \lambda_2 \alpha_2 && + k F \varphi Q_2(t) \\
\frac{d\alpha_3}{dt} &= \lambda_3 \eta_3 \alpha_2 - \lambda_3 \alpha_3 && + k F \varphi Q_3(t)
\end{aligned} .$$

These equations are re-cast into the linear systems format, using for now constant concentrations,

$$\mathbf{A} = \begin{pmatrix} -\lambda_1 & 0 & 0 \\ \eta_2 \lambda_2 & -\lambda_2 & 0 \\ 0 & \eta_3 \lambda_3 & -\lambda_3 \end{pmatrix} \qquad \mathbf{B} = \begin{pmatrix} 1 & 0 & 0 \\ 0 & 1 & 0 \\ 0 & 0 & 1 \end{pmatrix} ,$$

$$\mathbf{u} = \begin{pmatrix} Q_1 \\ Q_2 \\ Q_3 \end{pmatrix} k F \varphi \qquad \boldsymbol{\alpha} = \begin{pmatrix} \alpha_1 \\ \alpha_2 \\ \alpha_3 \end{pmatrix}$$

so that

$$\frac{d}{dt}\boldsymbol{\alpha} = \mathbf{A}\,\boldsymbol{\alpha} + \mathbf{B}\,\mathbf{u} .$$

The matrix **B** is the source-allocation matrix, which in this case is just an identity matrix, since each air concentration source term "drives" only that respective nuclide's activity. The activity vector **α** leads to the count rate vector via the efficiency-yield (abundance) product matrix **Ψ**

$$\boldsymbol{\Psi} \equiv \begin{pmatrix} \varepsilon_1 \gamma_1 & 0 & 0 \\ 0 & \varepsilon_2 \gamma_2 & 0 \\ 0 & 0 & \varepsilon_3 \gamma_3 \end{pmatrix} .$$

For background on the linear-systems approach, see [3] or [4]. The mathematical model for the time-dependent response of a rectangular-window (RW) moving-filter continuous particulate air monitor is then given by the matrix-exponential multiple integrals:

$$\boldsymbol{\alpha}_{RW}(t \le T) = \frac{1}{L}\left[\int_0^{vt} \int_{t-\frac{x}{v}}^{t} e^{\mathbf{A}(t-\tau)} \mathbf{B}\,\mathbf{u}(\tau)\, d\tau\, dx + \int_{vt}^{L} \int_0^{t} e^{\mathbf{A}(t-\tau)} \mathbf{B}\,\mathbf{u}(\tau)\, d\tau\, dx \right]; \tag{4-1}$$

$$\boldsymbol{\alpha}_{RW}(t \ge T) = \frac{1}{L} \int_0^{L} \int_{t-\frac{x}{v}}^{t} e^{\mathbf{A}(t-\tau)} \mathbf{B}\,\mathbf{u}(\tau)\, d\tau\, dx ; \tag{4-2}$$

$$\dot{\mathbf{C}}_{RW}(t) = \boldsymbol{\Psi}\,\boldsymbol{\alpha}_{RW}(t) = \begin{pmatrix} \dot{C}_1(t) \\ \dot{C}_2(t) \\ \dot{C}_3(t) \end{pmatrix} . \tag{4-3}$$

where **α** is a vector of decay-chain nuclide activities, disintegrations min^{-1}; t is the time, min; τ is an integration variable; $\dot{\mathbf{C}}(t)$ is a vector of time-dependent monitor net count rates, counts min^{-1}; x is the horizontal distance within the RW detection and deposition window, cm (inches); L is the length of RW deposition and detection window, cm (inches); v is the filter or tape speed, cm h^{-1} (inches h^{-1}); T is the transit time (L / v), h; **A** is the system transition matrix; **B** is the source allocation matrix; **u** is the source (air concentration) vector; **Ψ** is a matrix of detection efficiency-abundance products; λ_i is the nuclide i decay constant, h^{-1}; η_i is the branching ratio to nuclide i from its immediate parent; Q_i is the concentration of nuclide i in air, Bq m^{-3} (μCi cc^{-1}); k is a units reconciliation constant; F is the monitor flow rate, m^3 h^{-1} (ft^3 min^{-1}); φ is the product of the filter

collection and retention efficiency and line-loss fraction (this parameter could be subscripted on nuclide); ε_i is the detection efficiency, counts per emission, nuclide i; γ_i is the emission abundance, emission per disintegration, nuclide i.

This model is the extension to decay chains of the RW model reported in [1]. As discussed in that reference, the fundamental idea is to consider the moving-filter medium in the deposition window to be comprised of differential areas, each of which is a fixed filter for the length of time it is exposed in the window. The ODE system describes the variation of the activity on each differential element, and these elements are then integrated across the RW geometry. It can be shown that the circular-window (CW) case is covered by using the length

$$L_{CW} = \frac{16R}{3\pi}, \tag{4-4}$$

where R is the radius of the circular deposition window, in any solution to (4-1)-(4-3), as was shown in [1]. Note that the top-of-chain (first) nuclide's solutions from (4-1)-(4-3) will be the same as those developed using the scalar integrals in that reference, since the progeny do not affect their precursor nuclides.

Results

Example count rate solutions

Moving-filter monitors have two responses: the first, for time (t) less than the "transit time" (T), and the second, for time equal to or after the transit time. The transit time T is the length of the deposition window divided by the filter (tape) speed. The response is continuous across this time boundary. Time is measured from the start of the concentration transient. A zero initial condition is assumed in the count rate solutions; this condition refers to the lack of any fission products (FP) on the filter at time zero. However, radon-thoron is often present at time zero, and must be accounted for; more on this below.

In the case of a constant concentration the count rate for the first nuclide in the 3-chain for $t \le T$ will be:

$$\dot{C}_1(t) = \frac{\varepsilon_1 \gamma_1 k F \varphi Q_1}{\lambda_1}\left[\frac{v}{\lambda_1 L}\left(\lambda_1 t - 1 + e^{-\lambda_1 t}\right) + \left(1 - \frac{vt}{L}\right)\left(1 - e^{-\lambda_1 t}\right)\right], \tag{4-5}$$

and for $t \ge T$,

$$\dot{C}_1(t) = \frac{\varepsilon_1 \gamma_1 k F \varphi Q_1}{\lambda_1}\left[1 - \frac{v}{\lambda_1 L}\left(1 - e^{-\lambda_1 \frac{L}{v}}\right)\right]. \tag{4-6}$$

For the second nuclide in the chain, for $t \le T$,

$$\begin{aligned}\dot{C}_2(t) = {} & \frac{\varepsilon_2 \gamma_2 k F \varphi Q_2}{\lambda_2}\left\{\frac{v}{\lambda_2 L}\left(\lambda_2 t - 1 + e^{-\lambda_2 t}\right) + \left(1 - \frac{vt}{L}\right)\left(1 - e^{-\lambda_2 t}\right)\right\} \\ & + \frac{\varepsilon_2 \gamma_2 k F \varphi Q_1 \eta_2}{\lambda_2 - \lambda_1}\left\{\begin{array}{l}\frac{\lambda_2 v}{\lambda_1^2 L}\left(\lambda_1 t - 1 + e^{-\lambda_1 t}\right) + \frac{v}{\lambda_2 L}\left(\lambda_2 t - 1 + e^{-\lambda_2 t}\right) \\ + \left(1 - \frac{vt}{L}\right)\frac{\lambda_2 - \lambda_1}{\lambda_1}\left[1 - \lambda_2 \frac{e^{-\lambda_1 t}}{\lambda_2 - \lambda_1} + \lambda_1 \frac{e^{-\lambda_2 t}}{\lambda_2 - \lambda_1}\right]\end{array}\right\},\end{aligned} \tag{4-7}$$

and for $t \ge T$,

$$\dot{C}_2(t) = \frac{\varepsilon_2 \gamma_2 k F \varphi Q_2}{\lambda_2}\left[1 - \frac{v}{\lambda_2 L}\left(1 - e^{-\lambda_2 \frac{L}{v}}\right)\right] + \frac{\varepsilon_2 \gamma_2 k F \varphi Q_1 \eta_2}{\lambda_1(\lambda_2 - \lambda_1)}\left[\begin{array}{l}\lambda_1\left(\frac{v}{\lambda_2 L}\left(1 - e^{-\lambda_2 \frac{L}{v}}\right) - 1\right) \\ - \lambda_2\left(\frac{v}{\lambda_1 L}\left(1 - e^{-\lambda_1 \frac{L}{v}}\right) - 1\right)\end{array}\right]. \tag{4-8}$$

Note that both $t \geq T$ solutions are constants. The third nuclide's solution is algebraically cumbersome and not of direct interest here. It is not needed for the present work, but in passing it may be useful to observe that setting $v = 0$ in the $t \leq T$ solutions will yield the fixed-filter count rates for that situation.

If the nuclide of interest is "long-lived" (LL), that is, if its decay during the period of analysis is negligible, then the $t \leq T$ responses can be shown to be

$$\dot{C}_1(t) = \varepsilon_1 \gamma_1 k F \varphi Q_1 \left(t - \frac{vt^2}{2L} \right), \tag{4-9}$$

$$\dot{C}_2(t) = \varepsilon_2 \gamma_2 k F \varphi Q_2 \left(t - \frac{vt^2}{2L} \right), \tag{4-10}$$

and for $t \geq T$,

$$\dot{C}_1(t) = \varepsilon_1 \gamma_1 k F \varphi Q_1 \frac{L}{2v} , \tag{4-11}$$

$$\dot{C}_2(t) = \varepsilon_2 \gamma_2 k F \varphi Q_2 \frac{L}{2v} . \tag{4-12}$$

These LL results are found by taking the limit of the respective solutions as the decay constant approaches zero. The count rate for the "top-of-chain" nuclide is the solution that would be used for any single-nuclide situation. The matrix solution is not necessary to analyze a single nuclide (no decay chain), but there is considerable interest in the 3-chain for radon-thoron, so the matrix formulation will be used, for consistency.

Concentration estimation mathematical basis

Varying the filter speed in a computer-implemented solution to (4-1)-(4-3) showed that increasing this speed led to an apparent proportionality between the count rate for the top-of-chain nuclide and its non-constant concentration. At the nominal 2.54 cm h^{-1} (one inch h^{-1}) used in RW monitors, this proportionality is not present. Consider Fig. 4-1, where the count rate traces approach the shape of the concentration only as the filter speed becomes large. At the 2.54 cm h^{-1} (one inch h^{-1}) rate, that is, the way in which these monitors are usually operated, there is no evident relation between the count rate at any time, and the concentration at that time. In Fig. 4-2 is an expanded view of this situation, and it is seen that the 152.4 cm h^{-1} (60 inch h^{-1}) count rate shape is nearly identical to that of the concentration.

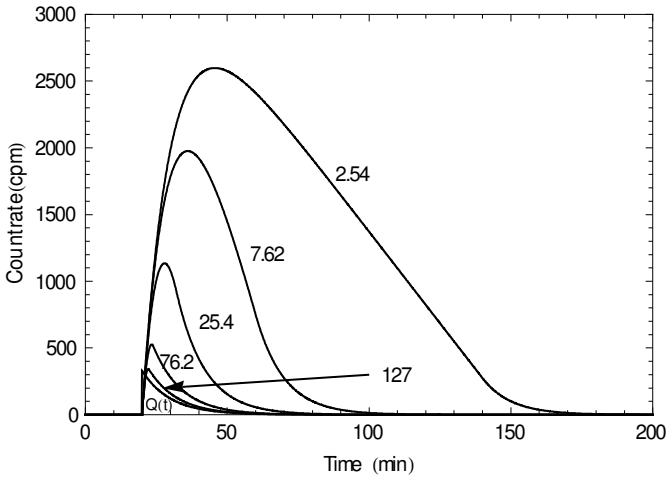

Figure 4-1. Count rate vs. time, for several filter (tape) speeds (2.54, 7.62, 25.4, 76.2, 127 cm h^{-1}). The exponential concentration Q(t) was scaled to fit on the count rate axis. The nuclide is ^{131}I, as an example of a fission product to be measured.

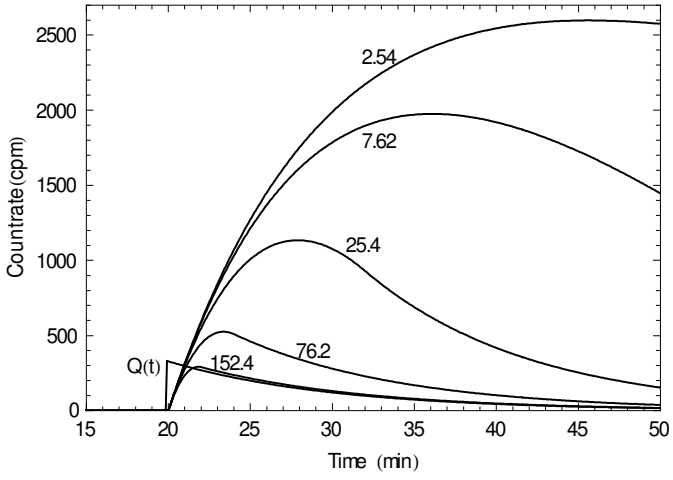

Figure. 4-2. Expanded-scale version of Fig. 4-1, with 152.4 cm h^{-1} (60 inch h^{-1}) instead of 127 cm h^{-1}(50 inch h^{-1}).

Fig. 4-3 makes the situation very clear, with still more zoom into the start of the transient. All the filter speed responses miss the initial rise of the concentration, but the 152.4 cm h^{-1} (60 inch h^{-1}) trace follows it closely after an initial delay of about two minutes. This delay is the transit time T for this monitor at this speed (L = 5.08 cm, or 2 inches); by contrast, at the nominal 2.54 cm h^{-1} (one inch h^{-1}) filter speed, T is about two hours.

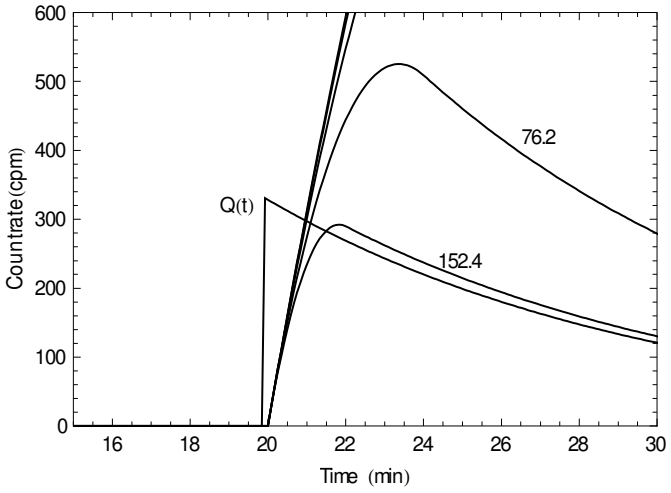

Figure 4-3. More-expanded version of Fig. 4-1. The 152.4 cm h^{-1} (60 inch h^{-1}) count rate tracks the concentration, after its transit time of two minutes.

Seeing this apparent proportionality, empirical numerical experiments were conducted to find a constant of proportionality so that dynamically-varying count rates could, perhaps, be converted into dynamically-varying concentration estimates. This constant turned out to be a particular collection of instrumental parameters, that is, parameters whose values would be known (measured) for a given instrument. The proportionality did not depend on knowledge of parameters that would only happen in a simulation context, e.g., the rate of decrease of an exponential concentration transient.

It was then found that expanding the RW count rate solutions, symbolically obtained, in a Taylor series in the filter speed v produced this same proportionality constant; it was the first-order term in the series expansion. To illustrate, consider a concentration behavior of simple single exponentials. This leads to the source definition

$$\mathbf{u} = \begin{pmatrix} Q_1 e^{-r_1 \tau} \\ Q_2 e^{-r_2 \tau} \\ Q_3 e^{-r_3 \tau} \end{pmatrix} k F \varphi,$$

where r_i is a rate constant controlling the exponential time-dependence of the concentrations. Note that the time variable in this source vector $\mathbf{u}$ is τ rather than t, in order to be integrated correctly in the monitor response model. When the $t \geq T$ solution (4-2)-(4-3) for this system is expanded in a Taylor series in v about infinity, or, in effect, the reciprocal of v about zero, the first three terms (the f are collections of factors that need not be presented here) are:

$$\begin{aligned}
\dot{C}_1(t) &\approx \frac{Q_1 e^{-r_1 t} \epsilon_1 \gamma_1 k F \varphi L}{2v} + \frac{Q_1 e^{-r_1 t} \epsilon_1 \gamma_1 k F \varphi (r_1 - \lambda_1) L^2}{6v^2} + \frac{Q_1 e^{-r_1 t} \epsilon_1 \gamma_1 F k \varphi (r_1 - \lambda_1)^2 L^3}{24 v^3} \\
\dot{C}_2(t) &\approx \frac{Q_2 e^{-r_2 t} \epsilon_2 \gamma_2 k F \varphi L}{2v} + \frac{f_{2,2}(Q_1, Q_2) L^2}{6v^2} + \frac{f_{2,3}(Q_1, Q_2) L^3}{24 v^3} \\
\dot{C}_3(t) &\approx \frac{Q_3 e^{-r_3 t} \epsilon_3 \gamma_3 k F \varphi L}{2v} + \frac{f_{3,2}(Q_2, Q_3) L^2}{6v^2} + \frac{f_{3,3}(Q_1, Q_2, Q_3) L^3}{24 v^3}
\end{aligned} \tag{4-13}$$

This is a remarkable and unexpected result, namely, that the concentration behavior for each nuclide in the decay chain is returned in the respective first-order term, multiplied only by known parameters**.** This result would not be especially obvious simply by examining the count rate solutions. For the first nuclide in the chain, the count rate expansion can be written as:

$$\dot{C}_1(t \geq T) \;\approx\; \epsilon_1 \gamma_1 k F \varphi Q_1 e^{-\eta_1 t} \left(\frac{L}{2v} + \frac{(r_1 - \lambda_1) L^2}{6v^2} + \frac{(r_1 - \lambda_1)^2 L^3}{24 v^3} \right). \tag{4-14}$$

From this and the other components of (4-13) it is seen that, when the second- (and higher-) order terms are negligibly small, the concentration of nuclide *i* can be estimated by

$$Q_i(t) \approx \frac{\dot{C}_i(t)}{\varepsilon_i \gamma_i k F \varphi \dfrac{L}{2v}}; \quad t \geq T\,. \tag{4-15}$$

This is the principal result. Replace *L* in (4-15) with (4-4) to use this estimation procedure for CW monitors; a Taylor expansion similar to (4-13) can be shown to produce this expression, for the analytical CW $t > T$ model [(1-13), with the scalars replaced by matrices]. Note that the transit time *T* is small, i.e, a few minutes, when the filter speed is fast. It is sometimes assumed that (4-15) holds for any RW monitor, at any time, but this is not the case; the estimator is only meaningful when the filter speed is fast enough to permit the use of only the first term in the expansion, and then, only after the transit time *T*. In fact, (4-15) would only apply, for the nominal filter speed situation, if the nuclide was LL *and* its concentration was constant *and* the time was greater than *T*.

The simple exponential used in (4-13) is only one of many possible *Q(t)* behaviors; several combinations of exponentials, as expected in most compartmental monitoring situations (see [5]), were checked with the expansion, and the result is consistent; the *Q(t)* is returned in the first term, multiplied by only instrumental (known) constants.

To verify that this relation (4-15) does produce reasonable concentration estimates, consider Fig. 4-4. This is an exponential concentration "spike" that abruptly rises and then decreases smoothly. Again it is seen that the nominal 2.54 cm h^{-1} (one inch h^{-1}) filter speed trace does not look anything like the concentration trace. As the filter speed increases, the agreement becomes better, and at 152.4 cm h^{-1} (60 inches h^{-1}) is nearly identical.

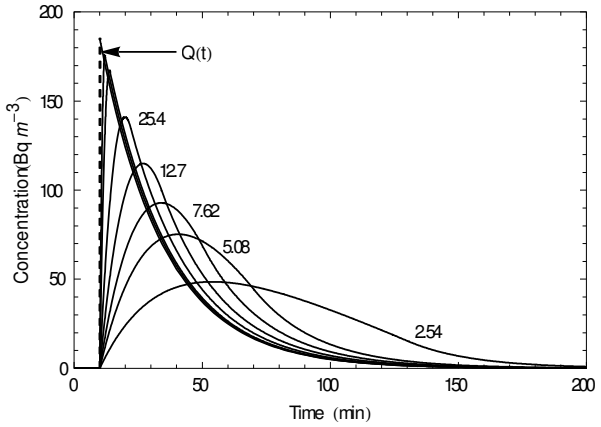

Figure 4-4. Concentration estimates for filter speeds (cm h^{-1}) indicated. The traces for 76.2 and 152.4 cm h^{-1} (30 and 60 inches h^{-1}) are very close to the concentration curve Q(t). The nuclide is again ^{131}I.

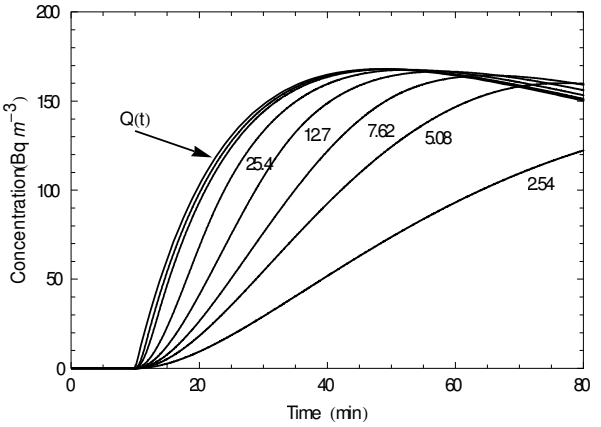

Figure 4-5. Concentration estimates for filter speeds (cm h^{-1}) indicated, for a slower transient than in Fig. 4-4. The traces for 76.2 and 152.4 cm h^{-1} (30 and 60 inches h^{-1}) are very close to the concentration curve Q(t). The nuclide is ^{131}I.

Figure 4-5 is another example of concentration estimation using (4-15), for a more slowly-increasing concentration profile. Again, the 2.54 cm h^{-1} (one inch h^{-1}) trace has no apparent relation to the concentration, while the 152.4 cm h^{-1} (60 inch h^{-1}) trace is nearly identical to it.

It might be expected that there would be some negative aspect to this good tracking ability at high filter speeds; this turns out to be a significantly reduced count rate. Consider Fig. 4-6, which shows the count rates for the same situation as in Fig. 5. The 2.54 cm h^{-1} (one inch h^{-1}) trace is by far the highest count rate, but this has no use in estimating the concentration. Clearly, the count rates are decreasing significantly as the filter speed increases.

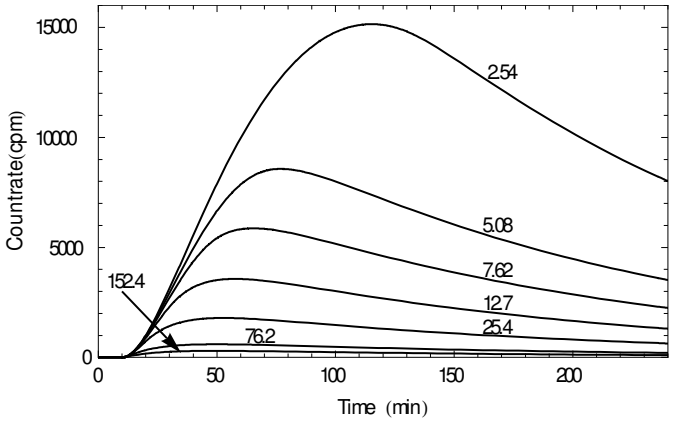

Figure 4-6. Count rate variation with filter speed; same cases as Fig. 5.

Fig. 4-7 shows the variation in count rate as a ratio to the count rate at the nominal 2.54 cm h^{-1} (one inch h^{-1}). It can be shown that this ratio of the count rates for constant concentrations at two filter speeds is

$$\frac{\lambda_1 L + v_2\left(e^{\lambda_1 \frac{L}{v_2}} - 1\right)}{\lambda_1 L + v_1\left(e^{\lambda_1 \frac{L}{v_1}} - 1\right)}. \tag{4-16}$$

This gives an idea of the magnitude of the count rate reduction; for LL activity the ratio is v_1 / v_2. Time-dependent concentrations will affect this ratio; since there are many possible time-dependences, a constant concentration was used in the figure.

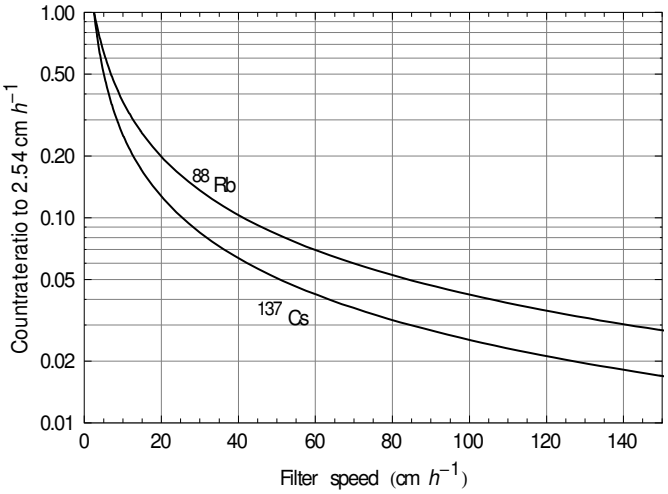

Figure 4-7. Count rate reduction vs. filter speed, for constant concentrations. The ratio is to the 2.54 cm h^{-1} (one inch h^{-1}) count rate.

One potential benefit of the count rate suppression at faster filter speeds is the reduction of detector saturation that can occur with higher levels of airborne particulate radioactivity, in post-accident situations. Another benefit of this count rate reduction is the suppression of radon-thoron interference. The radon-thoron count rate is significantly reduced at the higher filter speeds. Since a low-level detection capability is not desired, the radon-thoron suppression would not be of interest, except that there may be situations where a monitor is directly sampling outdoor air, with a full burden of radon-thoron, while at the same time "looking for" fission products. Reducing the interference from radon-thoron can help, in that situation. Fig. 4-8 shows the reduction as a function of filter speed.

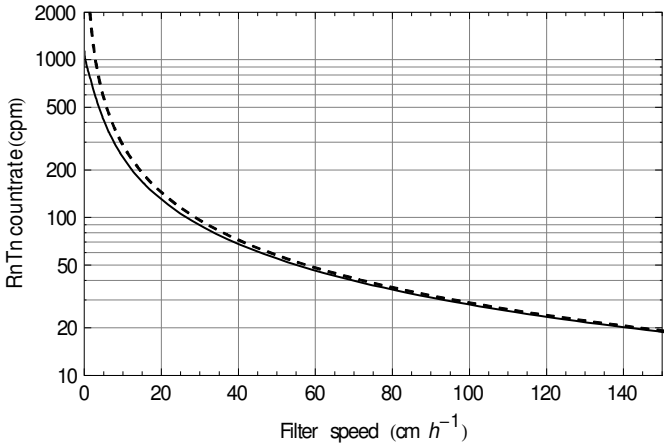

Figure 4-8. Reduction of total (six nuclides) radon-thoron count rate with filter speed. The dotted line is an approximation based on first-order terms from (4-13). Constant concentrations at 3.7 Bq m^{-3} (10^{-10} μCi cc^{-1}) for the radon chain, and 0.037 Bq m^{-3} (10^{-12} μCi cc^{-1}) for the thoron chain.

An intuitive way of looking at this fast-filter-speed approach is that the rapid removal of deposited activity from the detector window means that the monitor becomes almost “memoryless” and is responding mostly to the activity that is freshly deposited on the filter. That activity, in turn, is going to be more representative of the current level of the changing air concentration. This reasoning also applies to the decay chain progeny, which have a response driven almost entirely by the air concentration, and little from the “ingrowth” of their precursors. The latter activity is, again, removed from the detector’s view relatively quickly, so that most of what the detector sees is activity that is recently deposited, from the air.

Discussion

Higher-order terms

The issue of deciding when the filter speed is "fast enough" will be decided by the second-order terms in the expansion. When these terms are numerically small, the respective first term for the concentration calculation is used. For many fission-product monitoring situations there is concern only with the first nuclide in the chain; the second-order term for this nuclide, from (4-13), is

$$\frac{Q_1 e^{-r_1 t} \epsilon_1 \gamma_1 k F \varphi (r_1 - \lambda_1) L^2}{6 v^2} .$$

Here the concentration is a simple exponential, but it can be any function of time. The magnitude of this term is primarily dependent on the concentration; the decay constant; the filter speed, with the other parameters being fixed, for a given monitoring application.

As a special case, consider a constant concentration of LL activity. Then r_1 will be zero and λ will be very small, approaching zero. Then this term essentially vanishes (as do any higher-order terms), and all that remains is the first term. But the first term would then be identical to (4-11), as would be expected. Examination of the higher-order terms for the progeny will reveal that these terms all have the respective decay constant as a multiplicative factor. Thus, for constant-concentration, LL progeny

activity, (4-12) for the second nuclide, and a similar expression for the third, will apply, and these are the respective first-order terms in (4-13).

This mathematics says that the progeny count rates, under these rather restrictive conditions, will be driven only by their respective air concentrations. Relaxing the constant-concentration and LL restrictions, these expressions will still apply, approximately, but now only at high filter speeds, since that speed v appears in the denominators and thus the higher-order terms decrease to insignificance relatively quickly.

To illustrate, consider Fig. 4-9, which shows the magnitude of the second-order term for the top-of-chain nuclide, for some typical monitor parameter values (monitor flow rate F, 8.5 m^3 h^{-1} or 5 ft^3 min^{-1}; detection efficiency ε, 0.4; emission abundance γ, 1.0; collection efficiency φ, 0.7), for constant ^{131}I concentrations of 3.7, 37, 370 Bq m^{-3} (10^{-10}, 10^{-9}, and 10^{-8} µCi cc^{-1}), left to right. The higher concentrations require a faster filter speed to attain a given size of the term. Figure 4-10 shows an expanded view, for ^{137}Cs, which of course is a LL nuclide of considerable interest. Here the second-order term is small even at relatively slow filter speeds.

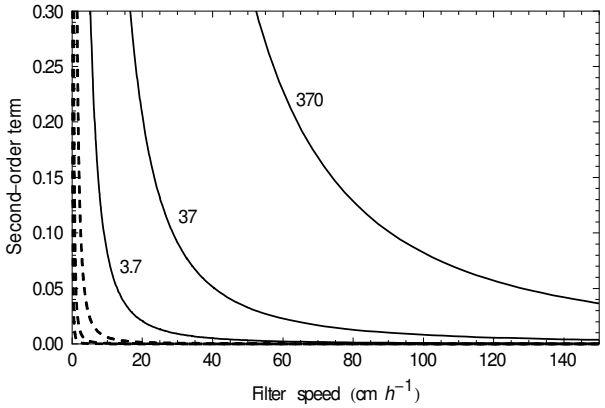

Figure 4-9. Magnitude of the second-order term in the series expansion vs. filter speed. Constant concentrations of ^{131}I indicated, in Bq m^{-3}. The dashed lines are ^{137}Cs at the same concentrations.

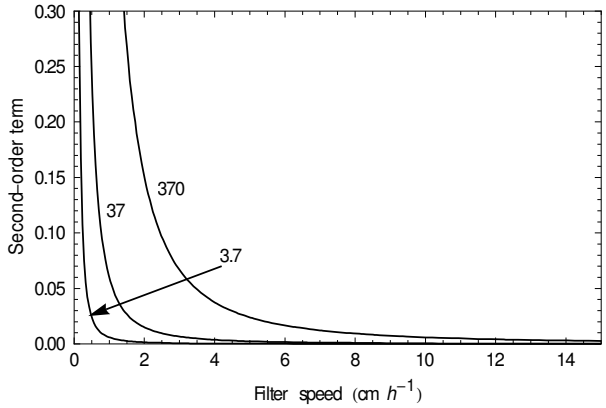

Figure 4-10. Magnitude of second-order term in expansion vs. filter speed for ^{137}Cs. The concentrations are as indicated, in Bq m^{-3}.

Concentration estimation uncertainty

It will be useful to have some idea of the uncertainty in these concentration estimates. Using the first-order term and considering the top-of-chain nuclide, the concentration estimate is

$$\hat{Q}_1 \approx \frac{\left(\dot{C}_1 + \dot{C}_{bkg} + \dot{C}_{RnTn}\right) - \dot{C}_{bkg} - \dot{C}_{RnTn}}{\varepsilon_1 \gamma_1 k F \varphi \frac{L}{2v}},$$

where $\dot{C}_{bkg}$ is the ambient background count rate, assumed constant, and $\dot{C}_{RnTn}$ is the efficiency-weighted sum of the count rates for the six radon-thoron nuclides; spectroscopy is not assumed. The quantity in parentheses is of course the “gross” count rate, as observed. The radon-thoron air concentrations are assumed known, and, for now, constant, although the model can handle time dependences such as a diurnal variation. Recall that the radon-thoron count rate is significantly suppressed at the higher filter speeds used here (Fig. 4-8).

In the model implementation, the monitor count rate is sampled every five seconds (i.e., the deterministic count rate mean from the model solution is multiplied by that digital time step) to get the mean number of counts in that sampling interval. That mean value is then used to draw a random sample from a Poisson distribution, to get a "noisy" number of observed counts in the digital register for that time step. That noisy data is then processed with a fixed-gain (θ) exponentially-weighted moving average (EWMA) variance reduction ("smoothing") algorithm, discussed in [6]; the output of that process is divided by the digital time-step to get a count rate estimate.

Consideration of the variances in this process, ignoring for now the uncertainties in the instrumental parameters, will show that, when a calculated value is used for the gross count rate, the estimated standard deviation for the concentration will be

$$\sigma_{\hat{Q}} = \frac{\sqrt{\frac{\theta}{(2-\theta)\Delta t}}}{\varepsilon \gamma k F \varphi \frac{L}{2v}} \sqrt{\varepsilon \gamma k F \varphi \frac{L}{2v} Q_t + \dot{C}_{bkg} + \dot{C}_{RnTn}} \quad , \tag{4-17}$$

while for the case where the gross count rate is directly observed, which it would of course be in practice, as opposed to a simulation, then

$$\sigma_{\hat{Q}} = \frac{\sqrt{\frac{\theta}{(2-\theta)\Delta t}}}{\varepsilon \gamma k F \varphi \frac{L}{2v}} \sqrt{\dot{C}_{gross}} \; . \tag{4-18}$$

The factor involving θ represents the variance reduction of the EWMA processing; see [6] and [7] for more information on this subject.

These expressions assume that the background and radon-thoron count rates are "well-known" and so have negligibly small variances (i.e., they are not observed during the concentration measurement); they are assumed to be, in effect, constants. In Fig. 4-11 is a plot showing the approximate 95% "confidence band" around the known concentration of ^{131}I, at a filter speed of 152.4 cm h^{-1} (60 inches h^{-1}). The jagged line shows the time-dependent concentration estimates; there are 2400 of them (200 minutes at 5 seconds per sample), and a direct count shows a fraction of 0.026 above the bound, and 0.031 below the bound. Ideally both would be about 0.025 for an approximate 95% interval.

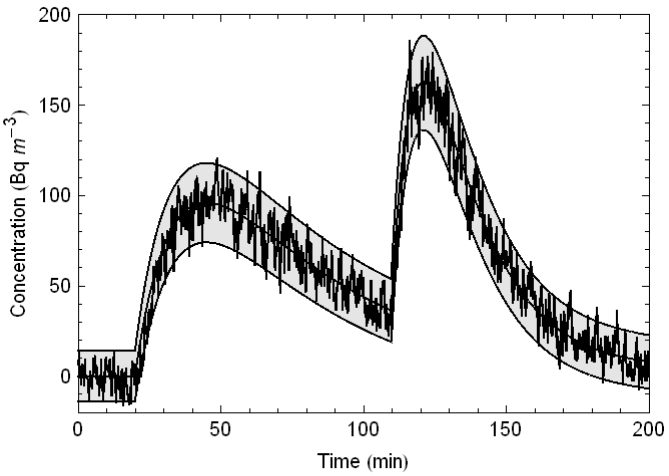

Figure 4-11. Estimated concentrations, with approximate 95% "confidence band." The nuclide is ^{131}I, and the filter speed is 152.4 cm h^{-1} (60 inches h^{-1}). The EWMA parameter θ is 0.2.

In Fig. 4-12 is a plot of relative error in the concentration estimate as a function of filter speed, at several (constant) concentrations. Since the variance of the gross count rate depends on the radon-thoron, and the latter varies with filter speed, some approximation must be used for that variation. Numerical experiments showed that, as indicated in Fig. 4-8, a function that is just a constant (about 48; see (4-19) below) divided by the filter speed is a reasonable approximation, at least at the higher filter speeds of interest; more than, e.g., 50.8 cm h^{-1} (20 inches h^{-1}).

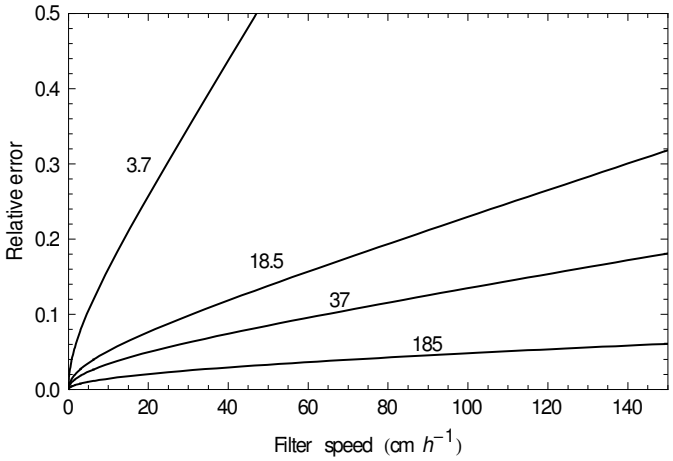

Figure 4-12. Relative error in concentration vs. filter speed. The radon-thoron contribution is approximated by 48/v, with v in cm h^{-1}; this is reasonably good above about 50.8 cm h^{-1} (20 inches h^{-1}). The curves are for concentrations of 3.7, 18.5, 37, 185 Bq m^{-3} (10^{-10}, $5x10^{-10}$, 10^{-9}, $5x10^{-9}$ μCi cc^{-1}), top to bottom. The higher concentrations have better relative error, as expected.

Smallest practical concentration

A reasonable question is to ask what is the lowest concentration that can reliably be measured, given a filter speed, and the background, and radon-thoron air concentrations. While for this monitoring approach minimum detectable concentrations (MDC) are not of interest in the usual way (i.e., for very low levels), it would still be useful to have at least an order of magnitude idea of when this fast-filter-speed method will work.

An important part of this calculation is the radon-thoron count rate. The model (4-1)-(4-3) provides solutions for chains of any length; since the radon and thoron chains do not interact, it will be simpler to treat them as 3-chains, separately, and then sum the results, as opposed to constructing a six-dimensional system. When the expansion (4-13) is done, the result for constant concentrations, using only the first-order terms is:

$$\dot{C}_{RnTn} \approx \frac{k\,F\,\varphi\,L}{2v}\sum_{i=1}^{6}\varepsilon_i\,\gamma_i\,Q_i \approx \frac{48(60)}{v} = \frac{2880}{v}\,, \tag{4-19}$$

where v is in cm h^{-1}, the monitor flow rate F is 8.5 m^3 h^{-1} (5 ft^3 min^{-1}), the window width L is 5.09 cm (two inches), and the remaining parameters have nominal values; with SI units the reconciliation factor k is unity. The air concentrations are at 3.7 Bq m^{-3} for radon and 0.037 Bq m^{-3} for thoron (10^{-10} and 10^{-12} μCi cc^{-1}). The count rate is in counts per minute. Next, consider the expected variation in the sum of the ambient background and this radon-thoron count rate. This will give

$$\sigma_{bkg} \approx \sqrt{\frac{\theta}{(2-\theta)\,\Delta t}\left(\dot{C}_{bkg} + \frac{2880}{v}\right)}\,. \tag{4-20}$$

Then, again using the first-order approximation for the fission-product (top-of-chain) nuclide,

$$\dot{C}_{FP} \approx \varepsilon_{FP}\,\gamma_{FP}\,k\,F\,\varphi\frac{L}{2v}\,Q_{FP}. \tag{4-21}$$

This count rate will be some multiple β of the variation in the background. Then

$$\dot{C}_{FP} > \beta\,\sigma_{bkg}\,,$$

so that, solving for the concentration,

$$Q_{FP} \approx \frac{2 v \beta}{\varepsilon_{FP} \gamma_{FP} k F \varphi L} \sigma_{bkg} , \tag{4-22}$$

or, more explicitly, with v in cm h^{-1} and the digital time step Δt in minutes,

$$Q_{FP} \approx \frac{v \beta}{30 \varepsilon_{FP} \gamma_{FP} k F \varphi L} \sqrt{\frac{\theta}{(2-\theta) \Delta t} \left(\dot{C}_{bkg} + \frac{2880}{v} \right)} \quad . \tag{4-23}$$

This variation with filter speed turns out to be essentially linear, and calculation for nominal parameter values suggests that at 152.4 cm h^{-1} (60 inches h^{-1}) a reasonable minimum concentration would be around 37 Bq m^{-3} (10^{-9} μCi cc^{-1}).

Conclusion

Numerical experimentation conducted while developing the extension of a moving-filter mathematical model to include decay chains revealed that the monitor count rates appear to closely track the time-dependent shape of the input air concentrations, if, and only if, the moving filter (tape) speed is much faster than the 2.54 cm h^{-1} (one inch h^{-1}) or so that is usually the case. That is, operating moving-filter continuous particulate air monitors at that typical filter speed does not provide a quantitative measurement of a changing air concentration of a fission product or other contaminant.

At the faster filter speeds, e.g., 76.2 or 152.4 cm h^{-1} (30 or 60 inches h^{-1}), the count rate trace has essentially the same shape as the concentration profile. A quantitative relation, namely (4-15), between the monitor's net count rate and a nonconstant concentration only applies when the filter speed is sufficiently fast that a Taylor series expansion of the monitor count rate can be reasonably well truncated at the first-order term. This mode of operation, which does not require any new monitor hardware, is capable of tracking rapidly-changing concentrations.

Since the fast filter speed also reduces the monitor's count rate, all else being equal, then the approach will best be used for relatively high-level concentrations, such as may occur in abnormal or "accident" conditions. The count rate suppression could be useful for reducing detector saturation that can occur with higher levels of airborne particulate radioactivity, in post-accident situations. Radon-thoron interference is also suppressed, which should be useful in those applications where ambient air is being monitored.

This new concentration tracking ability, as opposed to a simple just-above-background alarm function, could be of use for personnel protection in accident recovery efforts. Consider a situation where a worker opens a valve, and a rapidly-changing, high-level air concentration of one or more fission products results. It would be valuable to have an estimate in essentially real time of the level of this concentration, and, just as valuable, to know when it had decreased to a safer level. When operated at the slow typical filter speed, a short pulse of activity will produce an elevated count rate response long after the concentration has decreased, as in Fig. 4-1. At the faster speed, the concentration tracking is far better.

A negative aspect of this concentration tracking ability is that the filter tape will of course run out much faster than at the nominal speed, e.g., in perhaps a day rather than a month. However, if the monitor is only used at the fast speed during unusual working situations, namely, when it has been anticipated that there is the possibility of a rapid release of particulate airborne radioactivity, then this tape usage should not be a major issue, since these situations should not be routine. The ability to track rapidly-changing, high-level air concentrations in nearly real time would in any case readily justify the use of more filter tapes.

A useful future development would be a continuous filter tape that runs in a loop, so that the deposited activity would be removed by some means, after leaving the deposition and detection window, and perhaps collected for laboratory analysis, while the "erased" filter tape continues to move around in the loop at the (relatively) high speed necessary for dynamic tracking of rapidly-changing concentrations.

References

[1] W. C. Evans, "Mathematical models for the dynamic response of continuous particulate air monitors," *IEEE Trans. Nucl. Sci*., vol. 48, pp. 202-218, 2001.

[2] W. C. Evans, "Quantitative methods for continuous particulate air monitoring," *IEEE Trans. Nucl. Sci.,* vol. 48, pp. 1639-1657, 2001. Chapter 2.

[3] G. A. F. Seber and C. J. Wild, *Nonlinear Regression*, New York: Wiley, 1989.

[4] D. H. Anderson, *Compartmental Modeling and Tracer Kinetics.* New York: Springer-Verlag, 1983.

[5] W. C. Evans, "Concentration dynamics modeling for continuous particulate air monitor response prediction," *IEEE Trans. Nucl. Sci.,* vol. 49, pp. 2574-2598, 2002.

[6] W. C. Evans, "Digital count-rate estimation using adaptive exponentially weighted moving averages," *Trans. Am. Nucl. Soc.,* vol. 32, p. 133, 1979.

[7] D. C. Montgomery and L. A. Johnson, *Forecasting and Time Series Analysis.* New York: McGraw-Hill, 1976.

Chapter 5

Incorrect Interpretation of Moving-Filter Countrate Responses

Health Physics, 104(4), April 2013, 437-443

The graphs supplied by the vendors of moving-filter continuous particulate air monitors (CPAMs) in their sales literature show linear curves on a log-log scale, with net countrate on one axis and concentration on the other. The implication is that the monitor user is to read the concentration from the graph, given an observed net countrate, at any time. For the nominal filter speeds commonly used for these monitors, using the graph in this way is incorrect. The graphs do not state the limitations of the calculation: (a) the nuclide measured must be long-lived; (b) the concentration of that nuclide in the sampled air must remain constant; (c) the reading of the net countrate must be obtained after a specific time, called the "transit time." This time is typically on the order of several hours. Reading the net countrate at any time earlier than this will result in an incorrect concentration estimate. Given that a major purpose of a CPAM is to alert plant personnel to a change in airborne radioactivity concentrations, by definition when this happens the concentration is not constant. Thus, using the supplied curves will result in an incorrect estimate of that concentration. The solution is to use instead a fixed-filter CPAM and a previously-published quantitative method. With this approach there is no need to attempt to estimate a concentration, much less to assume that it is constant over long periods of time or that it can only change in a stair-step manner. With this alternative to a moving-filter CPAM a signal proportional to the time-integrated DAC-hour worker intake can be generated continuously, for any time-varying air concentration, including the sums-of-exponentials shapes expected during transient events in compartmental systems.

Introduction

CONTINUOUS PARTICULATE AIR MONITORS (CPAMs) are installed in nuclear power stations as part of the plant radiation monitoring system (RMS). There are two main types of CPAMs: fixed-filter, and moving-filter. Applications include occupational exposure control, process control, effluent monitoring, and reactor coolant leakage detection. Which type of CPAM to use for a given application in the plant is a matter of engineering judgment, since there is no relevant regulatory, nor standards, guidance on the subject.

To understand the current situation, some historical perspective will be useful. The engineers working at an architect/engineering (A/E) firm in the 1960s and 1970s, when the nuclear power stations operating today were designed, needed to specify air monitors for new plants. The engineers sent out letters to RMS vendors requesting information on the systems being offered, and what the vendors sent in return was all the data on these systems the engineers had to work with. There was little to nothing in textbooks or the published literature at the time on the technical performance characteristics of these monitors, as applied in the nuclear power industry. Also, the mathematical modeling of CPAMs, especially with regard to the development of quantitative relationships for these devices, was not part of the technical education of nuclear engineers or health physicists.

The A/E engineers were not in a position to design their own monitors, even if they somehow had obtained the necessary background; instead, they wrote performance specifications that could be met by instruments on the market at the time. These specifications were in turn based on the vendor information and the engineer's understanding and interpretation of the relevant regulatory requirements (which were not, and still are not, clearly defined). For their part, the vendors, in their sales literature, provided "calibration" expressions or curves which were presumably to be used to establish the quantitative relation between the monitor's net countrate and a concentration in the sampled air. Figures 5-1 and 5-2 show actual examples of these graphs. Other vendors provided calculations, such as shown in Fig. 5-3, taken from a vendor sales catalog, also of this time period.

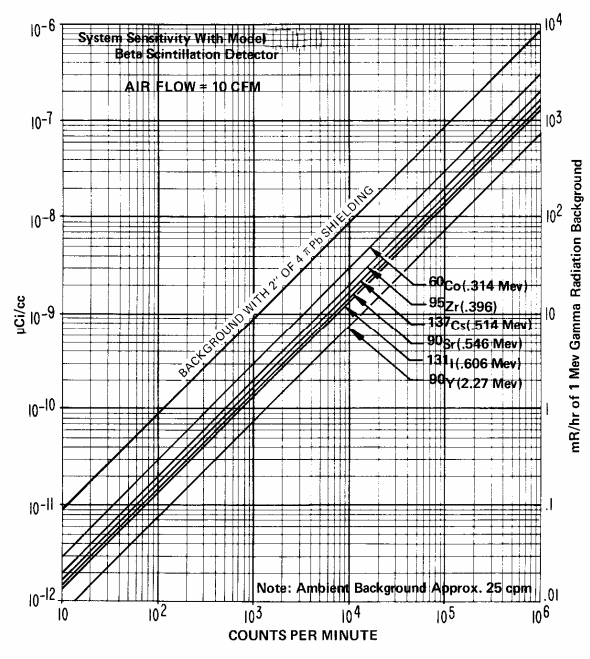

Fig. 5-1. Example CPAM "sensitivity" graph; vendor A, from time period of mid 1970s.

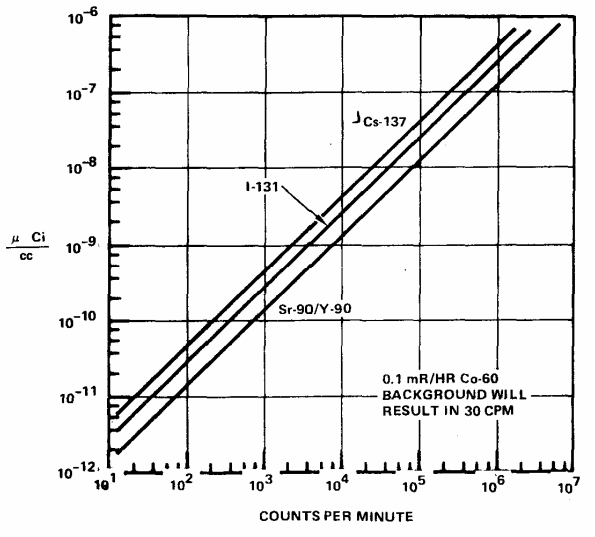

Fig. 5-2. Example CPAM "sensitivity" graph; vendor B, from time period of mid 1970s. Note that the monitor flow rate is not given.

The detector sensitivity for any system can be determined by applying the following formula:

$C/M/hr = YRA \times 3.74 \times 10^{10}$

Where C/M/hr = Count build up per hour of collection.
Y = Yield expressed in percent.
R = Pumping rate in CFM.
A = Activity in microcuries per cc.
3.74×10^{10} = Constant of proportionality.

As an example, assume the following conditions:
Using an SC-2B Beta Scintillation Detector with a 20% yield, 5 cfm pumping rate, and a concentration of activity of 10^{-10} uc/cc, applying the above formula we find:

$C/M/hr = YRA \times 3.74 \times 10^{10}$
$C/M/hr = 20 \times 5 \times 10^{-10} \times 3.74 \times 10^{10}$
$C/M/hr = 374\ C/M$

For a moving filter system, where filter transit is involved, the equation becomes:

$C/M = YRAT \times 1.37 \times 10^{10}$

Where Y = Detector yield, in percent.
R = Air flow rate, in cfm.
A = Activity in microcuries/cc.
T = Transit time, in hours.

Fig. 5-3. Example CPAM "sensitivity" calculations; vendor C, from time period of mid 1970s.

The vendor materials that were provided to the A/E design engineers clearly implied that, for a moving-filter CPAM, the user was to take the net countrate, presumably at any time, enter the graph for a given isotope, and then read off the presumably currently-existing concentration of that isotope in the sampled air. The implication was that moving-filter monitors could estimate concentrations directly. It has subsequently been shown that this is not the case, for the filter movement speeds typically used, i.e., 2.54 cm h^{-1} (1.0 in hr^{-1}) or in some cases even less.

To illustrate the false impression that existed concerning the capability of a moving-filter CPAM, three examples follow, taken from documents of this time period. First, a draft specification from a major A/E firm for a RMS, which stated in regard to an "atmospheric monitor" (emphasis added):

"Filter Movement: A combined fixed-filter and moving filter mode as desired, in order to enable selection of either a presentation of *accumulated data or current data*.**"**

This implies that a fixed-filter monitor provides the concentration integral (accumulated data) or a moving-filter provides the concentration itself (current data). The first is correct, the second is not. A second RMS specification draft from this A/E firm mentions "*Integrating samplers*" as opposed to "*Differential samplers*" (in context, "sampler" here is "monitor").

The implication is the same: that moving-filter monitors provide a real-time concentration estimate. The third example is from a published paper [1]:

"6.6 Alarm samplers
Alarm air samplers give an audible and/or visible warning when levels of airborne contaminants exceed preset values. The sampler therefore includes its own monitoring equipment. There are two basic types[,] which measure either the concentration or the exposure (concentration times time). The latter is more common and generally consists of a single filter viewed by a detector. *Measurement of concentration usually requires a moving strip of filter paper.*"

These examples illustrate what might be called "negative knowledge" that existed, and presumably still exists, in the nuclear power industry. Negative knowledge occurs when someone believes they understand something, but it turns out that what they believe is incorrect. In this case, A/E engineers and others apparently believed, based on the vendor sales literature, and absent any information to the contrary, that moving-filter monitors estimated concentrations in real time, and so with this (mis)understanding these devices were specified for various applications in nuclear power stations.

The primary purpose of this note is to ensure that this negative knowledge is not propagated into any future nuclear power station designs, and to provide a more mathematically-sound alternative.

Moving-Filter Sensitivity Graphs

Monitor "sensitivity" graphs such as Figs. 5-1 and 5-2 do not disclose the mathematical equation(s) being graphed. It can be inferred, however, that since there are straight lines in log-log space, the relation must be a power function. Examination of the curves shows that the slope is unity, so that the power is one. The simplest function, then, would be linear with a zero intercept, or something of the form

$$\hat{Q}(t) = \alpha \dot{C}(t),$$

with α a constant (often termed the "calibration constant"), $\hat{Q}$ the time-dependent estimated concentration, and $\dot{C}(t)$ the net, time-dependent monitor countrate. In Evans (2001a) these equations for the monitor countrates are derived:

$$\dot{C}_{RW}(t \geq T) = \bar{\varepsilon}\, \gamma k\, F\, \phi Q_0 \frac{L}{2v}, \tag{5-1}$$

$$\dot{C}_{CW}(t \geq T) = \bar{\varepsilon}\, \gamma k\, F\, \phi Q_0 \frac{8R}{3\pi v}, \tag{5-2}$$

where the parameters are as follows: RW is a rectangular-window deposition area, and CW is circular window; *L,* length of RW deposition window; *R*, radius of CW deposition window; *v*, filter (tape) speed; *T*, transit time[1]; Q_0,

[1] This is the time required for a differential area element to completely traverse the deposition area, i.e., for RW, L/v; for CW, $2R/v$.

constant concentration of nuclide in air; *k,* units reconciliation constant; *F*, monitor flowrate; φ, collection/retention efficiency and line-loss fraction product; γ, emission abundance; $\bar{\varepsilon}$, average detection efficiency.[2]

As is seen in [2], a considerable amount of mathematics is needed to arrive at these relatively simple expressions. In the absence of further information it will be assumed that these expressions are used to create the "sensitivity" graphs for moving-filter monitors. In fact, reverse-engineering actual vendor graphs, such as those in Figs. 5-1 and 5-2, using these equations produces plausible values for the detection efficiency, providing some assurance that these are the equations being graphed.

Returning to (5-1) and (5-2), the inversion to solve for the constant concentration is trivial, and these expressions are linear. That is, the limiting, constant $t \geq T$ countrate and the constant concentration are related by a multiplicative factor that consists of known instrumental parameters:

$$\hat{Q}_0 = \frac{1}{\bar{\varepsilon}\,\gamma\,k\,F\,\phi\,\dfrac{L}{2v}}\,\dot{C}_{RW}(t \geq T)\,; \tag{5-3}$$

$$\hat{Q}_0 = \frac{1}{\bar{\varepsilon}\,\gamma\,k\,F\,\phi\,\dfrac{8R}{3\pi v}}\,\dot{C}_{CW}(t \geq T)\cdot \tag{5-4}$$

Then in log-log space these functions, having zero intercept, will graph as straight lines with unity slope. The "calibration constant" α is the reciprocal quantity in (5-3) or (5-4), as appropriate for RW or CW, respectively. It is of interest to note that the only parameter in (5-3) or (5-4) that needs to be empirically estimated during the monitor calibration is the average detection efficiency, although some presumably conservative value must also be assumed for the line-loss parameter φ.

Vendor Graph Omissions

In order to derive (1) and (2), a number of assumptions had to be made. The graphs in Fig. 5-1 and 5-2 do not reveal what the limitations of these expressions are. In fact, these graphs have the following problems: (a) they do not specify RW or CW; (b) they do not provide the parameter values important to the calculations (*R* or *L,* or *v*); (c) they do not explain what is varying across the different lines for the several nuclides; (d) they do not explicitly state the transit time; (e) they do not explicitly state the restriction to long-lived nuclides;[3] (f) they do not explicitly state the restriction of the reading to times after the transit time *T*; (g) they do not explicitly state the restriction that the air concentration must remain constant over the entire transit time.

As for the calculations shown in Fig. 5-3, there are similar problems: (a) there is no derivation of the expressions used; (b) there is no derivation of the constant values used; (c) there is no reference to the literature as to where these expressions came from; (d) there is no statement of the assumptions, and thus limitations, of the calculations, similar to those listed above for the graphs. The moving-filter calculation shown is equivalent to (2) since this vendor's monitors were CW.

These graphs/calculations are for the limiting (or some would say "equilibrium") constant countrates attained for a constant concentration after the transit time, which, for the nominal filter speeds commonly used, is about two hours. The user cannot enter these graphs at any arbitrary time and read off a possibly time-dependent concentration; that is incorrect and a misuse of the monitor. The "quantitative method" (QM) in Figs. 5-1 to 5-3 is never explicitly stated, but implicitly consists of waiting for the transit time, with a constant concentration existing over that time, and then reading the attained constant net countrate.

---

[2] This is developed using the geometric efficiency averaged over the deposition window, for a given circular detector height above the plane of deposition. It can be demonstrated that using this average geometric efficiency produces a response within a few percent of that obtained using the explicit, position-dependent geometric efficiency. The latter response is not tractable analytically, and must be obtained numerically.

[3] It is the case that similar lines can be drawn on the graph for short-lived nuclides, e.g., ^{88}Rb. However, the equations necessary require knowledge of the mathematical models reported in [2], which was not available at the time these graphs were produced.

The fundamental issue is that, in general, a moving-filter monitor countrate response model cannot be inverted to solve for *Q(t)*. See [2] for the mathematical background. For some particular *Q(t)* cases this might be possible, but only if the parameters defining *Q(t)* are known. This would be most unusual. Therefore, there is no general way to get from the observed output (countrate) back to an estimate of the input (concentration). It follows that the simplifying assumptions of a constant concentration, and long-lived activity, and of using a reading only after the transit time are necessary in order to provide some form of QM for these monitors. Again, these critical restrictions are not stated in the example vendor materials shown in Figs. 5-1 to 5-3, nor in the accompanying written matter.

The transit time is an important parameter in the QM that is implicit in the graphs; it is by definition measured from the start of the concentration behavior. Two example ways to know that the transit time has elapsed are: (a) estimate the concentration start time (which is sometimes plainly evident) and then add the known transit time to this; (b) statistically test the countrate for a zero slope after an initial positive slope, indicating the constant countrate that is obtained after the transit time, if and only if the concentration is constant. These calculations are readily mechanizable with modern digital processing, although more difficult for older analog systems.

A more correctly-labeled monitor "sensitivity" graph is shown in Fig. 5-4. However, a crucial point is that, when the monitor is called upon to do its job, that is, indicating that the air concentration has changed, by definition that *Q(t)* is not constant, but the monitor "quantitative method" assumes that it *is* constant, and so this method fails. The simplistic conversion of countrate to concentration via the graph, even if better labeled, or, equivalently, via multiplication by a “calibration constant,” is still incorrect, at nominal filter speeds.

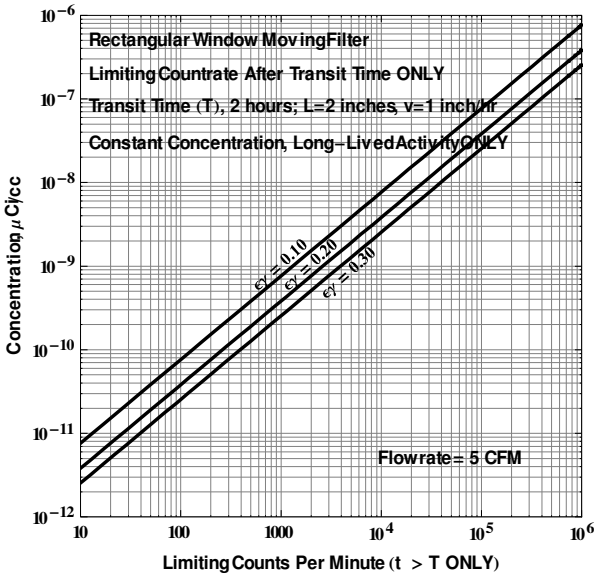

Fig. 5-4. Simulated CPAM “sensitivity” graph with more complete labeling, using (3) and units consistent with the vendor materials in Figs. 5-1to 5-3.

Examples

If this incorrect conversion is done the estimates for, e.g., an exponential *Q(t)* will look similar to that in Fig. 5-5. Clearly the concentration estimates are quite different from the actual *Q(t)* profile. It has very recently been shown, in [3], that the only way for this simple conversion to work correctly is when the filter speed is much faster than the usual 2.54 cm h^{-1} (1.0 in h^{-1}); a faster speed is shown in Fig. 5-6. It is interesting to note that this new fast-filter-speed approach does work the way the moving-filter misunderstanding would have it, i.e., an "instantaneous" concentration estimate, but this is unfortunately of little use for normal operations, due to a countrate suppression effect.

In Figs. 5-7 and 5-8 are the ratios of the estimated concentration to the true $Q(t)$ for an exponential and a constant Q, for several filter speeds v. It is seen that the ratio is far from the desired value of unity unless the filter speed is fast. Even for a constant Q (Fig. 5-8) a ratio of unity is only obtained after the transit time. The key is that the transit time is short, i.e., a few minutes, at the faster filter speeds. As discussed in [3], the price paid for this tracking ability is a reduced countrate, so that the fast-v method is only appropriate at higher concentrations.

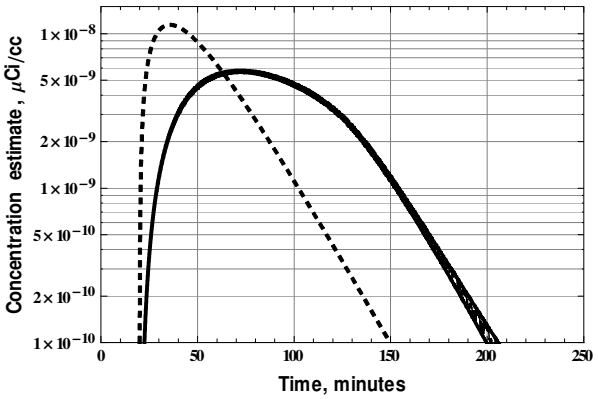

Fig. 5-5. Concentration estimates using (3) with a filter speed of 2.54 cm h^{-1} (1.0 in h^{-1}). Dashed curve is the true concentration behavior. For these plots the parameter values are as follows: RW monitor; long-lived nuclide; flow, 5 ft^3 min^{-1}; filter efficiency/line loss fraction, 0.7; window length, 4.547 cm (1.79 in); transit time, 107 minutes at 2.54 cm h^{-1} (1.0 in h^{-1}); window width, half the length, so that a rectangular region fits under a 2.54 cm (one-inch) radius detector; detector height above deposition plane, 1 cm; emission abundance, 1.0; average detection efficiency, 0.27.

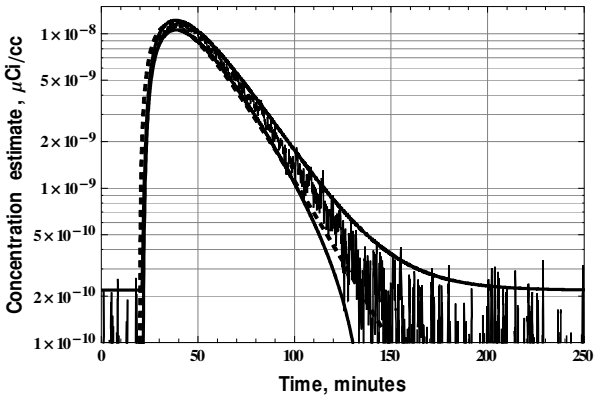

Fig. 5-6. Concentration estimates using (3) with a filter speed of 76.2 cm h^{-1} (30.0 in h^{-1}). The dashed curve is the true concentration behavior, and all other parameters are the same as in Fig. 5-5.

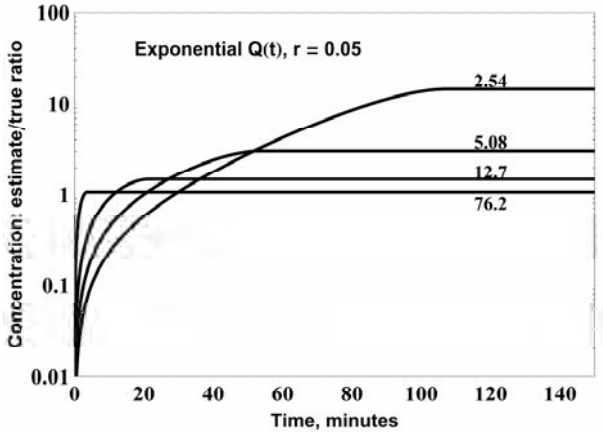

Fig. 5-7. Ratio of estimated to true concentrations for an exponential Q(t), with rate constant r. The filter speeds are as indicated, in cm h^{-1}. The transit time is about 100 minutes at 2.54 cm h^{-1} (1.0 in h^{-1}). Monitor parameter settings are the same as in Figs. 5-5 and 5-6.

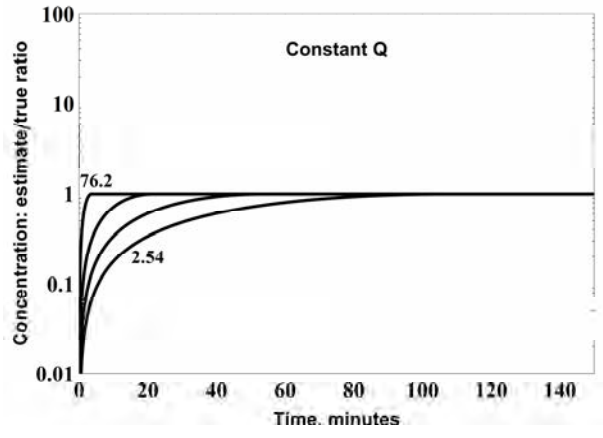

Fig. 5-8. Ratio of estimated to true concentrations for a constant Q. The filter speeds are slower toward the bottom, with the two inner lines at 5.08 and 12.7 cm h^{-1}. Note that even for a constant concentration the reading is not correct until after the transit time. Monitor parameter settings are the same as in Figs. 5-5 and 5-6.

Qualitative vs. Quantitative Use

The issue raised here is that moving-filter CPAM countrate responses can be misinterpreted, but this assumes that the device is being used quantitatively. That is, the monitor is taken to be a *measurement* device, having been calibrated in some manner on an absolute scale of a physical quantity, usually the air concentration of a specific nuclide. Note that this calibration does not consist of passing into the CPAM a known concentration of the nuclide as a particulate suspended in air, but rather is done via a selected QM, such as those in [4]. As mentioned above, the average detection efficiency must be experimentally measured as part of this QM-based calibration process; the estimation of this instrumental parameter is a necessary, but not sufficient, condition for calibration.

By contrast, however, the CPAM could also be operated as a qualitative device, assessing only *changes* in the countrate response (referred to as "trending"). In this case, no absolute-scale calibration would be necessary. The trending idea is to use the monitor to, by some criterion, lead to the taking of "grab" high-volume air samples, followed by laboratory analysis. Often the alarm or action level for this procedure is set just above the variation in the CPAM background, and thus has no quantitative or regulatory meaning. The grab sample will then, after some processing delay, lead to an estimate of the time integral of this changing concentration, which is then assumed to remain constant at the level calculated in the lab analysis. For long-lived activity only, it can be shown that this level will correspond to the average concentration in the compartment, averaged over the sampling interval. This average does not, of course, include the concentration behavior during the initial, trending, time period. How this process of "trend and grab" assists in controlling the intake of workers being actively exposed to a time-dependent air concentration is not evident.

Regulatory Guidance

There has been little regulatory guidance over the years as to exactly how the installed CPAMs are to be utilized in a power reactor health physics program. Notably, the issue of qualitative (trending) vs. quantitative (concentration estimates) is not addressed in any regulatory position. Simply saying that [5, Chapter 12]

> "The design objectives of the applicants' airborne radioactivity monitoring system are (1) to assist in maintaining occupational exposure to airborne contaminants ALARA, (2) to check on the integrity of systems containing radioactivity, and (3) to warn of unexpected release of airborne radioactivity to prevent inadvertent exposure of personnel."

does not provide sufficient information to permit the design and specification of such devices, nor, importantly, how they are to be used once installed in an operating plant. Regulatory Guide 8.8 says that the RMS can "give information on the ... concentration of airborne radioactive material." Stating that a system should "give information" is not particularly helpful to a monitor design engineer, nor to an A/E design engineer, nor to a nuclear power station health physicist. The single, rather hard-to-find regulatory CPAM performance specification is quantitative: [5, Chapter 12]

> "The monitoring system should be capable of detecting 10 DAC-hours of particulate and iodine radioactivity from any compartment that has a possibility of containing airborne radioactivity and that normally may be occupied by personnel, taking into account dilution in the ventilation system."

> "These airborne radioactivity monitors have the capability to detect [constant] derived air concentrations in air (DAC) of the most restrictive particulate and iodine radionuclides in the area or cubicle of lowest ventilation flow rate within 10 hours(s) (usually denoted as 10 DAC-hrs)."

DAC-hour Criterion and its Ambiguity

DAC-hours were expressed as MPC-hours in the mid-1970s, and CPAMs were specified on this basis, including in applications where this had no meaning (e.g., a BWR drywell monitor). However, it must first be recognized that the units of DAC-hours are ambiguous, since they also apply for the *time integral* of a possibly time-dependent concentration; this is of course related to the intake of a worker. It is not clear what health physics objective is met by simply "detecting" a concentration that is assumed to remain constant for many hours, including 10 hours, a longer time period than the usual 8-hour work shift. Also, as is well-known, detection (hypothesis test: has something changed) and measurement (how much has it changed) are not the same thing; it is not clear which is actually intended. Other regulatory guidance strongly implies the latter, i.e., measurement. For example, the definitions section of 10CFR20 states:

> "*Monitoring* ... means the measurement of ... concentrations, ... and the use of the results of these measurements to evaluate potential exposures and doses."

Clearly, there is no regulatory requirement to make these measurements of the air concentration instantaneously. However, that fact does not establish that no one in an operating plant today attempts to do so. If health physicists in nuclear power stations have devices, such as moving-filter CPAMs, that they truly believe could make such measurements, presumably they will use them, and write their procedures accordingly. There is no regulatory admonition *not* to do so.

Constant-Concentration Assumption

If A/E RMS designers were to attempt to show compliance with the 10 DAC-hr requirement, interpreted as a measurement of a concentration within some time interval, for a moving-filter CPAM, and all the information that was available to them was vendor materials such as in Figs. 5-1 to 5-3, there would be confusion, since these materials do not mention time at all. At the nominal filter speeds used, there is a lag time of some two hours (for some systems this could be as long as 8 hr) before the measurement is correct, and this is the case if, and only if, the very stringent assumption of a constant concentration *over this entire period* is made. Thus one might infer that the 10 DAC-hr requirement could be interpreted as being met by a moving-filter CPAM "detecting" a constant concentration of 5 DAC at its two hour transit time. It is not clear of what practical use this is, since, again, when the monitor is called upon to do its job of measuring a change in the air concentration, by definition that concentration is not constant, at 5 DAC or any other level.

There is a logical inconsistency between the assumption of a *constant* concentration for the supposed QM and the purpose of a monitoring instrument, that is, measuring a *changing* concentration. In spite of the "negative knowledge" in the nuclear power industry, it is a fact that a moving-filter CPAM operated at the nominal filter speed cannot measure a changing concentration. Again, one could then argue that it is not required to measure this change, in essentially real time, but simply to indicate it (trend; countrate increase). However, these monitors were specified and licensed as quantitative devices in the 1970s, at 1 MPC-hour, implying a concentration measurement in a finite time, so that using them qualitatively today is inconsistent with their licensing basis. Such use perhaps could be construed as a violation of licensing commitments, e.g., as stated in the plant FSAR.

It is important to recognize that existing regulatory guidance and vendor materials all assume that concentrations in nuclear power stations can only change in a square-wave or stair-step fashion, that is, from one constant level instantaneously to another constant level. This is, of course, not the case at all, since the plant buildings are compartmental systems and the time-dependent concentrations during transient events in such systems are sums of exponentials, as shown in, e.g., [6]. It is true that, at the design stage, A/E engineers assume a certain level of failed fuel, and then propagate those fission products through the various plant systems, with some assumed constant low-level leakage, to arrive at equilibrium air concentrations in the various compartments (e.g., equipment cubicles). However, that constant concentration is essentially a background or interference and of no direct monitoring interest in itself. What the CPAMs are there to do, presumably, is to detect changes in the air concentrations in the compartments, above this baseline level. The question, not addressed in any regulatory or standards guidance, is whether the CPAM is to *quantify* this change, or simply to *indicate* it, and, in either case, with what performance requirements.

The DAC-hour criterion assumes a constant concentration that must exist on a scale of several hours. This assumption avoids the need to find the time integral of a time-dependent concentration. The purpose, presumably, is to obtain an estimate of the intake of the workers in the area where this concentration exists. This estimate then becomes a simple product of the assumed constant concentration and the time the workers are exposed, given an assumed breathing rate. The basic approach is to, somehow, estimate that constant concentration and then to find the intake estimate. The moving-filter CPAM log-log graph reading discussed above is one way to obtain a concentration, but this estimate is incorrect unless taken after the several-hour transit time. It is not clear why this would be a good radiological protection strategy, or why this constant-concentration assumption would be thought to provide a reasonable estimate of worker intake while they are in all probability exposed to a time-dependent concentration.

Fixed-Filter Alternative

There is an alternative to the moving-filter approach already in the literature. A continuous, real-time signal that is proportional to the worker intake can be directly generated not by a moving-filter CPAM, but a fixed-filter CPAM:

$$\text{Intake}(\xi) = \frac{F_{breathing}\ \delta_{dilution}}{\overline{\varepsilon}\,\gamma k\, F_{monitor}\,\phi}\left[\dot{C}_{FF}(\xi) + \lambda\int_0^{\xi}\dot{C}_{FF}(t)\,dt\right] \tag{5-5}$$

where ξ is a time interval, λ is the decay constant of the nuclide of interest, and δ is a factor accounting for the dilution of the concentration that exists in the worker compartment, if the particulates are observed in a common HVAC duct. This is equation (1-21), with the dilution coefficient δ added, and it shows that a fixed-filter monitor can provide a time-dependent intake estimator, using the net countrate and integrated counts. The concentration itself need not be constant; it can have any arbitrary time-dependence. There is no need to estimate the concentration directly and there is no transit time delay. Note that for long-lived activity, the integral term becomes negligible, and the intake estimate is proportional to the attained countrate.

Given that, using (5-5), a fixed-filter monitor can track an estimate of worker uptake in real time, without the constant-concentration assumption, and without the wait until after a transit time, or without the delay involved with a trend alarm and subsequent grab sample, it is not clear why a moving-filter CPAM would be used, in any manner, for occupational personnel protection purposes. If dust loading is an issue, a step-advance fixed-filter monitor can be used, with a rapid filter advance and re-initialization of the (5-5) calculation, on low flow.[4] A step-advance can also be used if there is a constant long-lived airborne activity, such that the fixed-filter CPAM countrate would increase to unacceptable levels.

Conclusion

Several steps should be taken to resolve the issues discussed above. First, it should be made a standards or regulatory requirement that vendor materials for all CPAMs should clearly and explicitly state the methodology, the assumptions, and the limitations of the quantitative methods used in the devices. This is not the case today. Doing this would presumably eliminate the misleading log-log "sensitivity" plots for moving-filter CPAMs that have been around the industry since at least the 1970s. In fact such plots can still be found today, in vendor materials available on the internet, and they are still improperly labeled, and continue to propagate the same false implication regarding the monitor's quantitative capability.

Second, a study should be undertaken in the industry to evaluate the extent to which the incorrect interpretation of moving-filter CPAM responses discussed here might affect the radiological protection of nuclear power plant workers. What should be evaluated are the prevalence, and consequences, of this mistaken belief, in today's operating plants. Also, possible operational issues, notably related to reactor coolant leakage detection, should be evaluated, since these monitors are often used in this application. Further, a complete review of RMS procedures,

[4] The intake calculation of (5-5) assumes a constant monitor flow. If that flow decreases rapidly due to severe dust loading, another method from [4] should be selected, with that nonconstant flow taken into account.

not only for CPAMs, as they exist in current operating plants would be useful in identifying good, and poor, practices.

Third, a major need is for more detailed and accessible standards and regulatory guidance covering the acceptable use of installed CPAMs in nuclear power stations. Standards should address quantitative methods for CPAMs, including their limitations. A new Regulatory Guide with specific, unambiguous RMS performance and application requirements would be helpful to the industry. Most fundamentally this new guidance needs to define whether CPAMs are to be quantitative or qualitative instruments.

If CPAMs are to be quantitative, more meaningful performance requirements are needed for specification definition, to the level of detail that an appropriate method can be selected from the several available in, e.g., [4]. Measurement approaches must deal in a realistic manner with time-varying concentrations, i.e., anticipated operational occurrences. Measurement of the baseline constant concentration from normal leakage is not a performance requirement, except to account for it as an interference. Measurements should relate directly to the purpose of the monitor, e.g., for occupational exposure control, estimation of intake, not concentration, is appropriate. The nDAC-hr ambiguity (a constant concentration estimated over some time interval, vs. the time integral of a time-dependent concentration) must be resolved. Clear guidance should be provided on how CPAMs are to be routinely used, quantitatively, in a nuclear plant health physics program (ALARA).

If on the other hand CPAMs are to be qualitative, performance requirements must be defined so that systems can be designed to meet them. This must include a statistical analysis to find the minimum change to be reliably detected within some response time, taking into account the autocorrelation of variance-reduced countrate data. It must be recognized that expensive and time-consuming absolute calibrations will then no longer be necessary. The moving-filter concentration misinterpretation problem will vanish. For existing plants, it must be shown how qualitative use would not be a licensing-commitment violation.

Resolving these issues would be a good step toward improving RMS capabilities in a new generation of nuclear power stations.

References

[1] M. Marshall and D. C. Stevens, "The purposes, methods and accuracy of sampling for airborne particulate radioactive materials," *Health Physics,* vol. 39, pp.409-423, 1980.

[2] W. C. Evans, "Mathematical models for the dynamic response of continuous particulate air monitors," *IEEE Trans Nucl Sci*, vol. 48, pp. 202-218, 2001.

[3] W. C. Evans, "Estimation of high-level, rapidly-changing concentrations using moving-filter continuous particulate air monitors," *Health Physics*, vol. 102, pp. 410-418, 2012; Erratum vol. 102, p. 708, 2012.

[4] W. C. Evans, "Quantitative methods for continuous particulate air monitoring," *IEEE Trans Nucl Sci*, vol. 48, pp. 1639-1657, 2001.

[5] U. S. Nuclear Regulatory Commission. *NUREG 0800*; Standard review plan for the review of safety analysis reports for nuclear power plants: LWR edition; Revision 3, March 2007.

[6] D. H. Anderson, *Compartmental modeling and tracer kinetics*. New York: Springer-Verlag; 1983

Chapter 6

Geometric Efficiency Correction

Unpublished

Existing models assumed that the geometric efficiency variation was negligible across the detection window. Using an analytical model and Monte Carlo simulation, the geometric efficiency for RW, SQ (square), CW configurations was explored. It was demonstrated that the Monte Carlo results agree with the analytical integral. Detector height is now important. Using the correct geometric efficiency does reduce the indicated countrate of earlier models, not radically, but enough to need a correction. The correction is just a simple average efficiency, averaged over the detection window. Applying this to the existing models, in place of previously-assumed flat efficiency, brings earlier RW, CW models into reasonable, not exact, agreement with numerical solution which used the correct geometric efficiency (done with a numerical model). On the other hand, the FF correction is shown to be exact.

Existing Models

Under the assumption of a "flat" (constant, per nuclide) efficiency matrix $\boldsymbol{\psi}_0$, the original RW countrate model can be written

$$\dot{\mathbf{C}}_{RW}(t \le T) = \frac{\boldsymbol{\Psi}_0}{L}\left[\int_0^{vt}\int_{t-\frac{x}{v}}^{t} e^{\mathbf{A}(t-\tau)}\mathbf{B}\,\mathbf{u}(\tau)\,d\tau\,dx + \int_{vt}^{L}\int_0^{t} e^{\mathbf{A}(t-\tau)}\mathbf{B}\,\mathbf{u}(\tau)\,d\tau\,dx\right] \tag{1}$$

$$\dot{\mathbf{C}}_{RW}(t \ge T) = \frac{\boldsymbol{\Psi}_0}{L}\int_0^{L}\int_{t-\frac{x}{v}}^{t} e^{\mathbf{A}(t-\tau)}\mathbf{B}\,\mathbf{u}(\tau)\,d\tau\,dx \tag{2}$$

If the detection efficiency matrix is position-dependent, then this model is extended to be:

$$\dot{\mathbf{C}}_{RW}(t \le T) = \frac{1}{wL}\left[\begin{array}{l}\displaystyle\int_0^{w}\int_0^{vt}\int_{t-\frac{x}{v}}^{t} \boldsymbol{\Psi}(x,y)\,e^{\mathbf{A}(t-\tau)}\mathbf{B}\,\mathbf{u}(\tau)\,d\tau\,dx\,dy + \\ \displaystyle\int_0^{w}\int_{vt}^{L}\int_0^{t} \boldsymbol{\Psi}(x,y)\,e^{\mathbf{A}(t-\tau)}\mathbf{B}\,\mathbf{u}(\tau)\,d\tau\,dx\,dy\end{array}\right] \tag{3}$$

$$\dot{\mathbf{C}}_{RW}(t \ge T) = \frac{1}{wL}\int_0^{w}\int_0^{L}\int_{t-\frac{x}{v}}^{t} \boldsymbol{\Psi}(x,y)\,e^{\mathbf{A}(t-\tau)}\mathbf{B}\,\mathbf{u}(\tau)\,d\tau\,dx\,dy \tag{4}$$

where the efficiency matrix is now inside the integration. Similar expressions can be written for the CW case, but this is most practically handled by use of the "RW approximation" discussed in Chapter 1. That is, an effective window length

$$L_{CW} = \frac{16\,R_{dep}}{3\pi} \tag{5}$$

is used in these models; the responses will be a good approximation to those of the full CW models. R_{dep} is the radius of the deposition area, as opposed to the radius of the detector. These are often equal, but in general need not be. Note that, under the flat efficiency assumption, there is no need to specify the RW window width, nor the height of the detector above the plane of activity deposition. The assumption is that all the deposited activity is viewed by the detector, at the same efficiency.

Geometric Efficiency Function

However, there is of course a *geometric* detection efficiency variation across the deposition window. The issue is, can this variation be ignored, or must it be accounted for in some manner? The geometric efficiency Ω for a point source viewed by a circular detector is

$$\Omega(R_{det}, h, x, y) = \frac{1}{4\pi}\int_0^{R_{det}}\int_0^{2\pi} \frac{h}{\left[h^2 + r^2 + x^2 + y^2 + 2\,x\,r\cos(\theta) + 2\,y\,r\sin(\theta)\right]^{\frac{3}{2}}}\, r\,dr\,d\theta \tag{6}$$

where R_{det} is the radius of the circular detector, h is its height above the x-y plane of deposition, and (x, y) specifies the position of an emitting point in that plane. In the present case the emission "point" is for a differential area of filter material in the deposition window. This integral cannot be evaluated in closed form, so that a numerical solution is indicated.

One way to visualize the geometric efficiency is its variation along a radial distance, independent of the azimuth angle; this is shown in Fig. 1.

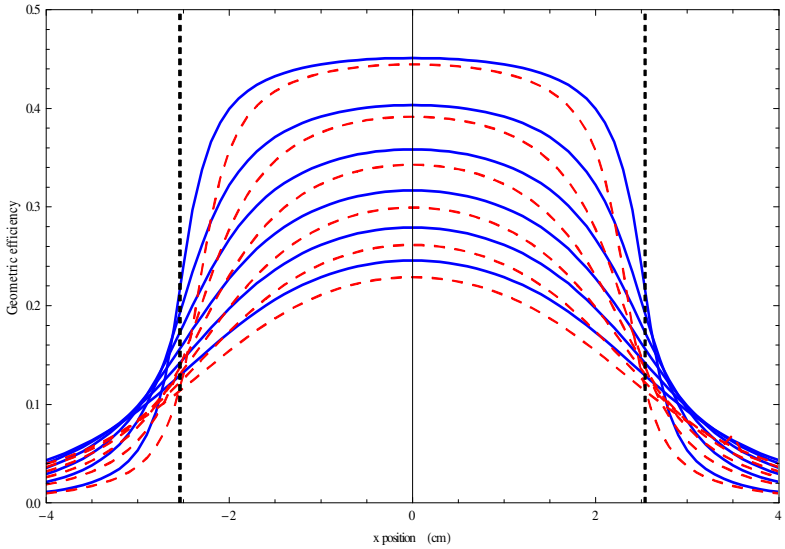

Fig. 1 Centerline geometric efficiency (blue), offset by 1 cm (red) for h=0.25 (top) to 1.5 (bottom) by 0.25. The vertical dashed lines represent the boundary of a 2.54 cm deposition area. For smaller h, the efficiency variation across the window is relatively mild until the emitting position is near the edge of the window.

In Figure 2 are 3D plots of Monte Carlo estimation of the geometric efficiencies for RW, CW, and SQ (square) deposition areas, for four detector heights h. It can be demonstrated that similar plots of the analytical function eqn(6) are indistinguishable from these.

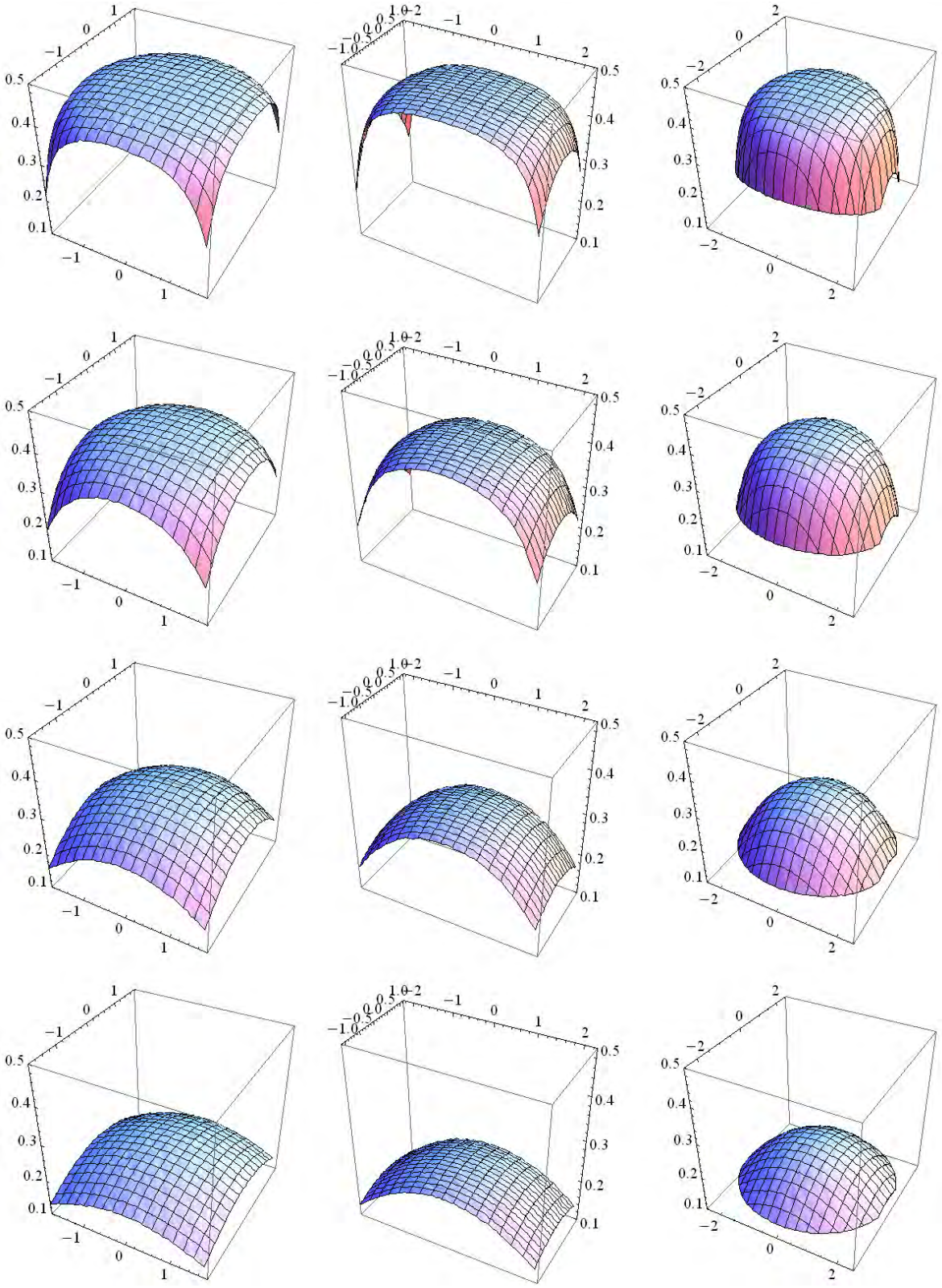

Figure 2. Plots of the geometric efficiency for SQ, RW, and CW deposition areas. The RW width is one-half the length. The detector height h is 0.25, 0.5, 1.0, 1.5 cm, top to bottom, while the detector radius is 2.54 cm.

Average Geometric Efficiency

One approach to correcting the countrate discrepancy noted above is to use an average geometric efficiency across the deposition window. That is, in a schematic form,

$$\bar{\Omega} = \frac{\int_{Area} \Omega(\,position)\; d(Area)}{Area} \tag{7}$$

More specifically, for the RW or SQ case,

$$\bar{\Omega} = \frac{1}{w\,L} \int_{-\frac{w}{2}}^{\frac{w}{2}} \int_{-\frac{L}{2}}^{\frac{L}{2}} \Omega\left(R_{det}, h, x, y\right)\, dx\, dy \tag{8}$$

where *(0,0)* is at the center of the detector. For the CW case,

$$\bar{\Omega} = \frac{1}{\pi R_{dep}^2} \int_{-R_{dep}}^{R_{dep}} \int_{-\sqrt{R_{dep}^2 - y^2}}^{\sqrt{R_{dep}^2 - y^2}} \Omega\left(R_{det}, h, x, y\right)\, dx\, dy \tag{9}$$

The CW case has radial symmetry, so that the azimuth angle (in the plane of deposition) has no effect on the efficiency; then

$$\bar{\Omega} = \frac{1}{\pi R_{dep}^2} \int_0^{2\pi} \int_0^{R_{dep}} \Omega\left(R_{det}, h, r, 0\right)\, r\, dr\, d\theta = \frac{2}{R_{dep}^2} \int_0^{R_{dep}} \Omega\left(R_{det}, h, r, 0\right) r\, dr \tag{10}$$

Note that this symmetry allows the use of a 1D interpolation in the CW countrate calculations, while the RW and SQ cases require a 2D interpolation, which is slower. These average geometric efficiencies can readily be calculated numerically. With the geometric efficiency defined, the overall detection efficiency is of course the product of the intrinsic efficiency v and the geometric efficiency Ω:

$$\varepsilon = \nu\, \Omega$$

In Fig. 3 is the *Mathematica* code to estimate the average efficiencies for RW and CW.

■ **Define the geometric efficiency function**

This is the usual point-source for a circular detector, extended to 3D.
x and y are the coordinates of the emitting cell.

```
Ω[R_, h_, x_, y_] := NIntegrate[h * r / (h^2 + x^2 + y^2 + r^2 + 2. x * r * Cos[ϕ] +
                                                                2. y * r * Sin[ϕ])^(3 / 2),
                                {r, 0., R}, {ϕ, 0., 2. Pi}, WorkingPrecision → 12,
                                AccuracyGoal → 5] / (4. Pi)
```

■ **Find the CW effic interpolation function (radial)**

This interpolation, even in 2D, is faster to execute than the direct efficiency function. The CW efficiency is independent of the azimuth angle, so it becomes a 1D interpolation, which is even faster.

```
Off[NIntegrate::inumr];
effCW = FunctionInterpolation[Ω[R, h, x, 0], {x, 0, R}];
```

■ **Find the RW effic interpolation function**

```
Off[NIntegrate::inumr];
effRW = FunctionInterpolation[Ω[R, h, x, y], {x, -L0 / 2, L0 / 2}, {y, -W / 2, W / 2}];
```

■ **Find CW average effic over window**

```
Off[NIntegrate::inumr];
CWavg = 2 * NIntegrate[r * effCW[r], {r, 0, R}] / (R * R)
```

■ **Find RW average effic over window**

```
Off[NIntegrate::inumr];
RWavg = NIntegrate[effRW[x, y], {x, -L0 / 2, L0 / 2}, {y, -W / 2, W / 2}] / (L0 * W)
```

Fig. 3. Mathematica code to find average geometric efficiencies, for RW and CW.

Countrate Difference and Correction

Having a geometric efficiency function, the next logical step is to implement it and find the countrate responses that result from this non-uniform detection efficiency. Then those responses can be compared to the previous model, which assumed a flat efficiency. The geometric efficiency function can be numerically integrated directly, but this is quite slow, so that a "function interpolation" was used.

In Figure 4 is a plot showing the RW countrates for a 3-chain, for the flat-efficiency model (solid lines) and the geometric-efficiency model; the latter includes Poisson noise and EWMA filtering. Clearly there is a significant difference, that needs to be corrected. Figure 5 shows the same thing for CW, and it also shows how well the RW approximation mimics the "exact" (numerical) CW response. The constant (flat) efficiency used in both figures is the *maximum* geometric efficiency, at the center of the detector. This would be the worst case, for the discrepancy comparison.

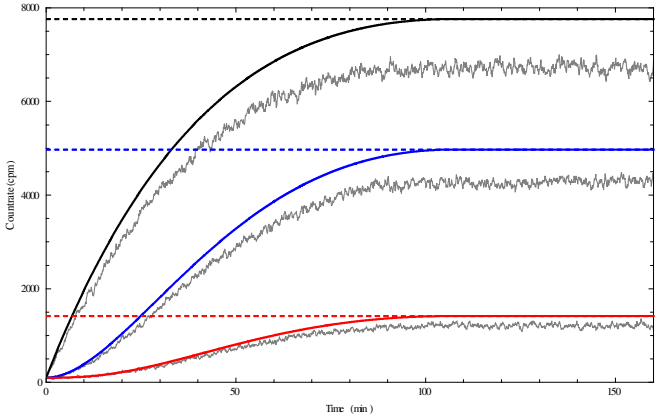

Figure 4. RW flat (max, centerline) efficiency countrate vs. geometric efficiency countrate, 3-chain.

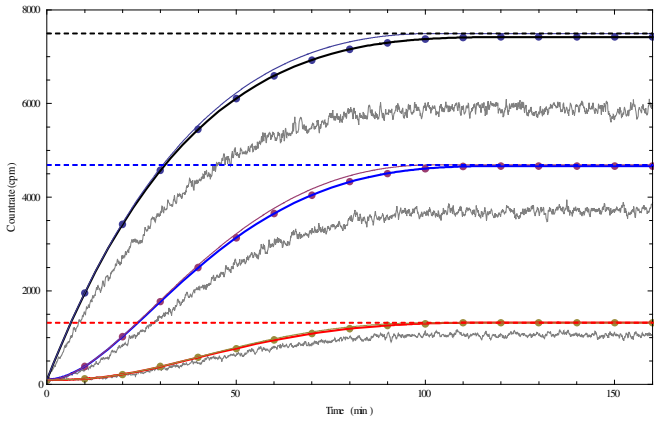

Figure 5. CW flat (max) efficiency: CW analytical (numerical triple integrals), dots and interpolated line; RW approximation, thin line; noisy countrates from geometric efficiency.

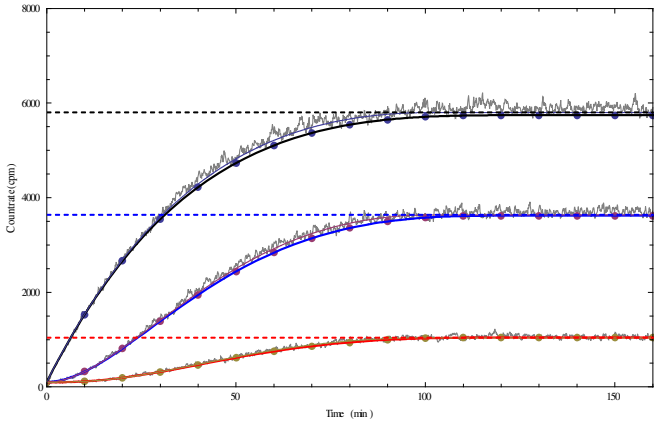

Figure 6. Similar to Fig.5, but now using the average geometric efficiency for the line plots, rather than the maximum efficiency. Clearly the agreement is far better; Fig.9 below shows that the fractional difference is a few percent.

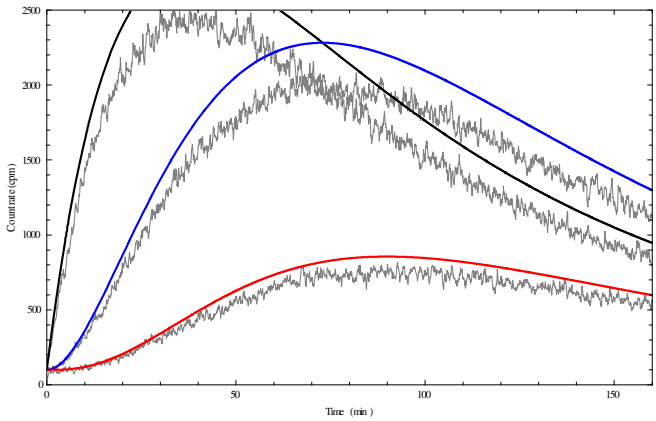

Figure 7. Fixed-filter (v=0.0001) 3-chain responses using maximum geometric efficiency. Overestimate is similar to RW, CW plots in Figs. 4, 5.

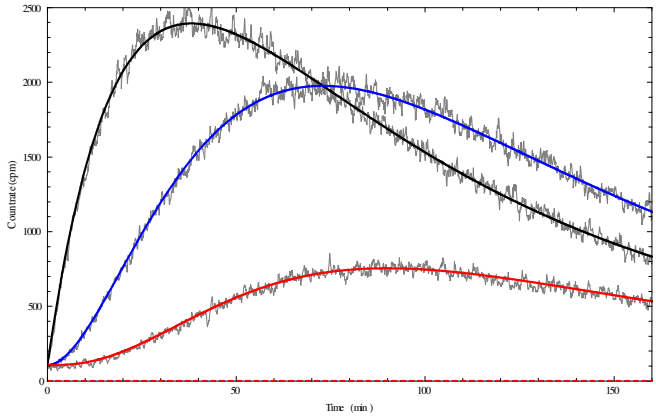

Figure 8. Same as Fig. 7, but using average geometric efficiency. Agreement is exact.

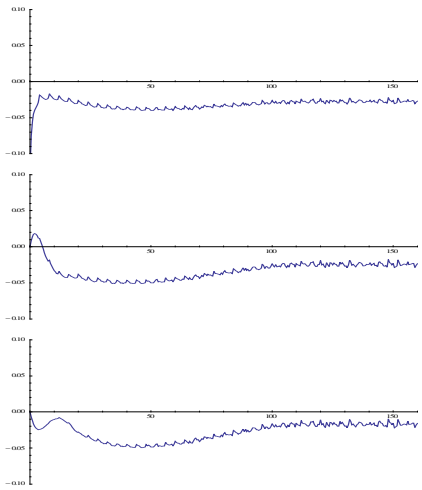

Figure 9. CW fractional differences when using average geometric efficiency. The difference is just a few percent.

Calibration

As was seen above, the use of the mathematical models requires an average efficiency for a given monitor. There are two ways to estimate this average efficiency: (1) use a distributed source, with radioactive material evenly spread across the deposition-window geometry; (2) a point source at the center of the detector, and a calculation of the average efficiency from this (observed) maximum efficiency.

For a source in the geometric configuration that will exist during monitor operation, with a known amount of a given nuclide evenly distributed over this area, the observed estimate of the efficiency will be

$$\bar{\varepsilon} = \frac{counts/time}{emissions/time} = \frac{\nu \int_{Area} \Omega(position)\Gamma(position)\, d(Area)}{\int_{Area} \Gamma(position)\, d(Area)} \tag{11}$$

where, again, ν is the intrinsic detection efficiency, and Γ is the activity per unit area on the filter medium, which in general can be a function of position in the deposition area. For a uniformly-deposited emitting material on the filter, however (or for a fixed-filter monitor), the activity per unit area is not position-dependent, so that

$$\bar{\varepsilon} = \frac{counts/time}{emissions/time} = \frac{\nu \int_{Area} \Omega(position)\, d(Area)}{\int_{Area} d(Area)} = \nu\,\bar{\Omega} \tag{12}$$

This is the efficiency that should be used in the monitor response models, or for fast-v. It is important to emphasize that the deposited calibration material must be in exactly the same geometric shape (rectangular, square, circular) and dimensions as the deposition area of the monitor.

Another approach is to use the maximum efficiency, which is found at the center of the detector

$$\varepsilon_{max} = \nu\ \Omega(R_{det},\, h,\, 0,\, 0)$$

and which can be estimated using a simple point source. Then the average efficiency for a given geometry can be calculated using the appropriate ratio

$$RWratio = \frac{\varepsilon_{avg}}{\varepsilon_{max}} = \frac{\nu}{w\,L\,\nu\,\Omega(R_{det},h,0,0)} \int_{-\frac{w}{2}}^{\frac{w}{2}} \int_{-\frac{L}{2}}^{\frac{L}{2}} \Omega(R_{det},h,x,y)\, dx\, dy \tag{13}$$

or

$$CWratio = \frac{\varepsilon_{avg}}{\varepsilon_{max}} = \frac{\nu}{\pi R_{dep}^2\,\nu\ \Omega(R_{det},h,0,0)} \int_{-R_{dep}}^{R_{dep}} \int_{-\sqrt{R_{dep}^2-y^2}}^{\sqrt{R_{dep}^2-y^2}} \Omega(R_{det},h,x,y)\, dx\, dy \tag{14}$$

These ratios are of course independent of the intrinsic efficiency. A *Mathematica* implementation for the CW case is as follows:

```
Ω[R_, h_, x_, y_] := NIntegrate[ h * r / (h^2 + x^2 + y^2 + r^2 + 2. x * r * Cos[ϕ] + 2. y * r * Sin[ϕ])^(3 / 2),
                                 {r, 0., R}, {ϕ, 0., 2. Pi} ] / (4. Pi);
 eff    = FunctionInterpolation[ Ω[R_det, h, x, y],
                                 {x, -2 R_dep, 2 R_dep}, {y, -2 R_dep, 2 R_dep} ] ;
maxeff = Ω[R_det, h, 0, 0];
avgeff = NIntegrate[eff[x, y] , {x, -R_dep, R_dep},
                {y, -Sqrt[R_dep^2 - x^2], Sqrt[R_dep^2 - x^2]} ] / (Pi R_dep^2 );
CWratio = avgeff / maxeff;
```

Then the estimated average efficiency is the product of this *CWratio* value and the observed point-source maximum efficiency (which, as measured, will implicitly include the intrinsic efficiency). For the RW or SQ case all that would change is the integration region, over the appropriate deposition area, to find the average efficiency. Note that the function interpolation is done out to twice the deposition area radius, to reduce edge effects. This interpolation is used because the direct integration of the efficiency function is very slow.

Conclusion

In earlier work it was incorrect to assume a flat efficiency. The geometric efficiency variation is significant, but not fatal; it can be corrected. Using the geometric efficiency averaged over the deposition area works quite well. One can always use the numerical model (Chapter 7) if the "exact" response is needed. Calibration can be done in the usual way with a uniform source, but of course it must be in the same geometry as the deposition area. Alternatively, and likely simpler and less expensive, one could use a point source at the center of detector and the calculation indicated above to find the average efficiency.

Chapter 7

Selected Formulas

Introduction

The purpose of this chapter is to present general mathematical models for the countrate response of, primarily, a rectangular-window (RW) moving filter continuous air monitor. A circular-window (CW) model is also presented, but an efficient approximation using the RW model solutions is preferred. Fixed-filter (FF) solutions are readily obtained from the RW results simply by substitution of a zero filter speed. Thus, a single model can provide solutions for all three monitor types. The model can provide countrate solutions for decay chains of any length, although length three, for radon-thoron (RnTn) is a practical maximum. Quantities derived from the countrate, e.g., derivatives and integrals, are also available. Solutions are obtained symbolically, using *Mathematica*. Commands for generating all solutions/equations are provided. Note that *Mathematica* outputs are often very cumbersome, and much hand-algebra is needed to obtain the equations given here.

A set of selected solutions is provided, but these are not comprehensive. The countrate responses are of course driven by the concentration behavior, which can take on many forms. A general procedure is given for finding solutions for any (integrable) concentration behavior, while various solutions are explicitly provided for the (1) constant, (2) single-exponential, (3) triple-exponential, and (4) Kr-Rb in containment concentration time-dependences.

The fundamental RW model is an extension to decay chains of the RW model reported in a series of papers in the *IEEE Transactions on Nuclear Science* (see references). Some of the solutions given here were presented in those papers, but other results are new. In particular, solutions for decay chains; for the Kr-Rb case; for RnTn; and some derivatives and integrals, are new. Another new result is a demonstration that a faster RW/CW filter speed can track a changing concentration very closely, although the countrate is reduced, so that this method would only be useful for accident situations.

The symbols used in the mathematical models are as follows:

$\boldsymbol{\alpha}$	vector of decay-chain nuclide activities, dpm;
$\dot{\mathbf{C}}(t)$	time-dependent monitor net countrate vector, cpm;
L	length of RW deposition/detection window, inches;
R	radius of CW deposition/detection window, inches;
v	filter (tape) speed, inches/hour;
T	transition time (L / v), hours;
$\mathbf{A}$	system matrix (here, decay constants);
$\mathbf{B}$	source allocation matrix;
$\mathbf{u}$	source (air concentration) vector;
$\boldsymbol{\Psi}$	matrix of detection efficiency-abundance products.
λ_i	nuclide i decay constant, 1/hr;
η_i	branching ratio to nuclide i;
Q_i	concentration of nuclide i in air, uCi/cc;
k	units reconciliation constant;
F	monitor or sampler flowrate, cfm;
φ	collection/retention efficiency and line-loss fraction product;
ε	detection efficiency, counts/emission;
γ	emission abundance, emission/disintegration.

Monitor Countrate Response Models

These models use the matrix exponential method of solution of the systems of differential equations that describe the activity accumulated on a differential area of filter. Those differential areas are then integrated across the RW or CW geometry to find the time they were exposed to the inflow of airborne activity. See [1]; these models are decay-chain extensions of the models reported there. A clean filter, zero initial condition, is assumed (except in 2.6, where the IC is included for more generality). Time is measured from the start of the concentration behavior.

2.1 Rectangular Window (RW) Moving Filter (T = L / v)

$$\boldsymbol{\alpha}_{RW}(t \le T) = \frac{1}{L}\left[\int_0^{vt}\int_{t-\frac{x}{v}}^{t} e^{\mathbf{A}(t-\tau)}\mathbf{B}\,\mathbf{u}(\tau)\,d\tau\,dx + \int_{vt}^{L}\int_0^{t} e^{\mathbf{A}(t-\tau)}\mathbf{B}\,\mathbf{u}(\tau)\,d\tau\,dx\right]$$

$$\boldsymbol{\alpha}_{RW}(t \ge T) = \frac{1}{L}\int_0^{L}\int_{t-\frac{x}{v}}^{t} e^{\mathbf{A}(t-\tau)}\mathbf{B}\,\mathbf{u}(\tau)\,d\tau\,dx$$

$$\dot{\mathbf{C}}_{RW}(t) = \boldsymbol{\Psi}\,\boldsymbol{\alpha}_{RW}(t)$$

2.2 Circular Window (CW) Moving Filter (T = 2R / v)

$$\boldsymbol{\alpha}_{CW}(t \le T) = \frac{2}{\pi R^2}\left\{\begin{array}{l}\displaystyle\int_{\sin^{-1}\left(\frac{vt}{2R}\right)}^{\frac{\pi}{2}}\int_{-R\sin(\alpha)+vt}^{R\sin(\alpha)}\int_0^{t} e^{\mathbf{A}(t-\tau)}\,\mathbf{B}\,\mathbf{u}(\tau)\,d\tau\,dx\,R\sin(\alpha)\,d\alpha \\ \displaystyle + \int_0^{\sin^{-1}\left(\frac{vt}{2R}\right)}\int_{-R\sin(\alpha)}^{R\sin(\alpha)}\int_{t-\frac{x+R\sin(\alpha)}{v}}^{t} e^{\mathbf{A}(t-\tau)}\,\mathbf{B}\,\mathbf{u}(\tau)\,d\tau\,dx\,R\sin(\alpha)\,d\alpha \\ \displaystyle + \int_{\sin^{-1}\left(\frac{vt}{2R}\right)}^{\frac{\pi}{2}}\int_{-R\sin(\alpha)}^{R\sin(\alpha)+vt}\int_{t-\frac{x+R\sin(\alpha)}{v}}^{t} e^{\mathbf{A}(t-\tau)}\,\mathbf{B}\,\mathbf{u}(\tau)\,d\tau\,dx\,R\sin(\alpha)\,d\alpha\end{array}\right\}$$

$$\boldsymbol{\alpha}_{CW}(t \ge T) = \frac{2}{\pi R^2}\int_0^{\frac{\pi}{2}}\int_{-R\sin(\alpha)}^{R\sin(\alpha)}\int_{t-\frac{x+R\sin(\alpha)}{v}}^{t} e^{\mathbf{A}(t-\tau)}\,\mathbf{B}\,\mathbf{u}(\tau)\,d\tau\,dx\,R\sin(\alpha)\,d\alpha$$

$$\dot{\mathbf{C}}_{CW}(t) = \boldsymbol{\Psi}\,\boldsymbol{\alpha}_{CW}(t)$$

2.3 Circular Window Moving Filter Approximation

It is shown in [1] that a good approximation for the CW response is given by using an "effective" length

$$L_{CW} = \frac{16R}{3\pi}$$

in the respective RW solutions given below. A graphical demonstration of this, for a 3-chain, is shown in Fig [xxx] in the Graphics section. The direct numerical solution of Eq(2.2) is possible, but slow, and this approximation is faster and quite good, especially after Poisson count variation is included.

2.4 Fixed Filter (FF): Matrix Exponential Solution

$$\boldsymbol{\alpha}_{FF}(t) \;=\; \int_0^t e^{\mathbf{A}(t-\tau)}\mathbf{B}\,\mathbf{u}(\tau)\,d\tau$$

$$\dot{\mathbf{C}}_{FF}(t) = \boldsymbol{\Psi}\,\boldsymbol{\alpha}_{FF}(t)$$

2.5 Fixed Filter: Zero Filter Speed RW Solution

Solutions obtained for the $t \le T$ RW case will have terms that are multiplied by the filter speed v. Setting this speed to zero will eliminate those terms, and lead to the FF response. Thus, any $t \le T$ RW solution implicitly also includes the FF solution for that case.

2.6 Fixed Filter: Laplace Transform Solution

$$\boldsymbol{\alpha}_{FF}(t) \;=\; \Im^{-1}\left[\left(s\mathbf{I}-\mathbf{A}\right)^{-1}\mathbf{B}\,\mathbf{u}(s)\right] \;+\; \Im^{-1}\left[\left(s\mathbf{I}-\mathbf{A}\right)^{-1}\boldsymbol{\alpha}_{FF}(0)\right]$$

$$\dot{\mathbf{C}}_{FF}(t) = \boldsymbol{\Psi}\,\boldsymbol{\alpha}_{FF}(t)$$

2.7 Fixed Filter: Iterated Scalar Convolution Integral Solution

$$\dot{C}_{FF,1}(t) = \varepsilon_1\,\gamma_1\,k\,F\,\phi\int_0^t Q_1(\tau)\,e^{-\lambda_1(t-\tau)}\,d\tau$$

$$\dot{C}_{FF,2}(t) = \varepsilon_2\,\gamma_2\,k\,F\,\phi\left\{\begin{array}{c}\displaystyle\int_0^t Q_2(\tau)\,e^{-\lambda_2(t-\tau)}\,d\tau \;+\\ \displaystyle\eta_2\lambda_2\int_0^t e^{-\lambda_2(t-\tau)}\int_0^\tau Q_1(\theta)\,e^{-\lambda_1(\tau-\theta)}\,d\theta\,d\tau\end{array}\right\}$$

$$\dot{C}_{FF,3}(t) = \varepsilon_3\,\gamma_3\,k\,F\,\phi\left\{\begin{array}{c}\displaystyle\int_0^t Q_3(\tau)\,e^{-\lambda_3(t-\tau)}\,d\tau \;+\\ \displaystyle\eta_3\lambda_3\int_0^t e^{-\lambda_3(t-\tau)}\int_0^\tau Q_2(\theta)\,e^{-\lambda_2(\tau-\theta)}\,d\theta\,d\tau \;+\\ \displaystyle\eta_2\eta_3\lambda_2\lambda_3\int_0^t e^{-\lambda_3(t-\tau)}\int_0^\tau e^{-\lambda_2(\tau-\theta)}\int_0^\theta Q_1(z)\,e^{-\lambda_1(\theta-z)}\,dz\,d\theta\,d\tau\end{array}\right\}$$

2.8 Source (Concentration) Modeling

The linear-systems approach used here for monitor response modeling is also well-suited for modeling the time-dependent concentrations that arise in various application situations. See [3] for a discussion. This approach will be used below for the Kr-Rb in containment (leak detection, RG 1.45) case. Once this concentration model is developed, it is used in the monitor models, above.

General Solution Method

There is not always a need for explicit algebraic solutions; the matrix exponential solution can be evaluated by mathematical software, and studies done, plots generated, without ever writing out the solutions algebraically. Those explicit solutions are usually needed only when exploring quantitative methods, for which the response models need to be inverted. One widely-used and readily-available mathematical system is *Mathematica*. To illustrate this process, below is an example procedure for finding a solution for a specified source behavior, using *Mathematica*.

First, the fundamental system of differential equations for the activities α of ,e.g., a 3-chain on a FF monitor or a differential area of a moving-filter monitor is

$$\begin{aligned}
\frac{d\alpha_1}{dt} &= -\lambda_1 \alpha_1 &&+ k F \phi Q_1(t) \\
\frac{d\alpha_2}{dt} &= \lambda_2 \eta_2 \alpha_1 - \lambda_2 \alpha_2 &&+ k F \phi Q_2(t) \\
\frac{d\alpha_3}{dt} &= \lambda_3 \eta_3 \alpha_2 - \lambda_3 \alpha_3 &&+ k F \phi Q_3(t)
\end{aligned}$$

which is written in matrix form as

$$\dot{\boldsymbol{\alpha}} = \mathbf{A}\,\boldsymbol{\alpha} + \mathbf{B}\,\mathbf{u}$$

with

$$\mathbf{A} = \begin{pmatrix} -\lambda_1 & 0 & 0 \\ \eta_2 \lambda_2 & -\lambda_2 & 0 \\ 0 & \eta_3 \lambda_3 & -\lambda_3 \end{pmatrix} \quad \mathbf{B} = \begin{pmatrix} 1 & 0 & 0 \\ 0 & 1 & 0 \\ 0 & 0 & 1 \end{pmatrix} \quad \mathbf{u} = \begin{pmatrix} Q_1 \\ Q_2 \\ Q_3 \end{pmatrix} k F \phi$$

This is the linear-systems formulation of the problem. The steps for a general solution are as follows:

1. Define source (concentration) time-dependent behavior, per nuclide (3-chain assumed), e.g.,

$$Q_1(\tau) = Q_0\, e^{-r\tau} \qquad Q_2(\tau) = 0 \qquad Q_3(\tau) = 0$$

Here only the top-of-chain nuclide is present in the monitored air. Note that the time variable is τ, not t, in order to be integrated correctly.

*2. Place these concentrations into the **u** vector:*

```
u = { { Q0*Exp[-r*τ] }, {0} , {0} } * k * F * φ;
```

*3. Define **B**, the source allocation matrix; usually just an identity matrix since each air concentration drives only that nuclide's activity:*

```
B = IdentityMatrix[3];
```

*4. Define **A**, the system matrix (which is developed from the ODE system for the decay chain);*

```
A = { { -λ1, 0, 0 }, { η2 λ2, -λ2, 0 }, { 0, η3 λ3, -λ3 } };
```

*5. Define the efficiency-abundance matrix (use the **average** geometric efficiency; see Chapter 6):*

```
Ψ = { {ε1 γ1, 0, 0},{0, ε2 γ2, 0},{0, 0, ε3 γ3} };
```

6. To preserve a symbolic solution do not define any parameters with numerical values at this point.

7. Find the RW activity vectors using Eq(2.1)

```
Activ = 1/L( Integrate[ MatrixExp[A(t-τ)].B.u, {x,0,v*t},{τ,t-x/v,t} ] +
             Integrate[ MatrixExp[A(t-τ)].B.u, {x,v*t,L},{τ,  0,  t} ]   );

ActivT = 1/L Integrate[ MatrixExp[A(t-τ)].B.u, {x,0,L},  {τ,t-x/v,t} ] ;
```

8. Find the CW activity vector functions using numerical integrations of Eq(2.2)

```
Activ[t_]:= 2/(Pi*R^2) * (
               NIntegrate[ MatrixExp[A(t-τ)].B.u*R*Sin[τ],
                           {τ,ArcSin[v*t/(2*R)],Pi/2},
                           {x, -R*Sin[τ]+v*t, R*Sin[τ]},
                           {τ,0,t} ] +
               NIntegrate[ MatrixExp[A(t-τ)].B.u*R*Sin[τ],
                           {τ,0,ArcSin[v*t/(2*R)]},
                           {x, -R*Sin[τ], R*Sin[τ]},
                           {τ,t-(x+R*Sin[τ])/v,t} ] +
               NIntegrate[ MatrixExp[A(t-τ)].B.u*R*Sin[τ],
                           {τ,ArcSin[v*t/(2*R)], Pi/2},
                           {x, -R*Sin[τ], -R*Sin[τ]+v*t},
                           {τ,t-(x+R*Sin[τ])/v,t}]         );
ActivT[t_]:= 2/(Pi*R^2) * (
               NIntegrate[ MatrixExp[A (t-τ)].B.u*R*Sin[τ],
                          {τ,0,Pi/2},
                          {x, -R*Sin[τ], R*Sin[τ]},
                          {τ, t-(x+R*Sin[τ])/v,t}  ] );
```

9. Find the countrate vectors:

```
CdotRW = Ψ.Activ;  CdotRWT = Ψ.ActivT;

CdotCW[t_]:= Ψ.Activ[t];   CdotCWT[t_]:= Ψ.ActivT[t];
```

10. If needed, show per-nuclide components algebraically; use these to take derivatives, integrals, limits, etc.

```
CdotRW[[1]]    CdotRW[[2]]    CdotRW[[3]]
```

For example, to find the long-lived activity result for nuclide 1,

```
CdotRWLL[[1]] = Limit[ CdotRW[[1]], λ1 → 0 ];
```

11. To find FF response vector:

```
CdotFF = CdotRW  /. v → 0;
```

12. To find approximate CW response vector:

```
CdotCWapp = CdotRW  /. L → 16 R/(3 Pi);
```

13. To combine the before- and after-T responses:

```
CdotRW1 = CdotRW[[1]]*Boole[t < L/v] + CdotRWT[[1]]*Boole[t ≥ L/v ];
CdotRW2 = CdotRW[[2]]*Boole[t < L/v] + CdotRWT[[2]]*Boole[t ≥ L/v ];
CdotRW3 = CdotRW[[3]]*Boole[t < L/v] + CdotRWT[[3]]*Boole[t ≥ L/v ];
```

14. To use numerical values, e.g., for plotting, and preserve the symbolic solutions, define a parameter list and use the replacement operator:

```
plist = {F→5, Q0→10^-10, k→6.3*10^10, r→0.1,  (etc) };

CdotRWplot = CdotRW  /. plist;
```

If symbolic solutions are not needed at all, then the parameters can be defined at the top of the notebook.

Selected-Application Solutions

This section presents some selected solutions for concentration cases of general interest. The constant-concentration case, while not physically realistic over longer time spans (several hours), is widely used, especially at the design stage, when more complicated dynamic behaviors require many assumptions to define. Results are given for a three-chain, although some expressions are so cumbersome that they are not given here. Algebraic solutions are not always needed; more complicated solutions can be explored graphically or numerically.

This is the *Mathematica* code for the solution; the source (concentration) vector **u** is different in the sections below.

```
B     = IdentityMatrix[3];
A     = { { -λ1, 0, 0 }, { η2 λ2, -λ2, 0 }, { 0, η3 λ3, -λ3 } };
Ψ     = { {ε1 γ1, 0, 0},{0, ε2 γ2, 0},{0, 0, ε3 γ3} };
Activ = 1/L( Integrate[ MatrixExp[A(t-τ)].B.u, {x,0,v*t},{τ,t-x/v,t} ] +
             Integrate[ MatrixExp[A(t-τ)].B.u, {x,v*t,L},{τ,  0,  t} ]   );
ActivT = 1/L Integrate[ MatrixExp[A(t-τ)].B.u, {x,0,L},  {τ,t-x/v,t} ] ;
CdotRW = Ψ.Activ;  CdotRWT = Ψ.ActivT;
```

4.1 First Nuclide, Constant Concentration

```
u     = { {Q1}, {Q2} , {Q3} } * k * F * φ;      (* all 3 constant concentrations *)
```

4.1.1 RW, $t \le L/v$ countrate, any halflife

`CdotRW[[1]];` [1] Eq(23)

$$\dot{C}(t) = \frac{\varepsilon_1 \gamma_1 k F \phi Q_1}{\lambda_1}\left[\left(1-\frac{vt}{L}\right)\left(1-e^{-\lambda_1 t}\right) + \frac{v}{\lambda_1 L}\left(\lambda_1 t - 1 + e^{-\lambda_1 t}\right)\right]$$

4.1.2 RW, $t \ge L/v$ countrate, any halflife

`CdotRWT[[1]];` [1] Eq(25)

$$\dot{C}(t) = \frac{\varepsilon_1 \gamma_1 k F \phi Q_1}{\lambda_1}\left[1 - \frac{v}{\lambda_1 L}\left(1 - e^{-\lambda_1 \frac{L}{v}}\right)\right]$$

4.1.3 RW, $t \le L/v$ countrate, LL

`Limit[ CdotRW[[1]], λ1 → 0 ];` [1] Eq(24)

$$\dot{C}(t) = \varepsilon_1 \gamma_1 k F \phi Q_1\left(t - \frac{vt^2}{2L}\right)$$

4.1.4 RW, $t \ge L/v$ countrate, LL

`Limit[ CdotRWT[[1]], λ1 → 0 ];` [1] Eq(26)

$$\dot{C}(t) = \varepsilon_1 \gamma_1 k F \phi Q_1 \frac{L}{2v}$$

4.1.5 CW, $t \le 2R/v$ countrate, any halflife

[1] Eq(27,33,34,35)

$$Z(a,b) \equiv \int_0^a e^{-\frac{b}{v}2R\sin(\alpha)} R\sin(\alpha)\, d\alpha \qquad \beta \equiv \frac{vt}{2R}$$

This is a nonelementary integral that must be evaluated numerically. Expanding the exponential in a series and integrating term-by-term can yield an acceptable approximation if enough (~10) terms are used. The approach in Section 2.3 is far easier and works well, including for decay-chain progeny.

$$\dot{C}_{CW} = \varepsilon_1 \gamma_1 k F \phi Q_0 \left\{ \begin{array}{l} \dfrac{1 - e^{-\lambda_1 t}}{\lambda_1}\left(1 - \dfrac{2}{\pi}\left[\beta\sqrt{1-\beta^2} + \sin^{-1}(\beta)\right]\right) \\ + \dfrac{2}{\lambda_1^2}\left(\lambda_1 t - 1 + e^{-\lambda_1 t}\right)\left(\dfrac{v}{\pi R}\right)\sqrt{1-\beta^2} \\ + \dfrac{2}{\pi\lambda_1}\left(\begin{array}{l} \sin^{-1}(\beta) - \beta\sqrt{1-\beta^2} \\ + \dfrac{v}{\lambda_1 R}\left(\dfrac{Z\left[\sin^{-1}(\beta), \lambda_1\right]}{R} + \sqrt{1-\beta^2} - 1\right) \end{array}\right) \end{array} \right\}$$

4.1.6 CW, $t \geq 2R/v$ countrate, any halflife [1] Eq(36)

$$\dot{C}_{CW} = \frac{\varepsilon_1 \gamma_1 k F \phi Q_0}{\lambda_1}\left[1 - \frac{2v}{\lambda_1 \pi R} + \frac{2v}{\lambda_1 \pi R^2} Z\left(\frac{\pi}{2}, \lambda_1\right)\right]$$

4.1.7 CW, $t \leq 2R/v$ countrate, LL [1] Eq(39)

$$\dot{C}_{CW} = \varepsilon_1 \gamma_1 k F \phi Q_0 \left\{ \begin{array}{l} t\left(1 - \dfrac{2}{\pi}\left[\beta\sqrt{1-\beta^2} + \sin^{-1}(\beta)\right]\right) \\ + \dfrac{8R}{3\pi v}\left(1 - \sqrt{1-\beta^2}\right) + \dfrac{2vt^2}{3\pi R}\sqrt{1-\beta^2} \end{array} \right\}$$

4.1.8 CW, $t \geq L/v$ countrate, LL [1] Eq(41)

$$\dot{C}_{CW} = \varepsilon_1 \gamma_1 k F \phi Q_0 \frac{8R}{3\pi v}$$

4.1.9 RW, $t \leq L/v$ derivative, any halflife `D[ CdotRW[[1]], t ]`

$$\frac{d\dot{C}}{dt} = \varepsilon_1 \gamma_1 k F \phi Q_1 e^{-\lambda_1 t}\left(1 - \frac{vt}{L}\right)$$

4.1.10 RW, $t \leq L/v$ derivative, LL `Limit[ D[ CdotRW[[1]], t ], λ1 → 0 ]`

$$\frac{d\dot{C}}{dt} = \varepsilon_1 \gamma_1 k F \phi Q_1\left(1 - \frac{vt}{L}\right)$$

4.1.11 RW, $t \leq L/v$ integral, any halflife `Integrate[ CdotRW[[1]], {t,0,ξ} ]`

$$\int_0^{\xi} \dot{C}(t)dt = \frac{\varepsilon_1 \gamma_1 k F \phi Q_1}{\lambda_1^2}\left[\lambda_1 \xi - \left(1 + \frac{v\xi}{L} + e^{-\lambda_1 \xi}\left(\frac{v\xi}{L} - 1\right)\right) + \frac{2v}{\lambda_1 L}\left(1 - e^{-\lambda_1 \xi}\right)\right]$$

4.1.12 RW, $t \le L/v$ integral, LL `Limit[ Integrate[ CdotRW[[1]], {t,0,ξ} ], λ₁ → 0 ]`

$$\int_0^{\xi} \dot{C}(t)dt = \frac{\varepsilon_1 \gamma_1 k F \phi Q_1 \xi^2}{2}\left(1 - \frac{v\xi}{3L}\right)$$

4.1.13 FF countrate, any halflife `CdotRW[[1]] /. v → 0;` [1] Eq(19)

$$\dot{C}(t) = \frac{\varepsilon_1 \gamma_1 k F \phi Q_1}{\lambda_1}\left[1 - e^{-\lambda_1 t}\right]$$

4.1.14 FF countrate, LL `Limit[ CdotRW[[1]] /. v → 0, λ₁ → 0];` [1] Eq(20)

$$\dot{C}(t) = \varepsilon_1 \gamma_1 k F \phi Q_1 t$$

4.1.15 FF derivative, any halflife `D[ CdotRW[[1]] /. v → 0, t ]`

$$\frac{d\dot{C}}{dt} = \varepsilon_1 \gamma_1 k F \phi Q_1 e^{-\lambda_1 t}$$

4.1.16 FF derivative, LL `Limit[ D[ CdotRW[[1]] /. v → 0, t ], λ₁ → 0 ]`

$$\frac{d\dot{C}}{dt} = \varepsilon_1 \gamma_1 k F \phi Q_1$$

4.1.17 FF integral, any halflife (Eberline equation) `Integrate[ CdotRW[[1]] /. v → 0, {t,0,ξ} ]`

$$\int_0^{\xi} \dot{C}(t)dt = \frac{\varepsilon_1 \gamma_1 k F \phi Q_1}{\lambda_1^2}\left[\lambda_1 \xi - \left(1 - e^{-\lambda_1 \xi}\right)\right]$$

4.1.18 FF integral, LL `Limit[ Integrate[ CdotRW[[1]] /. v → 0, {t,0,ξ} ], λ₁ → 0 ]`

$$\int_0^{\xi} \dot{C}(t)dt = \frac{\varepsilon_1 \gamma_1 k F \phi Q_1 \xi^2}{2}$$

4.2 Second Nuclide, Constant Concentration

4.2.1 RW, $t \le L/v$ countrate, any halflife `CdotRW[[2]]`

$$\dot{C}_2(t) = \frac{\varepsilon_2 \gamma_2 k F \phi Q_2}{\lambda_2}\left\{\left(1 - \frac{vt}{L}\right)\left(1 - e^{-\lambda_2 t}\right) + \frac{v}{\lambda_2 L}\left(\lambda_2 t - 1 + e^{-\lambda_2 t}\right)\right\}$$
$$+ \frac{\varepsilon_2 \gamma_2 k F \phi Q_1 \eta_2}{\lambda_2 - \lambda_1}\left\{\begin{array}{l}\left(1 - \frac{vt}{L}\right)\frac{\lambda_2 - \lambda_1}{\lambda_1}\left[1 - \lambda_2 \frac{e^{-\lambda_1 t}}{\lambda_2 - \lambda_1} + \lambda_1 \frac{e^{-\lambda_2 t}}{\lambda_2 - \lambda_1}\right] \\ + \frac{v}{L}\left[\frac{\lambda_2}{\lambda_1^2}\left(\lambda_1 t - 1 + e^{-\lambda_1 t}\right) - \frac{1}{\lambda_2}\left(\lambda_2 t - 1 + e^{-\lambda_2 t}\right)\right]\end{array}\right\}$$

4.2.2 RW, $t \geq L/v$ countrate, any halflife `CdotRWT[[2]]`

$$\dot{C}_2(t) = \frac{\varepsilon_2 \gamma_2 k F \phi Q_2}{\lambda_2}\left[1 - \frac{v}{\lambda_2 L}\left(1 - e^{-\lambda_2 \frac{L}{v}}\right)\right] + \frac{\varepsilon_2 \gamma_2 k F \phi Q_1 \eta_2}{\lambda_1(\lambda_2 - \lambda_1)}\left[\lambda_1\left(\frac{v}{\lambda_2 L}\left(1 - e^{-\lambda_2 \frac{L}{v}}\right) - 1\right) - \lambda_2\left(\frac{v}{\lambda_1 L}\left(1 - e^{-\lambda_1 \frac{L}{v}}\right) - 1\right)\right]$$

4.2.3 RW, $t \leq L/v$ countrate, LL `Limit[ CdotRW[[2]], λ₂ → 0 ]`

$$\dot{C}_2(t) = \varepsilon_2 \gamma_2 k F \phi Q_2\left(t - \frac{v t^2}{2L}\right)$$

4.2.4 RW, $t \geq L/v$ countrate, LL `Limit[ CdotRWT[[2]], λ₂ → 0 ]`

$$\dot{C}_2(t) = \varepsilon_2 \gamma_2 k F \phi Q_2 \frac{L}{2v}$$

4.2.5 FF countrate, any halflife `CdotRW[[2]] /. v → 0`

$$\dot{C}_2(t) = \frac{\varepsilon_2 \gamma_2 k F \phi Q_2}{\lambda_2}\left(1 - e^{-\lambda_2 t}\right) + \frac{\varepsilon_2 \gamma_2 k F \phi Q_1 \eta_2}{\lambda_1}\left(1 - \lambda_2 \frac{e^{-\lambda_1 t}}{\lambda_2 - \lambda_1} + \lambda_1 \frac{e^{-\lambda_2 t}}{\lambda_2 - \lambda_1}\right)$$

4.2.6 FF countrate, LL `Limit[ CdotRW[[2]] /. v → 0, λ₂ → 0 ]`

$$\dot{C}_2(t) = \varepsilon_2 \gamma_2 k F \phi Q_2 t$$

4.2.7 FF, derivative, any halflife `D[ CdotRW[[2]] /. v → 0, t ]`

$$\frac{d\dot{C}_2}{dt} = \varepsilon_2 \gamma_2 k F \phi Q_1 \eta_2 \frac{\lambda_2}{\lambda_2 - \lambda_1}\left[e^{-\lambda_1 t} - e^{-\lambda_2 t}\right] + \varepsilon_2 \gamma_2 k F \phi Q_2 e^{-\lambda_2 t}$$

4.2.8 FF, derivative, LL `Limit[ D[ CdotRW[[2]] /. v → 0, t ], λ₂ → 0 ]`

$$\frac{d\dot{C}_2}{dt} = \varepsilon_2 \gamma_2 k F \phi Q_2$$

4.2.9 FF, integral, LL `Limit[ Integrate[ CdotRW[[2]] /. v → 0, {t,0,ξ} ], λ₂ → 0 ]`

$$\int_0^{\xi} \dot{C}_2(t)\, dt = \varepsilon_2 \gamma_2 k F \phi Q_2 \frac{\xi^2}{2}$$

4.3 Third Nuclide, Constant Concentration

4.3.1 RW, $t \le L/v$ countrate, any halflife

`CdotRW[[3]]`

$$
\begin{aligned}
\dot{C}_3(t) = \quad & \frac{\varepsilon_3 \gamma_3 k F \phi Q_3}{\lambda_3}\left\{ \left(1-\frac{vt}{L}\right)\left(1-e^{-\lambda_3 t}\right) + \frac{v}{\lambda_3 L}\left(\lambda_3 t - 1 + e^{-\lambda_3 t}\right) \right\} \\
& + \frac{\varepsilon_3 \gamma_3 k F \phi Q_2 \eta_3}{\lambda_3-\lambda_2}\left\{ \begin{array}{l} \left(1-\frac{vt}{L}\right)\frac{\lambda_3-\lambda_2}{\lambda_2}\left[1-\lambda_3\frac{e^{-\lambda_2 t}}{\lambda_3-\lambda_2}+\lambda_2\frac{e^{-\lambda_3 t}}{\lambda_3-\lambda_2}\right]+ \\ \frac{v}{L}\left[\frac{\lambda_3}{\lambda_2^2}\left(\lambda_2 t - 1 + e^{-\lambda_2 t}\right) - \frac{1}{\lambda_3}\left(\lambda_3 t - 1 + e^{-\lambda_3 t}\right)\right] \end{array} \right\} \\
& + \frac{\varepsilon_3 \gamma_3 k F \phi Q_1 \eta_2 \eta_3}{(\lambda_1-\lambda_2)(\lambda_1-\lambda_3)}\left\{ \begin{array}{l} \left(1-\frac{vt}{L}\right)\frac{(\lambda_1-\lambda_2)(\lambda_1-\lambda_3)}{\lambda_1}\left[\begin{array}{l} 1+\frac{\lambda_2\lambda_3 e^{-\lambda_1 t}}{(\lambda_1-\lambda_3)(\lambda_2-\lambda_1)} \\ -\frac{\lambda_1\lambda_3 e^{-\lambda_2 t}}{(\lambda_2-\lambda_3)(\lambda_2-\lambda_1)} \\ -\frac{\lambda_1\lambda_2 e^{-\lambda_3 t}}{(\lambda_1-\lambda_3)(\lambda_2-\lambda_3)} \end{array}\right] \\ + \frac{v}{L}\left[\begin{array}{l} t\,\frac{\lambda_3^2(\lambda_1-\lambda_2)+\lambda_3\lambda_2^2}{\lambda_1(\lambda_2-\lambda_3)} - \frac{\lambda_2\lambda_3}{\lambda_1^2}\left(1-e^{-\lambda_1 t}\right) \\ +\frac{\lambda_2^2}{\lambda_3(\lambda_2-\lambda_3)}\left(1-\lambda_3 t - e^{-\lambda_3 t}\right) \\ -\frac{\lambda_3^2}{\lambda_2(\lambda_2-\lambda_3)}\left(1-e^{-\lambda_2 t}\right) \\ -\frac{\lambda_1}{\lambda_2\lambda_3(\lambda_2-\lambda_3)}\left[\begin{array}{l} \lambda_2^2\left(1-\lambda_3 t - e^{-\lambda_3 t}\right) \\ -\lambda_3^2\left(1-\lambda_2 t - e^{-\lambda_2 t}\right) \end{array}\right] \end{array}\right] \end{array} \right\}
\end{aligned}
$$

4.3.2 RW, $t \geq L/v$ countrate, any halflife `CdotRWT[[3]]`

$$\dot{C}_3(t) = \frac{\varepsilon_3 \gamma_3 k F \phi Q_3}{\lambda_3}\left[1 - \frac{v}{\lambda_3 L}\left(1 - e^{-\lambda_3 \frac{L}{v}}\right)\right]$$
$$+ \frac{\varepsilon_3 \gamma_3 k F \phi Q_2 \eta_3}{\lambda_2(\lambda_3 - \lambda_2)}\left[\lambda_2\left(\frac{v}{\lambda_3 L}\left(1 - e^{-\lambda_3 \frac{L}{v}}\right) - 1\right) - \lambda_3\left(\frac{v}{\lambda_2 L}\left(1 - e^{-\lambda_2 \frac{L}{v}}\right) - 1\right)\right]$$
$$+ \frac{\varepsilon_3 \gamma_3 k F \phi Q_1 \eta_2 \eta_3}{\lambda_2 \lambda_3 (\lambda_1 - \lambda_3)(\lambda_1 - \lambda_2)}\left\{\begin{array}{l} \frac{\lambda_2^2 \lambda_3^2}{\lambda_1}\left(1 - \frac{v}{\lambda_1 L}\left[1 - e^{-\lambda_1 \frac{L}{v}}\right]\right) \\ + \frac{\lambda_2^3\left(v\left[1 - e^{-\lambda_3 \frac{L}{v}}\right] - \lambda_3 L\right) - v\lambda_3^3\left(1 - e^{-\lambda_2 \frac{L}{v}}\right) + L\lambda_2\lambda_3^3}{(\lambda_2 - \lambda_3)L} \\ - \lambda_1 \frac{\left(\lambda_2^2 v\left[1 - e^{-\lambda_3 \frac{L}{v}}\right] - \lambda_3 \lambda_2^2 L\right) - v\lambda_3^2\left(1 - e^{-\lambda_2 \frac{L}{v}}\right) + L\lambda_2\lambda_3^2}{(\lambda_2 - \lambda_3)L} \end{array}\right\}$$

4.3.3 RW, $t \leq L/v$ countrate, LL `Limit[ CdotRW[[3]], λ3 → 0 ]`

$$\dot{C}_3(t) = \varepsilon_3 \gamma_3 k F \phi Q_3\left(t - \frac{v t^2}{2L}\right)$$

4.3.4 RW, $t \geq L/v$ countrate, LL `Limit[ CdotRWT[[3]], λ3 → 0 ]`

$$\dot{C}_3(t) = \varepsilon_3 \gamma_3 k F \phi Q_3 \frac{L}{2v}$$

4.3.5 FF countrate, any halflife `CdotRW[[3]] /. v → 0`

$$\dot{C}_3(t) = \frac{\varepsilon_3 \gamma_3 k F \phi Q_3}{\lambda_3}\left(1 - e^{-\lambda_3 t}\right) + \frac{\varepsilon_3 \gamma_3 k F \phi Q_2 \eta_3}{\lambda_2}\left(1 - \lambda_3 \frac{e^{-\lambda_2 t}}{\lambda_3 - \lambda_2} + \lambda_2 \frac{e^{-\lambda_3 t}}{\lambda_3 - \lambda_2}\right)$$
$$+ \frac{\varepsilon_3 \gamma_3 k F \phi Q_1 \eta_2 \eta_3}{\lambda_1}\left[1 + \frac{\lambda_2 \lambda_3 e^{-\lambda_1 t}}{(\lambda_1 - \lambda_3)(\lambda_2 - \lambda_1)} - \frac{\lambda_1 \lambda_3 e^{-\lambda_2 t}}{(\lambda_2 - \lambda_3)(\lambda_2 - \lambda_1)} - \frac{\lambda_1 \lambda_2 e^{-\lambda_3 t}}{(\lambda_1 - \lambda_3)(\lambda_2 - \lambda_3)}\right]$$

4.3.6 FF countrate, LL `Limit[ CdotRW[[3]] /. v → 0, λ3 → 0 ]`

$$\dot{C}_3(t) = \varepsilon_3 \gamma_3 k F \phi Q_3 t$$

4.4 FF, Constant Concentration Long-Term Equilibrium Countrates

It is shown in linear-systems analysis that, for a constant source, a system will reach equilibrium levels that can be calculated without explicitly solving the differential equation system. See Ref[3]. The system matrix **A** in effect is for the isotopic transitions on a FF.

```
u     = { {Q1}, {Q2} , {Q3} } * k * F * φ;       (* all 3 constant concentrations *)
        Ψ.(-Inverse[A].B.u)
```

$$\dot{\mathbf{C}}(t \to \infty) = \mathbf{\Psi}\left(-\mathbf{A}^{-1}\,\mathbf{B}\,\mathbf{u}\right) = \begin{pmatrix} \dfrac{\varepsilon_1 \gamma_1 Q_1}{\lambda_1} \\ \dfrac{\varepsilon_2 \gamma_2 Q_2}{\lambda_2} + \dfrac{\varepsilon_2 \gamma_2 Q_1 \eta_2}{\lambda_1} \\ \dfrac{\varepsilon_3 \gamma_3 Q_3}{\lambda_3} + \dfrac{\varepsilon_3 \gamma_3 Q_2 \eta_3}{\lambda_2} + \dfrac{\varepsilon_3 \gamma_3 Q_1 \eta_2 \eta_3}{\lambda_1} \end{pmatrix} k\,F\,\phi$$

4.5 First Nuclide, Single-Exponential Pulse Concentration

A single exponential "pulse" concentration can model events such as a sudden relief-valve lifting, or a pipe break, etc. The concentration rises very quickly, and then tails off exponentially, usually due to HVAC dilution in a compartment. Here, in this model, the concentration rises instantaneously, which of course would not happen in a monitored compartment unless the sampling point happened to be very close to the release point. Note that the time *t* here is *measured from the start of the release*; this reduces the clutter in the equations that would be needed to write them in terms of a time offset from an arbitrary zero time.

```
u = { {Q0*Exp[-r*τ]}, {0} , {0} } * k * F * φ;       (* only first nuclide source *)
```

4.5.1 RW, $t \le L / v$, countrate, any halflife

`CdotRW[[1]]`

$$\dot{C}(t) = \varepsilon_1 \gamma_1 k\,F\,\phi\,Q_0 \left\{ \begin{array}{c} \left(1 - \dfrac{v\,t}{L}\right)\dfrac{1}{\lambda_1 - r}\left(e^{-r t} - e^{-\lambda_1 t}\right) \\ + \dfrac{v}{L\left(\lambda_1 - r\right)^2}\left[e^{-r t}\left(t\left(\lambda_1 - r\right) - 1\right) + e^{-\lambda_1 t}\right] \end{array} \right\}$$

4.5.2 RW, $t \ge L / v$, countrate, any halflife

`CdotRWT[[1]]`

$$\dot{C}(t) = \frac{\varepsilon_1 \gamma_1 k\,F\,\phi\,Q_0\,e^{-r t}}{\left(\lambda_1 - r\right)^2}\left[\left(\lambda_1 - r\right) - \frac{v}{L}\left(1 - e^{\left(r - \lambda_1\right)\frac{L}{v}}\right)\right]$$

4.5.3 RW, $t \le L / v$, countrate, LL

`Limit[ CdotRW[[1]], λ1 → 0 ]`

$$\dot{C}(t) = \frac{\varepsilon_1 \gamma_1 k\,F\,\phi\,Q_0}{r}\left[\left(1 + \frac{v}{r\,L}\right)\left(1 - e^{-r t}\right) - \frac{v\,t}{L}\right]$$

4.5.4 RW, $t \geq L/v$, countrate, LL `Limit[ CdotRWT[[1]], λ1 → 0 ]`

$$\dot{C}(t) = \frac{\varepsilon_1 \gamma_1 k F \phi Q_0 e^{-rt}}{r}\left[\frac{v}{rL}\left(e^{r\frac{L}{v}} - 1\right) - 1\right]$$

4.5.5 FF countrate, any halflife `CdotRW[[1]] /. v → 0`

$$\dot{C}(t) = \varepsilon_1 \gamma_1 k F \phi Q_0 \left\{\frac{1}{\lambda_1 - r}\left(e^{-rt} - e^{-\lambda_1 t}\right)\right\}$$

4.5.6 FF countrate, LL `Limit[ CdotRW[[1]] /. v → 0, λ1 → 0 ]`

$$\dot{C}(t) = \frac{\varepsilon_1 \gamma_1 k F \phi Q_0}{r}\left[1 - e^{-rt}\right]$$

4.6 Second Nuclide, Single-Exponential Pulse Concentration

4.6.1 RW, $t \leq L/v$, countrate `CdotRW[[2]]`

$$\dot{C}_2 = \varepsilon_2 \gamma_2 k F \phi \eta_2 \lambda_2 Q_0 \left\{\begin{array}{l} \left(1 - \dfrac{vt}{L}\right)\left[\begin{array}{c} \dfrac{e^{-rt}}{(r-\lambda_1)(r-\lambda_2)} + \dfrac{e^{-\lambda_1 t}}{(r-\lambda_1)(\lambda_2-\lambda_1)} \\ - \dfrac{e^{-\lambda_2 t}}{(r-\lambda_2)(\lambda_2-\lambda_1)} \end{array}\right] \\ + \dfrac{v e^{-rt}}{L(\lambda_1-\lambda_2)}\left(\begin{array}{c} \dfrac{1 + rt - \lambda_1 t - e^{-\lambda_1 t}}{(r-\lambda_1)^2} \\ - \dfrac{1 + rt - \lambda_2 t - e^{-\lambda_2 t}}{(r-\lambda_2)^2} \end{array}\right) \end{array}\right\}$$

4.6.2 RW, $t \geq L/v$, countrate `CdotRWT[[2]]`

$$\dot{C}_2 = \frac{\varepsilon_2 \gamma_2 k F \phi \eta_2 \lambda_2 Q_0}{L(\lambda_1 - \lambda_2)}\left\{\begin{array}{c} \dfrac{v\left(1 - e^{\frac{L}{v}(r-\lambda_1)}\right) + L(r-\lambda_1)}{(r-\lambda_1)^2} \\ - \dfrac{v\left(1 - e^{\frac{L}{v}(r-\lambda_2)}\right) + L(r-\lambda_2)}{(r-\lambda_2)^2} \end{array}\right\}$$

4.6.3 FF, countrate `CdotRW[[2]] /. v → 0`

$$\dot{C}_2 = \varepsilon_2\,\gamma_2\,k\,F\,\phi\,\eta_2\,\lambda_2\,Q_0\left\{\frac{e^{-rt}}{(r-\lambda_1)(r-\lambda_2)}+\frac{e^{-\lambda_1 t}}{(r-\lambda_1)(\lambda_2-\lambda_1)}-\frac{e^{-\lambda_2 t}}{(r-\lambda_2)(\lambda_2-\lambda_1)}\right\}$$

4.7 First Nuclide, Three-Exponential Concentration

This concentration case is general; it covers a variety of possible behaviors just by changing parameters, rather than needing separate solutions. It was used in Ref[1] and so is included here. Note that the single-exponential case is included in these solutions, by using i = 3,3 in the summations. Thus there are correspondences to the solutions in section 4.5: 4.7.1, 4.5.1; 4.7.2, 4.5.5; 4.7.3, 4.5.3; 4.7.4, 4.5.6; 4.7.5, 4.5.2; 4.7.6, 4.5.4.

```
u = { {S /(r₂ - r₁)*( Exp[-r₁ τ]- Exp[-r₂ τ] ) + Q0 * Exp[-r₃ τ] },
                                                {0} , {0} } * k * F * φ;

B = IdentityMatrix[3];

A = { { -λ₁, 0, 0 }, { η₂ λ₂, -λ₂, 0 }, { 0, η₃ λ₃, -λ₃ } };

Ψ = { {ε₁ γ₁, 0, 0},{0, ε₂ γ₂, 0},{0, 0, ε₃ γ₃} };

Activ = 1/L( Integrate[ MatrixExp[A(t-τ)].B.u, {x,0,v*t},{τ,t-x/v,t} ] +
             Integrate[ MatrixExp[A(t-τ)].B.u, {x,v*t,L},{τ,  0,  t} ]   );

ActivT = 1/L Integrate[ MatrixExp[A(t-τ)].B.u, {x,0,L},  {τ,t-x/v,t} ] ;

CdotRW = Ψ.Activ;  CdotRWT = Ψ.ActivT;
```

4.7.1 RW, $t \le L/v$ countrate, any halflife `CdotRW[[1]];` [1] Eq(21)

$$\dot{C}_{RW} = \varepsilon_1\,\gamma_1\,k\,F\,\phi\sum_{i=1}^{3}\left\{\begin{array}{l}\dfrac{\Gamma_i}{(\lambda_1+\omega_i)^2}\dfrac{v}{L}\left[e^{\omega_i t}\left(t\left(\lambda_1+\omega_i\right)-1\right)+e^{-\lambda_1 t}\right]\\ +\dfrac{\Gamma_i}{\lambda_1+\omega_i}\left(1-\dfrac{vt}{L}\right)\left(e^{\omega_i t}-e^{-\lambda_1 t}\right)\end{array}\right\}$$

$$\Gamma_1 \equiv \frac{S}{r_2-r_1} \qquad \Gamma_2 \equiv \frac{-S}{r_2-r_1} \qquad \Gamma_3 \equiv Q_0 \qquad \omega_{1,2,3} \equiv -r_{1,2,3}$$

4.7.2 RW, $t \ge L/v$ countrate, any halflife `CdotRWT[[1]];` [1] Eq(22)

$$\dot{C}_{RW} = \varepsilon_1\,\gamma_1\,k\,F\,\phi\sum_{i=1}^{3}\left\{\frac{\Gamma_i}{(\lambda_1+\omega_i)^2}\left[\begin{array}{l}e^{\omega_i t}\left(\lambda_1+\omega_i-\dfrac{v}{L}\right)\\ +\dfrac{v}{L}e^{\omega_i\left(t-\frac{L}{v}\right)-\lambda_1\frac{L}{v}}\end{array}\right]\right\}$$

4.7.3 RW, $t \le L/v$ countrate, LL `CdotRW[[1]] /. λ1 → 0`

$$\dot{C}_{RW} = \varepsilon_1 \gamma_1 k F \phi \sum_{i=1}^{3} \left\{ \begin{array}{l} \dfrac{\Gamma_i}{\omega_i^2} \dfrac{v}{L} \left[e^{\omega_i t} \left(t\,\omega_i - 1 \right) + 1 \right] \\ + \dfrac{\Gamma_i}{\omega_i} \left(1 - \dfrac{v\,t}{L} \right) \left(e^{\omega_i t} - 1 \right) \end{array} \right\}$$

4.7.4 RW, $t \ge L/v$ countrate, LL `CdotRWT[[1]] /. λ1 → 0`

$$\dot{C}_{RW} = \varepsilon_1 \gamma_1 k F \phi \sum_{i=1}^{3} \frac{\Gamma_i}{\omega_i^2} \left[e^{\omega_i t} \left(\omega_i - \frac{v}{L} \right) + \frac{v}{L} e^{\omega_i \left(t - \frac{L}{v} \right)} \right]$$

4.7.5 FF countrate, any halflife `CdotRW[[1]] /. v → 0;` [1] Eq(18)

$$\dot{C}_{RW} = \varepsilon_1 \gamma_1 k F \phi \sum_{i=1}^{3} \left\{ \frac{\Gamma_i}{\lambda_1 + \omega_i} \left(e^{\omega_i t} - e^{-\lambda_1 t} \right) \right\}$$

4.7.6 FF countrate, LL `CdotRW[[1]] /. {v → 0, λ1 → 0}`

$$\dot{C}_{RW} = \varepsilon_1 \gamma_1 k F \phi \sum_{i=1}^{3} \left\{ \frac{\Gamma_i}{\omega_i} \left(e^{\omega_i t} - 1 \right) \right\}$$

4.7.7 CW $t \le 2R/v$ countrate, any halflife [1] Eq(28,29,30)

$$\dot{C}_{CW} = \varepsilon_1 \gamma_1 k F \phi \sum_{i=1}^{3} \left\{ \begin{array}{l} \dfrac{\Gamma_i}{\lambda_1 + \omega_i} \left(e^{\omega_i t} - e^{-\lambda_1 t} \right) \left(1 - \dfrac{2}{\pi} \left[\beta \sqrt{1 - \beta^2} + \sin^{-1}(\beta) \right] \right) \\ + \dfrac{2\Gamma_i}{\left(\lambda_1 + \omega_i \right)^2} \left(e^{-\lambda_1 t} + e^{\omega_i t} \left[t \left(\lambda_1 + \omega_i \right) - 1 \right] \right) \dfrac{v}{\pi R} \sqrt{1 - \beta^2} \\ + \dfrac{2\Gamma_i}{\lambda_1 + \omega_i} \dfrac{e^{\omega_i t}}{\pi} \left\{ \begin{array}{l} \sin^{-1}(\beta) - \beta \sqrt{1 - \beta^2} \\ + \dfrac{v}{R \left(\lambda_1 + \omega_i \right)} \left(\dfrac{Z\left(\sin^{-1}(\beta), \left(\lambda_1 + \omega_i \right) \right)}{R} + \sqrt{1 - \beta^2} - 1 \right) \end{array} \right. \end{array} \right\}$$

4.7.8 CW $t \ge 2R/v$ countrate, any halflife [1] Eq(32)

$$\dot{C}_{CW} = \varepsilon_1 \gamma_1 k F \phi \sum_{i=1}^{3} \frac{\Gamma_i e^{\omega_i t}}{\lambda_1 + \omega_i} \left\{ \begin{array}{l} 1 - \dfrac{2v}{\pi R \left(\lambda_1 + \omega_i \right)} \\ + \dfrac{2v}{\pi R^2 \left(\lambda_1 + \omega_i \right)} Z\left(\dfrac{\pi}{2}, \left(\lambda_1 + \omega_i \right) \right) \end{array} \right\}$$

4.8 Kr – Rb in Containment, Rb Monitored

This is the Reg Guide 1.45 situation- a leak of ^{88}Kr into containment, at some leakage rate, with some primary coolant concentration. The ^{88}Kr decays to ^{88}Rb in the air, and no ^{88}Rb is directly released. The first step is to find the dynamic behavior of the containment ^{88}Rb for this situation; then that is used to "drive" the RW monitor. Linear systems modeling is used for the concentration dynamics. Laplace transforms could be used to find the FF response, but it will be contained in the RW response.

Rb_{eff} is the "effective" removal rate for ^{88}Rb, including decay, plateout, and filtration. S_{Kr} is the source term of ^{88}Kr; the leak rate times the coolant concentration times the partition factor. The Q_{Rb} found is then the $\mathbf{u}(\tau)$ for the RW $t \le L / v$ countrate solution (this assumes no countrate contribution from the Kr). If there is no Rb loss other than decay, a separate solution is required. The matrix exponential solution will find this directly; the **A** matrix will be different for this case but the rest of the solution steps are the same.

```
        (* ------------ this is the concentration solution ------------- *)
(* SKr = leakrate * partition * coolant conc; V = containment volume *)
uQ = { {SKr}, {0} } / V;
BQ = IdentityMatrix[2];
AQ = { { -λKr, 0 }, { λRb, -λRbeff } };                    (* Rbeff is sum of Rb losses *)
AQ = { { -λKr, 0 }, { λRb, -λRb } };                             (* for decay-only case *)
Q  = Integrate[ MatrixExp[AQ(τ-κ)].BQ.uQ, {κ,0,τ} ];          (* conc vector; Kr, Rb *)
```

```
       (*  -------------- this is the countrate solution --------------- *)
u = { {Q[[2]]} } * k * F * φ;                        (* single-nuclide solutions (Rb88) *)
B = IdentityMatrix[1];                             (* don't really need matrix soln here *)
A = { { -λRb} };  Ψ = { {εRb γRb } };
Activ = 1/L( Integrate[ MatrixExp[A(t-τ)].B.u, {x,0,v*t},{τ,t-x/v,t} ] +
             Integrate[ MatrixExp[A(t-τ)].B.u, {x,v*t,L},{τ,  0,  t} ]  );
ActivT = 1/L Integrate[ MatrixExp[A(t-τ)].B.u, {x,0,L},  {τ,t-x/v,t} ] ;
CdotRW = Ψ.Activ;  CdotRWT = Ψ.ActivT;
```

4.8.1 Containment Concentrations

`Q[[1]]` `Q[[2]]`

$$Q_{Kr} = \frac{S_{Kr}}{\lambda_{Kr} V}\left(1 - e^{-\lambda_{Kr}\tau}\right) \qquad Q_{Rb} = \frac{\lambda_{Rb} S_{Kr}}{\left(\lambda_{Rb_{eff}} - \lambda_{Kr}\right) V}\left[\frac{1}{\lambda_{Kr}}\left(1 - e^{-\lambda_{Kr}\tau}\right) - \frac{1}{\lambda_{Rb_{eff}}}\left(1 - e^{-\lambda_{Rb_{eff}}\tau}\right)\right]$$

4.8.2 RW, $t \le T$, ^{88}Rb countrate from ^{88}Kr (only) source

`CdotRW[[1]]`

$$\dot{C}_{Rb}(t) = \frac{\varepsilon_{Rb}\,\gamma_{Rb}\,k\,F\,\phi\,S_{Kr}}{V}\left[\left(1-\frac{v\,t}{L}\right)\left\{\frac{1}{\lambda_{Kr}\lambda_{Rb_{eff}}}-\frac{\lambda_{Rb}e^{-\lambda_{Rb_{eff}}t}}{\lambda_{Rb_{eff}}\left(\lambda_{Kr}-\lambda_{Rb_{eff}}\right)\left(\lambda_{Rb}-\lambda_{Rb_{eff}}\right)}+\frac{e^{-\lambda_{Rb}t}}{\left(\lambda_{Kr}-\lambda_{Rb}\right)\left(\lambda_{Rb}-\lambda_{Rb_{eff}}\right)}-\frac{\lambda_{Rb}e^{-\lambda_{Kr}t}}{\lambda_{Kr}\left(\lambda_{Kr}-\lambda_{Rb}\right)\left(\lambda_{Kr}-\lambda_{Rb_{eff}}\right)}\right\}+\frac{v}{\lambda_{Rb}L}\left\{\frac{t\lambda_{Rb}-1}{\lambda_{Kr}\lambda_{Rb_{eff}}}+\frac{\lambda_{Rb}^2\left(t\left(\lambda_{Rb}-\lambda_{Kr}\right)-1\right)e^{-\lambda_{Kr}t}}{\lambda_{Kr}\left(\lambda_{Kr}-\lambda_{Rb}\right)^2\left(\lambda_{Kr}-\lambda_{Rb_{eff}}\right)}+\frac{\lambda_{Rb}^2\left(t\left(\lambda_{Rb}-\lambda_{Rb_{eff}}\right)-1\right)e^{-\lambda_{Rb_{eff}}t}}{\lambda_{Rb_{eff}}\left(\lambda_{Rb}-\lambda_{Rb_{eff}}\right)^2\left(\lambda_{Rb_{eff}}-\lambda_{Kr}\right)}+\frac{\left(\lambda_{Kr}\left(\lambda_{Rb_{eff}}-2\lambda_{Rb}\right)+\lambda_{Rb}\left(3\lambda_{Rb}-2\lambda_{Rb_{eff}}\right)\right)e^{-\lambda_{Rb}t}}{\left(\lambda_{Kr}-\lambda_{Rb}\right)^2\left(\lambda_{Rb}-\lambda_{Rb_{eff}}\right)^2}\right\}\right]$$

4.8.3 RW, $t \ge T$, ^{88}Rb countrate from ^{88}Kr (only) source

`CdotRWT[[1]]`

$$\dot{C}_{Rb}(t) = \frac{\varepsilon_{Rb}\,\gamma_{Rb}\,k\,F\,\phi\,S_{Kr}}{LV}\left\{\frac{v\,e^{-\lambda_{Rb}\frac{L}{v}}}{\lambda_{Kr}\,\lambda_{Rb}\,\lambda_{Rb_{eff}}}+\frac{\lambda_{Rb}L-v}{\lambda_{Kr}\,\lambda_{Rb}\,\lambda_{Rb_{eff}}}-\frac{\lambda_{Rb}\left(v+L\left(\lambda_{Rb_{eff}}-\lambda_{Rb}\right)\right)e^{-\lambda_{Rb_{eff}}t}}{\lambda_{Rb_{eff}}\left(\lambda_{Rb_{eff}}-\lambda_{Kr}\right)\left(\lambda_{Rb}-\lambda_{Rb_{eff}}\right)^2}-\frac{\lambda_{Rb}\left(v+L\left(\lambda_{Kr}-\lambda_{Rb}\right)\right)e^{-\lambda_{Kr}t}}{\lambda_{Kr}\left(\lambda_{Kr}-\lambda_{Rb_{eff}}\right)\left(\lambda_{Kr}-\lambda_{Rb}\right)^2}+\frac{v\lambda_{Rb}\,e^{-\lambda_{Kr}\left(t-\frac{L}{v}\right)-\lambda_{Rb}\frac{L}{v}}}{\lambda_{Kr}\left(\lambda_{Kr}-\lambda_{Rb_{eff}}\right)\left(\lambda_{Kr}-\lambda_{Rb}\right)^2}+\frac{v\lambda_{Rb}\,e^{-\lambda_{Rb_{eff}}\left(t-\frac{L}{v}\right)-\lambda_{Rb}\frac{L}{v}}}{\lambda_{Rb_{eff}}\left(\lambda_{Rb_{eff}}-\lambda_{Kr}\right)\left(\lambda_{Rb}-\lambda_{Rb_{eff}}\right)^2}\right\}$$

4.8.4 FF; ^{88}Rb countrate from ^{88}Kr (only) source[1]

`CdotRW[[1]] /. v → 0`

$$\dot{C}_{Rb}(t) = \frac{\varepsilon_{Rb}\,\gamma_{Rb}\,k\,F\,\phi\,S_{Kr}}{V}\left\{\begin{array}{l}\dfrac{1}{\lambda_{Kr}\lambda_{Rb_{eff}}} - \dfrac{\lambda_{Rb}e^{-\lambda_{Rb_{eff}}t}}{\lambda_{Rb_{eff}}\left(\lambda_{Kr}-\lambda_{Rb_{eff}}\right)\left(\lambda_{Rb}-\lambda_{Rb_{eff}}\right)} + \\ \dfrac{e^{-\lambda_{Rb}t}}{\left(\lambda_{Kr}-\lambda_{Rb}\right)\left(\lambda_{Rb}-\lambda_{Rb_{eff}}\right)} - \dfrac{\lambda_{Rb}e^{-\lambda_{Kr}t}}{\lambda_{Kr}\left(\lambda_{Kr}-\lambda_{Rb}\right)\left(\lambda_{Kr}-\lambda_{Rb_{eff}}\right)}\end{array}\right\}$$

4.8.5 RW, $t \le T$, ^{88}Rb countrate from ^{88}Kr (only) source; Rb Decay-Only Case

`CdotRW[[1]]`

$$\dot{C}_{Rb}(t) = \frac{\varepsilon_{Rb}\,\gamma_{Rb}\,k\,F\,\phi\,S_{Kr}}{V}\left\{\begin{array}{l}\left(1-\dfrac{v\,t}{L}\right)\left[\begin{array}{l}\dfrac{1}{\lambda_{Kr}\,\lambda_{Rb}} - \dfrac{\lambda_{Rb}\,e^{-\lambda_{Kr}t}}{\lambda_{Kr}\left(\lambda_{Kr}-\lambda_{Rb}\right)^2} \\ - \dfrac{t\,e^{-\lambda_{Rb}t}}{\left(\lambda_{Kr}-\lambda_{Rb}\right)} + \dfrac{\left(2\lambda_{Rb}-\lambda_{Kr}\right)e^{-\lambda_{Rb}t}}{\lambda_{Rb}\left(\lambda_{Kr}-\lambda_{Rb}\right)^2}\end{array}\right] \\ + \dfrac{v}{L}\left[\begin{array}{l}\dfrac{t^2e^{-\lambda_{Rb}t}}{2\left(\lambda_{Rb}-\lambda_{Kr}\right)} + \dfrac{t}{\lambda_{Kr}\,\lambda_{Rb}} - \dfrac{\left(1-e^{-\lambda_{Rb}t}\right)}{\lambda_{Kr}\lambda_{Rb}^2} \\ - \dfrac{t\lambda_{Rb}\,e^{-\lambda_{Kr}t}}{\lambda_{Kr}\left(\lambda_{Kr}-\lambda_{Rb}\right)^2} + \dfrac{\lambda_{Rb}\left(e^{-\lambda_{Rb}t}-e^{-\lambda_{Kr}t}\right)}{\lambda_{Kr}\left(\lambda_{Kr}-\lambda_{Rb}\right)^3}\end{array}\right]\end{array}\right\}$$

4.8.6 RW, $t \ge T$, ^{88}Rb countrate from ^{88}Kr (only) source; Rb Decay-Only Case

`CdotRWT[[1]]`

$$\dot{C}_{Rb}(t) = \frac{\varepsilon_{Rb}\,\gamma_{Rb}\,k\,F\,\phi\,S_{Kr}}{V}\left\{\begin{array}{l}\dfrac{1}{\lambda_{Kr}\,\lambda_{Rb}} + \dfrac{L\,e^{-\lambda_{Rb}t}}{2v\left(\lambda_{Rb}-\lambda_{Kr}\right)} - \dfrac{\lambda_{Rb}\,e^{-\lambda_{Kr}t}}{\lambda_{Kr}\left(\lambda_{Kr}-\lambda_{Rb}\right)^2} \\ - \dfrac{v}{L\,\lambda_{Kr}\,\lambda_{Rb}^2}\left(1-e^{-\lambda_{Rb}\frac{L}{v}}\right) \\ - \dfrac{v\,\lambda_{Rb}\,e^{-\lambda_{Kr}t}}{L\,\lambda_{Kr}\left(\lambda_{Kr}-\lambda_{Rb}\right)^3}\left[1 - e^{\left(\lambda_{Kr}-\lambda_{Rb}\right)\frac{L}{v}}\right]\end{array}\right\}$$

4.8.7 FF; ^{88}Rb countrate from ^{88}Kr (only) source, Rb Decay-Only Case

`CdotRW[[1]] /. v → 0`

$$\dot{C}_{Rb}(t) = \frac{\varepsilon_{Rb}\,\gamma_{Rb}\,k\,F\,\phi\,S_{Kr}}{V}\left\{\frac{1}{\lambda_{Kr}\,\lambda_{Rb}} - \frac{\lambda_{Rb}\,e^{-\lambda_{Kr}t}}{\lambda_{Kr}\left(\lambda_{Kr}-\lambda_{Rb}\right)^2} - \frac{t\,e^{-\lambda_{Rb}t}}{\left(\lambda_{Kr}-\lambda_{Rb}\right)} + \frac{\left(2\lambda_{Rb}-\lambda_{Kr}\right)e^{-\lambda_{Rb}t}}{\lambda_{Rb}\left(\lambda_{Kr}-\lambda_{Rb}\right)^2}\right\}$$

[1] This result was reported in [4].

4.8.8 Long-term equilibrium: Containment Concentrations

$$Q_{Kr}(t \to \infty) = \frac{S_{Kr}}{\lambda_{Kr} V} \qquad Q_{Rb}(t \to \infty) = \frac{\lambda_{Rb} S_{Kr}}{\lambda_{Kr} \lambda_{Rb_{eff}} V}$$

4.8.9 Long-term equilibrium: FF countrate

$$\dot{C}_{Rb}(t \to \infty) = \frac{\varepsilon_{Rb} \gamma_{Rb} k F \phi S_{Kr}}{\lambda_{Kr} \lambda_{Rb_{eff}} V} = \frac{\varepsilon_{Rb} \gamma_{Rb} k F \phi}{\lambda_{Rb}} Q_{Rb}(t \to \infty)$$

4.8.10 Long-term equilibrium: RW countrate

$$\dot{C}_{Rb}(t \to \infty) = \frac{\varepsilon_{Rb} \gamma_{Rb} k F \phi S_{Kr}}{\lambda_{Kr} \lambda_{Rb_{eff}} V} \left(1 - \frac{v}{\lambda_{Rb} L} \left[1 - e^{-\lambda_{Rb} \frac{L}{v}} \right] \right)$$

4.8.11 Long-term equilibrium: Containment Concentrations, Decay-Only Case

$$Q_{Kr}(t \to \infty) = \frac{S_{Kr}}{\lambda_{Kr} V} \qquad Q_{Rb}(t \to \infty) = \frac{S_{Kr}}{\lambda_{Kr} V}$$

4.8.12 Long-term equilibrium: FF countrate, Decay-Only Case

$$\dot{C}_{Rb}(t \to \infty) = \frac{\varepsilon_{Rb} \gamma_{Rb} k F \phi S_{Kr}}{\lambda_{Kr} \lambda_{Rb} V} = \frac{\varepsilon_{Rb} \gamma_{Rb} k F \phi}{\lambda_{Rb}} Q_{Rb}(t \to \infty)$$

4.8.13 Long-term equilibrium: RW countrate, Decay-Only Case

$$\dot{C}_{Rb}(t \to \infty) = \frac{\varepsilon_{Rb} \gamma_{Rb} k F \phi S_{Kr}}{\lambda_{Kr} \lambda_{Rb} V} \left(1 - \frac{v}{\lambda_{Rb} L} \left[1 - e^{-\lambda_{Rb} \frac{L}{v}} \right] \right)$$

These results are obtained by taking limits of the respective solutions for each case; for RW, use the $t \geq T$ solutions.

Quantitative Methods

These are some selected methods of "inverting" a response model, or quantities derived from such models, to solve for an estimate of the input concentration. Some of these methods were reported in Ref[2].

5.1 Fixed-Filter

5.1.1 FF Concentration, Initial Slope [2] Eq(7)

$$\hat{Q}(0) = \frac{1}{\varepsilon \gamma k F \phi} \left. \frac{d\dot{C}_{FF}}{dt} \right|_{t \approx 0}$$

5.1.2 FF, Concentration, Countrate and Derivative [2] Eq(5)

$$\hat{Q}(t) = \frac{1}{\varepsilon \gamma k F \phi}\left[\left.\frac{d\dot{C}_{FF}}{dt}\right|_t + \lambda \dot{C}_{FF}(t) \right]$$

5.1.3 FF, Constant Concentration, Derivative from 4.1.15

$$\hat{Q}_0 = \frac{\left.\frac{d\dot{C}_{FF}}{dt}\right|_t}{\varepsilon \gamma k F \phi e^{-\lambda t}}$$

5.1.4 FF, Constant Concentration, Countrate from 4.1.13

$$\hat{Q}_0 = \frac{\lambda \dot{C}_{FF}(t)}{\varepsilon \gamma k F \phi \left(1 - e^{-\lambda t}\right)}$$

5.1.5 FF, Constant Concentration, LL Countrate from 4.1.14

$$\hat{Q}_0 = \frac{\dot{C}_{FF}(t)}{\varepsilon \gamma k F \phi\, t}$$

5.1.6 FF, Constant Concentration, Counts (Eberline equation) [2] Eq(30); from 4.1.17

$$\hat{Q}_0 = \frac{\lambda^2 \int_0^{\xi} \dot{C}_{FF}(t)\, dt}{\varepsilon \gamma k F \phi \left[\lambda \xi - \left(1 - e^{-\lambda \xi}\right)\right]}$$

5.1.7 FF, Constant Concentration, LL Counts [2] Eq(31); from 4.1.18

$$\hat{Q}_0 = \frac{2 \int_0^{\xi} \dot{C}_{FF}(t)\, dt}{\varepsilon \gamma k F \phi \xi^2}$$

5.1.8 FF, Release, Counts and Countrate (Rb88 Method) [2] Eq(18)

$$R(\xi) = \frac{F_{stack}}{\varepsilon \gamma k F \phi}\left[\dot{C}_{FF}(\xi) + \lambda \int_0^{\xi} \dot{C}_{FF}(t)\, dt \right]$$

5.1.9 FF, Average Concentration, Counts and Countrate [2] Eq(22)

$$\bar{Q}(\xi) = \frac{1}{\varepsilon \gamma k F \phi \xi}\left\{ \left[\dot{C}_{FF}(\xi) - \dot{C}_{FF}(0) \right] + \lambda \int_0^{\xi} \dot{C}_{FF}(t)\, dt \right\}$$

5.2 Rectangular Window Moving Filter

5.2.1 RW Concentration, Initial Slope

[2] Eq(7)

$$\hat{Q}(0) = \frac{1}{\varepsilon \gamma k F \phi} \left. \frac{d\dot{C}_{RW}}{dt} \right|_{t \approx 0}$$

5.2.2 RW, Constant Concentration, Derivative

from 4.1.9

$$\hat{Q}_0 = \frac{\left. \frac{d\dot{C}_{RW}}{dt} \right|_t}{\varepsilon \gamma k F \phi e^{-\lambda t} \left(1 - \frac{vt}{L} \right)}; \quad t \le \frac{L}{v}$$

5.2.3 RW, Constant Concentration, Countrate

from 4.1.1

$$\hat{Q}_0 = \frac{\lambda^2 \dot{C}_{RW} \left(t \le \frac{L}{v} \right)}{\varepsilon \gamma k F \phi \left\{ \frac{v}{L} \left[\lambda t - 1 + e^{-\lambda t} \right] + \lambda \left(1 - \frac{vt}{L} \right) \left(1 - e^{-\lambda t} \right) \right\}}$$

5.2.4 RW, Constant Concentration, LL Countrate

from 4.1.3

$$\hat{Q}_0 = \frac{\dot{C}_{RW} \left(t \le \frac{L}{v} \right)}{\varepsilon \gamma k F \phi \left(t - \frac{vt^2}{2L} \right)}$$

5.2.5 RW, Constant Concentration, Limiting Countrate

from 4.1.2

$$\hat{Q}_0 = \frac{\dot{C}_{RW}(t \ge L/v)}{\varepsilon \gamma k F \phi \left[\frac{1}{\lambda} - \frac{v}{\lambda^2 L} \left(1 - e^{-\lambda \frac{L}{v}} \right) \right]}$$

5.2.6 RW, Constant Concentration, Limiting LL Countrate

from 4.1.4

$$\hat{Q}_0 = \frac{2v \dot{C}_{RW}(t \ge L/v)}{\varepsilon \gamma k F \phi L}$$

5.2.7 RW, Constant Concentration, Counts

from 4.1.11

$$\hat{Q}_0 = \frac{\lambda^2 \int_0^{\xi} \dot{C}_{RW}(t)\, dt}{\varepsilon \gamma k F \phi \left[\lambda \xi - \left(1 + \frac{v\xi}{L} + e^{-\lambda \xi} \left(\frac{v\xi}{L} - 1 \right) \right) + \frac{2v}{\lambda L} \left(1 - e^{\lambda \xi} \right) \right]}; \quad \xi \le \frac{L}{v}$$

5.2.8 RW, Constant Concentration, LL Counts from 4.1.12

$$\hat{Q}_0 = \frac{2\int_0^{\xi} \dot{C}_{RW}(t)\,dt}{\varepsilon\,\gamma\,k\,F\,\phi\,\xi^2\left(1-\frac{v\,\xi}{3L}\right)};\ \xi \le \frac{L}{v}$$

5.3 Rectangular or Circular Window Moving Filter; Fast Filter Speed

It can be demonstrated that if the filter speed is increased to, e.g., 30 inches/hr, the CW/RW monitor countrate will nearly track the concentration dynamic behavior. Taking the concentrations for the three nuclides in a chain to be simple exponentials, it can be shown that a Taylor series expansion to third order in the filter speed v about infinity, or in effect, in the reciprocal of v about zero, gives for the approximate $t \ge T$ RW countrates

$$\dot{C}_1(t) \approx \frac{Q_1 e^{-r_1 t}\,\epsilon_1\,\gamma_1\,k\,F\,\phi\,L}{2v} + \frac{Q_1 e^{-r_1 t}\,\epsilon_1\,\gamma_1\,k\,F\,\phi\,(r_1-\lambda_1)\,L^2}{6v^2} + \frac{Q_1 e^{-r_1 t}\,\epsilon_1\,\gamma_1 F\,k\,\phi\,(r_1-\lambda_1)^2\,L^3}{24v^3}$$

$$\dot{C}_2(t) \approx \frac{Q_2 e^{-r_2 t}\,\epsilon_2\,\gamma_2\,k\,F\,\phi\,L}{2v} + \frac{f_{2,2}(Q_1, Q_2)\,L^2}{6v^2} + \frac{f_{2,3}(Q_1, Q_2)\,L^3}{24v^3}$$

$$\dot{C}_3(t) \approx \frac{Q_3 e^{-r_3 t}\,\epsilon_3\,\gamma_3\,k\,F\,\phi\,L}{2v} + \frac{f_{3,2}(Q_2, Q_3)\,L^2}{6v^2} + \frac{f_{3,3}(Q_1, Q_2, Q_3)\,L^3}{24v^3}$$

The *f()* are collections of factors in the higher-order terms that are not of interest here. The remarkable feature is that the input concentration is returned in the first term, multiplied only by known (instrumental) parameters. This has been demonstrated for several shapes of *Q(t)*, including for the Kr-Rb case.

The conversion of countrate to concentration then is via

$$Q_i(t) \approx \frac{\dot{C}_i(t)}{\varepsilon_i\,\gamma_i\,k\,F\,\phi\,\frac{L}{2v}}\ \text{RW} \quad \text{or} \quad \frac{\dot{C}_i(t)}{\varepsilon_i\,\gamma_i\,k\,F\,\phi\,\frac{8R}{3\pi v}}\ \text{CW};\quad t \ge T$$

if v is fast enough to discard the second- and higher-order terms in the expansion. The CW case can be shown analytically, also via a Taylor expansion of those $t \ge T$ countrates. Note that the transit time T is on the order of a few minutes here, as opposed to hours when v is a more typical, e.g., one inch/hr. The estimated concentration in this method lags the true value slightly, but the tracking ability is excellent. This approach would be used only for high-level concentrations, as in accident situations; it is of no use for normal operations at lower concentrations. With this approach the filter tape would need to be changed about each day rather than once per month, but the monitor would not be used in this manner for extended periods, rather only when personnel need essentially real-time estimates of the concentration in their area. This approach was published in [5], and is also presented in Chapter 4.

The following material was attached to a document used in a conversation a few years ago with the NRC. That document was edited to become the published paper presented here as Chapter 5. For the moment this material will be left as-is; in a later edition it will be integrated with the other math in this chapter.

$\dot{\mathbf{C}}(t)$	time-dependent monitor net countrate vector, cpm;
L	length of RW deposition window, inches;
w	width of RW deposition window, inches;
h	height of detector above deposition plane, inches;
R_{det}	radius of detector, inches;
R_{dep}	radius of CW deposition window, inches;
v	filter (tape) speed, inches/hour;
T	transit time (L / v), hours;
$\mathbf{A}$	system matrix (here, decay constants);
$\mathbf{B}$	source allocation matrix;
$\mathbf{u}$	source (air concentration) vector;
$\mathbf{\Psi}$	matrix of detection efficiency-abundance products;
λ_i	nuclide i decay constant, 1/hr;
η_i	branching ratio to nuclide i;
Q_i	concentration of nuclide i in air, μCi/cc;
k	units reconciliation constant;
F	monitor flowrate, cfm;
φ	collection/retention efficiency and line-loss fraction product;
ξ	intrinsic detection efficiency, counts/intersection;
γ	emission abundance, emission/disintegration;
$\Omega(x,y)$	position-dependent geometric efficiency, intersection/emission.

General (decay chain) countrate response model RW

Extension of RW model reported in [2] to include decay chains and geometric efficiency

$$\dot{\mathbf{C}}_{RW}(t \le T) = \frac{1}{wL}\left[\int_0^w \int_0^{vt} \int_{t-\frac{x}{v}}^{t} \mathbf{\Psi}(x,y)\, e^{\mathbf{A}(t-\tau)} \mathbf{B}\,\mathbf{u}(\tau)\, d\tau\, dx\, dy \;+\; \int_0^w \int_{vt}^{L} \int_0^{t} \mathbf{\Psi}(x,y)\, e^{\mathbf{A}(t-\tau)} \mathbf{B}\,\mathbf{u}(\tau)\, d\tau\, dx\, dy\right]$$

$$\dot{\mathbf{C}}_{RW}(t \ge T) = \frac{1}{wL} \int_0^w \int_0^L \int_{t-\frac{x}{v}}^{t} \mathbf{\Psi}(x,y)\, e^{\mathbf{A}(t-\tau)} \mathbf{B}\,\mathbf{u}(\tau)\, d\tau\, dx\, dy$$

$$\mathbf{A} = \begin{pmatrix} -\lambda_1 & 0 & 0 \\ \eta_2 \lambda_2 & -\lambda_2 & 0 \\ 0 & \eta_3 \lambda_3 & -\lambda_3 \end{pmatrix} \qquad \mathbf{B} = \begin{pmatrix} 1 & 0 & 0 \\ 0 & 1 & 0 \\ 0 & 0 & 1 \end{pmatrix} \qquad \mathbf{u}(\tau) = \begin{pmatrix} Q_1(\tau) \\ Q_2(\tau) \\ Q_3(\tau) \end{pmatrix} k\, F\, \phi$$

$$\mathbf{\Psi}(x,y) = \Omega(x,y) \begin{pmatrix} \xi_1 \gamma_1 & 0 & 0 \\ 0 & \xi_2 \gamma_2 & 0 \\ 0 & 0 & \xi_3 \gamma_3 \end{pmatrix}$$

Countrate response model, single nuclide RW

Remove the matrices and vectors:

$$\dot{C}_{RW}(t \le T) = \frac{k\,F\,\phi}{w\,L}\left[\int_0^w \int_0^{vt} \int_{t-\frac{x}{v}}^{t} \Psi(x,y) e^{-\lambda(t-\tau)} Q(\tau)\, d\tau\, dx\, dy + \int_0^w \int_{vt}^{L} \int_0^{t} \Psi(x,y) e^{-\lambda(t-\tau)} Q(\tau)\, d\tau\, dx\, dy\right]$$

$$\dot{C}_{RW}(t \ge T) = \frac{k\,F\,\phi}{w\,L} \int_0^w \int_0^L \int_{t-\frac{x}{v}}^{t} \Psi(x,y) e^{-\lambda(t-\tau)} Q(\tau)\, d\tau\, dx\, dy \qquad \Psi(x,y) = \xi\,\gamma\,\Omega(x,y)$$

Geometric efficiency function, point source, circular detector

Need this to find an average efficiency, to remove the position-dependence

$$\Omega(R_{det}, h, x, y) = \frac{1}{4\pi} \int_0^{R_{det}} \int_0^{2\pi} \frac{h}{\left[h^2 + r^2 + x^2 + y^2 + 2\,x\,r\cos(\theta) + 2\,y\,r\sin(\theta)\right]^{\frac{3}{2}}}\, r\, dr\, d\theta$$

Average geometric efficiency across deposition window

Using the average efficiency produces an approximate response, within 3-5% of that which uses the full geometric efficiency

$$\bar{\Omega}_{RW} = \frac{1}{w\,L} \int_{-\frac{w}{2}}^{\frac{w}{2}} \int_{-\frac{L}{2}}^{\frac{L}{2}} \Omega\left(R_{det}, h, x, y\right)\, dx\, dy$$

$$\bar{\Omega}_{CW} = \frac{1}{\pi\, R_{dep}^2} \int_{-R_{dep}}^{R_{dep}} \int_{-\sqrt{R_{dep}^2 - y^2}}^{\sqrt{R_{dep}^2 - y^2}} \Omega\left(R_{det}, h, x, y\right)\, dx\, dy$$

Radial symmetry for CW:

$$\bar{\Omega}_{CW} = \frac{1}{\pi\, R_{dep}^2} \int_0^{2\pi} \int_0^{R_{dep}} \Omega\left(R_{det}, h, r, 0\right)\, r\, dr\, d\theta = \frac{2}{R_{dep}^2} \int_0^{R_{dep}} \Omega\left(R_{det}, h, r, 0\right) r\, dr$$

Overall effective detection efficiency:

$$\bar{\varepsilon} \equiv \xi\,\gamma\,\bar{\Omega}$$

Countrate response models with flat (effective) efficiency RW

Efficiency now comes outside integrals

$$\dot{C}_{RW}(t \le T) = \frac{\bar{\varepsilon}\,k\,F\,\phi}{w\,L}\left[\int_0^w \int_0^{vt} \int_{t-\frac{x}{v}}^{t} e^{-\lambda(t-\tau)} Q(\tau)\, d\tau\, dx\, dy + \int_0^w \int_{vt}^{L} \int_0^{t} e^{-\lambda(t-\tau)} Q(\tau)\, d\tau\, dx\, dy\right]$$

$$\dot{C}_{RW}(t \ge T) = \frac{\bar{\varepsilon}\,k\,F\,\phi}{w\,L} \int_0^w \int_0^L \int_{t-\frac{x}{v}}^{t} e^{-\lambda(t-\tau)} Q(\tau)\, d\tau\, dx\, dy$$

Removal of *y*-dependence eliminates outer integrals and *w*:

$$\dot{C}_{RW}(t \le T) = \frac{\bar{\varepsilon}\, k\, F\, \phi}{L}\left[\int_0^{vt}\int_{t-\frac{x}{v}}^{t} e^{-\lambda(t-\tau)}Q(\tau)\,d\tau\,dx + \int_{vt}^{L}\int_0^{t} e^{-\lambda(t-\tau)}Q(\tau)\,d\tau\,dx\right]$$

$$\dot{C}_{RW}(t \ge T) = \frac{\bar{\varepsilon}\, k\, F\, \phi}{L}\int_0^{L}\int_{t-\frac{x}{v}}^{t} e^{-\lambda(t-\tau)}Q(\tau)\,d\tau\,dx$$

These are the response models that would need to be inverted in the general case, with *Q(τ)* unknown.

Constant concentration countrate response RW

Need to select a concentration; choose constant for simplicity

$$\dot{C}_{RW}(t \le T) = \frac{\bar{\varepsilon}\, k\, F\, \phi\, Q_0}{\lambda}\left[\left(1-\frac{vt}{L}\right)\left(1-e^{-\lambda t}\right) + \frac{v}{\lambda L}\left(\lambda t - 1 + e^{-\lambda t}\right)\right] \tag{A-1}$$

This is (23) of [2]; next is (25) of [2].

$$\dot{C}_{RW}(t \ge T) = \frac{\bar{\varepsilon}\, k\, F\, \phi\, Q_0}{\lambda}\left[1 - \frac{v}{\lambda L}\left(1-e^{-\lambda\frac{L}{v}}\right)\right] \tag{A-2}$$

Formula for estimating a constant concentration, RW, any half-life, after transit time only:

$$\hat{Q}_0 = \frac{\lambda}{\bar{\varepsilon}\, k\, F\, \phi\left[1 - \frac{v}{\lambda L}\left(1-e^{-\lambda\frac{L}{v}}\right)\right]}\,\dot{C}_{RW}(t \ge T) \tag{A-3}$$

Constant concentration countrate response, long-lived RW

Take limit of above as lambda approaches zero (LL)

$$\dot{C}_{RW}(t \le T) = \bar{\varepsilon}\, k\, F\, \phi\, Q_0\left(t - \frac{vt^2}{2L}\right) \tag{A-4}$$

$$\dot{C}_{RW}(t \ge T) = \bar{\varepsilon}\, k\, F\, \phi\, Q_0\,\frac{L}{2v} \tag{A-5}$$

Formula for estimating a constant concentration, RW, long-lived only, after transit time only:

$$\hat{Q}_0 = \frac{1}{\bar{\varepsilon}\, k\, F\, \phi\,\frac{L}{2v}}\,\dot{C}_{RW}(t \ge T) \tag{A-6}$$

Constant concentration countrate response CW

The solution for $t \le T$ is complicated and need not be repeated here; see [2], (33-35). Then for $t \ge T$,

$$\dot{C}_{CW}\left(t \ge T\right) = \frac{\bar{\varepsilon}\, k\, F\, \phi\, Q_0}{\lambda}\left[1 - \frac{2v}{\lambda\pi R_{dep}} + \frac{2v}{\lambda\pi R_{dep}^2}\int_0^{\frac{\pi}{2}} e^{-\frac{\lambda}{v}2R_{dep}\sin(\alpha)} R_{dep}\sin\left(\alpha\right)d\alpha\right] \tag{A-7}$$

This is (36) of [2]. It can be shown that this nonelementary-integral expression can also be written

$$\dot{C}_{CW}\left(t \geq T\right) = \frac{\bar{\varepsilon}\, k\, F\, \phi Q_0}{\lambda}\left[1 - \frac{2v}{\lambda \pi R_{dep}} + \frac{v}{\lambda R_{dep}}\left\{\mathrm{L}_{-1}\left(\frac{2\lambda R_{dep}}{v}\right) - \mathrm{I}_1\left(\frac{2\lambda R_{dep}}{v}\right)\right\}\right] \tag{A-8}$$

where L_{-1} is the StruveL function and I_1 is a Bessel function. Either (A-7) or (A-8) can be evaluated numerically; or, we can find a good approximation by using the appropriate RW result with

$$L_{CW} = \frac{16 R_{dep}}{3\pi} \tag{A-9}$$

Note that for a given monitor system and a given nuclide, the quantity in brackets in (A-7, A-8) evaluates to a constant, so that a formula for estimating a constant concentration, CW, any half-life, after the transit time only, is

$$\hat{Q}_0 = \frac{\lambda}{\bar{\varepsilon}\, k\, F\, \phi\left[1 - \frac{2v}{\lambda \pi R_{dep}} + \frac{v}{\lambda R_{dep}}\left\{\mathrm{L}_{-1}\left(\frac{2\lambda R_{dep}}{v}\right) - \mathrm{I}_1\left(\frac{2\lambda R_{dep}}{v}\right)\right\}\right]}\, \dot{C}_{CW}\left(t \geq T\right) \tag{A-10}$$

Constant concentration countrate response, long-lived CW

$$\dot{C}_{CW}\left(t \leq T\right) = \bar{\varepsilon}\, k\, F\, \phi Q_0 \left\{ t\left(1 - \frac{2}{\pi}\left[\beta\sqrt{1-\beta^2} + \sin^{-1}\left(\beta\right)\right]\right) + \frac{8R_{dep}}{3\pi v}\left(1 - \sqrt{1-\beta^2}\right) + \frac{2vt^2}{3\pi R_{dep}}\sqrt{1-\beta^2} \right\} \tag{A-11}$$

$$\beta \equiv \frac{vt}{2R_{dep}} \tag{A-12}$$

This is (39) of [2].

$$\dot{C}_{CW}\left(t \geq T\right) = \bar{\varepsilon}\, k\, F\, \phi Q_0 \frac{8R_{dep}}{3\pi v} \tag{A-13}$$

(A-13) can be found most simply by substituting unity for β in (A-11); this corresponds to $t = T = 2R/v$. The countrate is continuous across the transit time boundary, and is constant thereafter. The same result follows by taking the limit of (A-8) as the decay constant approaches zero. Then a formula for estimating a constant concentration, CW, long-lived only, after the transit time only, is

$$\hat{Q}_0 = \frac{1}{\bar{\varepsilon}\, k\, F\, \phi Q_0 \frac{8R}{3\pi v}}\, \dot{C}_{CW}\left(t \geq T\right) \tag{A-14}$$

6.0 Circular Window Moving Filter Numerical Model (*Mathematica*)

Define geometric efficiency function

```
Ω[R_, h_, x_, y_] := NIntegrate[ h * r / (h^2 + x^2 + y^2 + r^2 + 2. x * r * Cos[ϕ] + 2. y * r * Sin[ϕ])^(3 / 2),
                                 {r, 0., R}, {ϕ, 0., 2. Pi} ] / (4. Pi)
```

Define various system parameters

```
R = 2.54; h = 1.0;   nvert = 100; ncells = 30;    v = 2.54 / 60.;
k = 2.2 * 10^6 * 2.832 * 10^4;  flow = 5.; phi = 0.7; kk0 = k * flow * phi;
L = 16 R / (3 Pi); alfa = 0.2; bkglevel = 100.;
tstart = 0.; tmax = 160.; tstep = 5. / 60.; nsteps = Round[(tmax - tstart) / tstep] + 1;
dx = v * tstep;
λ1 = Log[2.] / 60.; λ2 = Log[2.] / 20.; λ3 = Log[2.] / 10.; η2 = 1.; η3 = 0.36;
qstart = 0.; r1 = 0.05; r2 = 0.02; r3 = 0.; S = 0.; Q0 = 3.0 * 10^(-9);
```

Find geometric efficiency interpolating function

```
Off[NIntegrate::inumr];
efficCW = FunctionInterpolation[Ω[R, h, x, y], {x, -R, R}, {y, -R, R}];
```

Define concentration time-dependence functions

```
QA[r1_, r2_, r3_, S_, Q0_, qstart_, t_] :=
    If[(t ≥ qstart), S * (10^-10) / (r2 - r1) *
                     (Exp[-r1 * (t - qstart)] - Exp[-r2 * (t - qstart)]) +
                     Q0 * Exp[-r3 * (t - qstart)], 0.];
QB[Q0_, qstart_] := If[ (t ≥ qstart), 0. * Q0, 0.];
QC[Q0_, qstart_] := If[(t ≥ qstart), 0. * Q0, 0.];
QinA = Table[ QA[r1, r2, r3, S, Q0, qstart, t], {t, 0., tmax, tstep}];
QinB = 0. * QinA; QinC = 0. * QinA;                                    ;;
```

Define (x,y) coordinates of cells at time zero

```
dtheta = 0.99 Pi / nvert; theta = Table[ dtheta * i, {i, 1, nvert}];
eta = R * Sin[theta]; zeta = R * Cos[theta]; xlen = 2. * eta; dxlen = xlen / ncells;
yheight = Table[ (zeta[[i - 1]] - zeta[[i]]), {i, 2, nvert}]; dx2 = .5 * dxlen;
yheight = Prepend[ yheight, R - zeta[[1]] ];
diffeta = Table[ (eta[[i]] - eta[[i - 1]]), {i, 2, nvert}];
diffeta = Prepend[ diffeta, eta[[1]] ];
areacorr = yheight * diffeta; arearatio = 1 - diffeta / xlen;
darea = xlen * yheight - areacorr;
xleft = -eta;
xnow0 = Table[ xleft[[i]] + (j - 1) * xlen[[i]] / ncells,
                      {i, 1, nvert}, {j, 1, ncells}   ];
ynow0 = Table[zeta[[i]], {i, 1, nvert}, {j, 1, ncells}];
frac = Table[ darea[[i]], {i, 1, nvert}, {j, 1, ncells}] / (Pi * R^2 * ncells);
```

Define ODE recursive solution factors

```
alphaA = 1. - Exp[-λ1 * tstep]; alpha2A = 1. - alphaA;
alphaB = 1. - Exp[-λ2 * tstep]; alpha2B = 1. - alphaB;
alphaC = 1. - Exp[-λ3 * tstep]; alpha2C = 1. - alphaC;
kkA = frac * kk0 * alphaA / λ1;  kkB = frac * kk0 * alphaB / λ2;
kkC = frac * kk0 * alphaC / λ3;
kkBb = η2 * alphaB;  kkCc = η3 * alphaC; ;
```

MAIN CALCULATION LOOP

```
ii         = qstart / tstep;  k = 0;
xnow       = xnow0;
cellactvA = ConstantArray[0, {nvert, ncells}];
cellactvB = ConstantArray[0, {nvert, ncells}];
cellactvC = ConstantArray[0, {nvert, ncells}];
effic     = ConstantArray[0, {nvert, ncells}];
countCW   = ConstantArray[0, {nsteps, 3}];
Monitor[
Timing [
Do[  ii = ii + 1;
     cellactvA = kkA * QinA[[ii]]                  + alpha2A * cellactvA;
     cellactvB = kkB * QinB[[ii]] + kkBb * cellactvA + alpha2B * cellactvB;
     cellactvC = kkC * QinC[[ii]] + kkCc * cellactvB + alpha2C * cellactvC;
     Do[ If[ xnow[[i, j]] ≥ -xleft[[i]], xnow[[i, j]] = xleft[[i]];
                                      cellactvA[[i, j ]]  = 0.;
                                      cellactvB[[i, j ]]  = 0.;
                                      cellactvC[[i, j ]]  = 0.; ],
                                 { i, 1, nvert}, {j, 1, ncells}   ];

     effic = efficCW[ xnow, ynow0 ];
     xnow = xnow + dx;
     countCW[[ii, 1]] = Total[ effic * cellactvA * arearatio, 2 ];
     countCW[[ii, 2]] = Total[ effic * cellactvB * arearatio, 2 ];
     countCW[[ii, 3]] = Total[ effic * cellactvC * arearatio, 2 ]; ,
     {t, qstart, tmax, tstep }
  ]                            ]                    ,
  ProgressIndicator[ ii, {1, nsteps} ]  ]
  countCW = countCW + bkglevel;
```

Add Poisson noise, EWMA filter, find simulated countrates

```
countdataA = Table[countCW[[i, 1]] * tstep, {i, 1, nsteps } ];
countdataB = Table[ countCW[[i, 2]] * tstep, {i, 1, nsteps } ];
countdataC = Table[ countCW[[i, 3]] * tstep, {i, 1, nsteps } ];
```

```
noisycountsA = Table[ RandomInteger[PoissonDistribution[ countdataA[[i]] ] ], {i, 2, nsteps} ] ;
noisycountsB = Table[ RandomInteger[PoissonDistribution[ countdataB[[i]] ] ], {i, 2, nsteps} ] ;
noisycountsC = Table[ RandomInteger[PoissonDistribution[ countdataC[[i]] ] ], {i, 2, nsteps} ] ;

countrateA = ExponentialMovingAverage[ noisycountsA, alfa ] / tstep;
countrateB = ExponentialMovingAverage[ noisycountsB, alfa ] / tstep;
countrateC = ExponentialMovingAverage[ noisycountsC, alfa ] / tstep;
```

References

[1] W. C. Evans, "Mathematical Models for the Dynamic Response of Continuous Particulate Air Monitors", *IEEE Transactions on Nuclear Science* **48** (2), April 2001. Chapter 1, here.

[2] W. C. Evans, "Quantitative Methods for Continuous Particulate Air Monitoring", *IEEE Transactions on Nuclear Science* **48** (5), October 2001. Chapter 2.

[3] W. C. Evans, "Concentration Dynamics Modeling for Continuous Particulate Air Monitor Response Prediction", *IEEE Transactions on Nuclear Science* **49** (5), October 2002. Chapter 3.

[4] D. G. Weis, "Enhancement of Reactor Coolant Leakage Measurement Using Radiation Instrumentation", *IEEE Transactions on Nuclear Science* **46** (3), June 1999.

[5] W. C. Evans, "Estimation of High-Level, Rapidly-Changing Concentrations Using Moving-Filter Continuous Particulate Air Monitors", *Health Physics* **102** (4), April 2012. Chapter 4.

Chapter 8

Integrated-Count Processing for Fixed-Filter Continuous Particulate Air Monitors

Health Physics, 111(3), September 2016, 290-299

A calculation for estimating concentrations of long-lived airborne particulate radioactivity using fixed-filter continuous air monitors was given in an ISO standard. The method uses counts integrated over relatively long time intervals, rather than the "instantaneous" countrates that in digital systems are evaluated using much shorter time intervals and some form of variance-reduction filtering. This article presents three ways of deriving and interpreting this calculation, based on previously-published mathematical models that are themselves derived from first principles. The method is also extended here to apply for short-lived activity. Some statistical properties of the estimator are discussed, including its time-dependent variance and the presence of strong autocorrelation in the concentration estimates. An interactive simulation was used to examine the performance of the concentration estimation, using physically-plausible concentration time-dependence profiles; example plots are provided. The conclusion of these studies is that the method, as modified herein, can perform remarkably well in providing periodic average-concentration estimates for both long- and short-lived activity, and it should be considered an appropriate method in those situations where the tracking of a time-dependent concentration is deemed necessary. However, for personnel protection purposes the estimation of the time integral of the concentration is more useful, since it is directly proportional to a worker's inhalation uptake. This time integral can be found directly from the monitor response, without the estimation of the concentration at many time steps as is done with the method discussed here.

Introduction

Methods for the modeling and interpretation of the responses of continuous particulate air monitors (CPAMs) have been available for many years (Evans 2001a, 2001b). Most of these techniques rely on the use of some estimate of the "instantaneous" countrate from the monitor detector. In older analog systems the countrate was developed using an RC circuit, while in more modern digital systems this can be done by accumulating counts in a register for a few seconds and then applying some form of variance-reducing digital signal processing (filtering).

It is possible to estimate the dynamic, time-varying concentration (input) from the monitor response (output), in some circumstances. Why this would be necessary is not obvious, since the time integral of the concentration is more useful (it has a direct proportionality to the uptake of an exposed worker). It is important to recognize that the time integral of the concentration can be estimated from the monitor response, for fixed-filter CPAMs, without ever directly estimating the time-dependent concentration itself (Evans 2001b).

There was an ISO standard (originally issued as ISO 2005a and since revised as ISO 2010; cited in Lu and Whicker 2008) that contained a method for estimating concentrations for a fixed-filter CPAM; this method was restricted to long-lived activity. Although others have used it as well, for convenience this calculation will be referred to below as the "ISO method." The calculation does not use any form of countrate processing, but rather integrates counts over relatively long time intervals, much as would have been done decades ago with analog scalers. This leads to an *average* countrate over the integration interval. The integration interval is not specified, but at shorter intervals the integrated counts would be so small that the variability of the concentration estimate would be unacceptable. Since no variance reduction is provided, it is inferred that the integration interval must be relatively long, on the order of at least several minutes.

The purposes of this article are: (a) to derive the ISO method from available first-principles models and quantitative methods; (b) to extend it to apply to short-lived activity; (c) to characterize some statistical properties of the concentration estimates; (d) to study the method's performance against concentration profiles that are representative of those found in real-world compartmental systems. The latter means profiles that are sums of exponentials, continuously changing, as opposed to the "stairstep" or "square-wave" profiles often used, which, unrealistically, jump instantaneously from one constant level to another.

Discussion

Using notation consistent with earlier published work on CPAMs, the ISO concentration-estimation relation can be written

$$\hat{Q}_i = \frac{\dot{C}_i - \dot{C}_{i-1}}{\bar{\varepsilon}\, k\, \phi\, F_m\, \eta} = \frac{\frac{C_i}{\eta} - \frac{C_{i-1}}{\eta}}{\bar{\varepsilon}\, k\, \phi\, F_m\, \eta} = \frac{C_i - C_{i-1}}{\bar{\varepsilon}\, k\, \phi\, F_m\, \eta^2} \ , \tag{1}$$

where $\bar{\varepsilon}$ is the average detection efficiency[1], cpm/dpm; k is a units reconciliation constant; ϕ is the filter collection efficiency; F_m is the monitor flowrate, m^3/min, here assumed constant over the integration interval η, minutes; C is integrated (or "accumulated") counts; $\dot{C}$ is countrate, cpm; Q is concentration, Bq/m^3. The "hat" over Q means that it is an estimate. All countrates and integrated counts are assumed to be net, background/interference corrected. This estimator is restricted to long-lived (LL) activity only.

The ISO equation actually uses the sampled air volume, which could in principle allow for a time-dependent monitor flow rate, which then presumably is assumed to be integrated by the instrument, to give the volume. However, the development below will assume a constant flow rate, since its time-dependence, if any, is in general unknown. Also, the flow rate need only be considered constant over intervals of at most tens of minutes.

It is not clear whether this concentration estimate is to be interpreted as an average, or as a point value at some specific time. The calculation in eqn(1) is to be "slid along" as time progresses, so the notation implies that the concentration is a point estimate ("instantaneous," as opposed to an average over an interval), evaluated at the end of the i-th interval.

The countrates in eqn(1) are estimated *not* via some form of processing such as presented in eqn(4) of Evans 2001b but rather are based on counts integrated over comparatively long times. Again, countrate algorithms use short time intervals, on the order of a few seconds, to accumulate counts in a digital register, and then these counts are processed with some form of variance-reduction digital filtering. The ISO calculation uses time intervals on the order of several minutes, and does not apply any variance reduction processing.

The *two* countrate estimates needed in eqn(1) require integration of counts across *two* time intervals. However, the sequential nature of this calculation is such that the next concentration estimate will become available at the end of the next integration interval, of length η, even though the calculation requires a time interval of 2η. The fact that, in this sequential processing, a given observed integrated-count value is used in two adjacent concentration estimates has statistical consequences, to be discussed below.

It is essential to understand that the countrates estimated in the numerator of eqn(1) are *averages* over the respective integration intervals. For example, the counts C_1 accumulated over the interval t_1 to t_2 for a FF monitor will be (Evans 2001b)

$$C_1 \equiv C\left(t_1 \to t_2\right) = \int_{t_1}^{t_2} \bar{\varepsilon}\, k\, \phi \int_0^t Q(\tau)\, F_m(\tau) e^{-\lambda(t-\tau)}\, d\tau\, dt \ + \ \int_{t_1}^{t_2} \dot{C}_0\, e^{-\lambda t}\, dt \ , \tag{2}$$

where λ is the decay constant of the activity of interest, in min^{-1}, and $\dot{C}_0$ is the (net) countrate at time zero.

Figure 1 is a sketch showing the relationship of the time labels to the integrated counts. The time t in eqn(2) is measured in minutes from the time at which the monitor flow was started after a filter change, which also means that the initial-condition (net) countrate is taken to be zero. Thus, the zero time is considered known; it is not, as might be thought, the unknown time at which a concentration transient begins[2].

[1] The detection efficiency is the product of the intrinsic and geometric efficiencies; the latter is not constant across the detection region and must be averaged over this region. This averaging corrects fixed-filter responses exactly, while it is only approximate for moving-filter monitors.

[2] The latter is important, however, in the analysis of moving-filter CPAM responses (Evans 2001a).

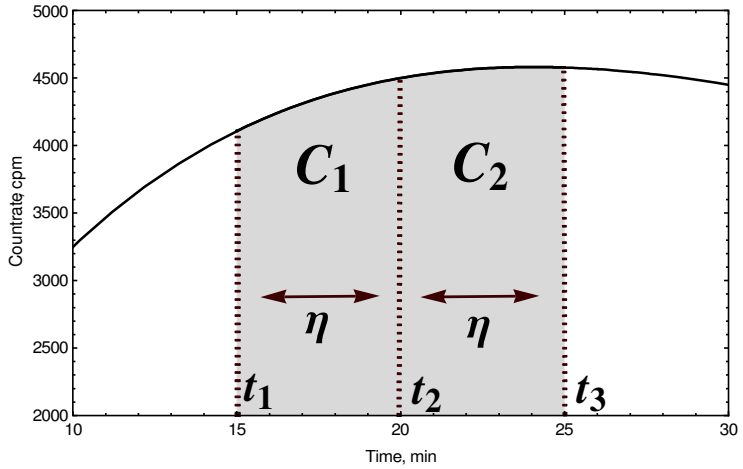

Fig. 1 Sketch of time intervals and integration regions. C is integrated counts.

As stated above, it is assumed that the monitor flowrate is constant over the integration interval, so that eqn(2) simplifies to

$$C_1 \equiv C\left(t_1 \to t_2\right) = \int_{t_1}^{t_2} \bar{\varepsilon}\, k\, F_m\, \phi \int_0^t Q(\tau)\, e^{-\lambda(t-\tau)}\, d\tau\, dt \ . \tag{3}$$

The average countrates over the intervals t_1 to t_2 and t_2 to t_3 will be

$$\bar{\dot{C}}_1 = \frac{C\left(t_1 \to t_2\right)}{\left(t_2 - t_1\right)} = \frac{C_1}{\eta} \qquad \bar{\dot{C}}_2 = \frac{C\left(t_2 \to t_3\right)}{\left(t_3 - t_2\right)} = \frac{C_2}{\eta} \ .$$

Derivation Using Numerical Derivative

In eqn(1) is an expression that appears as though it might be an attempt at a numerical, first-backward-difference derivative. It is well known that the differential equation for the time-dependent countrate of a fixed-filter monitor is (e.g., Evans 2001a)

$$\left.\frac{d\dot{C}}{dt}\right|_t = \bar{\varepsilon}\, k\, F_m\, \phi Q(t) - \lambda \dot{C}(t) \ . \tag{4}$$

The ISO formula is explicitly restricted to long-lived (LL) nuclides; it is seen immediately from eqn(4) that for LL nuclides (small value of λ) the instantaneous rate of change of the countrate at any time is proportional to the instantaneous concentration existing at that time. Thus, perhaps eqn(1) could be re-written as

$$\left.\frac{\Delta\dot{C}}{\Delta t}\right|_{t_2} \approx \bar{\varepsilon}\, k\, F_m\, \phi Q(t_2) \ . \tag{5}$$

From Fig. 1, time t_2 is the midpoint of the ISO calculation interval. The problem with this interpretation is that the interval Δt is, presumably, much too large to be considered a differential, in the calculus sense. The only way to make use of eqn(5) as an approximation to eqn(4) is to assume that the countrate is (essentially) linear over the interval Δt, so that the slope is (essentially) constant. That is, if the slope is not changing rapidly, then a wider Δt interval (on the order of minutes rather than seconds) will still provide a reasonable first-derivative estimate.

From this point, the restriction to LL nuclides will be lifted, so that

$$\left.\frac{\Delta \dot{C}}{\Delta t}\right|_{t_2} + \lambda \dot{C}(t_2) \approx \bar{\varepsilon}\, k\, F_m\, \phi Q(t_2) \tag{6}$$

will be the relation to develop. Since the ISO countrate estimates are averages, eqn(6) can be expressed as

$$\frac{\bar{\dot{C}}_2 - \bar{\dot{C}}_1}{\Delta t} + \lambda \dot{C}(t_2) \approx \bar{\varepsilon}\, k\, F_m\, \phi Q(t_2)\ . \tag{7}$$

The first two countrates on the LHS of eqn(7) are averages, for which there are estimates, while the third is an "instantaneous" value, for which there is not yet an estimator. (The ISO method's LL restriction eliminates the need for this "instantaneous" countrate.) At this point there are two problems to solve: (1) What is the appropriate time interval Δt to use for the difference of these two average countrates, and (2) How is the countrate at time t_2 to be estimated?

It can be shown with elementary algebra that under the linear-countrate assumption the average countrate value will occur at the midpoint of its respective integration interval. Both intervals are of width η, so the time difference Δt will also have value η. Since the time difference between each of the successive time markers t_1 t_2 t_3 is also η,

$$\frac{C_2 - C_1}{\eta^2} + \lambda \dot{C}(t_2) \approx \bar{\varepsilon}\, k\, F_m\, \phi\, Q(t_2)\ . \tag{8}$$

The remaining problem is how to estimate the countrate at the estimation midpoint, t_2 , given only the integrated counts in the two adjacent time intervals. For this, consider Fig. 2. The counts integrated in the indicated intervals, under the linear-countrate assumption, will be, from geometry (area of a trapezoid)

$$C_1 = \frac{\eta}{2}\left[\dot{C}(t_1) + \dot{C}(t_2)\right] \qquad C_2 = \frac{\eta}{2}\left[\dot{C}(t_2) + \dot{C}(t_3)\right].$$

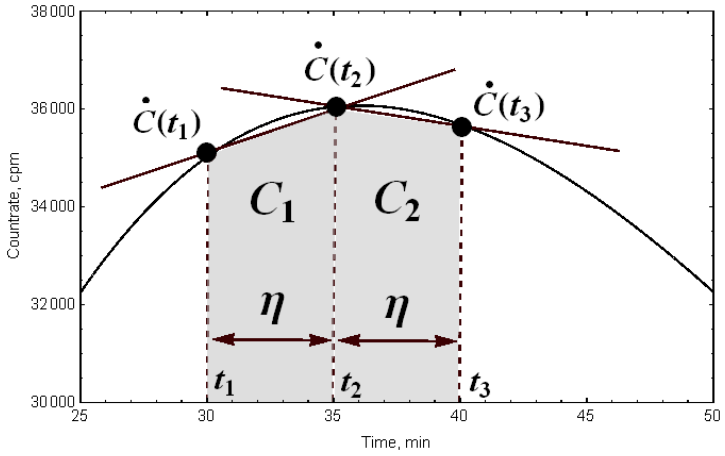

Fig. 2 Sketch showing trapezoidal areas, which, under the local-linearity assumption, approximate the areas for the integrated counts. This countrate trace is deliberately exaggerated to show these regions better; in most cases the curvature is so small that the trapezoidal area is for all practical purposes the same as the actual area. Even here the fractional difference in area is quite small.

Rearranging and adding the two equations,

$$\frac{2}{\eta}(C_1 + C_2) = \dot{C}(t_1) + \dot{C}(t_3) + 2\dot{C}(t_2)\ ,$$

from which

$$\dot{C}(t_2) = \frac{C_1 + C_2}{\eta} - \frac{\dot{C}(t_1) + \dot{C}(t_3)}{2} .$$

At this point recall that, with the linear-countrate assumption, the average of the two endpoint countrates will be the countrate at the midpoint of the overall calculation interval (of width 2η). Then the second term in the expression above is the countrate at time t_2, and using this leads to

$$\dot{C}(t_2) = \frac{C_1 + C_2}{2\eta} , \tag{9}$$

which is just the total counts divided by the total time. (In the figure, due to the high curvature used for illustration, this estimate is a bit low.) Using eqn(9) in eqn(8),

$$\frac{C_2 - C_1}{\eta^2} + \lambda \frac{C_1 + C_2}{2\eta} \approx \bar{\varepsilon}\, k\, F_m\, \phi\, Q(t_2) ,$$

which, with some rearrangement, leads to the final result for this interpretation of the ISO calculation; namely, as the estimated concentration at the midpoint t_2 of the estimation interval t_1 to t_3, not a point estimate at the endpoint time t_3, as implied in eqn(1):

$$\hat{Q}(t_2) \approx \frac{C_2\left(\frac{1}{\eta} + \frac{\lambda}{2}\right) - C_1\left(\frac{1}{\eta} - \frac{\lambda}{2}\right)}{\bar{\varepsilon}\, k\, F_m\, \phi \eta} . \tag{10}$$

Note that for LL activity this collapses to the form

$$\hat{Q}(t_2) \approx \frac{C_2 - C_1}{\bar{\varepsilon}\, k\, F_m\, \phi\, \eta^2} .$$

which amounts to eqn(1). Even though this concentration estimate applies at the midpoint t_2, it is not available until time t_3, which is taken to be the current time. Then the time assignment of this concentration estimate as a practical matter would be at the clock time corresponding to time t_3, since it was unavailable at the clock time corresponding to time t_2.

Uncertainty and Autocorrelation

An estimator for the uncertainty in this concentration value can be found using well-known propagation of uncertainty methods; the result for the variance of the estimated concentration is

$$Var[\hat{Q}] \approx \frac{C_2\left(\frac{1}{\eta} + \frac{\lambda}{2}\right)^2 + C_1\left(\frac{1}{\eta} - \frac{\lambda}{2}\right)^2}{\left(\bar{\varepsilon}\, k\, F_m\, \phi\, \eta\right)^2} , \tag{11}$$

since the integrated counts C will be Poisson distributed, and the mean and variance are of course equal for this data. This expression ignores the variances of the system parameters (average detection efficiency, flowrate, etc.), and in some situations these variances (and any possible covariances) should be considered and included in the uncertainty calculations.

While long-term constant concentrations are of little practical interest, they are useful in exploring the statistical behavior of an estimator such as eqn(10). Using an analytical model for the countrate response to a constant concentration Q_0 of activity of any half-life (from Evans 2001a), starting from a clean filter at time zero the countrate at any time thereafter will be:

$$\dot{C}(t) = \frac{\varepsilon k F_m \phi Q_0}{\lambda} \left[1 - \exp(-\lambda t) \right] .$$

Integrating this over two adjacent intervals, each of width η,

$$C_1 = \int_{t-2\eta}^{t-\eta} \dot{C}(\tau)\, d\tau \qquad C_2 = \int_{t-\eta}^{t} \dot{C}(\tau)\, d\tau \ ,$$

where τ is a dummy integration variable. Using the results of these integrations in the variance expression eqn(11) results in an algebraically-complicated function, the limit of which for LL activity can be shown to be

$$Var[\hat{Q}] = \frac{2Q_0}{\varepsilon k F_m \phi \eta^3} (t - \eta) \qquad t > \eta \ . \tag{12}$$

For short-lived (SL) activity, as time increases the variance approaches

$$Var[\hat{Q}] = \frac{Q_0}{2\varepsilon k F_m \phi \lambda \eta^3} \left(4 + \lambda^2 \eta^2 \right) \ , \tag{13}$$

and for, e.g., Rb-88 this variance level is attained after about two hours. Figs. 3 and 4 show the results of Monte Carlo simulation of the concentration estimation process, with lines showing the bounds for a "two-sigma" region, created using plus and minus two times the square root of eqn(12) or eqn(13). These bounds should contain about 95% of the observations. The fraction of observations, for a sample size of 15000 estimated concentrations, outside these bounds was very close to 0.05, in repeated experiments, at various concentration levels.

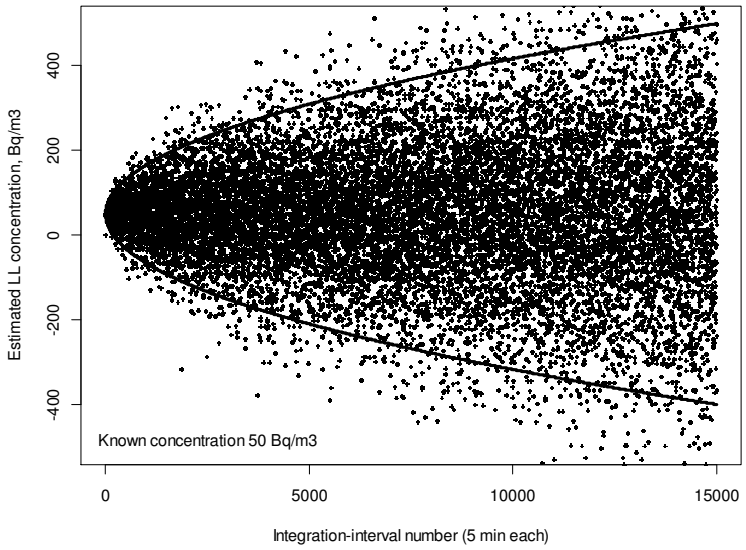

Fig. 3 Monte Carlo results for LL activity. The solid line represents an approximate 95% bound on the observations, based on eqn(12). Each dot represents one estimate of the constant LL concentration, with an integration interval of five minutes (so that the concentration averaging is done over ten minutes

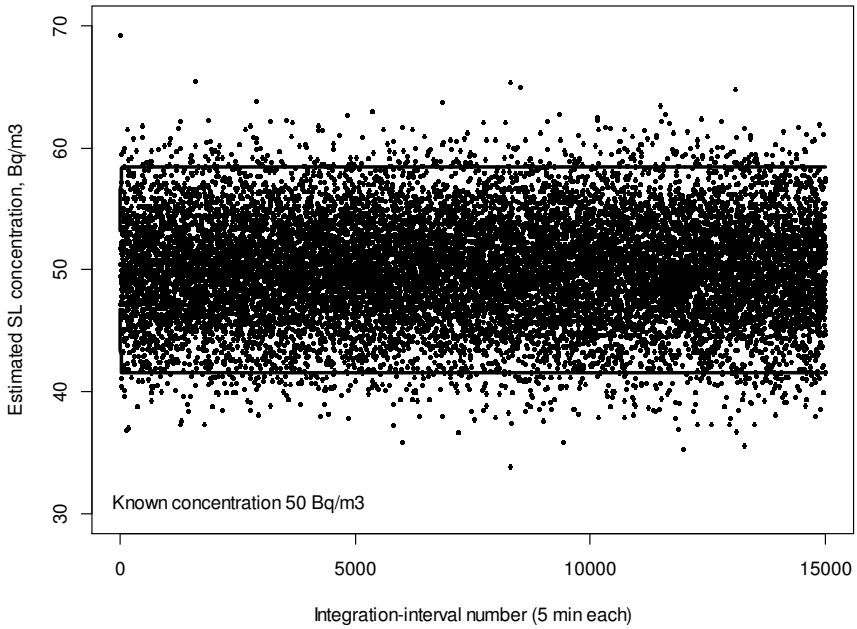

Fig. 4 Monte Carlo results for SL activity, similar to Fig. 3. The 95% bounds, from eqn(13), reach their limiting value very quickly on this time scale. There is actually some curvature in these bounds at early time values, that can be seen better in other figures

It is clear from eqn(12) and the evidence from the Monte Carlo experiments that the variance of LL concentration estimates increases with time, measured from the last replacement of the filter. This is due to the continued accumulation of activity on the filter; the concentration estimate is taking the difference of larger and larger numbers as time progresses[3]. For SL activity, on the other hand, the countrate reaches equilibrium and thus the concentration variance approaches a constant value.

Since adjacent concentration estimates use common data (C_2 for the current estimate is exactly C_1 for the next one), it should be expected that these estimates would be autocorrelated. The Monte Carlo simulation generates many thousands of concentration estimates; these do in fact show a very strong serial correlation, for both LL and SL activity. In the notation of the time-series literature (see e.g. Box and Jenkins 2008), the sequence of estimates follows an MA(1) process, with a negative autocorrelation coefficient.

MA stands for "moving average" and the "(1)" means that the serial correlation applies to "lag 1," i.e., immediately-adjacent values of the time series. The MA(1) process is also referred to as a "first-order moving average" random process. The identification of this process in the Monte Carlo output data, using standard time series analysis methods[4], is very clear and unambiguous. Similar analysis of output data from the full simulation (discussed below) also shows the MA(1) structure, although with much smaller sample sizes in those runs, the identification is more ambiguous.

The effect of this autocorrelation is to produce a rapid, high-frequency fluctuation in the concentration estimates as time progresses. This can be seen in Figs. 5, 6, and 7 where the "zig-zagging" of the estimates is evident; a higher value is followed by a lower one, and vice-versa. The negative correlation, and resulting high-frequency variation, is caused by the subtraction of the common integrated-count value. That is, in the current time step, observed count C_2 has a positive value in the ISO calculation, while in the next time step that exact same count result becomes C_1 and has a negative value (it is subtracted).

[3] This effect was noted in the discussion of eqn(22) in Evans 2001b.

[4] Plots of the autocorrelation function (ACF) and partial autocorrelation function (PACF) are used to identify a time series model.

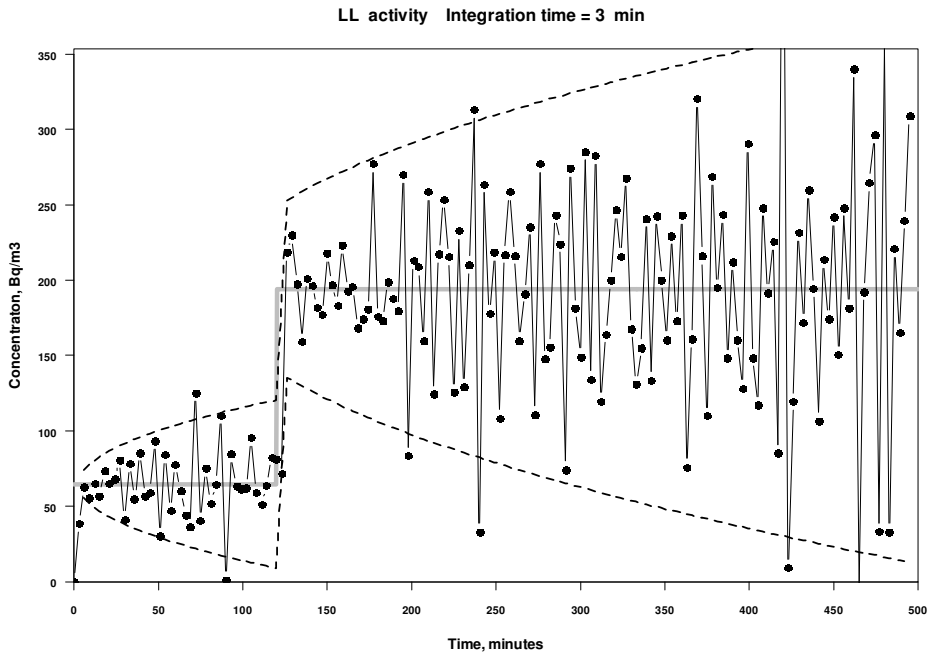

Fig. 5 This simulation run output shows the negative-autocorrelation effect of alternating high/low values. The dashed lines define the approximate 95% region. The monitor parameters (used in all plots) were: average detection efficiency, 0.2 cpm/dpm; monitor flowrate 0.001 m^3/s; collection/retention efficiency phi, 1.0.

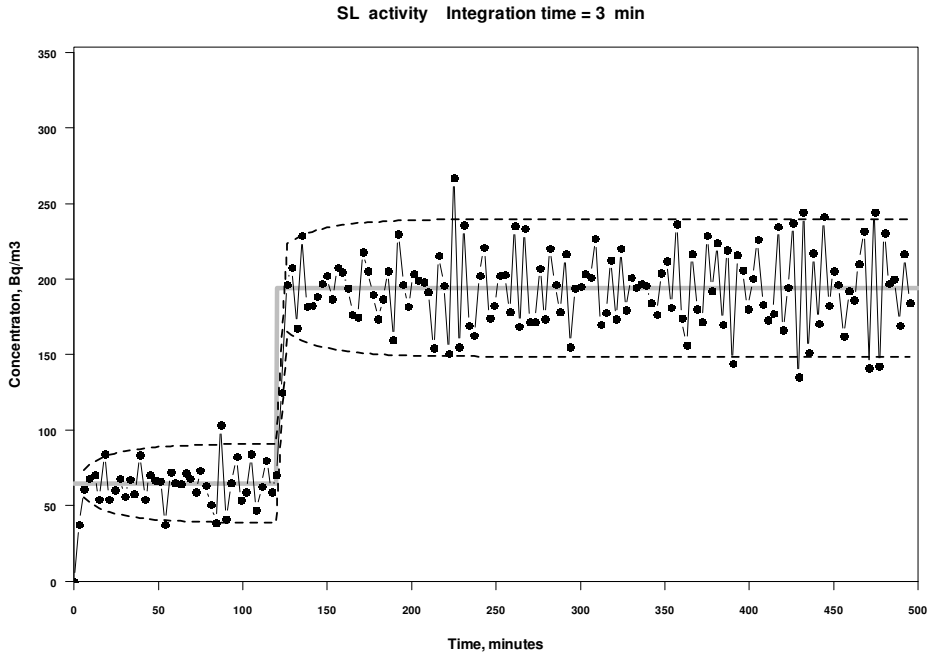

Fig. 6 Output of a simulation run the same as that in Fig. 5, but for SL activity (Rb-88). The autocorrelation effect is still noticeable. Time series analysis of the Monte Carlo data shows that both LL and SL have the MA(1) structure. pgm = singleexpoBW (first version)

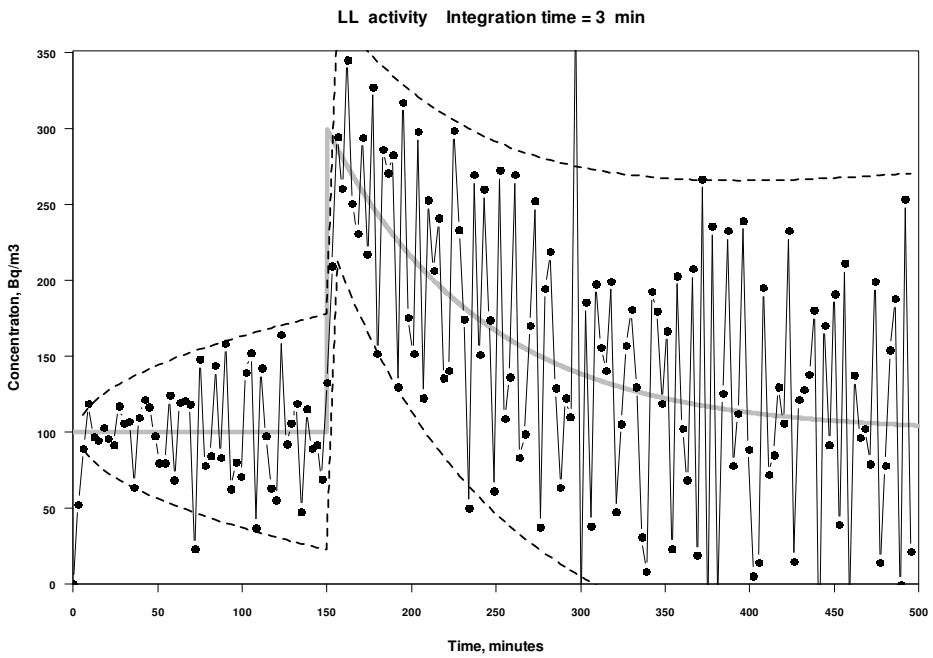

Fig. 7 Another example of the autocorrelation effect, for a time-varying concentration profile.

The practical consequences of this autocorrelation would be in the estimation of the variance of a sequence of these concentration estimates, perhaps as part of a concentration-change detection scheme. Such a scheme would be difficult to implement in any case, due to the time-dependent variance of LL activity. Autocorrelation has a significant impact on the estimation of the variance of a random process, and this must be taken into account. (See, e.g., Box and Jenkins 2008, p. 31; Law and Kelton 1991, p. 284.) However, this serial correlation should not have any effect on the estimated variance of an *individual* concentration estimate, using eqn(11).

Derivation Using the "Five-Minute Rb88 Method"

Another way to look at eqn(1) is to interpret it as an implementation of eqn(22) of Evans 2001b. This finds an average concentration over relatively short time intervals, e.g., five minutes, and applies for both LL and SL activities. Like the ISO calculation, it can be moved along in discrete steps across time, and this was demonstrated in Figures 8-10 of that reference. The countrates required by this estimation method are provided by a short-time-step (a few seconds) countrate processing algorithm, *not* by integrating counts over relatively long time intervals. Again, the latter provides an average countrate, while this Rb-88 method[5] requires "instantaneous" countrates.

It is shown in Evans 2001b that the average concentration over an interval $0 < t < \eta$ is estimated by

$$\bar{Q} = \frac{1}{\bar{\varepsilon}\, k\, F_m\, \phi \eta} \left[\dot{C}(\eta) - \dot{C}(0) \right] + \lambda \int_0^{\eta} \dot{C}(t)\, dt \ . \tag{14}$$

This calculation can be moved along a time span in a manner similar to eqn(1), so that, averaging over an interval from t_1 to t_3,

$$\bar{Q} = \frac{1}{\bar{\varepsilon}\, k\, F_m\, \phi (t_3 - t_1)} \left[\dot{C}(t_3) - \dot{C}(t_1) \right] + \lambda \int_{t_1}^{t_3} \dot{C}(t)\, dt \ .$$

[5] See Evans 2001b for the reasoning behind this terminology.

The time that might be assigned to this average is somewhat arbitrary, since the average can be considered to apply across the entire averaging interval. However, as with the derivative interpretation, the estimate itself is only available at time t_3 .

Returning to the ISO calculation, the integral in eqn(14) is the total counts obtained, so that

$$\bar{Q} = \frac{1}{\bar{\varepsilon}\, k\, F_m\, \phi\, 2\eta} \left[\dot{C}(t_3) - \dot{C}(t_1) \right] + \lambda (C_1 + C_2) \,. \tag{15}$$

Now the problem arises, similar to the discussion in the previous section, as to how the two countrates in the expression above are to be estimated using only the ISO-available integrated counts (rather than countrate-processing algorithm outputs, as originally intended). It is not mathematically legitimate to simply replace the instantaneous countrates in eqn(15) with the averages from the ISO method. The countrates in eqn(15) are at the endpoints of the averaging interval (t_1 to t_3), while the average countrates occur (i.e., match the actual time-dependent countrate value) somewhere inside that interval. What is needed is some relation between the difference of the *endpoint* countrates and the difference of the *average* countrates.

Once again, the linear-countrate assumption saves the day. With this, it can be shown by a geometric/algebraic development very similar to what was done in the derivative section above, that

$$\dot{C}(t_3) - \dot{C}(t_1) = 2 \left[\frac{C_2}{\eta} - \frac{C_1}{\eta} \right],$$

and this says that, for a linearly-varying countrate, the difference of the endpoint countrates is twice the difference of the average countrates. Using this in eqn(15) and rearranging,

$$\bar{Q} \approx \frac{C_2 \left(\frac{1}{\eta} + \frac{\lambda}{2} \right) - C_1 \left(\frac{1}{\eta} - \frac{\lambda}{2} \right)}{\bar{\varepsilon}\, k\, F_m\, \phi\, \eta} \,, \tag{16}$$

which looks very much like eqn(10). However, it is important to note that with this Rb-88-method interpretation of the ISO method, the estimator eqn(16) is for the *average* concentration over the interval t_1 to t_3 . In eqn(10) the interpretation was of a *point* estimate at time t_2. Finally, the uncertainty and autocorrelation aspects discussed in the previous section also apply here; all that has changed is the interpretation of the concentration estimator.

Derivation Using the "Eberline" Equation

The ISO use of integrated counts brings to mind eqn(30) of Evans 2001b, the "Eberline" concentration estimation method, which provides an estimate of the concentration given by

$$\hat{Q}_0 = \frac{\lambda^2\, C(\eta)}{\varepsilon\, k\, F_m\, \phi \left\{ \lambda\eta - \left[1 - \exp(-\lambda\eta) \right] \right\}} \,,$$

where $C(\eta)$ is the integrated count during the interval η. This approach uses resets of the system every so often, based on a control law. That is, the fixed filter is advanced and the calculations are reset. The ISO method uses differencing rather than resetting. The question is, could the Eberline equation function correctly if the filter was not advanced, and differencing was used?

The Eberline method assumes a constant concentration over the integration interval; since that interval is usually relatively short, this assumption is reasonable in some applications. As was demonstrated in the reference this approach can estimate time-varying concentrations quite well. Applying the mathematics of eqn(30) to the ISO situation, that is, using *differencing* of

integrated counts rather than the *resetting* that was the original design, results, after considerable effort, in the concentration estimator at time t_3 (again, this is the current time):

$$\hat{Q}_0(t_3) = \frac{\lambda^2 \left[C_2 - C_1\right]}{\overline{\varepsilon}\, k\, F_m\, \phi\, e^{-\lambda t_3} \left[1 + e^{\lambda\eta}\left(e^{\lambda\eta} - 2\right)\right]}\ , \tag{17}$$

and for LL activity (taking the limit as λ approaches zero) this is

$$\hat{Q}_0(t_3) = \frac{C_2 - C_1}{\overline{\varepsilon}\, k\, F_m\, \phi\, \eta^2}\ .$$

This is indeed eqn(1), now with the interpretation of a constant concentration, held constant over the integration interval. However, when implemented in a simulation eqn(17) fails for SL activity, since the countrate can reach equilibrium, remaining constant, so that the successive count differences are zero. This does not happen in eqn(10) or eqn(16), due to the multiplicative factors in the numerators. Thus this interpretation of the ISO method will indicate a zero concentration when the actual concentration is nonzero, which is of course unacceptable. It is therefore concluded, due to this lack of generality, that the Eberline method operated in a "differencing" mode does not provide an acceptable interpretation of the ISO calculation.

Countrate Curvature

The assumption of (approximate) linearity of the countrate was necessary in the developments above. Since the countrate of a fixed-filter monitor is the output of a first-order system, whose forcing function (i.e., the concentration) is itself usually the response of a low-order compartmental system, and thus mathematically "smooth," it could be expected that the countrate would in general also be a mathematically-smooth function of time. Such functions can be well approximated by a linear expansion over (relatively) small time intervals. These intervals need not be differentials, that is, extremely small; intervals on the order of a few minutes are acceptably small if the function (countrate) is reasonably smooth.

It has long been observed in CPAM mathematical modeling that countrate traces (graphs) do not show abrupt changes or discontinuities. See, for example, Figs. 9-15 in Evans 2001a or Figs. 4, 12, 13 of Evans 2002. In fact, for LL activity, the trace cannot decrease, and is usually a smooth (often linear) increase, or it may reach a limiting value and then remain constant. A countrate increase may be quite rapid, but it is still essentially linear. Thus, for LL activity the assumption of nearly linear countrate traces over modestly-sized time intervals (up to, say, 10 or 15 minutes) is entirely reasonable.

For SL activity, some concentration profiles do result in a countrate "peak," where there is a definite curvature of the countrate trace. However, this maximum does not often occur over very short time intervals, so that a linear approximation is still plausible; see Fig. 2. Even if there is significant curvature in the SL-peak case, the only implication is that the concentration estimates near the peak will be incorrect, if the concentration-estimation integration interval is too large. This estimation bias likely would be overwhelmed by the uncertainty of the estimate. In any case, even if there is some bias in these situations, there is no known regulatory, nor practical, requirement to track time-varying concentrations to a high degree of accuracy.

One way to demonstrate the reasonableness of this local-linearity assumption is simply to show that the modified method does produce remarkably good concentration estimates for physically-plausible concentration profiles, especially those that are continuously changing. This good performance should not be possible unless the conditions under which the method was derived were met, and that of course includes the countrate linearity assumption. Such demonstrations will be presented in the next section.

Example Plots

The numerical simulation discussed in Evans 2001a was adapted to include the ISO calculation, for testing purposes. This simulation finds the monitor responses by solving sets of differential equations; it does not use the analytical models presented in that reference; in fact, it was created as an independent test of those analytical solutions. This interactive simulation permits the adjustment of a variety of parameters, especially those controlling the concentration profile.

The simulation handles activity of any half-life, and for SL activity Rb-88 is generally used (18 minute half-life) since this is a commonly-occurring particulate fission product. The simulation also produces plots of the integrated counts as they accumulate, and plots of the actual monitor countrate (these are not presented here). The simulation runs at a small time step, intended to emulate a digital monitor; five seconds is the usual setting. Poisson "noise" can optionally be added to the counting data.

The plotted output includes the concentration estimate, its "error bar" (plus/minus one sigma), a short line behind the point, indicating the period over which the averaging was done, i.e., the integration intervals, and a short line ahead of the point indicating the time during which that estimate applies, until the next one becomes available. Also shown are the plus/minus "two-sigma" bounds that result from using the known concentration level and the known (noise-free) counts with the square root of the variance expression, eqn(11).

For testing the ISO method, two basic concentration profiles were used: (1) an exponential decrease from an initial value; (2) the concentration behavior in a single compartment with first-order losses and constant-level sources turning on and off at two different times (Evans 2002). Adjustments of these profiles produced a wide variety of test situations, against which the ISO method was exercised. In no case did the method fail to produce reasonable estimates of the time-dependent concentration. In short, it performed remarkably well.

Figure 8 shows deterministic (no Poisson noise in the counts) concentration estimates for the compartmental system, for LL activity. There are two source "events," illustrated by the rectangles at the bottom of the plot. These sources are scaled arbitrarily to fit onto the plot region, although their relative heights are proportional to their input levels. These sources are active for relatively long times, in order to allow the concentration profile to develop.

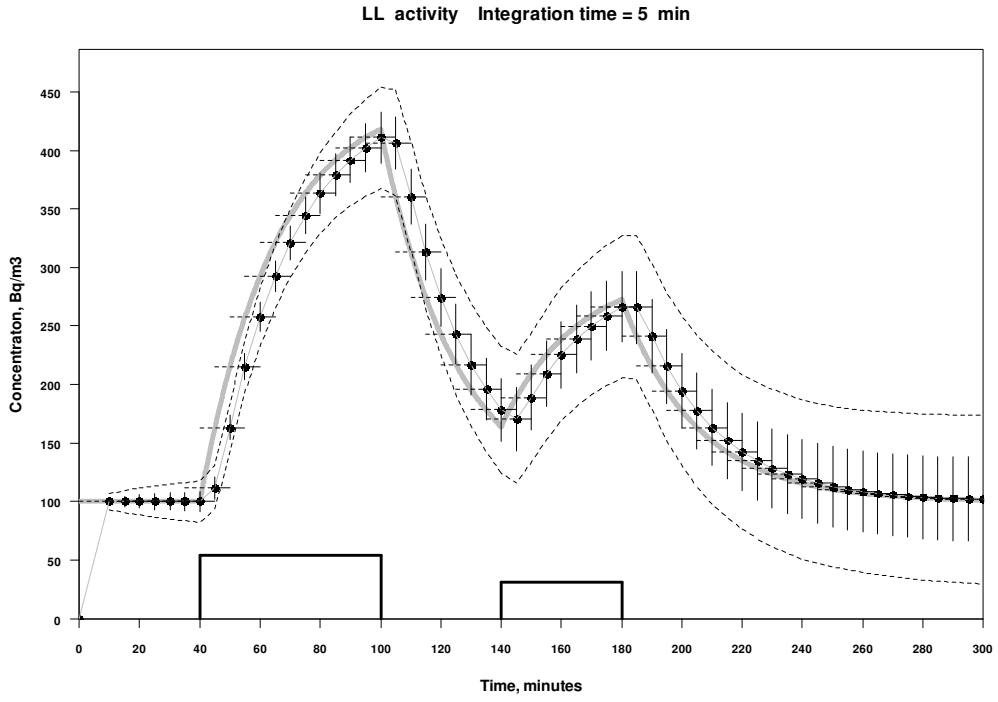

Fig. 8 Simulation output for a single-compartment system, driven by an intermittent source term (rectangles). This no-noise run shows the tracking ability of the estimation. Note that, although the source term is a "square wave" the resulting concentration time-dependence in the monitored compartment is exponential. The source rectangles are scaled arbitrarily to fit on the plot, but have correct relative heights.

One interpretation of this situation, if the source-active times were much shorter than in this figure, might be the sudden lifting of a pressure relief valve, which stays open for some time, and then abruptly closes. As the pressure builds up again, this could

be repeated many times. The rate at which activity is injected into the compartment could remain constant while the valve is open. The point is that even though the source term driving the concentration behavior in the compartment is discontinuous and could be considered a "square wave," the resulting concentration in the compartment is continuous and will be defined by sums of exponentials.

In Figure 9 is the same situation, but with Poisson variability added to the counts. Note that the variability of the estimates increases with time. Figure 10 shows this situation for SL activity, ^{88}Rb. In this case, the decay of the ^{88}Rb acts as another first-order loss term, in addition to those for HVAC dilution/filtration and plateout. Thus the system reaches equilibrium faster, and also the rate of removal is faster. Note also that the 95% bounds are narrower and they do not increase in width with time, unlike those in Figs. 8 and 9. The increase of these bounds toward their limit, given in eqn(13), can just be seen at the early part of the run. The width of the bounds remains constant after about 120 minutes.

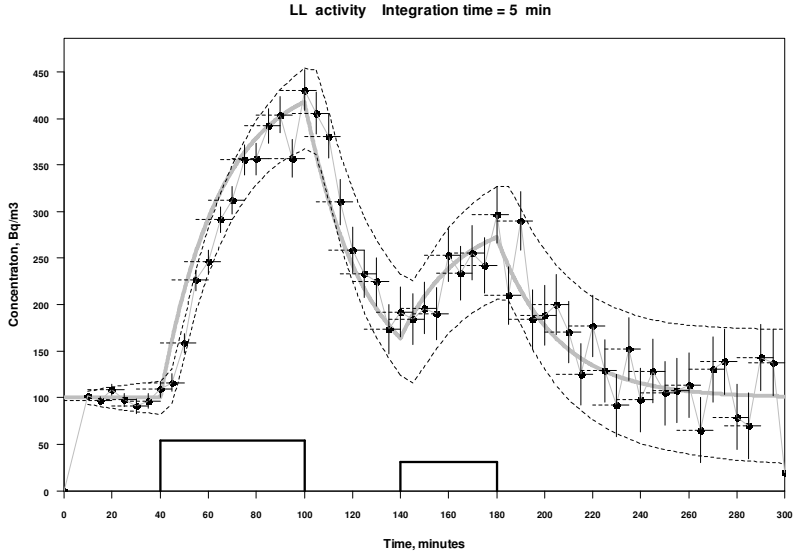

Fig. 9 Same setup as Fig. 8, but with Poisson noise added.

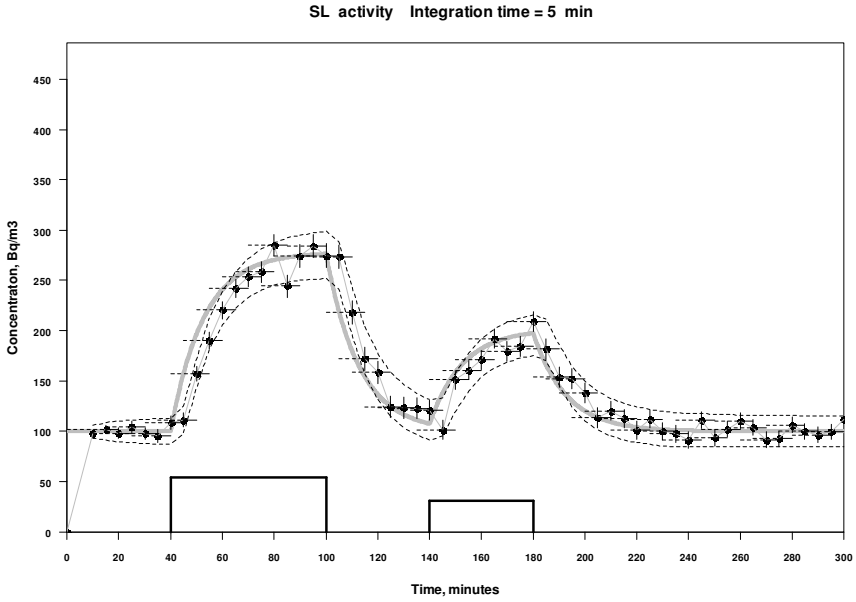

Fig. 10 Also the same setup as Fig. 8 but for SL (Rb-88) activity. Note that decay is a loss term from the compartment, so that the buildup and decrease of the concentration are both faster than when only other first-order losses (e.g. dilution, plateout) are considered.

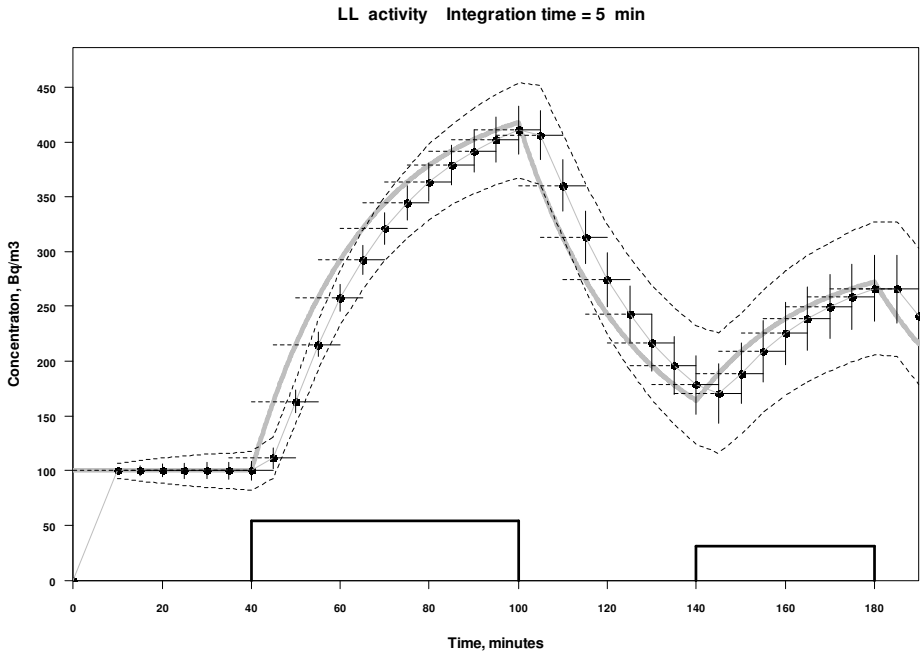

Fig. 11 The same case as Fig. 8, but an expanded view. It can be seen that the average concentration, at the midpoint of the averaging interval (horizontal dashed line segments), is nearly equal to the concentration at that same time.

Figure 11 is the same as Fig. 8, but zoomed in to see the behavior of the estimates more clearly. It can be seen that the average value of the concentration over the interval shown by the dashed horizontal lines nearly matches the level of the concentration at the midpoint of the averaging interval. This effect has been observed in many test runs and other mathematical analyses. It appears to result from the fact that, similar to the countrate, the concentration is essentially linear over reasonably short time intervals. However, the implication of this is that the current estimate of the average concentration over the last (e.g.) ten minutes was the actual concentration five minutes ago. It is not clear that this information, while interesting, has any practical use.

Conclusion

It has been shown that a relatively simple calculation such as the ISO approach for estimating a concentration from a fixed-filter CPAM response can lead to several different interpretations. This estimator might be considered a new "quantitative method," but it appears that it is not, since it can be derived from other, previously-published methods. The difference is in the implementation, notably the use of simple countrate integration (and, implicitly, averaging) rather than the estimation of an "instantaneous" countrate via digital signal processing. The latter approach is especially appealing today, with so much computing power readily available and affordable.

After applying the modification that permits the estimation of concentrations for SL activity, considerable exercising of this method in simulation studies has shown that there is no doubt that the method works. However, these studies also demonstrated that this method produces concentration estimates that are strongly autocorrelated, and for which the variance increases with time elapsed since the filter was changed (LL activity). These are not desirable properties.

Again assuming that it is for some reason important to attempt to track a time-varying concentration, rather than directly estimate its time integral, further work will need to be done to optimize the integration-time parameter of the calculation. This will need to consider the usual tradeoff of response time against some form of variance reduction. The latter can be done with what amounts to finite impulse response (FIR) filtering; this combines several concentration observations into a new concentration estimate (Lu and Whicker 2008).

Another approach is to use infinite impulse response (IIR) filtering; this is recursive, such as the exponentially weighted moving average (EWMA) or its adaptive version (AEWMA), both discussed in Evans 2001b. There, this filtering was applied to countrate estimation, but it can just as well be used for variance reduction of the concentration estimates. In fact, the EWMA filtering approach has been implemented and tested on the ISO method, and it does work as expected. The variance of the concentration estimates is reduced, which is particularly useful at shorter integration times, but this is at the price of lagging a changing concentration profile.

Which form of filtering will work best, and with what filter parameters, with simultaneous regard to transient response and variance reduction, remains to be studied. One approach to this study might be to use a root-mean-square error measure; this would reflect both bias (violation of assumptions; lag) and statistical variability. Such tests should use physically-reasonable concentration profiles, notably, those with continuously-changing concentrations.

Based on the work reported here the ISO calculation can be interpreted in the following ways:

(1) as a point estimate of the concentration at the endpoint of the second integration interval;
(2) as a point estimate of the concentration at the midpoint of the two integration intervals ;
(3) as an average concentration across both integration intervals;
(4) as an estimate of a constant concentration across both integration intervals.

Of these the most appealing is (3), since the idea of averaging a time-dependent concentration across an interval of perhaps tens of minutes seems more reasonable than assigning a concentration value to one specific time point in that interval, or of assuming it to be constant over the interval. The averaging approach, or interpretation, only requires the countrate over the integration intervals to be (nearly) linear, and this is not a particularly limiting assumption.

The usefulness of a concentration-tracking ability, as evidenced for the ISO method in Figs. 8-11, would be in the dynamic estimation of personnel inhalation uptake, especially in circumstances where the concentration is changing significantly during the worker's exposure. The idea is to use the monitor to control the uptake during the episode rather than assess the uptake after the fact. The ISO concentration estimates generated (e.g., every 5 min) are to be multiplied by the counting time and summed in what amounts to a numerical integration, the result of which will be proportional to the worker's inhalation uptake.

However, in eqn(19) of Evans 2001b we have a direct-integration alternative to the ISO numerical method, for a dynamic, real-time estimate of worker uptake $U(t)$ at any time t after an arbitrary start time t_1, with constant breathing rate F_b, namely

$$U(t) = F_b \int_{t_1}^{t} Q(\tau)\, d\tau = \frac{\dot{C}(t) - \dot{C}(t_1) + \lambda \int_{t_1}^{t} \dot{C}(\tau)\, d\tau}{\varepsilon\, k\, F_m\, \phi}$$

This says that all that is needed to estimate the uptake that has been integrated from some start time up to the current time is to subtract the (net) countrate at the start time from that at the current time t, and, for SL activity, also use the total net counts integrated over this time interval. This interval need not be short, it can be of arbitrary length (e.g., a work shift of several hours). Knowledge of the time when any concentration transients started or ended, or their profile, is not required. The start time t_1 could, but need not, coincide with a clean-filter restart of the monitor.

A comparison of these two approaches was briefly explored, and it was demonstrated that both can perform acceptably in terms of tracking ability and variance reduction. The latter was somewhat surprising for the ISO method, since that would involve adding up a large number (e.g. every 5 min over an 8 hr shift is 96 terms) of autocorrelated terms that have variances which increase with time, so that the summation of these terms might be expected to have a very large variance, to the point where the uptake estimate would not be of any practical use. As it happens, this "variance explosion" does not occur, due to a telescoping-series or cancellation effect in the summation, such that the resulting sume amounts to only the first and last terms. In any case, a full exploration and comparison of the uptake-control capabilities of the ISO and above equation methods is beyond the scope of this work and needs further research.

References

Box, GEP; Jenkins, GM; Reinsel, GC Time Series Analysis, Forecasting and Control, 4th Ed. Wiley (2008).

Evans WC. Mathematical models for the dynamic response of continuous particulate air monitors. IEEE Trans Nucl Sci, 48:202-218; 2001a.

Evans WC. Quantitative methods for continuous particulate air monitoring. IEEE Trans Nucl Sci, 48:1639-1657; 2001b.

Evans WC. Concentration dynamics modeling for continuous particulate air monitor response prediction. IEEE Trans Nucl Sci, 49:2574-2598; 2002.

International Standardization Organization (ISO), Determination of the detection limit and decision threshold for ionizing radiation measurement- part 5; Section B.5 Counting measurements on filters during accumulation of radioactive material; Geneva:ISO, ISO Standard 11929-5:2005.

Law, AM; Kelton, WD Simulation Modeling and Analysis, 2nd Ed., McGraw Hill (1991).

Lu, Z.; Whicker, J. Considerations for data processing by continuous air monitors based on accumulation sampling techniques, Health Phys 94:s4-s15, 2008.

Chapter 9

Reactor Coolant Leakage Rate Estimation

Unpublished

Detection of reactor coolant leakage is discussed in Regulatory Guide 1.45, in which it is stated that particulate air monitors are an acceptable method for detecting an increase in coolant leakage rate. In this paper a method is presented for the use of fixed-filter and moving-filter continuous particulate air monitors for not only the detection, but the estimation of the magnitude of increased coolant leakage. Following the standard ISA-67.03-1982, a well-mixed, single-compartment containment is assumed, with a step increase in the coolant leakage rate over some nominal, equilibrium leakage. The ^{88}Kr-^{88}Rb decay chain is used, with the ^{88}Rb observed by either a fixed- or moving-filter monitor. Models are developed for the time-dependent concentrations of these nuclides in containment, and from those the countrate responses of these monitors are found. The countrate models are in turn used to estimate the leakage rate from the observed monitor response, once a threshold has been crossed, using nonlinear estimation. The threshold (setpoint) calculation takes into account the autocorrelated nature of countrate data. A simulation study was performed, using a prototype implementation of these concepts, and the leakage rate was found to be estimated to within about 20% for leakage rates varying from 0.1 to 1.5 gpm, with a delay time of about 20 minutes after the threshold crossing.

Introduction

This chapter concerns the use of RW CPAMs for Kr-Rb leak detection. Mainly, can the leak rate be estimated from observed cpm, esp for RW? This is the Reg Guide 1.45 situation- a leak of ^{88}Kr into containment, at some leakage rate, with some primary coolant concentration. The ^{88}Kr decays to ^{88}Rb in the air, and no ^{88}Rb is directly released. Note that this same pathway can be the case for ^{137}Cs and ^{138}Cs (Xe precursors). So when we say Kr-Rb here, it could also be Xe-Cs. The first step is to find the dynamic behavior of the containment ^{88}Rb for this situation; then that is used to "drive" the RW monitor. Linear systems modeling is used for the concentration dynamics. Laplace transforms could be used to find the FF response, but it will be contained in the RW response.

Rb_{eff} is the "effective" removal rate for ^{88}Rb, including decay, plateout, and filtration. S_{Kr} is the source term of ^{88}Kr; the leak rate times the coolant concentration times the partition factor. The Q_{Rb} found is then the $\mathbf{u}(\tau)$ for the RW $t \le L / v$ countrate solution (this assumes no countrate contribution from the Kr). If there is no Rb loss other than decay, a separate solution is required. The matrix exponential solution will find this directly; the **A** matrix will be different for this case but the rest of the solution steps are the same.

Source (Concentration) Modeling

Linear Systems Approach: Single Compartment

Assume a reactor coolant liquid leak that "instantaneously" mixes uniformly into a single-compartment containment volume, with a recirculating filtration HVAC operating. The ordinary differential equations (ODE) that govern the Kr-Rb system are

$$\begin{aligned} \frac{d\alpha_{Kr}}{dt} &= \Gamma q_{Kr} \psi_{Kr} - \lambda_{Kr}\alpha_{Kr} - \rho_{Kr}\alpha_{Kr} - \Theta_{Kr}\frac{f_H}{V}\alpha_{Kr} \\ \frac{d\alpha_{Rb}}{dt} &= \Gamma q_{Rb} \psi_{Rb} + \lambda_{Rb}\alpha_{Kr} - \lambda_{Rb}\alpha_{Rb} - \rho_{Rb}\alpha_{Rb} - \Theta_{Rb}\frac{f_H}{V}\alpha_{Rb} \end{aligned} \quad (1)$$

where:

- α activity, Bq;
- Γ liquid leakage rate, m^3/min;
- q reactor coolant concentration, Bq/m^3;
- ψ partition factor (fraction of activity in liquid phase that becomes airborne);

λ decay constant, min^{-1};
ρ plateout factor (fraction of airborne activity that deposits on surfaces);
Θ filtration efficiency;
f_H HVAC recirculation volumetric flow rate, m^3/min;
V containment free-air volume, m^3

Under uniform mixing, the concentrations $Q(t)$ are just these activities $\alpha(t)$ divided by the volume V. Clearly, instantaneous mixing is not physically possible; in fact the time-dependent concentration for a single well-mixed compartment would follow an exponential buildup, controlled by the air exchange rate of the HVAC recirculation. However, for the present purpose, this initial mixing-time delay will be ignored.

The next step is to recognize that some of the parameters in the general eqn(1) are either exactly or effectively zero. These parameters are: (1) the plateout rate of Kr; (2) the filtration efficiency of Kr; (3) the partition factor of Rb, which does not become airborne directly from the liquid. Then the system can be re-written as

$$\begin{aligned} \frac{d\alpha_{Kr}}{dt} &= \Gamma q_{Kr} \psi_{Kr} - \lambda_{Kr}\alpha_{Kr} \\ \frac{d\alpha_{Rb}}{dt} &= \lambda_{Rb}\alpha_{Kr} - \lambda_{Rb}\alpha_{Rb} - \rho_{Rb}\alpha_{Rb} - \Theta_{Rb}\frac{f_H}{V}\alpha_{Rb} \end{aligned} \tag{2}$$

The first-order loss terms for Rb can be collected into a single parameter:

$$\lambda_{Rbeff} = \lambda_{Rb} + \rho_{Rb} + \Theta_{Rb}\frac{f_H}{V}$$

and then we have the ODE system

$$\begin{aligned} \frac{d\alpha_{Kr}}{dt} &= \Gamma q_{Kr} \psi_{Kr} - \lambda_{Kr}\alpha_{Kr} \\ \frac{d\alpha_{Rb}}{dt} &= \lambda_{Rb}\alpha_{Kr} - \lambda_{Rbeff}\alpha_{Rb} \end{aligned}$$

There are many ways to solve these equations; the linear-systems approach is particularly useful. The ODE are expressed in a matrix-vector format as follows:

$$\frac{d}{dt}\boldsymbol{\alpha} = \mathbf{A}\boldsymbol{\alpha} + \mathbf{B}\mathbf{u}; \qquad \mathbf{A} = \begin{pmatrix} -\lambda_{Kr} & 0 \\ \lambda_{Rb} & -\lambda_{Rbeff} \end{pmatrix}$$

$$\mathbf{B} = \begin{pmatrix} 1 & 0 \\ 0 & 1 \end{pmatrix} \qquad \mathbf{u} = \begin{pmatrix} \Gamma q_{Kr} \psi_{Kr} \\ 0 \end{pmatrix}$$

A solution for the time-dependent activity vector $\boldsymbol{\alpha}$ can then be found using the matrix exponential

$$\boldsymbol{\alpha}(\tau) = \int_0^{\tau} e^{\mathbf{A}(\tau-\kappa)}\mathbf{B}\mathbf{u}\, d\kappa \tag{3}$$

where the time variable is τ, for use in the countrate solution integrals, below. Solving this yields the time-dependent activities

$$\boldsymbol{\alpha}(\tau) = \Gamma q_{Kr} \psi_{Kr} \begin{pmatrix} \dfrac{1-e^{-\lambda_{Kr}\tau}}{\lambda_{Kr}} \\ \lambda_{Rb}\left(\dfrac{1}{\lambda_{Kr}\lambda_{Rbeff}} + \dfrac{e^{-\lambda_{Kr}\tau}}{\lambda_{Kr}(\lambda_{Kr}-\lambda_{Rbeff})} - \dfrac{e^{-\lambda_{Rbeff}\tau}}{\lambda_{Rbeff}(\lambda_{Kr}-\lambda_{Rbeff})} \right) \end{pmatrix} \tag{4}$$

If there should be a situation where there is no Rb loss other than decay, then we would have $\lambda_{Rbeff} = \lambda_{Rb}$, and the activity solutions become

$$\boldsymbol{\alpha}_0(\tau) = \Gamma q_{Kr} \psi_{Kr} \begin{pmatrix} \dfrac{1-e^{-\lambda_{Kr}\tau}}{\lambda_{Kr}} \\ \left(\dfrac{1}{\lambda_{Kr}} + \dfrac{\lambda_{Rb}\, e^{-\lambda_{Kr}\tau}}{\lambda_{Kr}(\lambda_{Kr}-\lambda_{Rb})} - \dfrac{e^{-\lambda_{Rb}\tau}}{(\lambda_{Kr}-\lambda_{Rb})}\right) \end{pmatrix} \tag{5}$$

The time derivatives of the activities in eqn(4) are

$$\frac{d}{d\tau}\boldsymbol{\alpha}(\tau) = \Gamma\ q_{Kr}\ \psi_{Kr} \begin{pmatrix} e^{-\lambda_{Kr}\tau} \\ \dfrac{\lambda_{Rb}}{\lambda_{Kr}-\lambda_{Rbeff}}\left(e^{-\lambda_{Rbeff}\tau} - e^{-\lambda_{Kr}\tau}\right) \end{pmatrix} \tag{6}$$

from which we see that, at time zero, when the leakage begins (or begins at a new, higher level), the initial slope of the Kr activity is positive, while that of the Rb is zero. Also of interest is the long-term equilibrium attained, assuming that the leakage rate and coolant concentrations both remain constant over a long period; if this is this case, then

$$\boldsymbol{\alpha}\left(\tau \to \infty\right) = -\mathbf{A}^{-1}\mathbf{B}\mathbf{u} = \Gamma\ q_{Kr}\ \psi_{Kr} \begin{pmatrix} \dfrac{1}{\lambda_{Kr}} \\ \dfrac{\lambda_{Rb}}{\lambda_{Kr}\,\lambda_{Rbeff}} \end{pmatrix} \tag{7}$$

In the decay-only case, the equilibrium activities are of course equal. Figure 1 shows the time-dependent concentrations of Kr and Rb for a constant source term; the dashed lines are the equilibrium values just found. Note that it takes many (about twenty) hours to attain equilibrium.

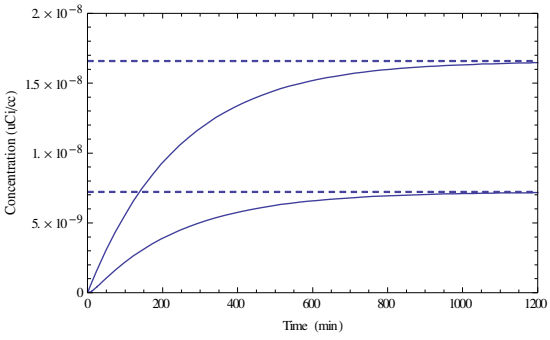

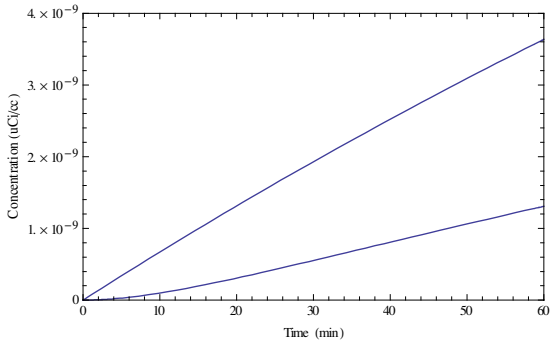

Figure 1 (left): Concentrations for a 0.5 gpm leakage rate, 0.001 uCi/cc coolant Kr concentration, partition factor unity, Rb_{eff} 0.05 larger than λ_{Rb} , containment volume 10^6 ft^3. The top curve is Kr. Dotted lines are the long-term equilibria. Figure 2 (right); an expanded view of the first hour of this time-dependent variation in the concentrations. The Rb has a zero initial slope, and is clearly in no way at any sort of equilibrium value in this first hour, as required in RG1.45. (The initial Kr mixing time into the containment air, ignored here, would delay this even further.)

Linear Systems Approach: Two Compartments

This section needs filling out, in a later edition- this is a placeholder for now. Likely just Mathematica code, these will be very complicated solutions. Here is the system matrix; 2 nuclides in 2 compartments, so a 4x4 system.

$$\mathbf{A} = \begin{pmatrix} -\lambda_{Kr}-k_{21} & k_{12} & 0 & 0 \\ k_{21} & -\lambda_{Kr}-k_{12} & 0 & 0 \\ \lambda_{Rb} & 0 & -\lambda_{Rb_{eff}} & k_{12} \\ 0 & \lambda_{Rb} & k_{21} & -\lambda_{Rb}-k_{12} \end{pmatrix}$$

Standard ISA-S67.03-1982

This document, "Standard for Light Water Reactor Coolant Pressure Boundary Leak Detection," asserts that it covers "identification and quantitative measurement of reactor coolant system leakage...". In section 7.2.1(a) it is stated that "Sufficient data and understanding of the principles are needed to properly interpret an increase in radiation monitor readout in terms of coolant leakage." However, no guidance is given on how one would in fact go about this interpretation.

Realizing that standards are not prescriptive, nonetheless there should be a requirement that however this interpretation is to be done, the methodology involved must be well-documented. An example of how to do this interpretation could be presented in an Appendix, to provide some guidance as to acceptable methods.

Further, in section 7.2.1(c)(2) it is said that "only Rb-88 which is in secular equilibrium with its parent isotope Kr-88 need be considered." It is not clear if this means equilibrium in the coolant or the air. Since, upon a leak, Rb is not released directly to the air, its concentration in the coolant is irrelevant. It attains equilibrium in the air, with its only source being the decay of Kr-88, after many hours.

This standard, in its Appendix B.3.1, has the following differential equation, for a single radioisotope; written in the present notation,

$$\frac{1}{V}\frac{d\alpha}{dt} = \Gamma q \; - \lambda \alpha V - \rho \Gamma \; q - \phi \alpha \tag{8}$$

with ϕ a "purge rate" for containment dilution, zero if there is no dilution. This equation appears to be incorrect, in that: (1) there is no partition factor in the source term; (2) the plateout factor is incorrectly applied to the source term rather than the airborne activity α; (3) there is no term accounting for HVAC recirculation and filtration. *Most fundamentally, the Kr-Rb leakage detection problem requires* ***two*** *differential equations.*

A solution is presented in this appendix for the "activity concentration in the containment atmosphere as a function of time..." which "may be used to estimate the radioactivity transient in the containment atmosphere" in order to "form the basis for estimating monitor response to a leak." It is not defined how one is to use this (incorrect) solution for a time-dependent concentration to estimate the monitor response. Doing so would require the use of the mathematical models for monitor response published in [1], some twenty years after this standard was released. And, even if one had the monitor response models, and thus could estimate the monitor response, how then would one estimate the leakage rate?

RG1.45 says that "it is important to quantify the reactor coolant leakage" and, again, "the ability to quantify the leakage rate is important" but this standard provides no guidance on how to go about accomplishing that. RG1.45 goes on to say "However, signals from other leakage monitoring systems [e.g., air monitors] may not readily convert to a leakage rate." Providing such a conversion method, for leakage rate estimation using air monitors, is the purpose of this paper.

Source Behavior

This is a placeholder, to be completed in later editions.

Monitor Response Modeling

Moving-Filter Countrate Model

Models for predicting the time-dependent response of moving- and fixed-filter continuous particulate air monitors were developed in [1]. What is required for a solution is to have a mathematical representation of the time-dependent concentration that drives the monitor response. In the general application of air monitors, the concentration time dependence is not known, but for the Kr-Rb in containment situation, we do have this knowledge.

A moving-filter monitor response has two parts; one before the "transit time" (T) and another after this time, which is the time required for a differential filter element to traverse the entire length L of the deposition/detection window. With a filter speed v, this is just $T = L / v$, and is typically about two hours. In [1] it was shown that the activities on the monitor filter are given by

$$\alpha_{RW}(t \le T) = \frac{k F \phi}{L}\left[\int_0^{vt}\int_{t-\frac{x}{v}}^{t} Q_{Rb}(\tau)\, e^{-\lambda_{Rb}(t-\tau)}\, d\tau\, dx + \int_{vt}^{L}\int_0^{t} Q_{Rb}(\tau)\, e^{-\lambda_{Rb}(t-\tau)}\, d\tau\, dx\right] \tag{9}$$

$$\alpha_{RW}(t \ge T) = \frac{k F \phi}{L}\int_0^{L}\int_{t-\frac{x}{v}}^{t} Q_{Rb}(\tau)\, e^{-\lambda_{Rb}(t-\tau)}\, d\tau\, dx \tag{10}$$

where F is the monitor flow rate, φ is a collection efficiency (including a line-loss fraction), and k is a units reconciliation constant. Then the countrate is obtained from

$$\dot{C}_{RW}(t) = \varepsilon_{Rb}\ \gamma_{Rb}\, \alpha_{RW}(t) \tag{11}$$

where ε is the detection efficiency and γ is the abundance of the emission being counted. Here RW stands for "rectangular window." It was shown in [1] that a good approximation for the circular window (CW; window radius R) response is obtained by using the "effective" window length

$$L_{CW} = \frac{16R}{3\pi} \tag{12}$$

in the RW solutions. Fixed-filter (FF) countrates are found by using a filter speed of zero ($v=0$) in the RW $t<T$ solutions. Thus, one solution method contains results for all three monitor types.

Since Kr is not collected on the particulate filter medium, the monitor response will be due only to the Rb, and we have its concentration in the second element in eqn(4), after dividing by the containment free-air volume V. Using that expression in the multiple integrals above yields the $t \le T$ solution, 4.8.2 in Chapter 7, and for $t \ge T$, 4.8.3 therein; the FF response is 4.8.4. For the case when there is no Rb loss other than decay, separate solutions are needed. These are, for $t \le T$, 4.8.5; $t \ge T$, 4.8.6, and for the FF case, 4.8.7.

The long-term equilibrium expressions are, for RW:

$$\dot{C}_{Rb}(t \to \infty) = \frac{\varepsilon_{Rb}\, \gamma_{Rb}\, k\, F\, \phi \Gamma\, q_{Kr}\, \psi_{Kr}}{\lambda_{Kr}\, \lambda_{Rb_{eff}}\, V}\left(1 - \frac{v}{\lambda_{Rb} L}\left[1 - e^{-\lambda_{Rb}\frac{L}{v}}\right]\right) \tag{13}$$

and for FF,

$$\dot{C}_{Rb}(t \to \infty) = \frac{\varepsilon_{Rb}\, \gamma_{Rb}\, k\, F\, \phi \Gamma\, q_{Kr}\, \psi_{Kr}}{\lambda_{Kr}\, \lambda_{Rb_{eff}}\, V} = \frac{\varepsilon_{Rb}\, \gamma_{Rb}\, k\, F\, \phi}{\lambda_{Rb}} Q_{Rb}\left(t \to \infty\right) \tag{14}$$

which are equivalent to 4.8.9, 4.8.10. For the decay-only case, use λ_{Rb} for λ_{Rbeff}.

ISA Calibration Issues

In Appendix B.3.4(c) a process termed a "calibration" is discussed. Item (3) states that this calibration should include "introducing a laboratory-calibrated concentration of the reference or control isotope into the sampler, and recording the counting rate above background." This seems to be confusing a volumetric monitor, such as a liquid or noble gas monitor, with the integrating particulate monitors. It is not explicitly stated which kind of monitor is being calibrated. There is also no discussion of fixed vs. moving filters for the particulate monitors, nor how the calibration procedure would differ for these, nor how to handle the time-dependent response of these monitors (see below).

There is one sentence in paragraph (c) that says "Aerosol detectors are calibrated by cross-referenced standards." There is no further discussion of what this means, or what, exactly, the calibration procedure would be. The remaining material seems to apply only to volumetric monitors, but this is not explicitly stated. There is a requirement that "A plot of the concentration of the reference isotope in terms of micro-curies/cc versus the net counting rate produced should then be drawn on log-log scales. This plot should be used as a calibration curve in the field." Such a curve would only apply to volumetric monitors; *this curve has no meaning for particulate air monitors*, especially as applied to the Kr-Rb leakage detection/measurement problem.

A correct calibration process for the particulate monitors would at least consist of choosing a quantitative method, often based on inverting a monitor response model, and the estimation of the instrumental parameters required by that model, notably the detection efficiency as a function of energy, so that an interpolating function can be found. This latter is, apparently, what is implied by the term "cross-calibration" in the footnote "These referenced isotopes [Cs-137 for particulate monitors] are used for instrument calibration, therefore, monitor sensitivity should be cross-calibrated to the isotopes listed in Paragraph 7.2.1(c) [for particulate monitors, Rb88]."

The energy dependence of the monitor detection efficiency should be defined by a mathematical interpolating function, based on direct measurements of the detection efficiency over the range of energies appropriate for the monitoring application. The interpolating function should be estimated using regression techniques, rather than by drawing a "curve" on a piece of graph paper, and should include parameter and prediction (interpolation) uncertainties. The detection efficiencies can be measured by depositing a calibrated, traceable level of activity of the selected nuclide onto a matrix that is similar in properties to the monitor collection (filter) medium.

As the standard reads, it would appear that we are to feed a known airborne concentration of, e.g., Cs137 to the particulate monitor, and observe its response. But that response is not a single value, it is time-dependent. The actual response for RW for a constant concentration is, for $t<T$, for a nuclide of any half-life (these relations are given in Section 4.1 of Chapter 7, repeated here for convenience),

$$\dot{C}_{RW}(t) = \frac{\varepsilon \gamma k F \phi Q}{\lambda}\left[\left(1-\frac{vt}{L}\right)\left(1-e^{-\lambda t}\right) + \frac{v}{\lambda_{Rb} L}\left(\lambda t - 1 + e^{-\lambda t}\right) \right] \tag{15}$$

and for $t>T$

$$\dot{C}_{RW}(t) = \frac{\varepsilon \gamma k F \phi Q}{\lambda}\left[1 - \frac{v}{\lambda L}\left(1 - e^{-\lambda \frac{L}{v}}\right)\right] \tag{16}$$

The limit of these as λ becomes small (LL) for $t< T$

$$\dot{C}_{RW}(t) = \varepsilon \gamma k F \phi Q\left(t - \frac{vt^2}{2L}\right) \tag{17}$$

and for $t>T$

$$\dot{C}_{RW}(t) = \varepsilon \gamma k F \phi Q \frac{L}{2v} \tag{18}$$

These are plotted in Fig 3.

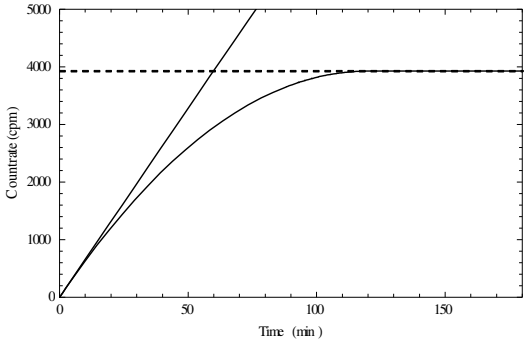

Figure 3. Response of FF (straight line) and RW to constant, LL input. Limiting cpm, dashed line.

It is true that an RW monitor will attain a limiting countrate, when driven by a constant concentration (dashed line in Fig 3). One could plot that single countrate vs. several input concentrations, assuming that such a particulate concentration generation was available. But it is not the case that the net countrate can be read off the monitor, at any time, and that countrate be converted to a concentration estimate. Such "calibration curves," as discussed in the standard, have been around for many years.

The implication is that an instantaneous net countrate is proportional to the concentration that exists at the time of the reading. This is not valid, for either FF or RW monitors. (See Chapter 5.) The fundamental issue with this portion of the standard is that it does not make clear what kind of monitor is being calibrated, and it in fact has no useful information on how to go about calibrating a particulate monitor for *any* purpose, much less specifically for the Kr-Rb problem.

Estimation of Leakage Rate

Prototype leakage-rate estimation

The basic approach is to "fit" a countrate response model to observed countrate data, and to obtain from that nonlinear regression an estimate of the leakage rate. To test this concept, specific techniques, parameter values, etc., were implemented in a prototype simulation program, and they worked well. However, it is recognized that much of this methodology can be refined and improved for implementation in real-world monitoring systems. What is important here is not the details of the test implementation, but rather the proof of concept; that this overall approach can provide a reasonable estimate of the leakage rate. And of course it must be noted that this estimate is only as good as the fundamental assumptions used in defining the problem.

The leakage rate estimation process is the same for both FF and RW monitors, with the obvious exception of the specific countrate models used. The process begins with an estimate of the assumed-constant baseline countrate, which consists of the sum of the ambient background and the long-term equilibrium countrate, from a constant, nominal (relatively low) leakage rate. Next, the variability of this baseline countrate is estimated, using the observed standard deviation over some time window, corrected for the autocorrelation induced by the EWMA filtering [Anderson, TSA]:

$$\hat{\sigma} = \frac{s_{observed}}{\sqrt{1 - \frac{2}{n-1}\sum_{k=1}^{n}\left\{\left(1-\frac{k}{n}\right)(1-\alpha)^{k}\right\}}} \tag{19}$$

The autocorrelation function for the EWMA is the last term in the summation (see MDC Appendix). With this estimate, an upper bound or threshold is established for the baseline countrate; this is just twice the "sigma" estimate. A simple crossing of this threshold is not a sufficient trigger to start the leakrate estimation process, since EWMA-smoothed data will exhibit pseudo-trends, i.e., runs above or below the mean. Thus, in this prototype it is required that the countrate stay above the threshold for three minutes (30 samples, at 0.1 min per digital time step); optimizing this will of course need further research.

When this condition is met, the next step is to use the radar-filter derivative estimator (see p. 2-5) to find an approximation for the start time. This is done by taking an average of five rate estimates on either side of the threshold-crossing time, and then "walking this down" the derivative vs. time curve until this average rate is near zero. (Recall that the initial slope of the countrate response is zero.) When the rate appears to be near zero, a correction is applied to account for the lag of the radar filter, and the result is an initial estimate of the start time.

With this start-time estimate, bounds are defined to create a dataset for the regression. The lower bound is the estimated start time minus a time step of about seven minutes, to provide some data *before* the start, for estimating the baseline. The upper bound is about 20 minutes above the start time. This, in a real system, would be a wait time, after the threshold was crossed. A longer window of data would help the regression, but would increase the wait time. In simulation studies, 20 minutes was a reasonable compromise; this, again, needs further investigation.

With the bounds defined, the regression dataset is assembled. The model to be estimated from this dataset is

$$\dot{C}_{RW} = \Gamma\, q_{Kr}\, \psi_{Kr}\, k_1 \left\{ \begin{array}{l} \left(1 - \dfrac{v\,(t-t_0)}{L}\right)\left(a_1 + a_2\, e^{-\lambda_{Rbeff}(t-t_0)} + a_3\, e^{-\lambda_{Rb}(t-t_0)} + a_4\, e^{-\lambda_{Kr}(t-t_0)}\right) \\ + \dfrac{v}{\lambda_{Rb}\, L}\left[\begin{array}{l} a_1\left(\lambda_{Rb}\,(t-t_0)-1\right) + \left(a_5\,(t-t_0)-1\right)a_6\, e^{-\lambda_{Kr}(t-t_0)} \\ + \left(a_7\,(t-t_0)-1\right)a_8\, e^{-\lambda_{Rbeff}(t-t_0)} + a_9\, e^{-\lambda_{Rb}(t-t_0)} \end{array}\right] \end{array} \right\} + \dot{C}_{base} \tag{20}$$

where k_1 and the a are collections of constant parameters, as follows:

$$k_1 \equiv \frac{\varepsilon_{Rb}\,\gamma_{Rb}\,k\,F\,\phi\,q_{Kr}\,\psi_{Kr}}{V} \tag{21}$$

and

$$\begin{aligned}
a_1 &\equiv \frac{1}{\lambda_{Kr}\,\lambda_{Rbeff}} \qquad a_2 \equiv \frac{\lambda_{Rb}}{\lambda_{Rbeff}\left(\lambda_{Kr}-\lambda_{Rbeff}\right)\left(\lambda_{Rb}-\lambda_{Rbeff}\right)} \qquad a_3 \equiv \frac{1}{\left(\lambda_{Kr}-\lambda_{Rb}\right)\left(\lambda_{Rb}-\lambda_{Rbeff}\right)} \\
a_4 &\equiv \frac{\lambda_{Rb}}{\lambda_{Kr}\left(\lambda_{Kr}-\lambda_{Rb}\right)\left(\lambda_{Kr}-\lambda_{Rbeff}\right)} \qquad a_5 \equiv \lambda_{Rb}-\lambda_{Kr} \qquad a_6 \equiv \frac{\lambda_{Rb}^2}{\lambda_{Kr}\left(\lambda_{Kr}-\lambda_{Rb}\right)^2\left(\lambda_{Kr}-\lambda_{Rbeff}\right)} \\
a_7 &\equiv \lambda_{Rb}-\lambda_{Rbeff} \qquad a_8 \equiv \frac{\lambda_{Rb}^2}{\lambda_{Rbeff}\left(\lambda_{Rb}-\lambda_{Rbeff}\right)^2\left(\lambda_{Rbeff}-\lambda_{Kr}\right)} \qquad a_9 \equiv \frac{\lambda_{Kr}\left(\lambda_{Rbeff}-2\lambda_{Rb}\right)+\lambda_{Rb}\left(3\lambda_{Rb}-2\lambda_{Rbeff}\right)}{\left(\lambda_{Kr}-\lambda_{Rb}\right)^2\left(\lambda_{Rb}-\lambda_{Rbeff}\right)^2}
\end{aligned} \tag{22}$$

For FF, the model is

$$\dot{C}_{FF} = \Gamma\,q_{Kr}\,\psi_{Kr}\,k_1\left\{a_1 + a_2\,e^{-\lambda_{Rbeff}(t-t_0)} + a_3\,e^{-\lambda_{Rb}(t-t_0)} + a_4\,e^{-\lambda_{Kr}(t-t_0)}\right\} + \dot{C}_{base} \tag{23}$$

For the decay-only case, a-factors similar to those defined above are developed in a straightforward way. The leakage rate Γ and the baseline countrate C_{base} enter these models linearly, so that a "partial linear" nonlinear estimation procedure is used. With this approach to the regression problem, the only initial estimate needed is for the single nonlinear parameter, the start time t_0.

Simulation results

(Some preliminary results; more detail and conclusions to follow later.)

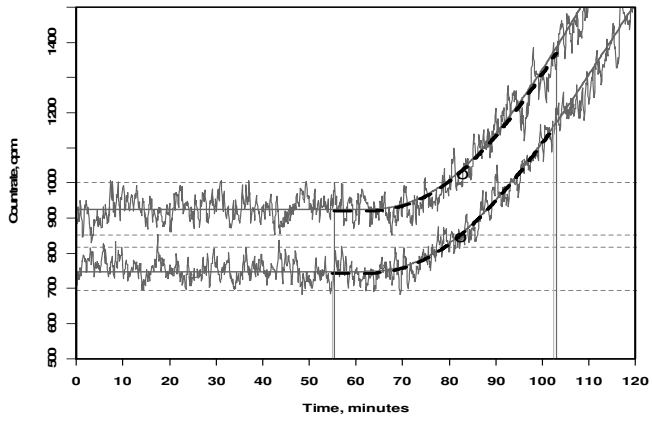

Figure 4. FF (top) and RW (bottom) cpm and "fitted" response; start time 60 min, leakage rate 0.5 gpm; vertical lines indicate regression dataset windows; solid smooth line is deterministic countrate.

Estimation results for this example (known leak rate LR = 0.50):

t0	***base***	***LR***	
62.35 (0.54)	*744.2 (2.3)*	*0.57 (0.02)*	*RW*
56.75 (0.65)	*916.0 (2.6)*	*0.43 (0.02)*	*FF*

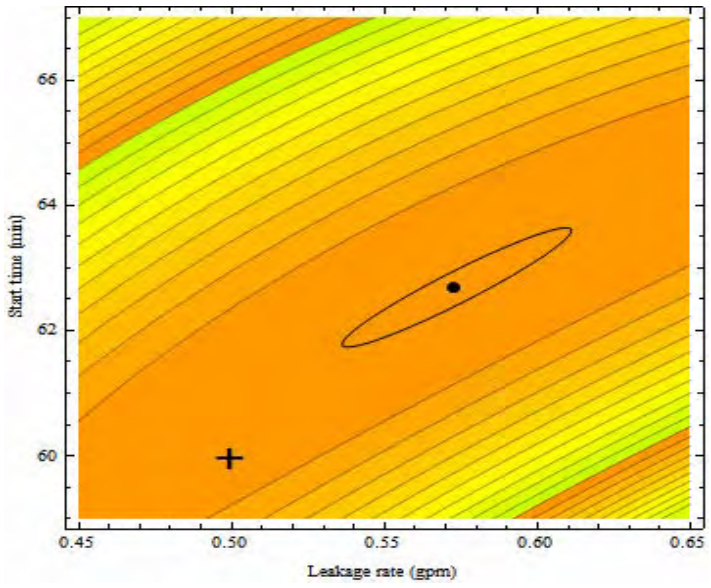

Figure 5. Contours from the nonlinear estimation process for RW. The cross is the known point- start time 60 min, LR 0.50 gpm. The dot is the point estimate. Note positive correlation (tilt of ellipse).

Patent

There is a patent (US5343046, 1994) that uses a shaped collimator or shield to, allegedly, produce a "first-order" response in a moving-filter monitor. Somehow this is supposed to allow estimation of reactor coolant leakage rate. The patent does not indicate how this is to be done and indeed the "methodology," such as it is, seems to be completely wrong.

There are sketches of countrate profiles in the patent. In Appendix D is a collection of some profiles that assume a flat efficiency, while more-correct 3D versions (i.e., that include geometric efficiency) are in Chapter 6. None of these look like those in the patent, and at that, those are contradictory- they assume LL but this application is supposed to be for Rb^{88}, which of course is SL. Below is some math to try to make sense of what is given in the patent (which has only trivial math):

$$\alpha(t) = \frac{k\,F\,\phi}{area}\left\{\int_0^{vt}\int_{y_1(x)}^{y_2(x)}\int_{t-\frac{x}{v}}^{t} Q_{Rb}(\tau)\,e^{-\lambda_{Rb}(t-\tau)}d\tau\,dy\,dx + \int_{vt}^{L}\int_{y_1(x)}^{y_2(x)}\int_{t-\frac{x}{v}}^{t} Q_{Rb}(\tau)\,e^{-\lambda_{Rb}(t-\tau)}d\tau\,dy\,dx\right\} \tag{24}$$

$$y_1(x) = -\frac{w}{2}e^{-rx} \qquad y_2(x) = \frac{w}{2}e^{-rx} \tag{25}$$

$$area = \int_0^L w\,e^{-rx}\,dx = \frac{w}{r}\left(1 - e^{-rL}\right) \tag{26}$$

$$\alpha(t) = \frac{k\,F\,\phi}{area}\left\{\int_0^{vt} w\,e^{-rx}\int_{t-\frac{x}{v}}^{t} Q_{Rb}(\tau)\,e^{-\lambda_{Rb}(t-\tau)}d\tau\,dx + \int_{vt}^{L} w\,e^{-rx}\int_{t-\frac{x}{v}}^{t} Q_{Rb}(\tau)\,e^{-\lambda_{Rb}(t-\tau)}d\tau\,dx\right\} \tag{27}$$

which leads to the $t < T$ activity solution

$$\alpha(t) = \frac{k\,F\,\phi\,r}{1 - e^{-rL}}\left\{\int_0^{vt} e^{-rx}\int_{t-\frac{x}{v}}^{t} Q_{Rb}(\tau)\,e^{-\lambda_{Rb}(t-\tau)}d\tau\,dx + \int_{vt}^{L} e^{-rx}\int_{t-\frac{x}{v}}^{t} Q_{Rb}(\tau)\,e^{-\lambda_{Rb}(t-\tau)}d\tau\,dx\right\} \tag{28}$$

Using the Q_{Rb} found above in this leads to a very complicated solution that is clearly no improvement over the expressions given above and in Chapter 7. The response is far from "first order" (i.e. FF) and even if that were the case, the FF solution still requires the Q start time. Most importantly, the patent does not describe how to get from this modified monitor response to an estimate of S_{Kr}. The patent is an interesting and creative idea that does not appear to have sufficient mathematical foundation to be of any practical use.

Appendix A

Nonconstant Flowrate Effects in Sampling

Health Physics, 82(1) January 2002; 114-119

Correction for a nonconstant flowrate during particulate air sampling is often done by taking the arithmetic average of the initial and final flowrates. This average is then used in concentration calculations as if the flowrate had been constant at that value during the entire sampling period. For long-lived activity this approach is reasonable, but for shorter-lived activity and longer sampling times, the estimated concentrations can be biased low. This note examines the magnitude of this bias, and also provides expressions for estimating the concentration, given an observed count, assuming an exponential flowrate time-dependence. One expression uses an estimate of the exponential time-dependence, while another expression uses a linear approximation for the flowrate time-dependence. Both of these are shown to be superior to the use of the average flowrate. The parameters used in these expressions are estimated from the same initial and final flowrates used in the arithmetic average.

Introduction

When collecting particulate air samples it is usually assumed that the sampler flowrate is constant, and, often, this is not unreasonable. However, regulatory guidance (e.g., [1]) suggests that, if the flowrate at the end of the sampling period is ten percent or more below the initial value, we should use the arithmetic average of the two flowrates in the concentration calculations. The purpose of this note is to examine the accuracy of this approach. A similar analysis was done for radon daughters in [2], although the thrust there was for concentration variations rather than flowrate variations.

Let us pose the problem as it would occur in the field. We are given a sampler's initial and final flowrates, and the sampling interval; the sampler is not a constant-volume unit. To illustrate, say we have an initial rate of 20 cfm, a final rate of 15 cfm, and a sample duration of one hour. This represents a 25 percent decrease in flow in one hour. We could (a) use the average of the two flowrates, 17.5 cfm, as if it had been constant across the hour, as the regulatory guidance suggests, in estimating the concentration, or (b) we could use an exponential flowrate relation to estimate the concentration, or (c) we could use a linear flowrate relation to estimate the concentration. In the latter two cases we can estimate the necessary parameters from the observed flowrate data.

Our purpose is to develop methods (b) and (c), and compare them to (a), in addition to showing the bias caused by (a) when the true flowrate behavior is taken to be exponential. First we develop a general expression for the counts, then we solve it for the three hypothesized flowrate behaviors (constant, exponential, linear). This leads to relations for the estimated constant concentration for these cases. Next we attempt to establish that an exponential behavior for the flowrate decrease is a reasonable assumption for the true behavior. Using that, we next find ratios which permit evaluation of the bias in the concentration estimates, for the three assumed behaviors, when the true behavior is exponential. Finally, we plot these ratios for some selected parameter values.

Expected Sample Counts

It will be useful to briefly review the basis for the estimation of particulate air concentrations using a sampling process, to establish notation and the basic expressions that will be needed below. The starting point for this analysis is the ordinary differential equation (ODE) for the countrate on a fixed filter:

$$\frac{d\dot{C}}{dt} = \varepsilon k \gamma \phi F(t) Q(t) - \lambda \dot{C} \qquad (1)$$

where $\dot{C}$ is the countrate; ε is the detection efficiency; γ is the gamma abundance; k is a units-conversion constant; λ is the decay constant; ϕ is the collection efficiency; Q is the time-dependent concentration in the sampled air; F is the time-dependent sampler flowrate. Expressions similar to this have been in the literature for many years; two early examples are [3], [4]. A convenient way to write the solution for this ODE is to use the scalar convolution integral (e.g., [5]):

$$\dot{C}(t) = \varepsilon k \gamma \phi \exp(-\lambda t) \int_0^t Q(\tau) F(\tau) \exp(\lambda \tau) d\tau + \dot{C}_0 \exp(-\lambda t) \tag{2}$$

We are considering a single nuclide; parent-progeny applications such as radon-thoron can be treated by extending (2) to use a matrix convolution. The filter is assumed to be new at the start of sampling, so that the initial countrate is zero, and the second term in (2) vanishes. Since we are discussing a sampler, as opposed to a monitor, the countrate (2) is not observed. (For detailed models of fixed- and moving-filter particulate monitor dynamic countrate responses, for time-varying concentrations, see [6].) Instead, at the end of the sampling interval T_s we secure the flow, remove the filter and prepare it for counting. This takes some time T_d, which we may deliberately increase, e.g., to permit interfering natural activity to decay.

At the end of the decay interval we begin a count, of duration T_c. The countrate at the end of the sampling period is (2) with T_s in place of t. The countrate at the start of the counting period is then $\dot{C}(T_s) \exp(-\lambda T_d)$ and this countrate continues to decay during the counting interval, during which we integrate that decaying countrate to obtain the observed counts. All of these operations can be collected into a single expression for the counts accumulated from a sample filter:

$$C(T_s, T_d, T_c) = \int_0^{T_c} \left\{ \left[\varepsilon k \gamma \phi \exp(-\lambda T_s) \int_0^{T_s} Q(\tau) F(\tau) \exp(\lambda \tau) \, d\tau \right] \exp(-\lambda T_d) \right\} \exp(-\lambda t) dt \tag{3}$$

Clearly, the observed counts are controlled by the product of the concentration and the flowrate (this is the essence of the source term in the ODE). The inner integral in (3) will determine how we are to interpret a count from a sample. The key fact is that (3) is a single-point estimate, so we need to have a single concentration value, for the estimation to be meaningful. There are two obvious choices for single values: (a) a constant concentration, or (b) an average concentration over the sampling interval.

Exploring the behavior of (3), we will find that for long-lived activity (negligible decay during sampling/analysis period), the exponentials will vanish and we can find an average concentration if the flowrate is constant. This is not the case for shorter-lived nuclides, where the inner-integral exponential cannot be ignored. That is,

$$\frac{1}{T_s} \int_0^{T_s} Q(\tau) \exp(\lambda \tau) d\tau \neq \frac{1}{T_s} \int_0^{T_s} Q(\tau) d\tau = \bar{Q}$$

Similarly, if the concentration is constant, for long-lived activity we can find an average flowrate, or the total air volume sampled, to estimate the concentration. Again, for shorter-lived nuclides this is not the case, for the same reason as for the average concentration. We do not want to restrict the analysis to long-lived nuclides, so that we must keep the exponentials in (3).

In the general case, with unspecified concentration and flowrate time-dependencies, we cannot find a meaningful single-point estimate of a varying concentration from a single sample. Also, it would be most unusual to have *a priori* knowledge of the concentration dynamic behavior, including the necessary parameter values, and if we did, there would be little need for a sample. However, for the flowrate we have a separate measurement, at least at the start and finish of the sample, and, perhaps, dynamically during the sampling interval. Therefore, the only single-value estimate we will use is that of a constant concentration, with the possibility of a time-dependent flowrate, since the latter can be independently measured.

Concentration Estimation

The next step is to develop the expressions to be used in estimating the constant concentration from a sample, given an observed count, the initial and final flowrates, and the sampling interval. These are derived by using the appropriate $F(t)$ in (3), evaluating the expected count, then solving for the constant concentration using an observed count.

Constant (average) flowrate

This case assumes a constant flowrate $F(t)=F_0$ in (3), which will lead to the counts

$$C(T_s,T_d,T_c) = \frac{\varepsilon k \gamma \phi Q_0 F_0}{\lambda^2} \exp(-\lambda T_d)\left[1 - \exp(-\lambda T_c)\right]\left[1 - \exp(-\lambda T_s)\right] \tag{4}$$

and this is easily solved for the constant concentration, using the observed counts and observed average flowrate:

$$\hat{Q}_{avg} = \frac{\lambda^2 C_{obs}}{\varepsilon k \gamma \phi F_{avg} \exp(-\lambda T_d)\left[1 - \exp(-\lambda T_c)\right]\left[1 - \exp(-\lambda T_s)\right]} \tag{5}$$

with

$$F_{avg} = 0.5\left(F_{initial} + F_{final}\right)$$

Exponential flowrate

For this case we have

$$F(t) = F_{initial} \exp(-r t) \tag{6}$$

where $F_{initial}$ is the initial flowrate and r is a parameter controlling the rate of decrease. Using this in (3) to obtain the expected count and then solving for the constant concentration we find

$$\hat{Q}_{\exp} = \frac{\lambda(\lambda - \hat{r})\, C_{obs}}{\varepsilon k \gamma \phi F_{initial} \exp(-\lambda T_d)\left[1 - \exp(-\lambda T_c)\right]\left[\exp(-\hat{r} T_s) - \exp(-\lambda T_s)\right]} \tag{7}$$

with the parameter r estimated using

$$\hat{r} = \frac{1}{T_s}\ln\left(\frac{F_{initial}}{F_{final}}\right) \tag{8}$$

Equation (7) applies when the estimate (8) is not equal to λ. If it is equal, then we use

$$\hat{Q}_{\exp} = \frac{\lambda C_{obs}}{\varepsilon k \gamma \phi F_{initial} \exp(-\lambda T_d)\left[1 - \exp(-\lambda T_c)\right] T_s \exp(-\lambda T_s)} \tag{9}$$

Linear flowrate

Next, suppose that we assume the observed decrease in flow was due to a linear flowrate behavior

$$F(t) = F_{initial} - b t$$

where b is the slope or linear rate of change of the flowrate. Using this in (3) we obtain the expected count and then solve for the concentration to find

$$\hat{Q}_{lin} = \frac{\lambda^2 C_{obs}}{\varepsilon k \gamma \phi \exp(-\lambda T_d)\left[1 - \exp(-\lambda T_c)\right] \Psi} \tag{10}$$

$$\Psi = F_{initial}\left[1 - \exp(-\lambda T_s)\right] + \frac{\hat{b}}{\lambda}\left[1 - \lambda T_s - \exp(-\lambda T_s)\right]$$

with

$$\hat{b} = \frac{1}{T_s}\left(F_{initial} - F_{final}\right)$$

Next we explore one possible behavior for the flowrate and then use it to see what the consequences would be of using the above concentration estimation relations when the counts were in fact produced by that flowrate behavior.

Actual Flowrate Behavior

Let us now consider what the "true" time-dependent variation in the flowrate might be. It seems reasonable that the variation would be exponential, since any dust (particulate matter which may or may not contain activity) pulled onto the filter would at first block the available penetrations in the filter, while later in the sampling period it would have more difficulty in finding an open penetration to block. Therefore we would expect that the flowrate would decrease more rapidly at the start of sampling, and more slowly later. This concept was explored with a simple Monte Carlo experiment. Particles were randomly, uniformly scattered across a rectangular area, and the number of "hits" in equal-sized "cells" (representing openings in the filter) were tabulated. There were 10^4 cells, in a 100x100 grid. If a cell received at least one particle, that flow path was considered blocked.

The size of the particulate population was increased, stepwise, simulating the effect of a constant dust loading rate being sampled for increasing lengths of time. Five replicates were done at each setting of the number of particles. The measured quantity was the fraction of the available cells which were not blocked (did not receive at least one hit). Presumably the flowrate would be proportional to the fraction of open paths (cells). The results are shown in Fig. 1, along with an exponential function estimated from the data, via a transformed linear regression.

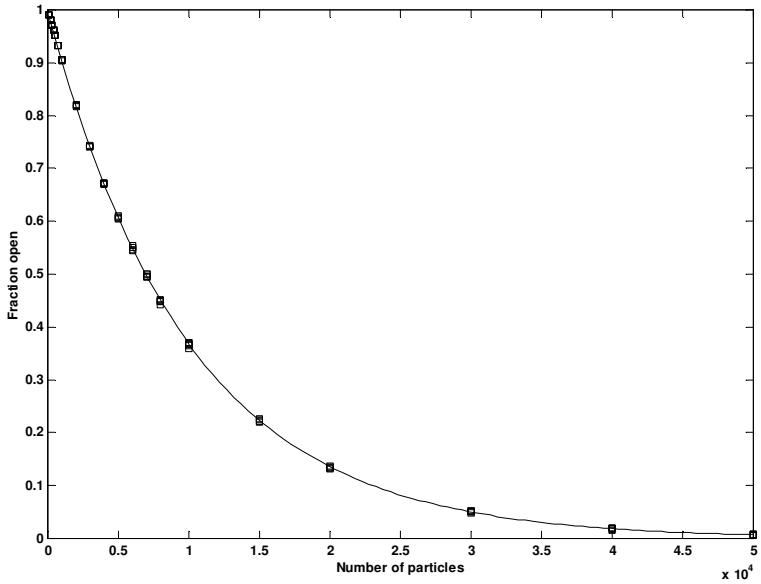

Figure 1. Monte Carlo filter flow results. Five replicates at each particle-number setting. 100x100 cells. Exponential regression to data indicated by solid line.

The agreement is excellent, lending support to the assumption that the true variation in the sampler flowrate is exponential. Of course this function is also mathematically convenient. In some applications the flowrate may follow some other time-dependence, or it may be quite erratic, due to sampler problems, power fluctuations, and so forth. In order to make progress, however, we must use some closed form for the flowrate variation, and since exponential behaviors occur so frequently, this seems a reasonable choice. Note that [2] also used an exponential variation in the "collection rate," which is the product of the concentration and flowrate in (1).

Concentration-Estimate Ratios

Next we develop the expected counts when the true flowrate behavior is exponential, and use these to create ratios of the resulting concentration estimates to the correct concentration.

Constant (average) flowrate

In accordance with the regulatory procedure, we would estimate the average flowrate over the sampling time from the observed initial and final flowrates. When the true $F(t)$ is exponential this average will be

$$\bar{F}_{\exp}(T_s) = \frac{F_{initial}}{2}\left[1 + \exp(-rT_s)\right] \tag{11}$$

What is of interest is to compare the concentration estimates obtained using (11), a constant value, in (3), as opposed to using the correct dependence (6) in (3). The count accumulated if we use the observed average flowrate (11) as if the true flowrate had been constant at that value across the entire sampling time T_s for a constant concentration Q_0 is given by

$$C_{avg}(T_s,T_d,T_c) = \frac{\varepsilon k \gamma \phi Q_0}{\lambda^2}\exp(-\lambda T_d)\left[1 - \exp(-\lambda T_c)\right]\left[1 - \exp(-\lambda T_s)\right]\frac{F_{initial}}{2}\left[1 + \exp(-rT_s)\right] \tag{12}$$

However, what actually has happened is that the flowrate has followed (6), so we should use that in (3). This gives, again for a constant concentration Q_0, and when r is not equal to λ, the count

$$C_{\exp}(T_s,T_d,T_c) = \frac{\varepsilon k \gamma \phi\, Q_0\, F_{initial}}{\lambda(\lambda - r)}\exp(-\lambda T_d)\left[1 - \exp(-\lambda T_c)\right]\left[\exp(-rT_s) - \exp(-\lambda T_s)\right] \tag{13}$$

Note that if r is zero, (12) and (13) reduce to (4), as we would expect, since this implies a constant flowrate. If r is equal to λ then we must return to (3), and we will find that the count will then be given by

$$C_{\exp}(T_s,T_d,T_c) = \frac{\varepsilon k \gamma \phi\, Q_0\, F_{initial}}{\lambda}\exp(-\lambda T_d)\left[1 - \exp(-\lambda T_c)\right]\left[T_s\exp(-\lambda T_s)\right] \tag{14}$$

To avoid the need to have two equations for each scenario we will assume henceforth that r and λ are not equal, but this requirement must be kept in mind, and special solutions developed if it is not met.

To see what effect the use of the average flowrate has, we will compare the concentration estimate we would obtain from an observed count, if we use (12), when in fact the flowrate variation was exponential, i.e., (13). We can find an estimate of the constant concentration Q_0 from (12), using the counts that would have been generated by the true flowrate behavior, i.e., (13). That is, we have the estimate

$$\hat{Q}_{avg} = \frac{\lambda^2 C_{\exp}(T_s,T_d,T_c)}{\varepsilon k \gamma \phi \exp(-\lambda T_d)\left[1 - \exp(-\lambda T_c)\right]\left[1 - \exp(-\lambda T_s)\right]\frac{F_{initial}}{2}\left[1 + \exp(-rT_s)\right]}$$

which is equivalent to (5), with (11) used for F_{avg} and C_{exp} used for C_{obs}, and this will reduce to

$$\hat{Q}_{avg} = Q_0 \left\{ \frac{2\lambda}{\lambda - r} \frac{\exp(-rT_s) - \exp(-\lambda T_s)}{[1 + \exp(-rT_s)][1 - \exp(-\lambda T_s)]} \right\} = Q_0 R_{avg}(\lambda, r, T_s) \quad (15)$$

If the ratio R_{avg} is close to unity, then the concentration estimate found by using the average flowrate will be close to the correct value Q_0. By taking the limit of R_{avg} as the decay constant approaches zero it can be shown that for long-lived activity the ratio is essentially unity for any sampling time. It is also unity when the parameter r is zero. If r is not zero, the limit as the sampling time becomes large is zero. Values of R_{avg} less than unity mean that concentration estimates which use the average flowrate are biased low, or underestimated.

Exponential flowrate

If we use the exponential relation (13) to estimate the concentration when the true behavior is exponential then we could form a ratio R_{exp} similar to R_{avg}; this ratio will be unity if our estimate of the exponential parameter r is correct. Since we should not assume that it will be correct, we can write a ratio which includes a fractional or scaling adjustment w to r, simulating a bias in its estimation. This will lead to a concentration-estimate ratio of

$$R_{\exp} = \frac{(\lambda - r)[\exp(-wrT_s) - \exp(-\lambda T_s)]}{(\lambda - wr)[\exp(-rT_s) - \exp(-\lambda T_s)]} \quad (16)$$

When w is unity, R_{exp} is also unity, since we would then be using the correct value of r in estimating Q_0.

Linear flowrate

For this case we use the linear $F(t)$ in (3) to find the counts

$$C_{lin}(T_s, T_d, T_c) = \frac{\varepsilon k \gamma \phi Q_0}{\lambda^2} \exp(-\lambda T_d)[1 - \exp(-\lambda T_c)] \left\{ F_{initial}[1 - \exp(-\lambda T_s)] + \frac{b}{\lambda}[1 - \lambda T_s - \exp(-\lambda T_s)] \right\} \quad (17)$$

Note that if the slope b is zero, (17) reduces to (4). Given the observed flowrates and sampling time we would estimate this slope from

$$\hat{b} = \frac{F_{initial} - F_{final}}{T_s}$$

However, by hypothesis, the actual flowrate is exponential, so that this would amount to

$$\hat{b} = \frac{F_{initial}[1 - \exp(-rT_s)]}{T_s} \quad (18)$$

Using this for b in (17) and solving for the concentration, again using the counts we would observe from the true exponential flowrate behavior, from (13), we obtain the concentration-estimate ratio

$$\hat{Q}_{lin} = Q_0 \left\{ \frac{\lambda}{\lambda - r} \frac{\exp(-rT_s) - \exp(-\lambda T_s)}{[1 - \exp(-\lambda T_s)] + \frac{1}{\lambda T_s}[1 - \exp(-rT_s)][1 - \lambda T_s - \exp(-\lambda T_s)]} \right\} = Q_0 R_{lin}(\lambda, r, T_s) \quad (19)$$

The limit of R_{lin} as the decay constant approaches zero (long-lived activity) is unity, as it is if the exponential parameter r is zero. If r is nonzero, the limit as the sample time becomes large is zero.

Results

The ratio R_{avg} is plotted as solid lines in Fig. 2 as a function of the sample time, for a short-lived nuclide, ^{88}Rb (half-life 18 minutes), for three example values of the exponential parameter r. These correspond to flowrate decreases of 5, 20, and 50 percent in one hour, using

$$r(f) = \frac{1}{T_s} \ln\left(\frac{1}{1-f}\right)$$

where f is the fractional decrease in the sampling interval T_s (here, one hour). This is an arbitrary spread of loading rate values, intended to approximate a low, medium, and high dust loading rate. The dotted lines are for a somewhat longer half-life, of about three hours. Fig. 2 shows the fraction of the correct concentration we can expect to estimate if we use the observed initial and final flowrates as an arithmetic average when in fact the flowrate was decreasing exponentially, for these three rates of flowrate decrease.

For ^{88}Rb we see in Fig. 2 that there is a small bias in the estimated concentration for shorter sampling times, but as this time becomes larger, the bias becomes larger (more underestimation), particularly at higher rates of flowrate decrease. For the longer-lived nuclide the bias is reduced, but it still becomes large at longer sample times and higher loading rates. All of this is as we would expect intuitively; what is useful here is to have some quantitative sense of how much effect there is, as a function of these parameters. For longer sampling times, shorter-lived nuclides, and higher dust loading rates, it would be advisable to estimate the parameter r using (8), and then find the concentration estimate using (7), as opposed to using the arithmetic-average calculation (5).

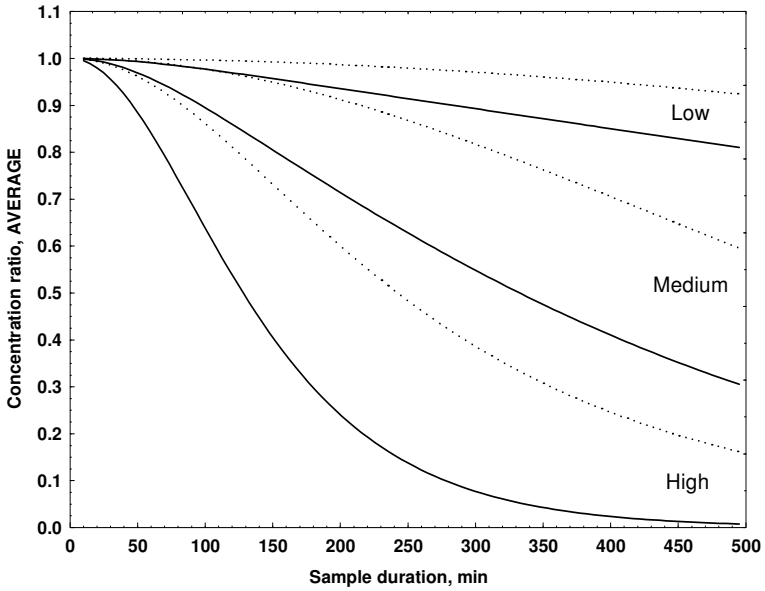

Figure 2. Estimated concentration ratios vs. sample time, for dust loading at 5, 20, 50 percent flowrate decrease in one hour. Solid lines are average-flowrate ratios (15) for ^{88}Rb (half-life 18 minutes), dotted lines are ratios for a nuclide with a half-life of 180 minutes.

In Fig. 3 we have plots of R_{lin} as a function of the sampling interval, again for low, medium, and high dust loading rates, for ^{88}Rb and a three-hour half-life nuclide. We see that using the linear flowrate is consistently better (ratio closer to unity) than is the use of the average flowrate (Fig. 2), for given values of r and T_s. Also note that when the product rT_s is small, the ratio R_{lin} is close to unity, since the (true) exponential and (approximate) linear relations are very close. This is because

$$F(t) = F_{initial} \exp(-rT_s) \approx F_{initial}\left(1 - rT_s\right) = F_{initial} - rF_{initial}T_s$$

so that the slope b is $rF_{initial}$. That is, for small values of rT_s, the flowrate decrease is essentially linear.

In Fig. 4 we have a plot showing R_{exp} for values of w of 0.9 and 1.1, for the three loading rates. As we might expect, at the higher loading rates and longer sampling intervals, the concentration bias will be larger if our parameter estimate r is, e.g., ten percent high or low. This plot illustrates the importance of having a good estimate of the exponential rate parameter r. If flowrate data is available periodically during the sampling period then we could use that data to estimate r, via a regression, rather than relying on only the start and end flowrates, i.e., (8).

In conclusion, if we are willing to assume an exponential flowrate decrease during the sampling period, the concentration-estimate ratios (15), (16), and (19) provide a means to assess the possible bias of using, respectively, an arithmetic-average constant flowrate, an exponential flowrate, or a linear flowrate, in estimating a concentration from a sample count. For shorter-lived nuclides, longer sampling times, and higher dust loading rates, using an arithmetic-average constant flowrate will produce concentration values that may be underestimated sufficiently to be a cause for concern. With reasonably good parameter estimates, the exponential and linear flowrate concentration results can be less biased than the arithmetic-average flowrate concentration result.

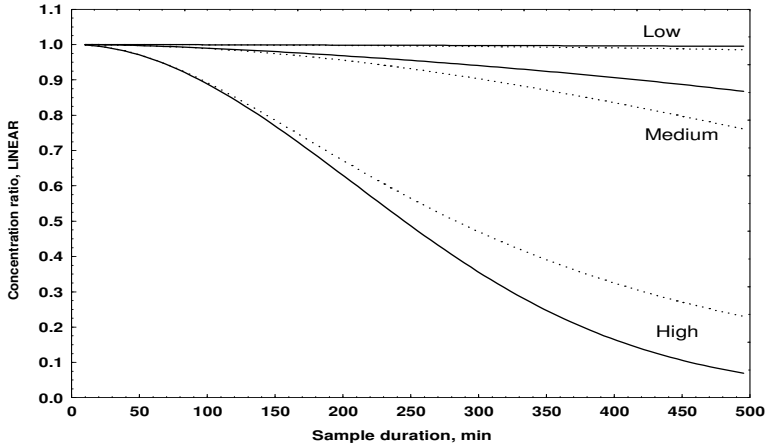

Figure 3. Estimated concentration ratios vs. sample time, for dust loading at 5, 20, 50 percent flowrate decrease in one hour. Solid lines are linear-flowrate ratio (19) estimates for ^{88}Rb, dotted lines are ratios for a nuclide with a half-life of 180 minutes.

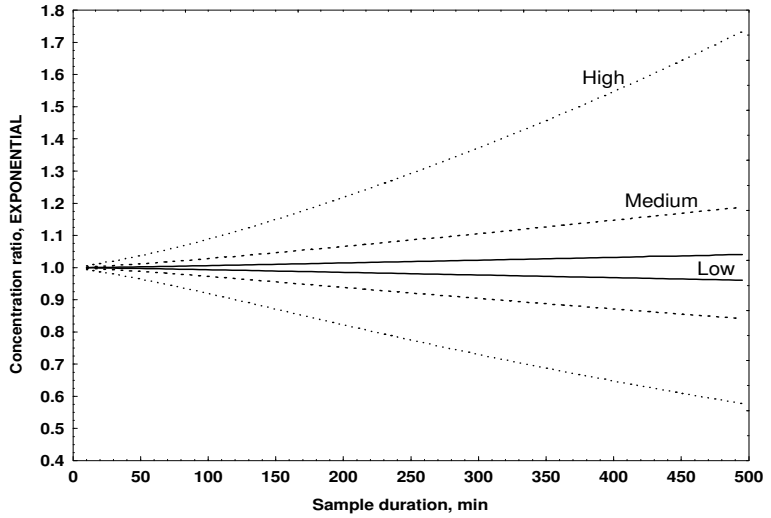

Figure 4. Estimated concentration ratios vs. sample time, for dust loading at 5, 20, 50 percent flowrate decrease in one hour. Lines above unity are for exponential ratio (16) with scaling factor w of 0.9, lines below unity are for scaling factor 1.1.

References

[1] United States Nuclear Regulatory Commission, Regulatory Guide 8.25, "Air Sampling in the Workplace," Section 5.5, June 1992.

[2] A. G. Scott, "The Bias in Radon Daughter Concentration Estimates Caused by Concentration Variations During Sampling," *Health Physics*, vol. 44, pp. 267-271, 1983.

[3] G. L. Helgeson, "Determination of Concentrations of Airborne Radioactivity," *Health Physics*, vol. 9, pp. 931-942, 1963.

[4] R. D. Evans, "Engineer's Guide to the Elementary Behavior of Radon Daughters," *Health Physics*, vol. 17, pp. 229-252, 1969.

[5] W. J. Palm, *Modeling, Analysis and Control of Dynamic Systems*, New York:Wiley, 1983, p. 178.

[6] W. C. Evans, "Mathematical Models for the Dynamic Response of Continuous Particulate Air Monitors," *IEEE Transactions on Nuclear Science,* vol. 48, pp. 202-218, 2001. Chapter 1 here.

Appendix B

Decay Chain Air Concentration Estimation Using a Sampler with an Exponentially-Decreasing Flowrate

Unpublished

Introduction

This report presents equations for (a) calculating the air concentrations for a three-component decay chain, given observed counts (usually from gamma spectroscopy) or (b) for predicting the counts to be observed for that chain, given the air concentrations. The sampler flow rate can decrease exponentially; using zero for the decrease parameter yields the previous results for a constant flow. The predicted counts are compared to CTBT air sample spectral results (from AU), and they agree within about 2 percent. A summing correction was needed for one of the peaks. Variances are found; QQ plots of Monte Carlo data show that these are correct and that the PDF of the concentration estimates is Normal. These variances are for Poisson counts only; flow and efficiency uncertainties are not considered, so that these variances are minimums. Numerical experiments show the importance of not exceeding a reasonable decay time, such that a given nuclide's activity deposited from the air will still remain on the filter at counting time. If not, it is impossible to estimate the air concentration for that nuclide (the process estimates zero, with a large variance).

Discussion

The differential equations governing the time-dependent activity on the sampler filter, for a decay chain of length three, are (the symbols will be defined below):

$$\begin{aligned}
\frac{d\alpha_1}{dt} &= -\lambda_1 \alpha_1 &&+ k F \phi Q_1(t), \\
\frac{d\alpha_2}{dt} &= \lambda_2 \eta_2 \alpha_1 - \lambda_2 \alpha_2 &&+ k F \phi Q_2(t), \\
\frac{d\alpha_3}{dt} &= \lambda_3 \eta_3 \alpha_2 - \lambda_3 \alpha_3 &&+ k F \phi Q_3(t).
\end{aligned} \tag{1}$$

This is more compactly expressed as

$$\frac{d}{dt}\boldsymbol{\alpha} = \mathbf{A}\boldsymbol{\alpha} + \mathbf{B}\mathbf{u} \tag{2}$$

with

$$\boldsymbol{\alpha} = \begin{pmatrix} \alpha_1 \\ \alpha_2 \\ \alpha_3 \end{pmatrix} \quad \mathbf{A} = \begin{pmatrix} -\lambda_1 & 0 & 0 \\ \eta_2 \lambda_2 & -\lambda_2 & 0 \\ 0 & \eta_3 \lambda_3 & -\lambda_3 \end{pmatrix} \quad \mathbf{B} = \begin{pmatrix} 1 & 0 & 0 \\ 0 & 1 & 0 \\ 0 & 0 & 1 \end{pmatrix} \tag{3}$$

The source-allocation matrix **B** is an identity matrix since the sources (air concentrations) drive only the activities of the respective nuclides. The source term for an exponentially-decreasing sampler flowrate, which terminates at the end of the sampling interval T_s can be written as

$$\mathbf{u}(t) = \begin{pmatrix} Q_1 \\ Q_2 \\ Q_3 \end{pmatrix} k \phi F_0 \, e^{-rt} \left[1 - \Phi(t - T_s)\right] \tag{4}$$

Here $\Phi(t\text{-}T_s)$ is the "Heaviside Operator" which acts to turn off the air flow at the end of the sampling time T_s. This operator has a value of zero for times less than T_s, and is unity at, and after, this time. This formulation of the source term for the sampling application (as opposed to monitoring) is very useful because the Heaviside operator has a Laplace transform. This in turn permits one solution to be developed that covers the entire time period from the start of sampling until the end of the counting time of the sample.

The time-dependent activity solution is found using Laplace transforms:

$$\boldsymbol{\alpha}(t) \; = \; \Im^{-1}\left[\left(s\mathbf{I} - \mathbf{A}\right)^{-1} \mathbf{B}\,\mathbf{u}(s)\right] \; + \; \Im^{-1}\left[\left(s\mathbf{I} - \mathbf{A}\right)^{-1} \boldsymbol{\alpha}(0)\right] \tag{5}$$

where

$$\mathbf{u}(s) = \begin{pmatrix} Q_1 \\ Q_2 \\ Q_3 \end{pmatrix} \frac{k \phi F_0}{s + r} \left(1 - e^{-(r+s)T_s}\right) \tag{6}$$

and the vector $\boldsymbol{\alpha}(0)$ of initial activities is taken to be zero for a clean filter at the start of sampling. The vector of Laplace transforms of the activities is then

$$\boldsymbol{\alpha}(s) = \begin{pmatrix} \dfrac{Q_1}{(s+\lambda_1)} \\ \dfrac{Q_2}{(s+\lambda_2)} + \dfrac{Q_1 \eta_2 \lambda_2}{(s+\lambda_1)(s+\lambda_2)} \\ \dfrac{Q_3}{(s+\lambda_3)} + \dfrac{Q_2 \eta_3 \lambda_3}{(s+\lambda_2)(s+\lambda_3)} + \dfrac{Q_1 \eta_2 \eta_3 \lambda_2 \lambda_3}{(s+\lambda_1)(s+\lambda_2)(s+\lambda_3)} \end{pmatrix} \frac{k \phi F_0}{s+r} \left(1 - e^{-(r+s)T_s}\right) \tag{7}$$

The inverse Laplace transform of this gives, after premultiplying by the efficiency-abundance matrix $\boldsymbol{\Psi}$, the countrates:

$$\dot{\mathbf{C}}(t) \; = \boldsymbol{\Psi}\; \boldsymbol{\alpha}(t) \; = \boldsymbol{\Psi}\; \Im^{-1}\left[\left(s\mathbf{I} - \mathbf{A}\right)^{-1} \mathbf{B}\,\mathbf{u}(s)\right] \tag{8}$$

where

$$\boldsymbol{\Psi} = \begin{pmatrix} \varepsilon_1 \gamma_1 & 0 & 0 \\ 0 & \varepsilon_2 \gamma_2 & 0 \\ 0 & 0 & \varepsilon_3 \gamma_3 \end{pmatrix} \tag{9}$$

The results of these operations are the (unobserved) countrates during and after the sample collection time T_s. After this time, the sample decays for some time T_d and then is counted for a time T_c. Counting is a time integral, such that

$$\mathbf{C}(T_c) = \int_{T_s + T_d}^{T_s + T_d + T_c} \dot{\mathbf{C}}(t)\, dt \tag{10}$$

Since the integration time (i.e., counting time) is after the sampling time, the Heaviside operator is unity in the countrate expressions. Using this fact, carrying out the integrations, and factoring yields the desired results for the integrated counts.

$\boldsymbol{\alpha}$	vector of decay-chain nuclide activities, dpm;
$\dot{\mathbf{C}}(t)$	time-dependent countrate vector, cpm;
$\mathbf{A}$	system matrix (here, decay constants);
$\mathbf{B}$	source allocation matrix;
$\mathbf{u}$	source (air concentration) vector;
$\boldsymbol{\Psi}$	matrix of detection efficiency-abundance products.
λ_i	nuclide *i* decay constant, 1/hr;
η_i	branching ratio to nuclide *i*;
Q_i	concentration of nuclide *i* in air, uCi/cc;
k	units reconciliation constant;
F	monitor or sampler flowrate, cfm;
ϕ	collection/retention efficiency and line-loss fraction product;
ε	detection efficiency, counts/emission;
γ	emission abundance, emission/disintegration.

```
u          = { {Q₁},{Q₂},{Q₃} } * F₀ * Exp[-r t] * k * φ *
                                  ( 1 - HeavisideTheta[t - Ts] );
B          = IdentityMatrix[3];
A          = { { -λ₁, 0, 0 }, { η₂ λ₂, -λ₂, 0 }, { 0, η₃ λ₃, -λ₃ } };
Ψ          = { {ε₁ γ₁, 0, 0},{0, ε₂ γ₂, 0},{0, 0, ε₃ γ₃} };
LaplActiv  = Inverse[ s*IdentityMatrix[3] - A ] . B .
                 LaplaceTransform[u,t,s, Assumptions → Ts > 0];
Cdot       = Ψ . InverseLaplaceTransform[ LaplActiv,s,t ];
Counts     = Integrate[ Cdot /. HeavisideTheta[t-Ts] → 1, { t, Ts+Td, Ts+Td+Tc } ];
```

Figure 1. Mathematica code for the sampling problem

It may be of interest to note in passing that during the sampling time, if the concentrations and flowrate remain constant, the long-term equilibrium activities can be obtained without explicitly solving for the time-dependent countrates, using

$$\boldsymbol{\alpha}(t \to \infty) = -\mathbf{A}^{-1}\mathbf{B}\,\mathbf{u} = \begin{pmatrix} \dfrac{Q_1}{\lambda_1} \\ \dfrac{Q_2}{\lambda_2} + \dfrac{Q_1 \eta_2}{\lambda_1} \\ \dfrac{Q_3}{\lambda_3} + \dfrac{Q_2 \eta_3}{\lambda_2} + \dfrac{Q_1 \eta_2 \eta_3}{\lambda_1} \end{pmatrix} k\, F_0\, \phi \tag{11}$$

This result makes it easy to see that, if the only source is Q_1 and the branching ratios η are unity, then the equilibrium activities will be equal. The equilibrium (unobserved) countrates are then found from

$$\dot{\mathbf{C}}\left(t \to \infty\right) = \boldsymbol{\Psi}\,\boldsymbol{\alpha}\left(t \to \infty\right)$$

The time required to attain these countrates of course depends on the respective half-lives. The three-chain system as a whole will approach approximate equilibrium after about five half-lives of the longest half-life (smallest decay constant, or minimum eigenvalue of the system matrix **A**) nuclide.

The flowrate parameter *r* can readily be estimated using

$$\hat{r} = \frac{1}{T_s} \ln\left(\frac{F_{initial}}{F_{final}}\right) \tag{12}$$

Note that, mathematically, this value of *r* must not be equal to any of the decay constants λ. If there is equality, separate solutions must be developed. However, in practice, exact equality is unlikely; implementations of these calculations can check for this condition and add a small increment to *r* to avoid divide-by-zero problems. Also, if the estimated value of *r* is small, the implication is that the flowrate decrease was approximately linear during the sampling interval. ***For a constant flowrate, set r to zero (or a very small number) in the solutions presented below.***

Countrate Solutions

During the sampling time, the "countrates" from the filter are of course not observed, but it is still useful to understand how they would have behaved had they been observed in the time leading up to the counting interval. These countrates are contained in the variable **Cdot** in the *Mathematica* code shown in Fig. 1. The efficiencies and emission abundances used are those for the counting system that is used to analyze the filter after removal from the sampler. The countrate solutions for the first two nuclides in the chain are presented below.

The unobserved countrate for the first (top-of-chain) nuclide will be:

$$\dot{C}_1(t) = \frac{\varepsilon_1 \gamma_1 k F \phi Q_1}{\lambda_1 - r}\left\{\left(e^{-rt} - e^{-\lambda_1 t}\right) - \Phi\left(t - T_s\right)\left(e^{-rt} - e^{-\lambda_1 (t-T_s)}\, e^{-rT_s}\right)\right\} \tag{13}$$

and for the second nuclide:

$$\begin{aligned}\dot{C}_2(t) = {} & \frac{\varepsilon_2 \gamma_2 k F \phi Q_2}{\lambda_2 - r}\left\{\left(e^{-rt} - e^{-\lambda_2 t}\right) - \Phi\left(t - T_s\right)\left(e^{-rt} - e^{-\lambda_2 (t-T_s)}\, e^{-rT_s}\right)\right\} + \\ & \varepsilon_2 \gamma_2 k F \phi \eta_2 Q_1 \lambda_2 \left\{\begin{array}{l} \left(\dfrac{e^{-rt}}{(\lambda_1 - r)(\lambda_2 - r)} - \dfrac{e^{-\lambda_1 t}}{(\lambda_2 - \lambda_1)(\lambda_1 - r)} + \right. \\ \left. \dfrac{e^{-\lambda_2 t}}{(\lambda_2 - \lambda_1)(\lambda_2 - r)}\right) \\ -\Phi\left(t - T_s\right)\left(\dfrac{e^{-rt}}{(\lambda_1 - r)(\lambda_2 - r)} - \dfrac{e^{-\lambda_1 (t-T_s)}\, e^{-rT_s}}{(\lambda_2 - \lambda_1)(\lambda_1 - r)} + \right. \\ \left. \dfrac{e^{-\lambda_2 (t-T_s)}\, e^{-rT_s}}{(\lambda_2 - \lambda_1)(\lambda_2 - r)}\right) \end{array}\right\}\end{aligned} \tag{14}$$

The third-nuclide countrate solution is complicated and need not be presented here; it is contained in the *Mathematica* variable **Cdot[[3]]**.

Integrated Counts

For the integrated counts, it will prove to be useful to first define several collections of constant factors that result from the integration of the Laplace countrate solutions (variable **Counts** in Fig. 1). It is essential to recognize that these are simply numbers, for a given sampling scenario; all the parameters in the expressions below will have numerical values:

$$a_1 = \frac{\varepsilon_1 \gamma_1 k F_0 \phi}{\lambda_1 (\lambda_1 - r)} \left(e^{-rT_s} - e^{-\lambda_1 T_s} \right) \left(1 - e^{-\lambda_1 T_c} \right) e^{-\lambda_1 T_d} \tag{15}$$

$$a_2 = \frac{\varepsilon_2 \gamma_2 k F_0 \phi}{\lambda_2 (\lambda_2 - r)} \left(e^{-rT_s} - e^{-\lambda_2 T_s} \right) \left(1 - e^{-\lambda_2 T_c} \right) e^{-\lambda_2 T_d} \tag{16}$$

$$a_3 = \frac{\varepsilon_2 \gamma_2 k F_0 \phi \eta_2 \lambda_2}{(\lambda_2 - \lambda_1)(\lambda_1 - r)(\lambda_2 - r)} \left[\begin{array}{l} \frac{\lambda_2 - r}{\lambda_1} \left(e^{-rT_s} - e^{-\lambda_1 T_s} \right) \left(1 - e^{-\lambda_1 T_c} \right) e^{-\lambda_1 T_d} \\ - \frac{\lambda_1 - r}{\lambda_2} \left(e^{-rT_s} - e^{-\lambda_2 T_s} \right) \left(1 - e^{-\lambda_2 T_c} \right) e^{-\lambda_2 T_d} \end{array} \right] \tag{17}$$

$$a_4 = \frac{\varepsilon_3 \gamma_3 k F_0 \phi}{\lambda_3 (\lambda_3 - r)} \left(e^{-rT_s} - e^{-\lambda_3 T_s} \right) \left(1 - e^{-\lambda_3 T_c} \right) e^{-\lambda_3 T_d} \tag{18}$$

$$a_5 = \frac{\varepsilon_3 \gamma_3 k F_0 \phi \eta_3 \lambda_3}{(\lambda_3 - \lambda_2)(\lambda_2 - r)(\lambda_3 - r)} \left[\begin{array}{l} \frac{\lambda_3 - r}{\lambda_2} \left(e^{-rT_s} - e^{-\lambda_2 T_s} \right) \left(1 - e^{-\lambda_2 T_c} \right) e^{-\lambda_2 T_d} \\ - \frac{\lambda_2 - r}{\lambda_3} \left(e^{-rT_s} - e^{-\lambda_3 T_s} \right) \left(1 - e^{-\lambda_3 T_c} \right) e^{-\lambda_3 T_d} \end{array} \right] \tag{19}$$

$$a_6 = \varepsilon_3 \gamma_3 k F_0 \phi \eta_2 \eta_3 \left[\begin{array}{l} \frac{\lambda_2 \lambda_3}{\lambda_1 (\lambda_1 - \lambda_2)(\lambda_1 - \lambda_3)(\lambda_1 - r)} \left(e^{-rT_s} - e^{-\lambda_1 T_s} \right) \left(1 - e^{-\lambda_1 T_c} \right) e^{-\lambda_1 T_d} \\ + \frac{\lambda_3}{(\lambda_2 - \lambda_1)(\lambda_2 - \lambda_3)(\lambda_2 - r)} \left(e^{-rT_s} - e^{-\lambda_2 T_s} \right) \left(1 - e^{-\lambda_2 T_c} \right) e^{-\lambda_2 T_d} \\ + \frac{\lambda_2}{(\lambda_3 - \lambda_1)(\lambda_3 - \lambda_2)(\lambda_3 - r)} \left(e^{-rT_s} - e^{-\lambda_3 T_s} \right) \left(1 - e^{-\lambda_3 T_c} \right) e^{-\lambda_3 T_d} \end{array} \right] \tag{20}$$

Then the integrated counts are simply expressed as

$$C_1 = a_1 Q_1 \qquad C_2 = a_2 Q_2 + a_3 Q_1 \qquad C_3 = a_4 Q_3 + a_5 Q_2 + a_6 Q_1 \tag{21}$$

These relations, for constant flow ($r = 0$), have been tested against a large set of high-volume air sample gamma-ray spectral results. The 238 keV line of ^{212}Pb, 727 keV of ^{212}Bi, and 583 keV of ^{208}Tl were used to check count predictions from these equations. For these samples the decay time was long (several hours), so that the only counts observed for the progeny came from the top-of-chain parent. The median ratios of observed to predicted counts were: ^{212}Pb, 0.99; ^{212}Bi, 1.01; ^{208}Tl, 1.02.

The plots in Fig. 2 show the ratio of observed to predicted counts for the peaks indicated. The thicker horizontal line is the median of the ratios. The top-of-chain nuclide ^{212}Pb has essentially perfect matching, since it was used as the starting point for the prediction of the progeny counts. That is, Q_2 and Q_3 were assumed to be (essentially) zero since, due to the long decay time, any air activity from them would produce negligible counts during the counting interval; there was no estimate available for them in any case. Then the predicted counts are found using

$$C_1 = a_1 Q_1 \qquad C_2 = a_3 Q_1 \qquad C_3 = a_6 Q_1 \tag{22}$$

with Q_1 provided by the spectrum analysis. Interestingly, it was necessary to apply a cascade-summing correction to the 583 keV line of ^{208}Tl; the median ratio was only about 0.85 before this correction was applied.

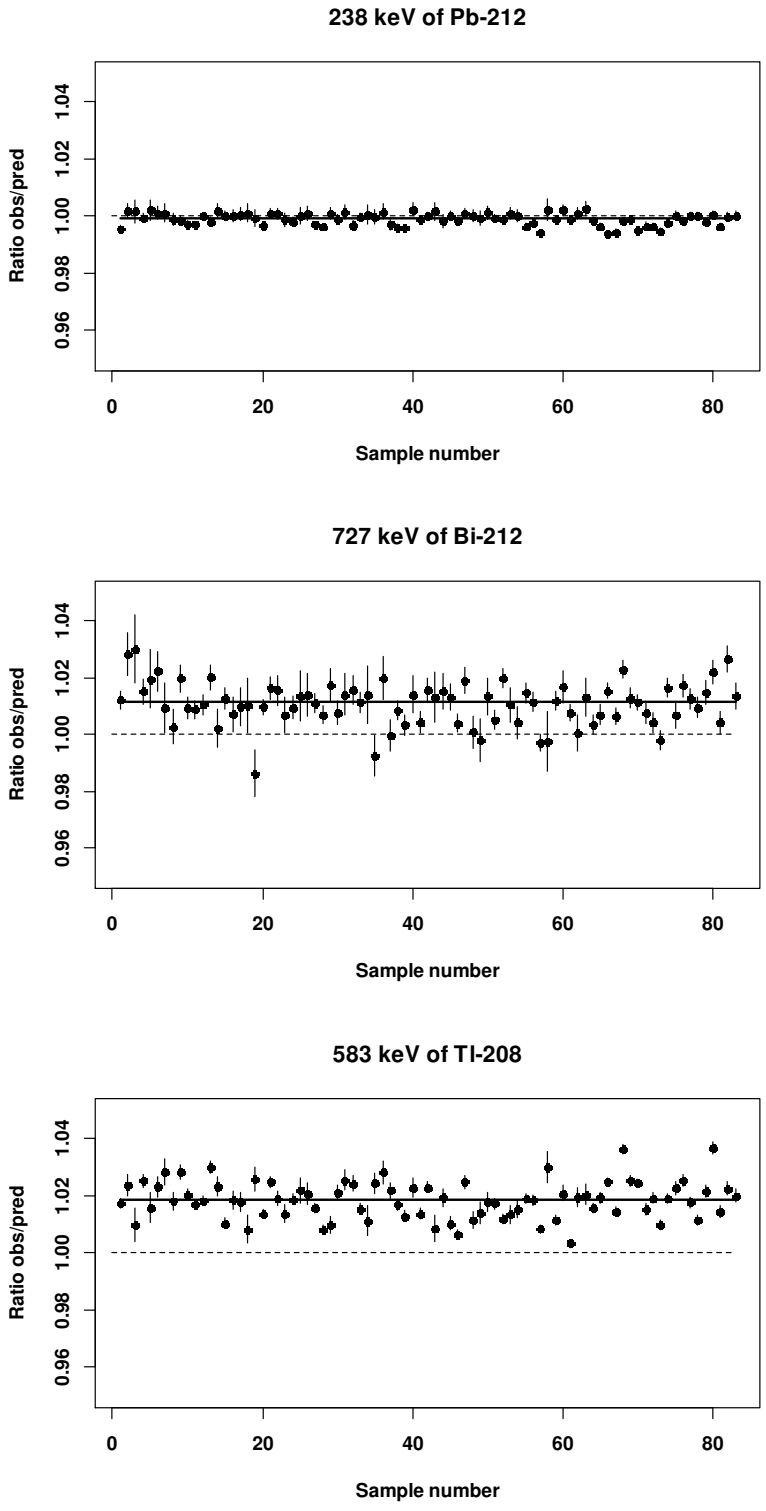

Figure 2. Comparison of predicted and observed decay-chain counts

Concentration Estimation

Given the observed counts, the concentrations are estimated using

$$\hat{Q}_1 = \frac{1}{a_1} C_1 \tag{23}$$

$$\hat{Q}_2 = \frac{1}{a_2} C_2 - \frac{a_3}{a_1 a_2} C_1 \tag{24}$$

$$\hat{Q}_3 = \frac{1}{a_4} C_3 - \frac{a_5}{a_2 a_4} C_2 - \left(\frac{a_6}{a_1 a_4} - \frac{a_3 a_5}{a_1 a_2 a_4} \right) C_1 \tag{25}$$

Note that eqn(23) is equivalent to eqn(7) in Appendix A. The estimation of the air concentration of a progeny nuclide depends on the presence of enough activity from air-deposited material to exceed the subtracted contributions from the precursors. Thus, if the decay time between the end of sampling and the start of counting is long enough for the air-deposited activity to (effectively) vanish, then it will not be possible to estimate the air concentration for that nuclide. In that situation all the observed counts will be from ingrowth, with none from the air-deposited activity.

The variances of the concentration estimates can be calculated from the following expressions; these ignore any uncertainties in the detection efficiencies or sampler flow rate, and are thus minimum variances:

$$Var\left(\hat{Q}_1\right) = \frac{1}{a_1^2} C_1 \tag{26}$$

$$Var\left(\hat{Q}_2\right) = \frac{1}{a_2^2} C_2 + \left(\frac{a_3}{a_1 a_2} \right)^2 C_1 \tag{27}$$

$$Var\left(\hat{Q}_3\right) = \frac{1}{a_4^2} C_3 + \left(\frac{a_5}{a_2 a_4} \right)^2 C_2 + \left(\frac{a_6}{a_1 a_4} - \frac{a_3 a_5}{a_1 a_2 a_4} \right)^2 C_1 \tag{28}$$

A Monte Carlo simulation was developed to generate many thousands of concentration estimates, using Poisson counts. One example QQ plot of the Monte Carlo output (n=50000), shown in Fig. 3, demonstrates that: (1) the concentration estimates follow a Normal distribution, and (2) the variances given above are correct. These plots also can indicate when the process is estimating a zero mean concentration, which happens when the decay time is long compared to the half-life of the nuclide in question. That is, the actual air concentration may not be, and likely is not, zero, but this estimation process cannot produce any sensible concentration value when the information it needs (counts due to the air activity, not from ingrowth) is not present.

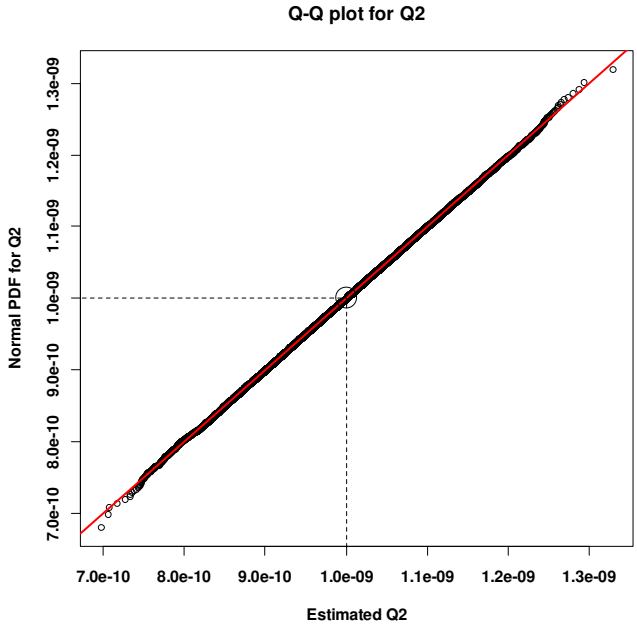

Fig. 3 *QQ plot for Bi212*

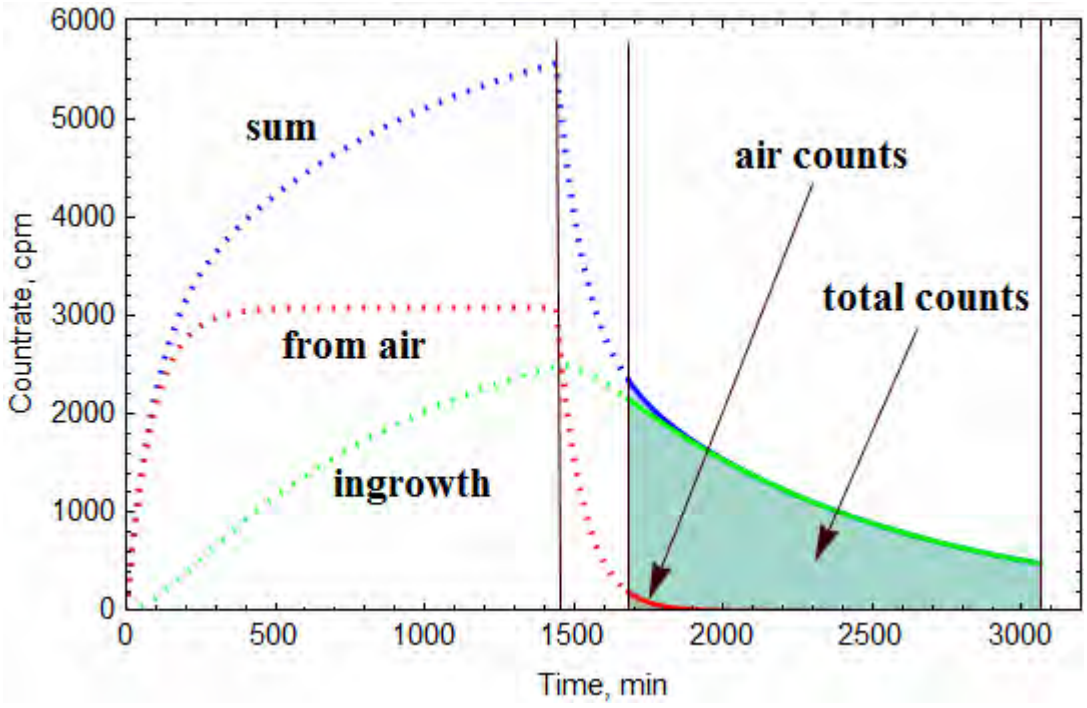

Fig. 4 *These plots shows Bi212 behavior. They also show that if the decay time is long cf. halflife, the counts available from the air activity will be a very small fraction of the total counts.*

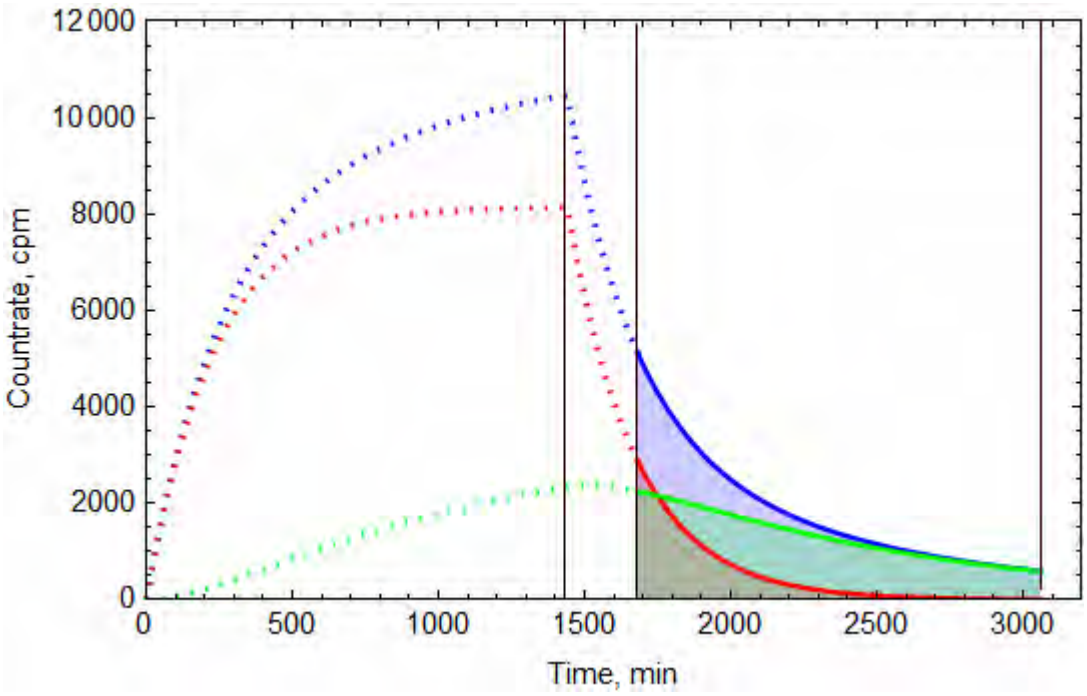

Fig. 5 *Same thing as Fig. 4 but "Bi212" changed to 160 min halflife. More air counts available now.*

Appendix C

Bias in MDC Estimates Due to Autocorrelation of Monitor Background Countrate Readings

Unpublished

Introduction

The estimation of the detection capability of a radioactivity monitor is based on an assessment of the variability of the instrument's background readings. The usual measure of this variability is the standard deviation, which is found from a series of repeated observations of the background, and this data is processed using the well-known formula

$$s_b = \hat{\sigma}_b = \sqrt{\frac{\sum_{i=1}^{N}\left(x_i - \bar{x}\right)^2}{N-1}} \qquad (1)$$

where N is the number of measurements and σ_b is the true, but unknown, standard deviation of the background. This numerical estimate is then used in one of several possible MDC (or MDA) expressions.

However, the output of most monitoring instruments is a real-time count*rate*, as opposed to an integrated *count* over some time interval. Integrated counts, as with a lab scaler, are statistically uncorrelated, since the scaler is reset for each count and thus one result has no influence on the next. With ratemeters, whether analog or digital, this is not the case, and readings of the instrument output are serially correlated (also known as "autocorrelation"). The filtering used in the rate-generation process induces this dependence of the current reading on (all) prior readings.

It can be shown [1] using results from the statistical discipline of time-series analysis (TSA) that the estimate from eqn(1) has the expected value

$$\mathrm{E}(s_b) = \sigma_b \sqrt{1 - \frac{2}{N-1}\sum_{k=1}^{N-1}\left(1 - \frac{k}{N}\right)\rho_k} \qquad (2)$$

where ρ_k is the autocorrelation function (ACF) of the data. This function expresses the dependence of the data points that are separated by k lags (time steps), and it can be found analytically, with some considerable algebraic effort, for the output of most digital filters, such as those used in monitoring applications.

From eqn(2) it is apparent that, if the ACF consists of positive values, then the expected value of our estimator of the background variability will not be σ_b, but some value less than that. In other words, **eqn(1) is a biased estimator** of σ_b if the ACF is nonzero; if the ACF is positive, as is generally the case for instrumental data, then the estimate s_b will be biased low, *making the instrument's MDC look better than it really is.*

To gain some insight into the effect of autocorrelation, consider Figure 1. This shows the ratio of s_b to σ_b as a function of sample size N for several levels of autocorrelation; that autocorrelation was generated by a certain type of digital filter (EWMA), to be discussed momentarily. The larger numbers labeling the lines, at the right side of the plot, represent stronger autocorrelation. In this plot, a complete lack of bias is represented by the line at 1.0 at the top of the figure. We see that this is not attained, even for relatively large sample sizes. The circle shown in the figure represents a sample size N = 20, at a level of autocorrelation in the data that would be reasonable to expect in a monitoring instrument; we see that the resulting s_b is less than half what it should be.

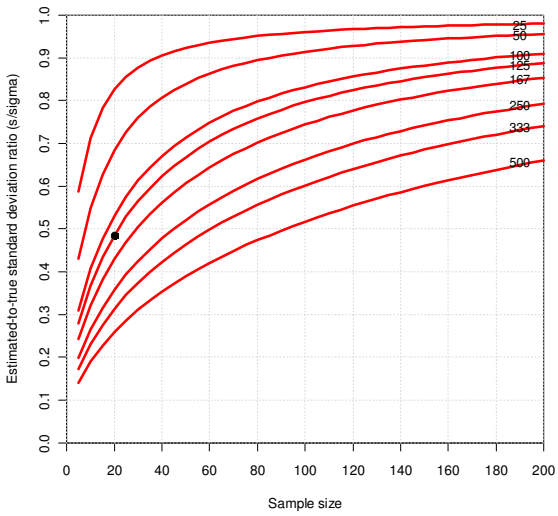

Figure 1. Ratio of estimated to true standard deviation as a function of sample size and RC circuit time constant (seconds) for EWMA digital representation of analog RC circuit. Based on eqn(2) with ACF derived for EWMA.

A familiar type of rate display is the analog RC circuit. However, modern instruments are more likely to use a digital rate display, which in turn is based on some form of digital filter. The purpose of the filter, and of the RC circuit, is to reduce the inherent variability of the raw detector output pulses. Since there are many types of digital filters, we will focus on one particular type that is specifically intended to mimic the familiar RC circuit behavior.

To aid in this process, a simulation was developed to show the time-dependent output of an RC circuit, driven by Poisson-distributed count data. The output of this simulation is a "strip-chart recording" over some time interval. This can be used to compare the digital filter output so that we can have some assurance that the latter really does respond similarly to the RC circuit.

To find a digital filter that "matches" the RC dynamics, we use some results from digital signal processing. This begins with finding the transfer function H of the analog circuit; using Laplace transforms on the ODE of the circuit, we find that

$$H(s) = \frac{1}{1 + s\,RC} \tag{3}$$

where s is the Laplace variable. Then, using the "Impulse Invariance" approach [2] to go from continuous time (analog, Laplace transform) to discrete time (digital, z-transform) it can be shown that

$$z_k = \left(1 - \frac{\Delta t}{RC}\right) z_{k-1} + \frac{\Delta t}{RC}\, x_k \tag{4}$$

where z is the filter output, x is the input, and Δt is the time step over which the filter accumulates counts (typically a few seconds). This result assumes that Δt is smaller than the "time constant" RC, which is usually quite reasonable. This "register time" is a critical parameter in the design of a digital filter for monitoring applications

This is an example of a recursive filter (since its output depends on prior outputs), and this particular one is widely used, in many disciplines, from economics to missile systems. It is known as an Exponentially-Weighted Moving Average (EWMA), and is usually written in one of the following forms

$$z_k = z_{k-1} + \alpha\left(x_k - z_{k-1}\right) = \alpha\, x_k + \left(1 - \alpha\right) z_{k-1} \tag{5}$$

The parameter α is often called the EWMA gain; this recursion can be considered as a constant-gain Kalman filter. Returning to eqn(4) and comparing to eqn(5) we recognize that for the RC-emulation task it will be the case that

$$\alpha \approx \frac{\Delta t}{RC} \tag{6}$$

and the approximation symbol is used since eqn(4) was based on a series expansion of an exponential. As we will soon see, the approximation is very good for reasonable values of the "register time" Δt (the short interval used to accumulate counts from the detector) and the RC time constant.

It is worth noting, although we will not pursue this in detail, that if we go back to the continuous-time transfer function eqn(3) and use a somewhat different method, the "bilinear transformation" [2], then we can derive another digital filter, and that filter also models the RC circuit behavior very well.

Digital Filter Model of RC Circuit

To aid in the analysis of the digital filtering, a simulation of an *analog* RC circuit driven by Poisson-distributed detector pulses was developed. The digital representation, or approximation, to this circuit was then found using continuous-time to discrete-time transformation methods discussed in any text on digital signal processing[1] (e.g., Impulse Invariance). Then, it can be shown that a good representation of the RC low-pass analog filter circuit is obtained with a digital filter that turns out to be what is known in TSA as an Exponentially Weighted Moving Average (EWMA).

This filter is usually written as

$$z_t = \alpha x_t + (1 - \alpha) z_{t-1} \tag{7}$$

where x is the input (here, from the detector) and z is the output. Note that this is a recursive, IIR filter, since the current output depends on the prior output(s). When the parameter (gain, α) of this filter is appropriately chosen, the EWMA will mimic the low-frequency behavior of the RC circuit; this is shown in Figure 2. In the derivation of the EWMA it can be shown that a gain of

$$\alpha = \frac{\Delta t}{\Delta t + RC} \tag{8}$$

will follow the RC circuit very closely. Also, when the analog time constant RC is significantly larger than the "register" time Δt, as it most often would be, we have the useful approximation

$$\alpha \approx \frac{\Delta t}{RC} \tag{9}$$

This approximate result, eqn(5), can also be obtained via other transformation methods.[2]

Note that the EWMA operates on counts accumulated over the time step Δt, usually on the order of a few seconds, while the RC circuit reacts to each pulse as it arrives. So, by a Nyquist sort of reasoning, the EWMA cannot react any more quickly than the Δt, and it naturally does not follow the higher-frequency fluctuations of the ratemeter.

The statistical properties of the EWMA (mean, variance, ACF) were derived; the mean and variance results are readily available in the TSA literature, but the ACF result appears to be novel. With these properties known, it will be convenient to use the EWMA to generate the autocorrelated data for this study. Other filter designs are of course possible, and some were explored, notably a filter based on the Bilinear Transform, but the results were no different from those obtained using the simpler (and widely-used) EWMA filter.

[1] For example, Oppenheim and Schafer, *Digital Signal Processing*, Prentice-Hall (1975), Chapter 5.

[2] See, e.g., Bendat and Piersol, *Random Data: Analysis and Measurement Procedures*, 2nd Ed. Wiley-Interscience (1986), p367.

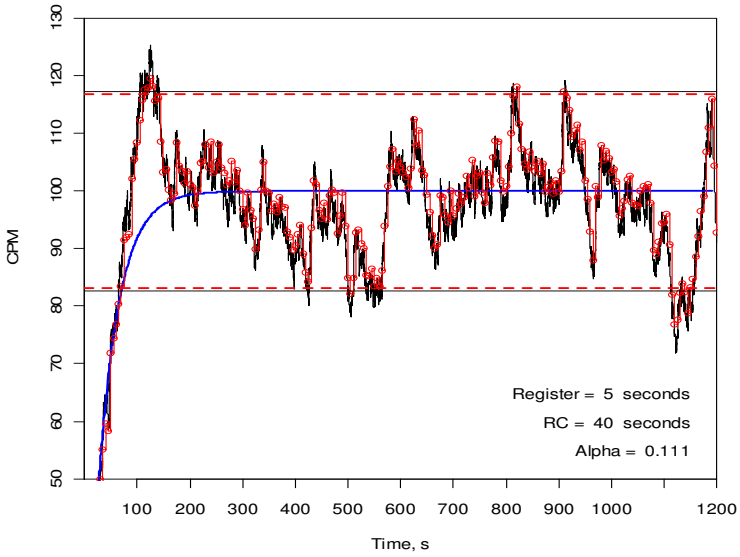

Figure 2. Analog RC circuit ratemeter and EWMA countrates. Trace with circles is EWMA. Bounds indicate EWMA and RC approximate 95% limits.

In Figure 2 we have a plot of the analog RC ratemeter simulation and the EWMA; the agreement is excellent. Note that the EWMA does not follow all the "high-frequency" variations of the RC, since the EWMA is a low-pass filter, this is to be expected. The "low-frequency" variations are modeled very well.The bounds indicated on the plot will be discussed below. The simulation also generates the observed (i.e., estimated) ACF for the EWMA and for the RC circuit sampled at the same time interval (Δt) that the EWMA uses. This is shown in Figure 3; they are essentially identical.

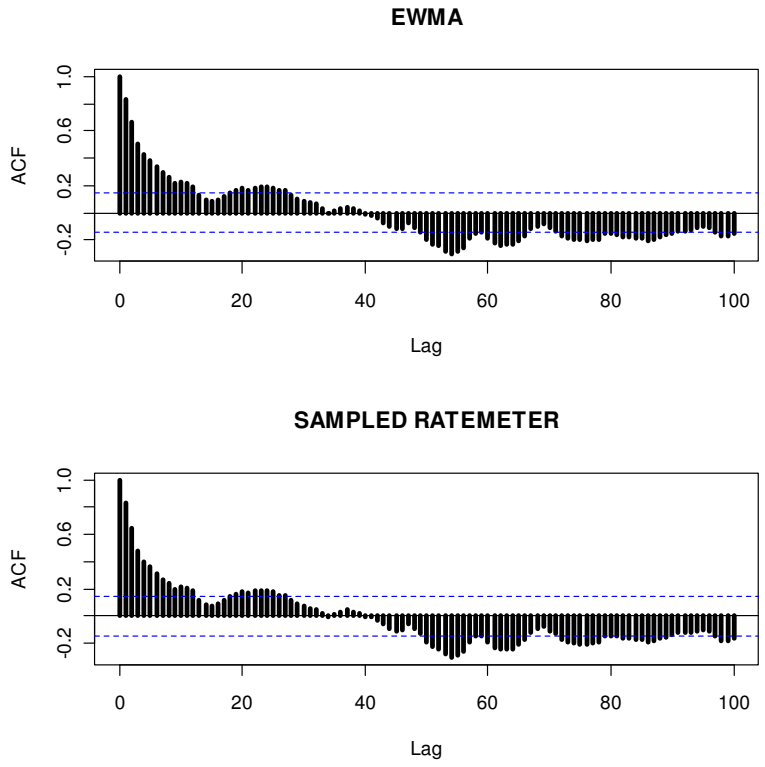

Figure 3. Estimated autocorrelation functions (ACF) for EWMA and a ratemeter.

Statistical Properties of EWMA

We will need to know the mean (expected value), variance, and ACF of the EWMA. The expected value is found by taking expectations of both sides of eqn(7), recalling that α is a constant, and assuming that the input x_k is constant:

$$\begin{aligned} \mathrm{E}[z_k] &= \alpha \mathrm{E}[x_k] + (1-\alpha)\mathrm{E}[z_{k-1}] \\ \mathrm{E}[z_k] - (1-\alpha)\mathrm{E}[z_{k-1}] &= \alpha \mathrm{E}[x_k] \\ \mathrm{E}[z_k]\{\, 1 - (1-\alpha)\,\} &= \alpha \mathrm{E}[x_k] \\ \mathrm{E}[z_k] &= \mathrm{E}[x_k] \end{aligned}$$

The third line follows from the second since the expected value of a stationary process is the same at any lag. Thus we have shown that *the mean of the EWMA output equals the mean of the (constant) input*.

The variance and ACF can be derived together, since the ACF is found via the autocovariance function γ_k, and then the variance is just γ_0. The ACF is defined to be

$$\rho_k = \frac{\gamma_k}{\gamma_0}$$

so the problem is to find the autocovariance function. The first step is to redefine the z_k of eqn(7) to be the variation around the mean level of the process, so that the expected value of this new process will be zero. With that, we have

$$\gamma_k = \mathrm{E}[z_t\, z_{t-k}] = \mathrm{E}\Big[\big(\alpha x_t + (1-\alpha) z_{t-1}\big)\big(\alpha x_{t-k} + (1-\alpha) z_{t-1-k}\big)\Big]$$

where t is any arbitrary lag (or time step). Expanding this, and recognizing that the input x to the EWMA is uncorrelated, i.e., random pulses from a detector, it can be shown with some expectation-value algebra that

$$\gamma_0 = \frac{\alpha}{2-\alpha}\,\sigma_x^2 \tag{10}$$

This important result also appears in various TSA references. Now we can define a useful quantity, the variance reduction ratio (VRR), as

$$VRR_{EWMA} = \frac{\alpha}{2-\alpha} \tag{11}$$

and this will be less than unity when α is less than unity.

These results were derived for a lag k of zero. To get the general autocovariance function, k will not be zero, and we proceed with a considerable amount of tedious expectation-value algebra, to finally obtain

$$\gamma_k = \frac{\alpha(1-\alpha)^k}{2-\alpha}\,\sigma_x^2 \tag{12}$$

and it can be seen that for $k = 0$ this agrees with eqn(11), as it must. Then the ACF is readily found to be

$$\rho_k = \frac{\gamma_k}{\gamma_0} = (1-\alpha)^k \tag{13}$$

which is a result of central importance. Since alpha is less than unity, this ACF will be a converging geometric series, as can be seen in Figure 4, which shows the observed (estimated) ACF for a very long EWMA sequence, along with the ACF points as found from eqn(10). The agreement is excellent.

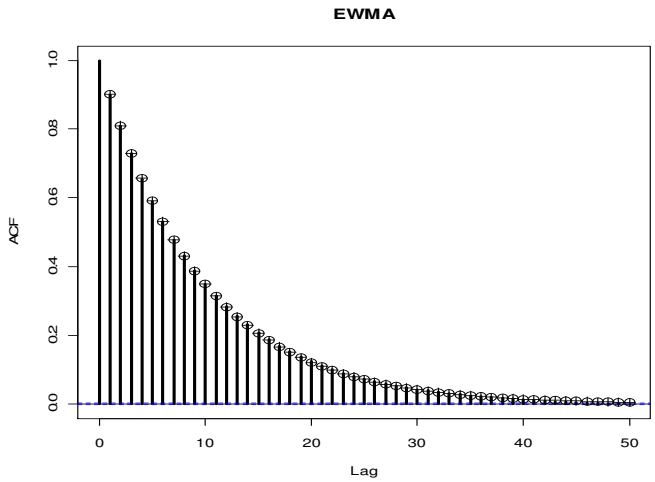

Figure 4. Estimated vs. theoretical ACF for EWMA.

Next we bring these calculations into the radiation monitoring context by recognizing that the input data sequence x_k is a sequence of pulses from a detector, and these pulses are Poisson distributed. Since the mean and variance of Poisson data are equal, we then can write for the standard deviation of the constant background countrate

$$\sigma_b^{raw} = \sqrt{\frac{\dot{C}_b}{\Delta t}} \tag{14}$$

as is well-known. Combining this with eqn(11) we find that

$$\sigma_b^{EWMA} = \sqrt{\frac{\alpha}{2-\alpha}} \sqrt{\frac{\dot{C}_b}{\Delta t}} \tag{15}$$

Using another well-known result, for the analog ratemeter,

$$\sigma_b^{ratemeter} = \sqrt{\frac{\dot{C}_b}{2RC}} \tag{16}$$

Returning to Figure 2, the horizontal lines are "two-sigma" bounds found using eqn(16) for the ratemeter (solid lines), and using eqn(15) for the EWMA (dotted lines). Since the EWMA is specifically designed to model at least the low-frequency behavior of the RC circuit, these two sets of bounds agree closely, as is seen in the figure. Note that both the RC circuit and the EWMA are driven by exactly the same input (detector) data in this figure. The EWMA accumulates counts over the register time Δt, five seconds in this case, while the RC circuit responds to these counts (pulses) as they occur in real time.

As a further check on the appropriateness of the EWMA as a digital representation of the RC circuit, let us equate the VRR of the EWMA and the RC circuit and solve for the EWMA gain α that would be necessary for equality. Using eqn(15) and (16) we find that equal VRR implies

$$\frac{1}{\sqrt{2RC}} = \sqrt{\frac{\hat{\alpha}}{(2-\hat{\alpha})\,\Delta t}}$$

and a bit of algebra will yield

$$\hat{\alpha} = \frac{2}{1 + 2\dfrac{RC}{\Delta t}}$$

which doesn't look too promising unless RC is significantly greater than Δt, as is usually the case, and then

$$\hat{\alpha} \approx \frac{\Delta t}{RC}$$

as we had already found in eqn(6). In fact there are several ways to find this gain α, and the result is always this same approximate value.

Bias Demonstration

Next we proceed to generate some EWMA output data and observe the estimates of the σ_b (i.e., s_b) that result. These will be compared to the σ_b that is known to be correct; the quantity graphed in Figure 5 will be observed (simulated) values of

$$R \equiv \frac{s_b}{\sigma_b}$$

If the s_b were not biased, then on average this ratio would be unity. In Figure 5 we see the bias in s_b reflected in the mean (circle) and median (bar) of two thousand replications of eqn(1) as a function of sample size N. The rectangles are based on the 0.025 and 0.975 quantiles, so that each box contains 95% of the s_b data generated at that N. The mean values follow the prediction from eqn(2) reasonably well (curved line); this is the same function as graphed in Figure 1.

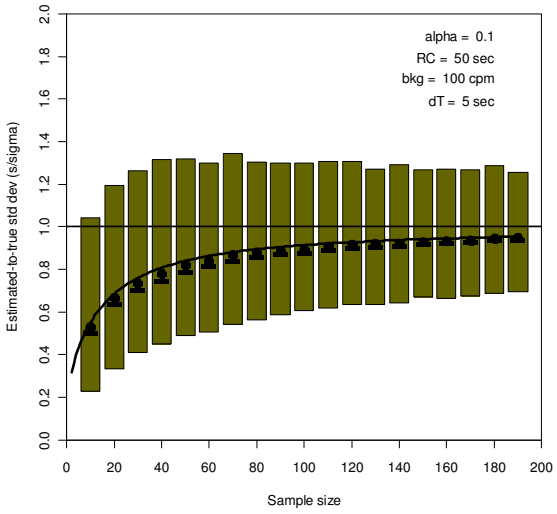

Figure 5. Simulated EWMA-processed count data; estimated standard deviation divided by known standard deviation. Boxes contain 95% of data at each N.

Not only are the estimates s_b biased, but as is evident in the plot, they also have a large amount of scatter, and their PDF is skewed. Running the simulation for other values of α yields plots that look very similar to Figure 5, and they follow the trends shown in Figure 1. By way of comparison, consider Figure 6, where there is zero autocorrelation. The bounds are based on the chi-square distribution, and we see that this data is behaving exactly as expected for uncorrelated data.

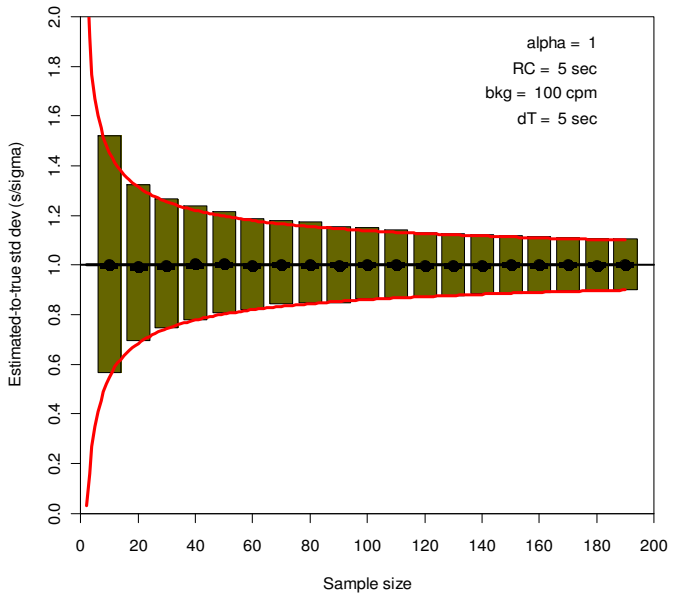

Figure 6. Standard deviation ratio for uncorrelated data; 95% boxes.

In these simulation runs there is a correction applied to the s_b found using eqn(1), that is noticeable only at very small sample sizes (e.g., $N < 20$). This correction is due to the fact that eqn(1) is not unbiased, even for uncorrelated data, and eqn(1) must be multiplied by

$$a = \sqrt{\frac{N-1}{2}}\ \frac{\Gamma\left(\frac{N-1}{2}\right)}{\Gamma\left(\frac{N}{2}\right)} \tag{17}$$

to remove this bias. This effect is noticeable in the simulation output if the correction is not applied.

Bias Correction

If the parameter α is known for a given EWMA filter, then it would seem logical to use eqn(2) to correct the s_b estimates. We can do this by using eqn(13) in eqn(2), so that our corrected, unbiased, estimate of σ_b is found using

$$s_b^{corrected} = \frac{a\ s_b}{\sqrt{1\ -\ 2\sum_{k=1}^{N-1}\left(1-\frac{k}{N}\right)(1-\alpha)^k}} \tag{18}$$

Applying this in the simulation we obtain the results shown in Figure 7. The bias is greatly decreased, but the scatter is still unacceptably large.

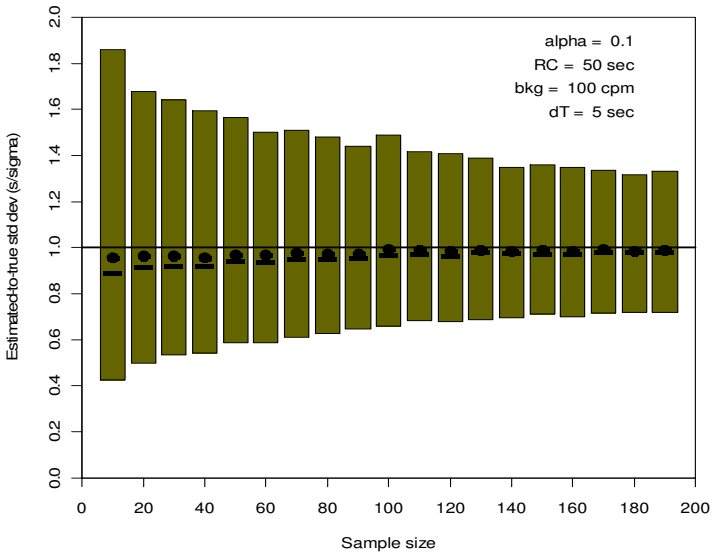

Figure 7. Bias-corrected standard deviation ratios; 95% boxes.

If the filter characteristics are not known *a priori*, a reasonable approach would seem to be to estimate the ACF directly from the data, and then use that in eqn(2) to correct the bias. This method was also simulated, and the results are not usable; this is because the estimated ACF is biased and is poorly estimated for any sample size N that would be used in monitor calibration (i.e., N less than several thousand observations). Graphing these results looks very much like Figure 5, where no bias correction was applied. **Bias correction of s_b requires a known ACF**.

Using the Mean Countrate

An alternative approach is possible due to the fact that the input data for the EWMA is Poisson distributed, and so there is a known relation between the *level* of the countrate (the mean) and the *variability* of the countrate (the standard deviation). The variability is what we seek, for MDC calculations. This was expressed above in eqn(15), repeated here

$$\sigma_b^{EWMA} = \sqrt{\frac{\alpha}{2-\alpha}}\sqrt{\frac{\dot{C}_b}{\Delta t}}$$

which we could write as

$$\sigma_b^{EWMA} = \sqrt{\frac{\alpha}{(2-\alpha)\Delta t}}\sqrt{\dot{C}_b} = k_{EWMA}\sqrt{\dot{C}_b} \qquad (19)$$

We could write similar relations for the RC circuit or for the bilinear digital filter. The variability of the (constant) background countrate is directly proportional to the square root of the countrate level. The proportionality constant is a function of the filtering parameter(s).

If these parameters are constant, and known, then we can use eqn(19), or its equivalent for the other filters, to find an estimate of σ_b from the countrate. That, in turn, is simply estimated by its mean value over some number of replicated measurements. Note that these measurements are taken in sequence *exactly as the monitor would use them in its quantitative method*; there is no "waiting for three time constants between measurements" as is sometimes specified in order to try to obtain uncorrelated data. (See Chapter 2 for a discussion of various quantitative methods.)

If the filtering is adaptive, where the filter gain changes randomly, then the approach would be to use Monte Carlo simulation to characterize a relation similar to eqn(19). Thus we would simulate the filtering process and estimate

the proportionality constant. Using the AEWMA filtering discussed in Chapter 2 (eqn 2-4) as an example, the data in Figure 9 was generated.

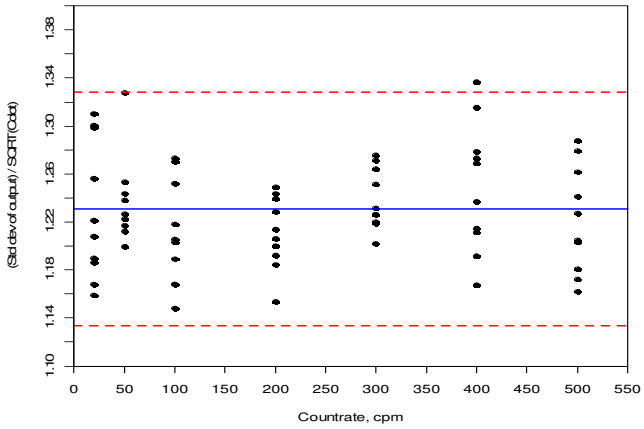

Figure 8. AEWMA proportionality constant Monte Carlo plot; estimate was 1.23±0.05

This approach was used in the calibration of air monitors in the Digital Radiation Monitoring System for the Shoreham Nuclear Power Station, in the early 1980s. One hundred measurements of the background were taken for each instrument, and the mean calculated, and the proportionality constant applied (it was 1.3 for that system) to find the estimator of σ_b to use in the MDC calculations. Note that in these simulations very large sample sizes, i.e., several thousands of points, are used, to eliminate the need for a bias correction in the observed s_b data. (The AEWMA output is autocorrelated.)

Mean Countrate Results

Let us apply the method of eqn(19) in the simulation; the results are shown in Figure 9, along with the previous method of correcting the estimated s_b. Clearly the mean-method is estimating the correct σ_b, and, most notably, its scatter is dramatically smaller than that of the corrected s_b.

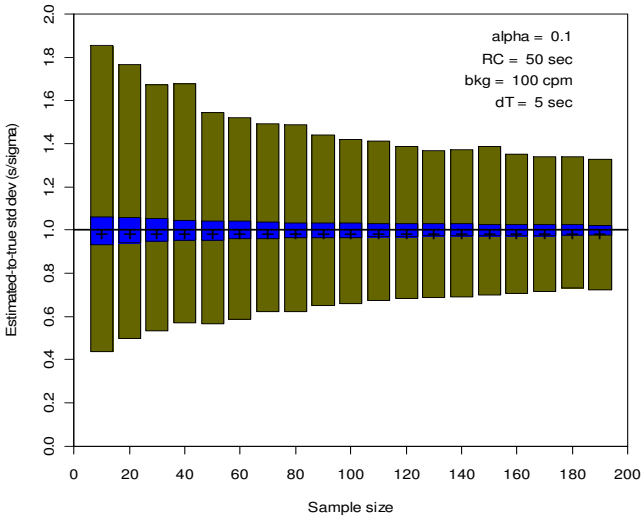

Figure 9. Estimation of countrate variability using the mean (blue boxes) and bias-corrected s_b (green boxes). All boxes 95% level.

What is being graphed in the blue boxes in this figure is the ratio of eqn(19) divided by eqn(15):

$$R = \frac{k_{EWMA}\sqrt{\bar{C}_b}}{\sqrt{\frac{\alpha}{(2-\alpha)\Delta t}}\sqrt{\dot{C}_b}} = \sqrt{\frac{\bar{C}_b}{\dot{C}_b}}$$

and since the expected value of the mean EWMA-filtered countrate is just the constant background countrate (as was shown above), the expected value of this ratio is unity. This is reflected in the figure.

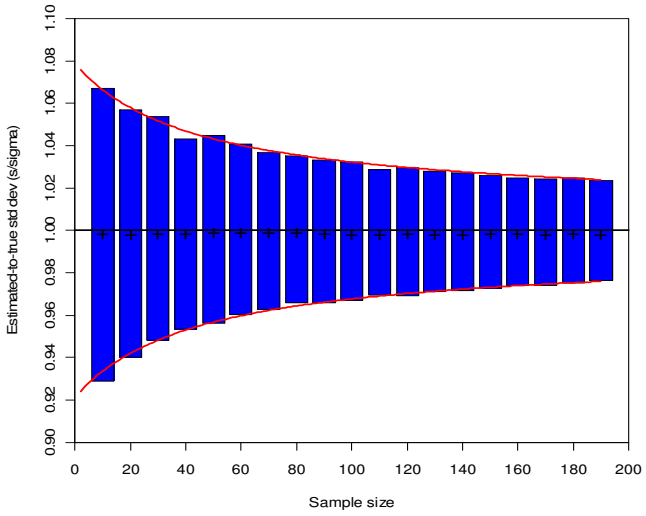

Figure 10. Mean-method estimates of sigma-b, with 95% bounds.

Bias-Correction Methods

There are three methods that might be used to remedy this bias situation. The assertions stated below can be proven analytically and/or demonstrated with simulation results that will not be presented here, for brevity:

1. Use eqn(1) s_b and correct it for autocorrelation using eqn(2) and the filter ACF.

Must know ACF *analytically* and must take samples in Δt (time-ordered) sequence.

ACF estimated from observed data is biased (see [1]); *it will not work.* Also, empirical ACFs require impractical sample sizes.

Corrected s_b has no bias but has large scatter.

2. Use s_b with spaced samples ("wait ≥ three time-constants between measurements").

Does eliminate autocorrelation; must be able to find minimum wait time, could need ACF for this.

Not biased, but still large scatter.

Not the way the instrument operates in practice, hence these are artificial measurements.

3. Establish relation of mean to σ_b then estimate *mean* (not s_b) from monitor data.

Only possible when input data is Poisson (as we have for detector pulses).

Mean can be shown to be unbiased in presence of autocorrelation.

This method is independent of timing; samples can be at each Δt, with wait time, or random intervals.

Will work for nonconstant-gain (adaptive) digital filters.

Either analytical or Monte Carlo to establish how σ_b varies with mean cpm.

This method, using Monte Carlo, was successfully used in the calibration of the Shoreham DRMS, which had an adaptive countrate filter.

Dramatically smaller scatter in σ_b estimates, especially at practical sample sizes, and thus better MDC estimates.

To see that the bias is removed, and to see the relative scatter in the σ_b estimates, consider Figure 11. This shows the Method 2 and 3 results for a simulation run where both methods used the same EWMA data, and both used the same wait time. The mean values of both sets of data are very close to unity, showing that the bias has been removed. The widths of the boxes represent, as in previous figures, 95% of the data at each sample size. Clearly Method 2 results in *much* more dispersion of the σ_b estimates than does Method 3, for a given sample size.

The "wait time" for Methods 2 and 3 in these plots is 44 time steps (of 5 seconds each), and this was calculated by finding the number of lags needed to reduce the autocorrelation to 0.01. This calculation is possible, as is the bias correction in Method 1, only because the ACF of the EWMA has been derived. (Note that Method 3 does not **depend** on this wait time; it was convenient in coding the simulation to use the same delta-t for both methods.)

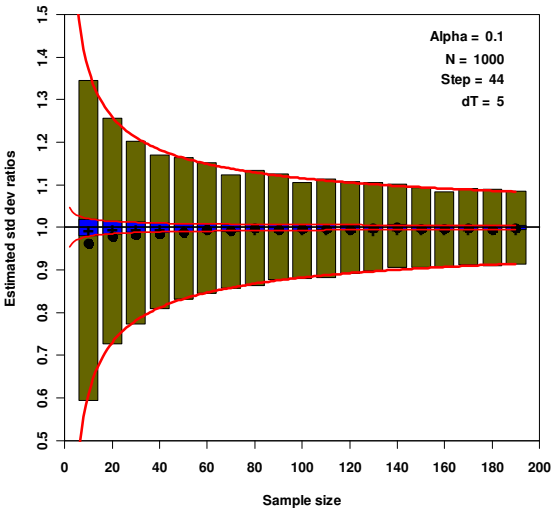

Figure 11. Bias-correction sigma ratios for Method 2 (green boxes) and Method 3 (blue boxes).

Another, concise, way to show the relative precision of these methods is a plot representing the "normalized" scatter (i.e., the relative error) in the σ_b estimates for each method. This is shown in Figure 12. The dots represent quantile estimates from simulation data, while the curves are based on analytical functions. The quantiles are those that represent a "one-sigma" range of observed σ_b estimate values.

Figure 12 shows that the precision of the Method 3 estimates is about one percent or less, and is a weak function of the sample size, while Method 2 varies from around 15% at N=20 to about 5% at N=200. Method 1 results in the worst-precision estimates. All three methods do eliminate the bias, but they differ significantly in precision. As a general principle of data analysis, we would presumably want to use the minimum-variance, unbiased estimator, and, here, that is Method 3.

As a practical matter in conducting measurements, it is also important to emphasize again that Method 3 does not depend on any particular timing requirement, e.g., at each Δt or at some wait time between samples. This is because, for a constant-mean random process, *where* (or more correctly, *when*) we sample that process will have no effect on our estimate of the mean level of the process. And the underlying autocorrelation structure of the *process itself* (as opposed to the ACF of the spaced samples) is not altered by the spacing of the samples.

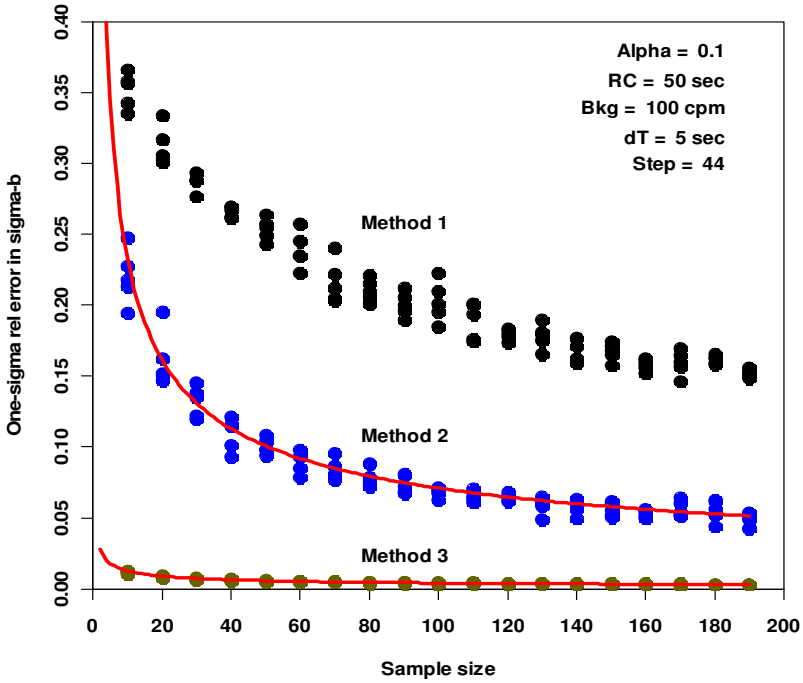

Figure 12. "One-sigma" relative error in estimates of σ_b for indicated method. Points are simulation results. Methods 2 and 3 use 44-step wait time, Method 1 used all samples, in sequence.

Conclusion

At a minimum there should be some discussion in the MDC calculation documentation of this bias and precision issue, when using s_b to estimate σ_b for the MDC calculations, for ratemeter-based instruments. A recommended method for resolving the bias, perhaps Method 3 above, should be presented in an Appendix. Any alternative to that method, that users choose to apply, should be carefully justified statistically, and should be thoroughly documented.

References

[1] Anderson, T.W. *The Statistical Analysis of Time Series*, Wiley (1994); Chapter 8.

[2] Oppenheim and Schafer, *Digital Signal Processing*, Prentice-Hall (1975); Chapter 5.

Appendix D

Activity / Countrate Profiles

Unpublished

This appendix contains 2D plots of activity and 3D plots of countrate, on RW and CW filters. The 2D plots are for a constant input concentration, as well as an exponentially-decreasing concentration, for both a LL nuclide and Rb^{88}. The activity is shown in two columns, increasing in time from the top left to bottom right, with the elapsed time indicated. The transit time is 120 min. These profiles will represent countrates, if a flat (constant) detection efficiency is assumed. The 3D versions are for countrates; these show the effect of the nonconstant geometric efficiency that actually applies. The observed countrate is the volume under these surfaces.

The 2D profiles in this Appendix can be considered a "side view" of 3D surfaces that are generated using a flat efficiency (constant across *both* dimensions of the RW deposition area). One purpose of creating these profiles was to show that those sketched in the patent mentioned in Chapter 9 are not consistent with these. The profiles in the patent could apply for a LL nuclide (they are linear), but the purpose of the patent relates to Rb^{88} (leak detection), and those profiles can be seen herein to be curved. Thus the patent is internally inconsistent.

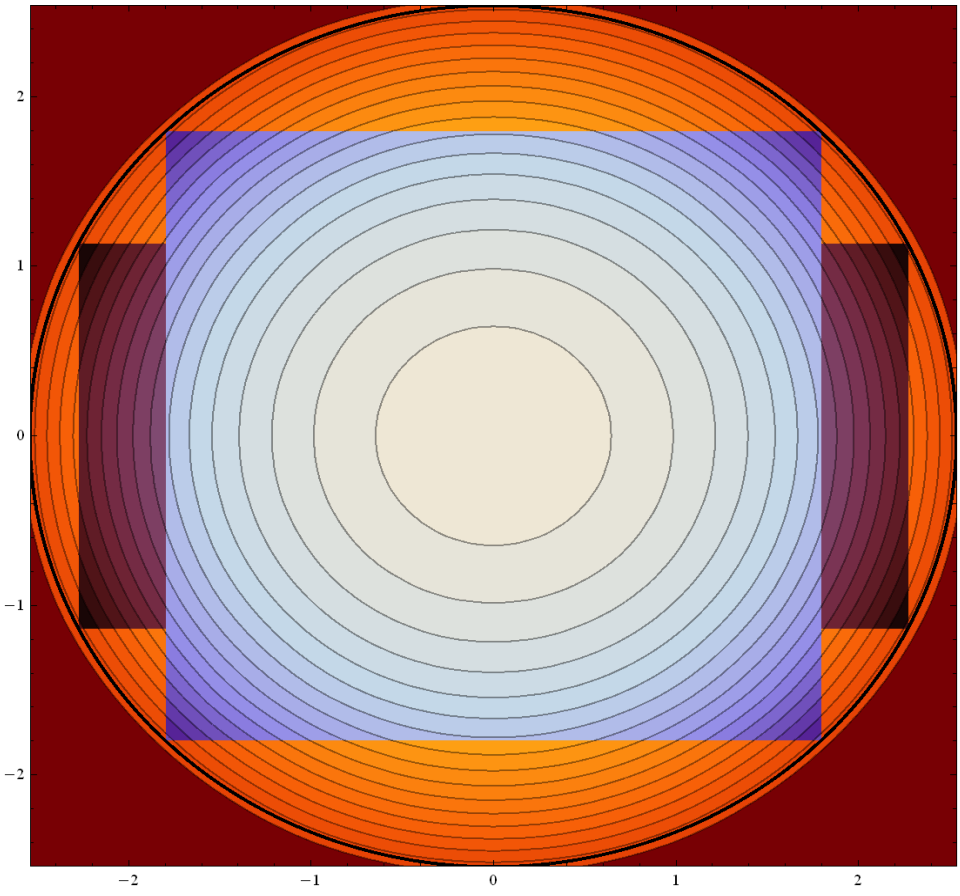

The regions of a circular deposition area viewed by the three window types. The square and rectangular windows in the plots below are sized to just fit within the circular window region.

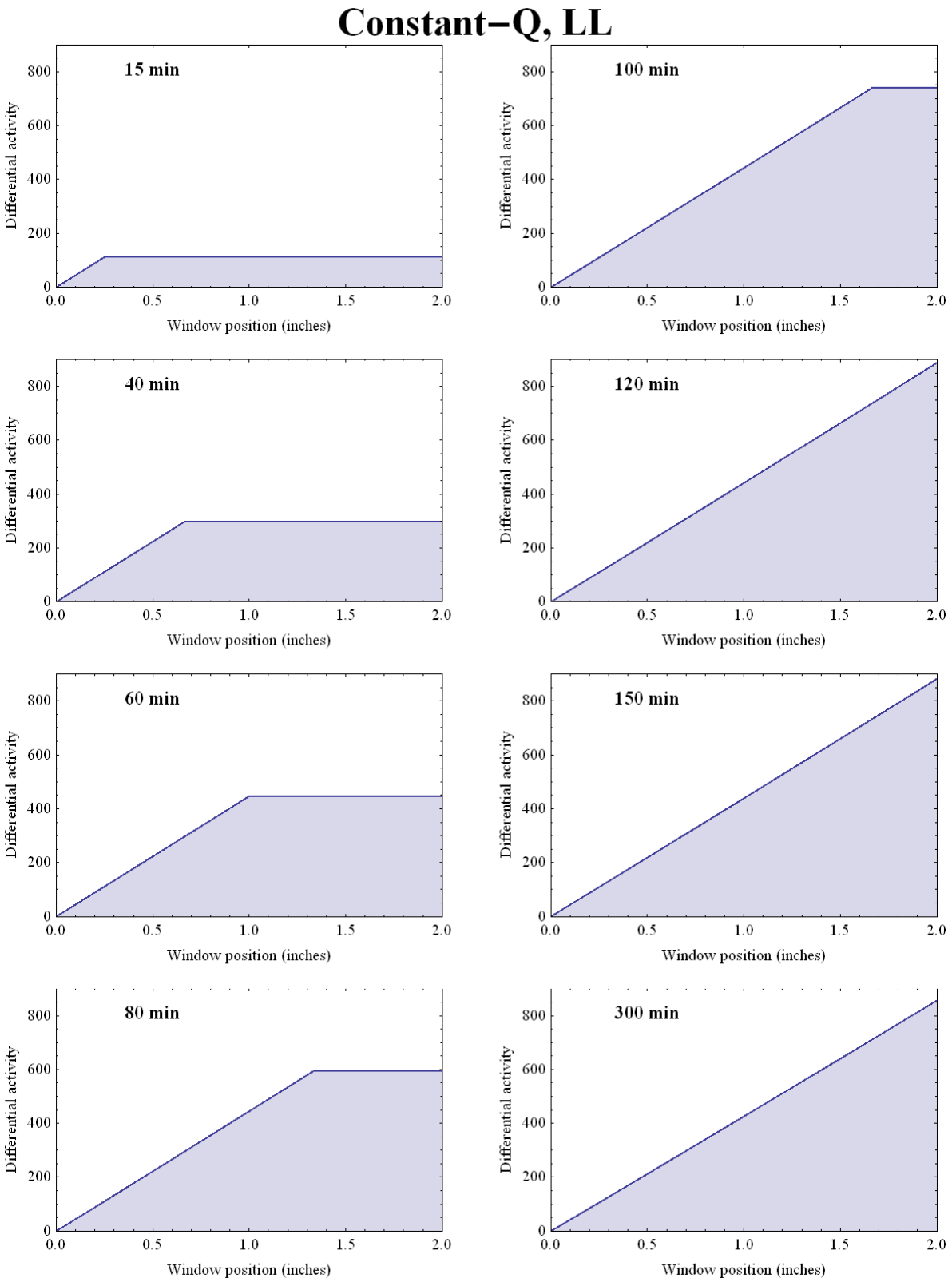

Figure 1. Activity profiles, activity per unit area vs. window position, RW, at various times.

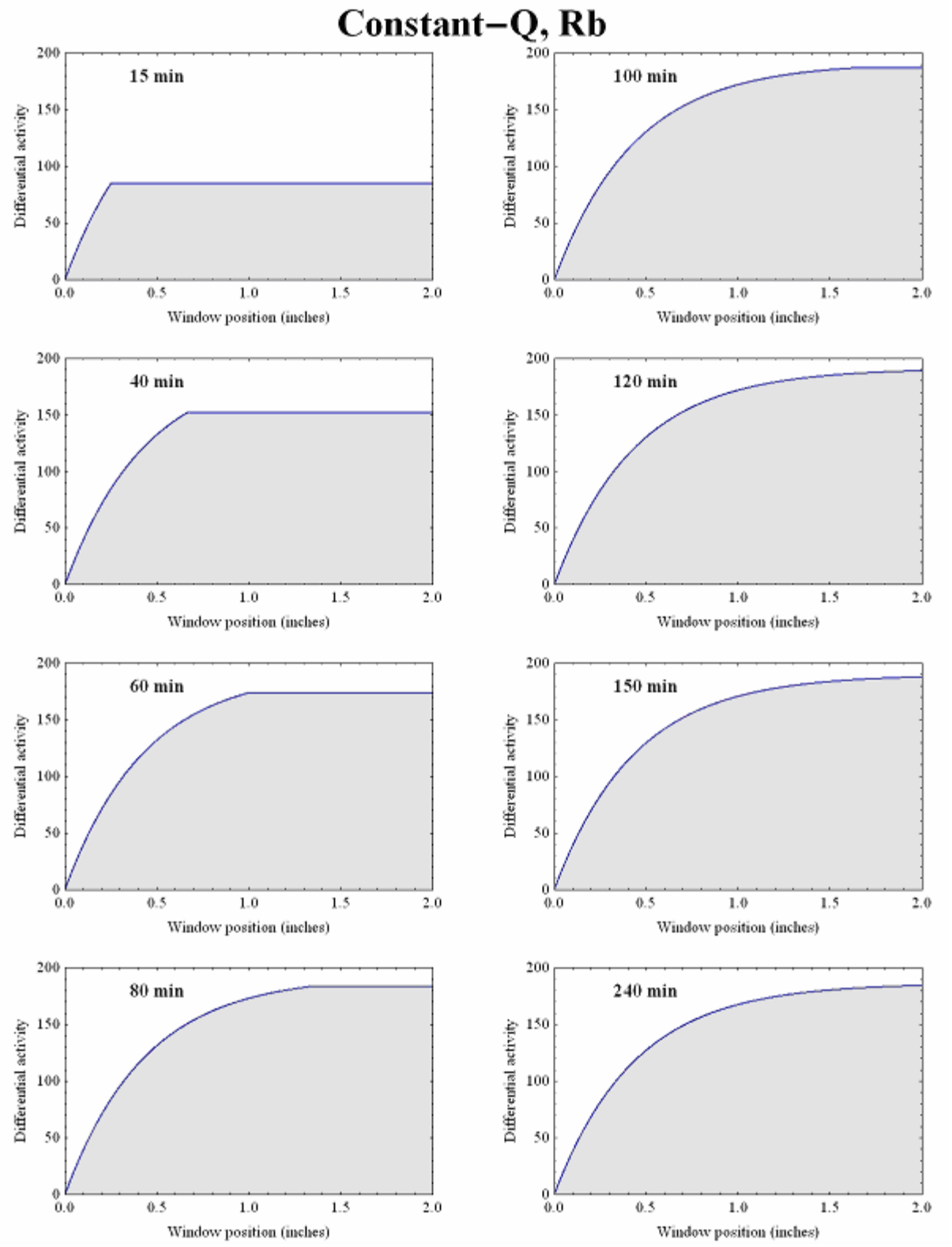

Figure 2. Same as Fig. 1, for Rb-88.

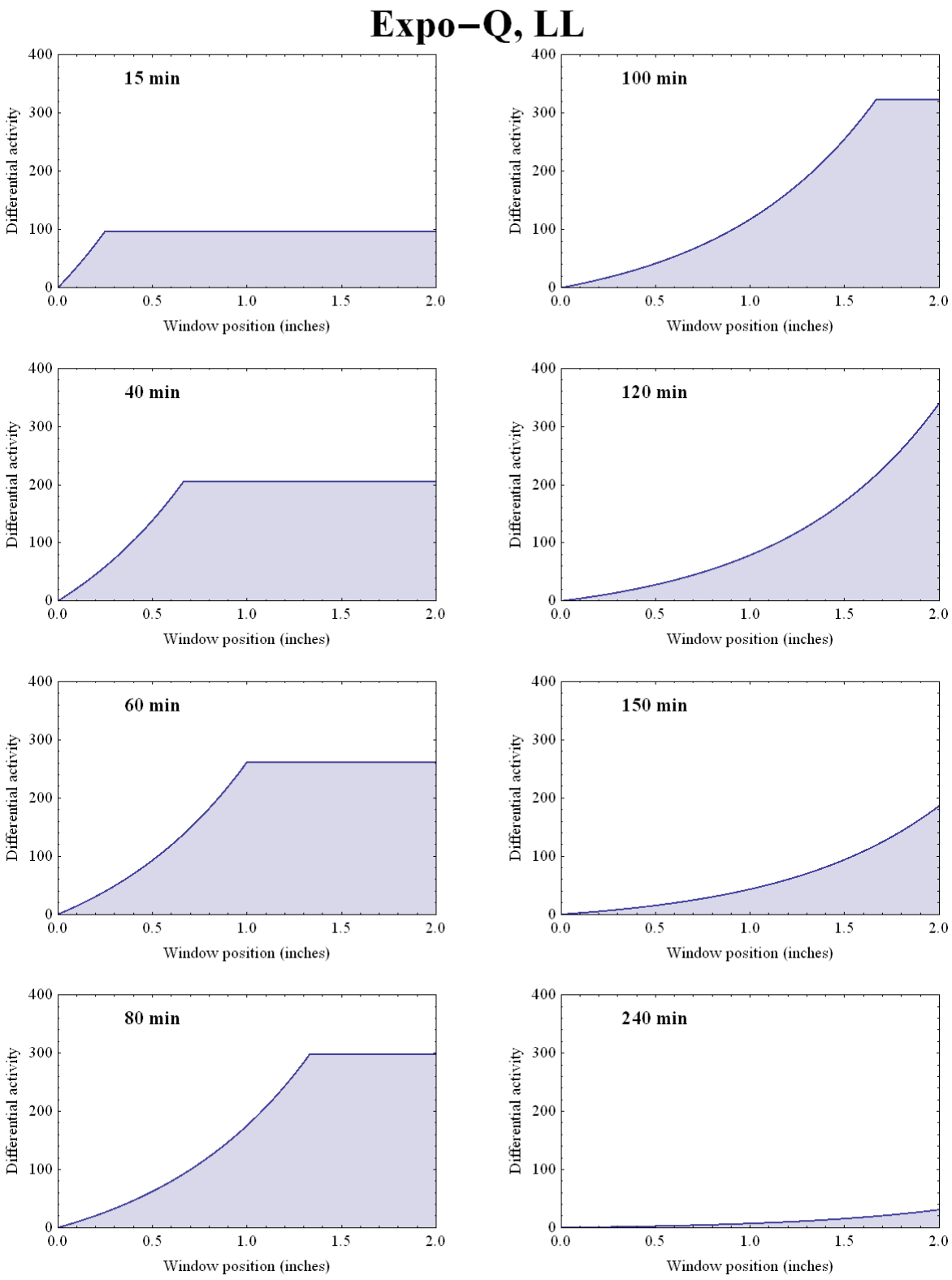

Figure 3. Same as Fig. 1, for an exponentially-decreasing input concentration.

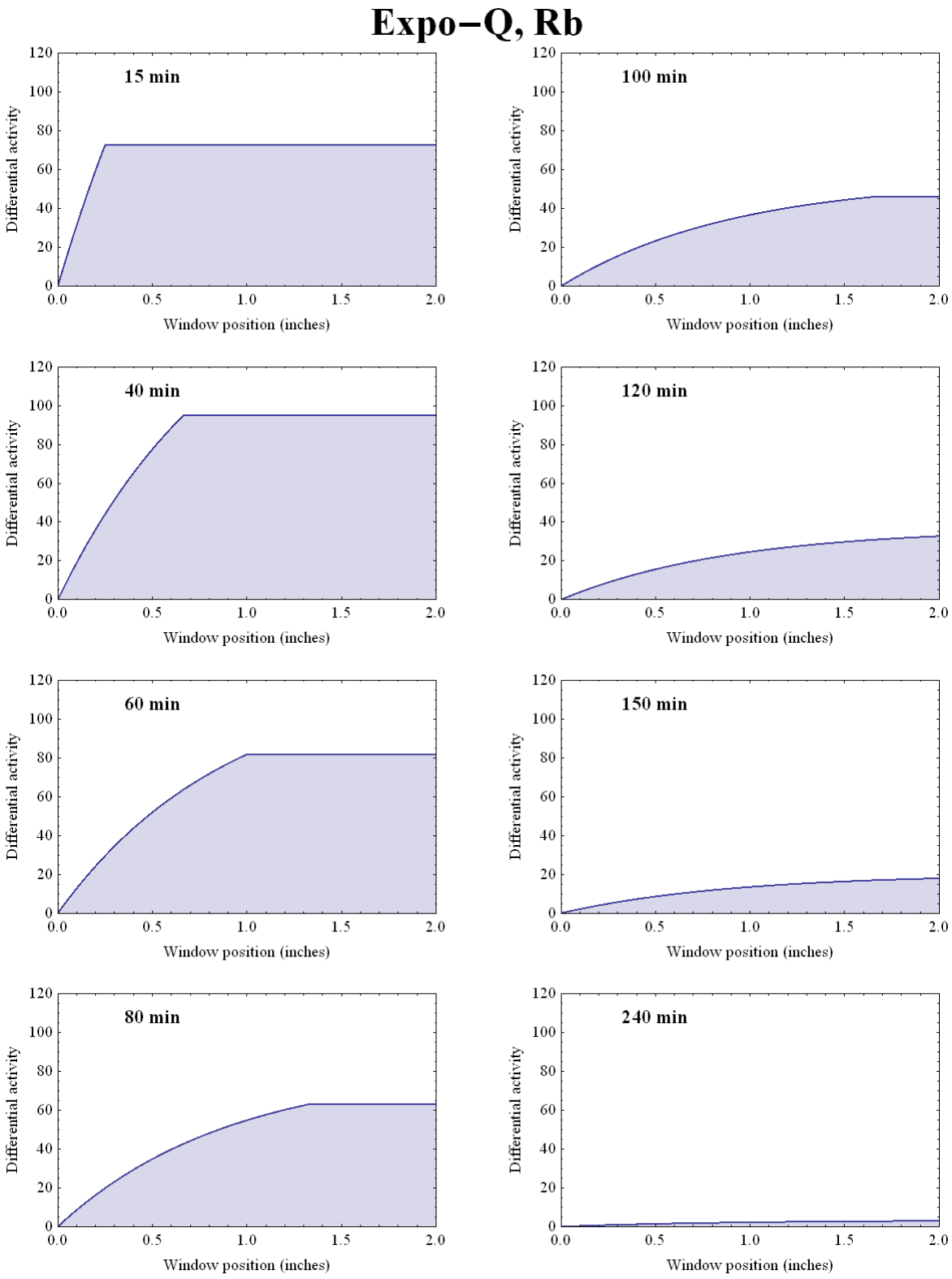

Figure 4. Same as Fig. 2, for an exponentially-decreasing input concentration.

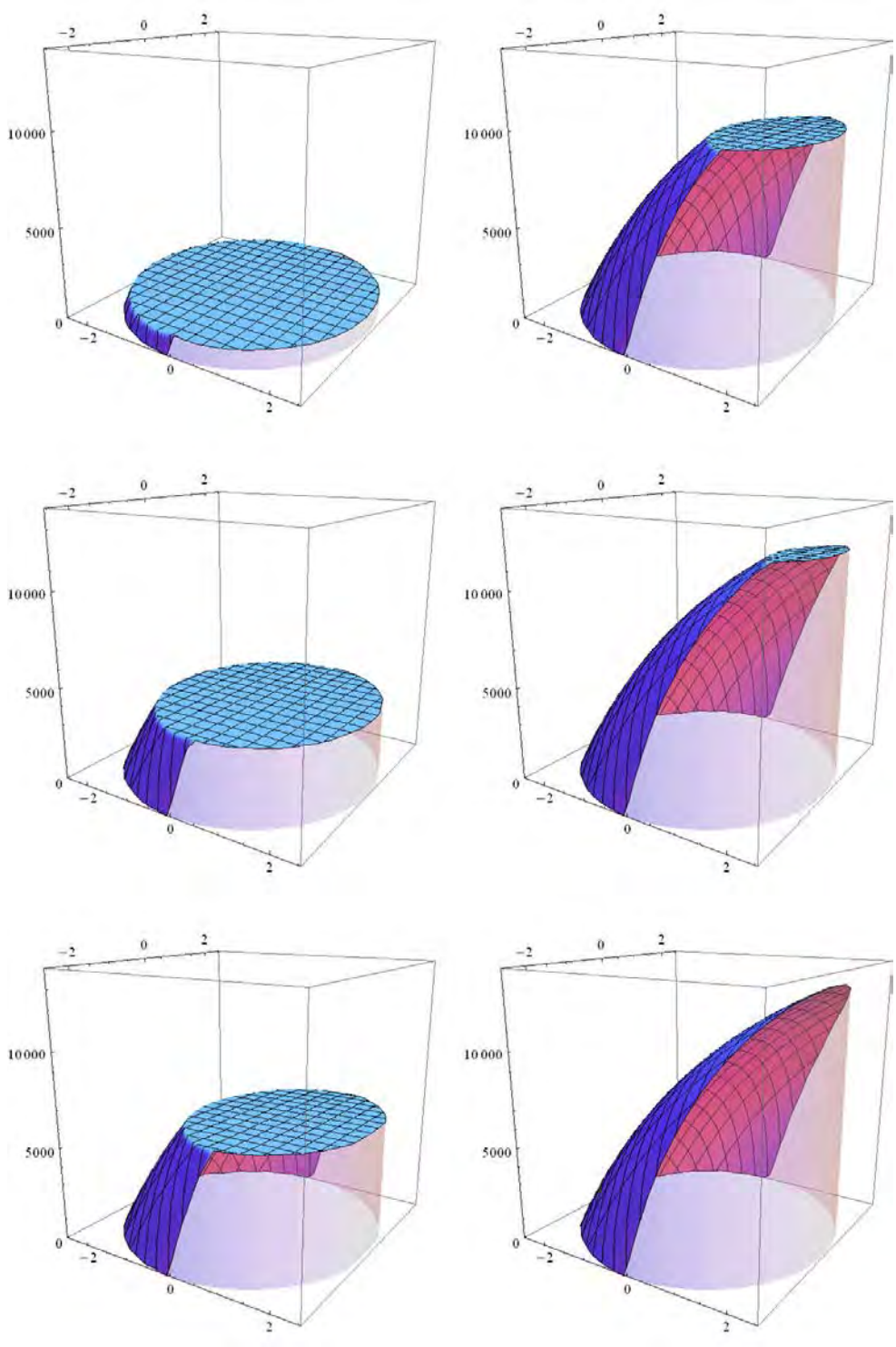

Figure 5. CW flat-efficiency countrate-per-unit-area surfaces.These surfaces are directly proportional to the activity per unit area Γ(x,y), for the top nuclide (60 min halflife) in a 3-chain, at six time steps, increasing down the columns, left to right. In the early stages the activity per unit area is constant, but over a decreasing portion of the deposition window. By the last time step the activity is continuously changing across the window.The total countrate is the volume under the surfaces.

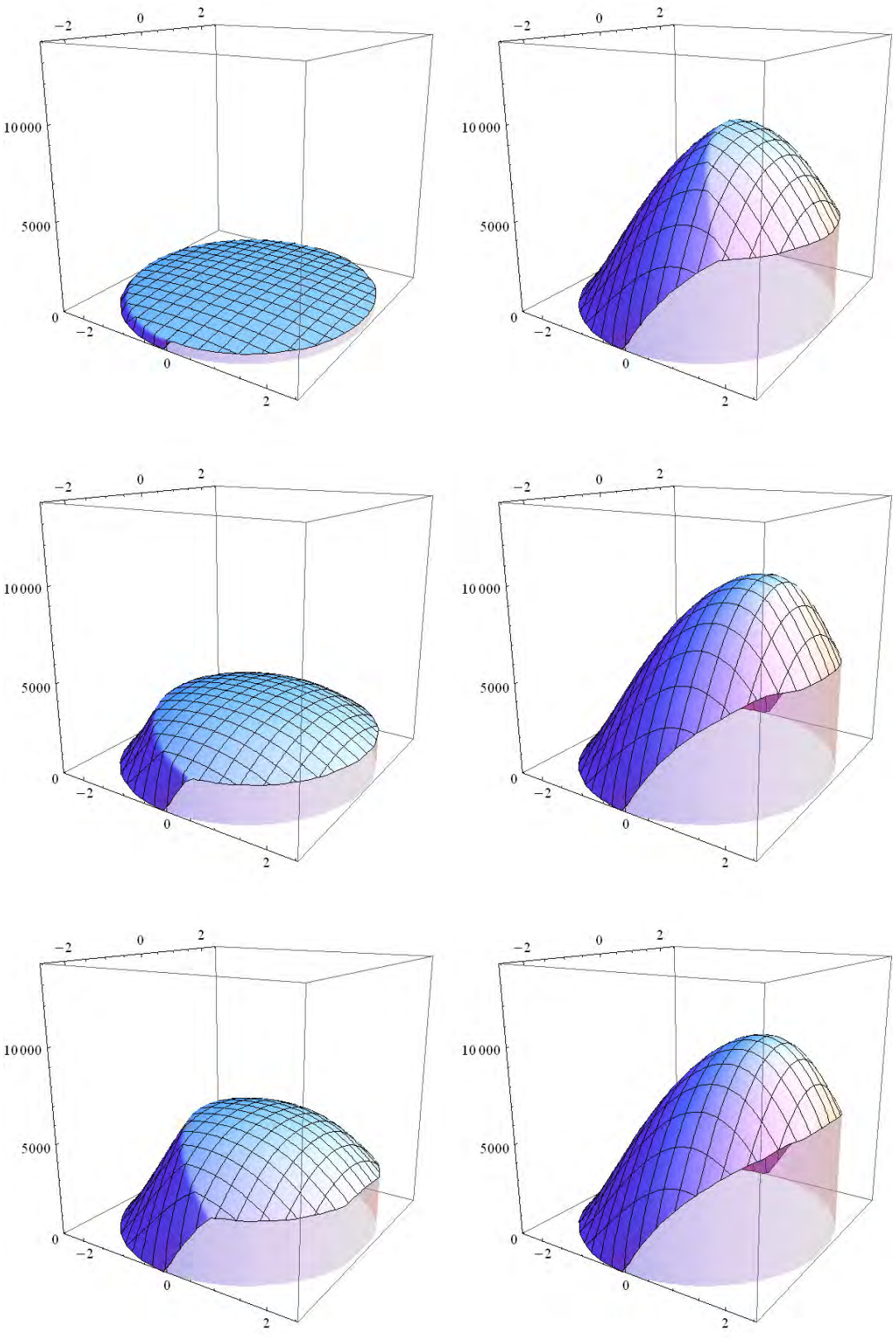

Figure 6. Same as Fig. 5, but with geometric efficiency applied.

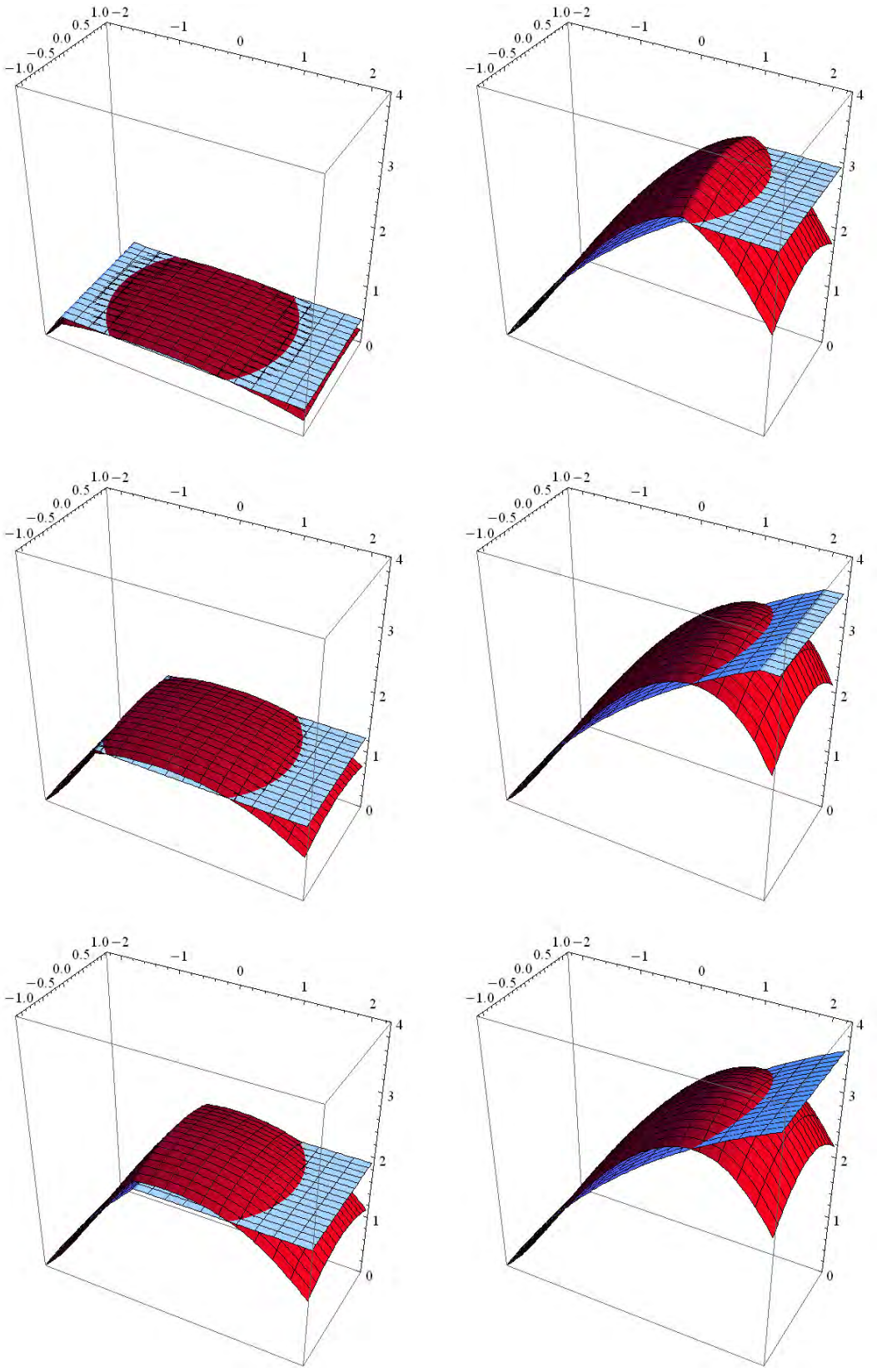

Figure 7. RW, 3-chain, top nuclide differential cpm/area surfaces, with flat, average efficiency (blue), geometric = red. The nuclide has a halflife of 60 min, so is not considered LL and thus there is some slight curvature.

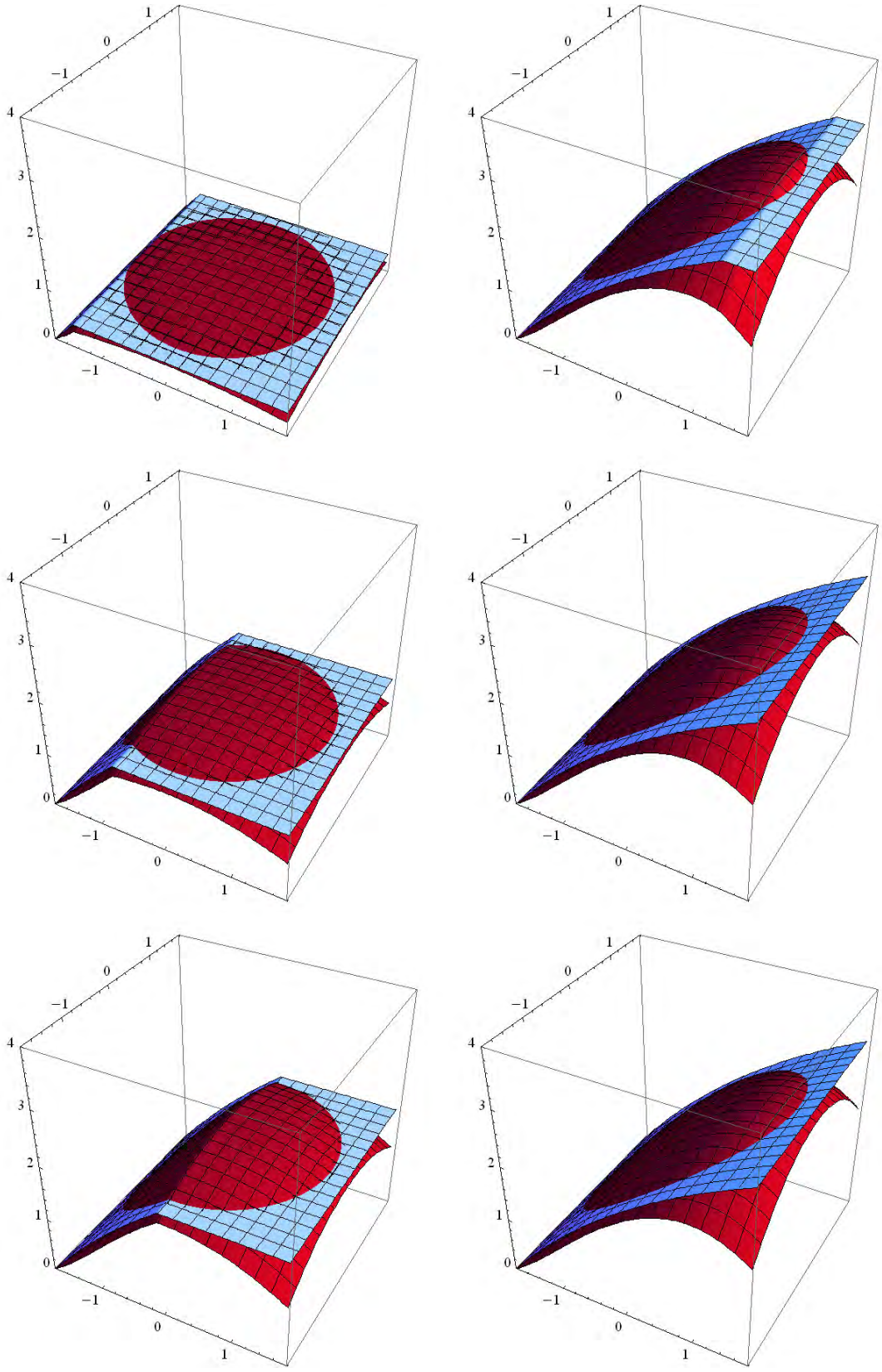

Figure 8. Same as Fig.7 for a square deposition area

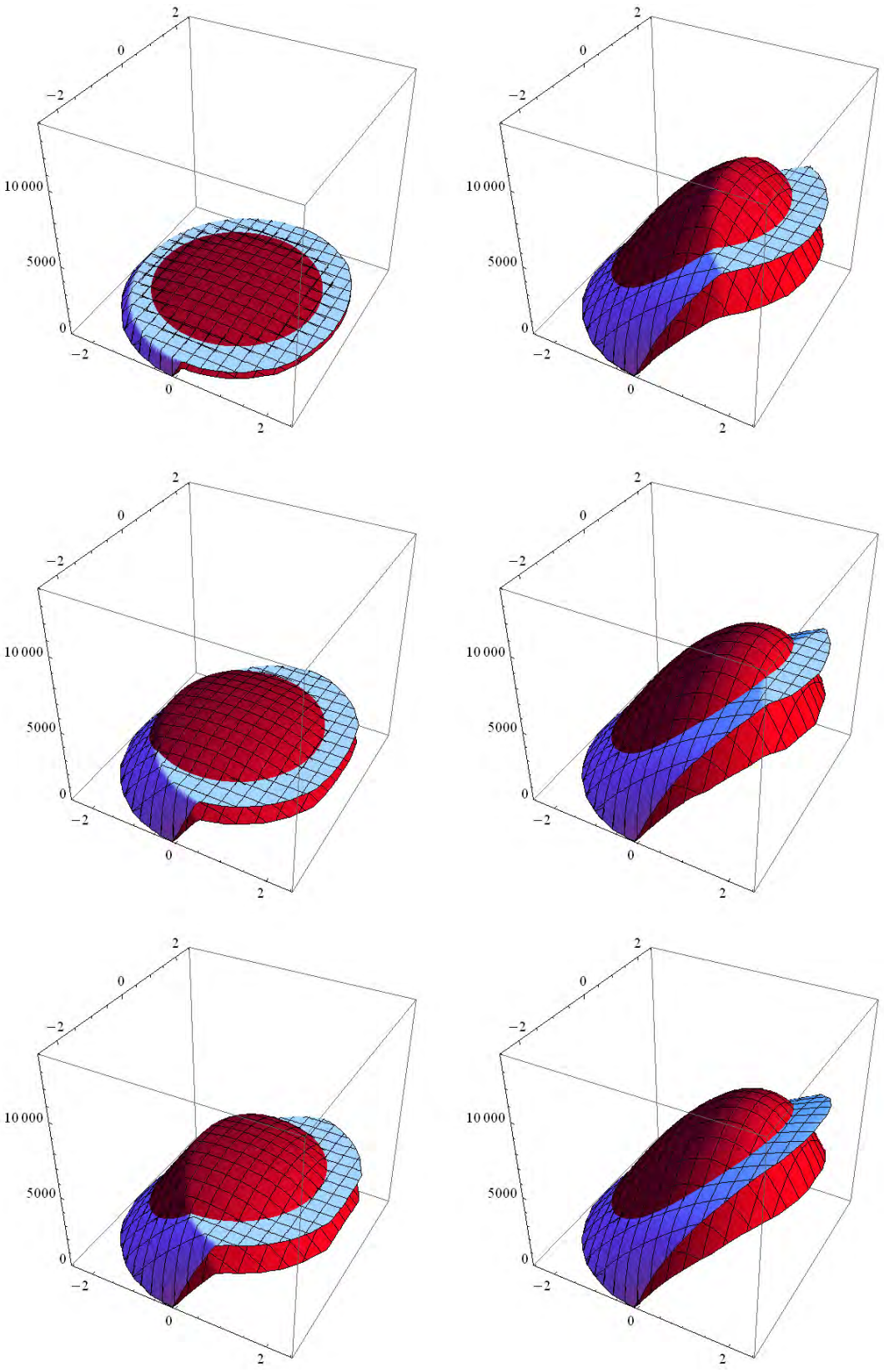

Figure 9. Same as Fig. 7 for a circular deposition area.